

<https://doi.org/10.15388/vu.thesis.501>
<https://orcid.org/0000-0002-2715-067X>

VILNIUS UNIVERSITY

Andrius Sakalauskas

Understanding Inhibition of Protein Amyloid Fibril Formation

DOCTORAL DISSERTATION

Technological Sciences,
Chemical Engineering (T 005)

VILNIUS 2023

The dissertation was prepared between 2019 and 2023 at Vilnius University. The research was supported by Research Council of Lithuania (KD-19076).

Academic supervisor – Dr. Vytautas Smirnovas (Vilnius University, Technological Sciences, Chemical engineering, T 005).

This doctoral dissertation will be defended in a public meeting of the Dissertation Defence Panel:

Chairman – Prof. Dr. Rolandas Meškys, (Vilnius University, Technological sciences, Chemical Engineering, T 005).

Members:

Dr. Zuzana Bednarikova (Institute of Experimental Physics, Natural Sciences, Biochemistry, N 004),

Dr. Indrė Kučinskaitė-Kodžė (Vilnius University, Technological Sciences, Chemical engineering, T 005),

Doc. Dr. Jolanta Sereikaitė (Vilnius Gediminas Technical University, Technological Sciences, Chemical Engineering, T 005),

Prof. Dr. Salvador Ventura (Universitat Autònoma de Barcelona, Natural Sciences, Biochemistry, N 004).

The dissertation shall be defended at a public meeting of the Dissertation Defence Panel at 10:00 hour on 05 September 2023 in Room R401 of the Life Sciences Center (Vilnius University)

Address: Sauletekio av. 7., Room No. R401, Vilnius, Lithuania

Tel. +370 631 55555; e-mail: andrius.sakalauskas@gmc.vu.lt

The text of this dissertation can be accessed at the libraries of Vilnius University as well as on the website of Vilnius University:

www.vu.lt/lt/naujienos/ivykiu-kalendorius

<https://doi.org/10.15388/vu.thesis.501>
<https://orcid.org/0000-0002-2715-067X>

VILNIAUS UNIVERSITETAS

Andrius Sakalauskas

Baltymų amiloidinės agregacijos slopinimo tyrimai

DAKTARO DISERTACIJA

Technologijos mokslai,
Chemijos inžinerija (T 005)

VILNIUS 2023

Disertacija rengta 2019 – 2023 metais Vilniaus universitete.
Mokslinius tyrimus rėmė Lietuvos mokslo taryba (KD-19076).

Mokslinis vadovas – dr. Vytautas Smirnovas (Vilniaus universitetas, technologijos mokslai, chemijos inžinerija, T 005)

Gynimo taryba:

Pirmininkas – prof. Dr. Rolandas Meškys (Vilniaus universitetas, technologijos mokslai, chemijos inžinerija, T 005).

Nariai:

Dr. Zuzana Bednarikova (Eksperimentinės fizikos institutas, gamtos mokslai, biochemija, N 004),

Dr. Indrė Kučinskaitė-Kodžė (Vilniaus universitetas, technologijos mokslai, chemijos inžinerija, T 005),

Doc. Dr. Jolanta Sereikaitė (Vilniaus Gedimino technikos universitetas, technologijos mokslai, chemijos inžinerija, T 005),

Prof. Dr. Salvador Ventura (Universitat Autònoma de Barcelona, gamtos mokslai, biochemija, N 004).

Disertacija ginama viešame Gynimo tarybos posėdyje 2023 m. rugsėjo mėn.5 d. 10 val. Vilniaus universiteto Gyvybės mokslų centro R401 auditorijoje.

Adresas: Saulėtekio al. 7, R401, Vilnius, Lietuva,

Tel. +370 631 55555; e-mail: andrius.sakalauskas@gmc.vu.lt

Disertaciją galima peržiūrėti Vilniaus universiteto bibliotekose ir VU interneto svetainėje adresu: <https://www.vu.lt/naujienos/ivykiu-kalendorius>

ACKNOWLEDGEMENTS

The journey I embarked on to complete this dissertation was filled with challenges, but with unwavering support from my colleagues, academic supervisor, family, and friends, I was able to overcome every obstacle.

My involvement with the Amyloid Research Group in the Department of Biothermodynamics and Drug Design at Vilnius University began during my undergraduate studies. It was there that I met my first mentor, Darius Šulskis, who introduced me to the fundamentals of research methods and allowed me to delve into the study of amyloids. I am deeply grateful to Tomas Šneideris for guiding my experiments, which ultimately led to a remarkable publication. His comprehensive knowledge of amyloid-beta purification and its aggregation proved invaluable. I extend my heartfelt appreciation to Mantas Žiaunys for showing the ways how to write scientific manuscripts and for his support with publications.

I would like to express my sincere gratitude to my supervisor, Dr. Vytautas Smirnovas, for accepting me as his student, providing unwavering support, sharing his insightful thoughts, and injecting humor into our scientific discussions. I am also thankful to the other members of our Amyloid Research Sector - Kamilė, Rūta, Dominykas, Lukas, and our students - for their support, engaging discussions, and for fostering an extraordinary atmosphere in the lab. I extend my thanks to Daumantas Matulis, Mantas Žvirblis, Gediminas Žvinys, Virginija Dudutiene, and other members of the Biothermodynamics and Drug Design team for their important contributions, stimulating meetings, successful collaborations, and opportunities to work together.

I am deeply grateful to my other collaborators—Justina Versockienė, Eglė Lastauskienė, Laimonas Stančaitis, Simona Strazdaitė, Gediminas Niaura, Audrius Zakšauskas, Rebecca Strenke-Hoffman, Alexander K. Buell, Saeid Hadi Ali Janvand, and Daniel E. Otzen. Your contributions have been instrumental in enabling me to undertake various enlightening studies.

Lastly, I am indebted to my family and friends whose unwavering encouragement, love, and understanding have sustained me throughout

this challenging journey. Your belief in me has been my greatest motivation. Thank you all for being there for me.

ABBREVIATIONS

A β	Amyloid-beta
A β_{40}	Amyloid-beta (1-40)
A β_{42}	Amyloid-beta (1-42)
aCSF	Artificial cerebrospinal fluid
AD	Alzheimer's disease
AFM	Atomic force microscopy
APP	Amyloid precursor protein
CSF	Cerebrospinal fluid
DMSO	Dimethyl sulfoxide
EGCG	Epigallocatechin-3-gallate
FTIR	Fourier-transform infrared spectroscopy
GA	Gallic acid
GAO	Oxidized gallic acid
GuSCN	Guanidine thiocyanate
HCF	Fibrils formed at higher protein concentration
HPLC	High-performance liquid chromatography
HSA	Human serum albumin
ISF	Interstitial fluid
LCF	Fibrils formed at lower protein concentration
NFT	Neurofibrillary tangle
oDHF	Oxidized 2'3'-dihydroxyflavone
oDHF _{HW}	High molecular weight components of oDHF
oDHF _{LW}	Low molecular weight components of oDHF
PD	Parkinson's disease
PBS	Phosphate buffered saline
SEC	Size-exclusion chromatography
SP	Senile plaque
TBS	Tris buffered saline
ThT	Thioflavin-T
UV/Vis	Ultraviolet/Visible

CONTENTS/TURINYS

ACKNOWLEDGEMENTS	5
ABBREVIATIONS.....	7
ABSTRACT	10
1. LITERATURE OVERVIEW	13
1.1. Neurodegenerative diseases	13
1.1.1. History of neurodegenerative diseases.....	13
1.1.2. Alzheimer’s disease	14
1.1.3. Parkinson’s disease	15
1.2. Therapy of neurodegenerative diseases	16
1.2.1. Medications on AD	16
1.2.2. Future medications on AD	17
1.2.3. Polyphenols as anti-amyloid compounds.....	18
1.3. Protein aggregation	19
1.3.1. Protein aggregation mechanism	19
1.3.2. Protein aggregation polymorphism.....	21
1.3.3. Inhibition mechanism.....	21
1.4. Protein aggregation <i>in vitro</i>	22
1.4.1. Aggregation monitoring.....	22
1.4.2. Protein aggregation kinetics.....	23
1.4.3. Fibril morphology and secondary structure	24
1.5. Proteins used in this thesis.....	25
1.5.1. Amyloid- β	25
1.5.2. α -synuclein	26
1.5.3. Insulin.....	26
2. METHOD OVERVIEW	27
2.1. Protein purification	27
2.2. Protein aggregation studies	28
2.3. Kinetic data analysis	28
2.4. Protein inhibition studies	29
2.5. Autoxidation and separation of polyphenolic molecules	29
2.6. Atomic force microscopy	30
2.7. Fourier-transform infrared spectroscopy.....	31
3. RESULT OVERVIEW	32
3.1. Article 1.....	32
3.2. Article 2.....	33
3.3. Article 3.....	35
3.4. Article 4.....	36
3.5. Article 5.....	39
4. DISCUSSION.....	42
4.1. Autoxidation of polyphenols.....	42
4.1.1. Gallic acid autoxidation	42
4.1.2. Flavone autoxidation.....	42
4.1.3. Scavenging the inhibitor within the flavone autoxidation mixture	44

4.2. Insulin polymorphism	45
4.3. Altering the <i>in vitro</i> screening.....	45
CONCLUSIONS	47
SUMMARY IN LITHUANIAN LANGUAGE	49
REFERENCES/BIBLIOGRAFIJA	69
CURRICULUM VITAE	79
LIST OF PUBLICATIONS INCLUDED IN THE DISSERTATION.....	81
LIST OF PUBLICATIONS NOT INCLUDED IN THE DISSERTATION	83
LIST OF SCIENTIFIC EVENTS.....	86
COPIES OF PUBLICATIONS/PUBLIKACIJŲ KOPIJOS	88

ABSTRACT

Neurodegenerative disorders such as Alzheimer's and Parkinson's diseases are considered incurable, and they worsen the life quality significantly. As life expectancy continues to rise, the incidence of neurodegenerative diseases is projected to increase at an exponential rate. Protein accumulation into fibrillar aggregates that possess β -sheet-rich regions is commonly considered to be involved with the onset and progression of these disorders. The search for a cure for these neurological conditions has been ongoing for several decades. In turn, scientists have been developing approaches to target different processes, one of which is the inhibition of protein aggregation. However, this search led to many unsuccessful clinical trials with only a few drugs that slow the progression of the disease but also introduce significant side effects. This is why it is critical to continue the research and development of potential drugs, especially focusing on primary steps that may help avoid expensive investments during the course of the drug development. Improvement of *in vitro* screening procedures and pre-clinical trial analysis of potential medications can improve efficacy and speed up the development processes.

In this work, the main focus was on the molecules of polyphenolic nature and their potency to inhibit the protein aggregation process. As a number of these molecules failed clinical trials in this field of research (e.g. epigallocatechin-3-gallate, curcumin, resveratrol), a more thorough *in vitro* analysis was dedicated to their stability and impact on protein aggregation. The results displayed the instability of molecules at neutral or higher pH that covers the physiological conditions where the molecule is supposed to be active. Part of these tested molecules autoxidize, which involves a complex mechanism; however, this process is vital for the inhibitory effect on amyloid-beta ($A\beta_{42}$) and insulin aggregation. Interestingly, the most potent inhibitor (2'3'-dihydroxyflavone) on the fibrillation of $A\beta_{42}$, α -synuclein and insulin was found to autoxidize, forming different molecular compounds (small molecules and polymers), with only polymeric molecules being involved in the inhibitory mechanism.

The second part of this study was focused on improving the *in vitro* screening procedure. Typically, protein aggregation assay *in vitro* is performed using phosphate or tris buffered saline solutions or even buffers which were used at the final step of purification. While this methodology reduces the complexity of data assessment, the aggregation mechanism as well as the inhibitory effect could be different from the process in the brain. This is why, distinct medium mimicking cerebrospinal fluid (CSF) composition

was formulated that allowed to assess how major components of CSF affect A β ₄₂ aggregation inhibition using epigallocatechin-3-gallate and fluorinated benzenesulfonamide VR16-09. The results were completely different from those acquired when using PBS, affirming the importance of altered medium during *in vitro* drug screening experiments. Artificial cerebrospinal fluid (aCSF) could be a new medium used for screening anti-amyloid compounds. This mixture could replace currently popular PBS or TBS formulations and lower the difference between *in vitro* and *in vivo* assay.

Aim

To examine the role of polyphenolic compounds in regulating protein amyloid aggregation process.

Objectives

1. To characterize the inhibitory effect of gallic acid and its oxidized products on the insulin aggregation process.
2. To determine the link between the autoxidation process of hydroxy-flavones and their inhibitory potential for A β ₄₂ and insulin aggregation.
3. To examine the autoxidation products of 2'3'-dihydroxyflavone and distinguish particles involved in inhibiting A β ₄₂ and α -synuclein aggregation.
4. To compare how cerebrospinal fluid components and artificially created medium affect the inhibition of A β ₄₂ by oxidized epigallocatechin-3-gallate and fluorinated benzenesulfonamide VR16-09.

Scientific novelty

This study shows that the link between polyphenolic compounds and their anti-amyloid characteristics is due to their chemical properties change upon autoxidation. This process happens at neutral or higher pH resulting in shifted inhibitory mechanism that can lead to wrong data interpretation. The experiments of this work given the opportunity to analyse anti-aggregation characteristics of polyphenols before the autoxidation process and when it is complete. This analysis allowed to understand why the inhibitory effect is not visible under certain reaction conditions. This process helped to prove that

gallic acid does not possess anti-amyloid characteristics, while its oxidized form does. Analysis of protein aggregation inhibition with gallic acid led to finding a new insulin aggregate conformation that is dependent on the peptide concentration.

The autoxidation process of flavones is very complex and is not thoroughly analysed. There are plenty of molecules that form during this process, however, there was no direct link between the polymers formed in the resulting mixture and the inhibitory features of polyphenols. Therefore, the conversion of polyphenolic molecules and their anti-amyloid characteristics were further analysed and discussed within this work. Furthermore, the investigation into the inhibitory properties of molecules at distinct reaction conditions led to figuring out that the commonly used medium during *in vitro* screening assay may lead to wrong data interpretation. This allowed us to formulate a distinct artificial cerebrospinal fluid medium that could minimize the bridge between the *in vitro* and *in vivo* experiments.

Defending statements

1. The autoxidation of polyphenolic compounds is a critical factor that enables their potential to inhibit protein amyloid formation.
2. Autoxidation of flavones leads to the formation of polymeric molecules that are primary contributors to their inhibitory activity against A β ₄₂ and aSyn fibrillation.
3. Components of cerebrospinal fluid alter the inhibitory potential of anti-amyloid compounds.

1. LITERATURE OVERVIEW

1.1. Neurodegenerative diseases

The terms “neurodegeneration” or “neurodegenerative” are thought to be universally understood. However, there is no singular accurate definition that may fit into a sentence but rather into a paragraph covering many processes that may or may not be linked together. This word is a combination of “neuro”, meaning the nerve cells or neurons and “degeneration”, which specifies the loss of function or structure in the cells or “to become degenerate”. Accordingly, to these definitions, neurodegeneration could mean the primary loss of function in the nerve cells. However, in reality, it covers many different mechanisms related to a number of distinct neurological diseases that are located in different regions of the spinal cord or brain and possess particular pathological hallmarks [1]. The list of different common neurodegenerative disorders and their pathologies is summarized in Table 1.

Table 1. Common neurodegenerative disorders and their neuropathology [2–4].

Neurological disorder	Type	Main neuropathology	Main anatomic vulnerability
Alzheimer’s disease	Sporadic	Senile plaques, Neuronal Tau inclusions, amyloid angiopathy	Basal forebrain, frontal/temporal lobes, limbic structures.
Parkinson’s disease	Sporadic, familial	Neuronal inclusions of α -synuclein (Lewy bodies)	Hippocampus, Substantia nigra, cerebellum
Prion diseases: Creutzfeldt-Jakob disease, fatal insomnia and others	Sporadic, familial, iatrogenic, infectious	Spongiform changes, prion protein accumulation and plaques	Cerebral cortex, Cerebellum
Amyotrophic lateral sclerosis	Sporadic, familial	TDP-43 immunoreactive neuronal cytoplasmic inclusions	Motor cortex, brainstem and spinal cord motor neurons

1.1.1. History of neurodegenerative diseases

The concept of neurodegenerative diseases has gone through many centuries and had multiple names indicating symptoms or societal beliefs of

that time. A common proposed aetiology ranged from being the supernatural (e.g. caused by gods, demons or even ghosts), caused by reproductive organs (e.g. the displaced uterus interference with functions of other organs), traumatic experiences and cognitive biases towards bodily symptoms [5]. However, as early as 2000 B.C. Egyptians described memory declines in older people as a common expression. Later on, Pythagoras referred to old age as when the mind declines to a level of a baby. Similar observations were also recorded by Hippocrates, Plato, and Marcus Tullius Cicero, continuing to the modern era, where presumably William Shakespeare portrayed symptoms of some type of dementia [6].

The first mention of degeneration was by George Gulliver in 1843 [7]. Later, in 1894, Charles Fere developed the term neurological disorder and talked about observing biological phenomena and pathological heredity [8]. After some time, the hypothesis on degeneration was further developed by Francis Galton, who proposed that good and bad temper or even intelligence were transmitted in families and that there could be an “improvement of humanity through selective breeding” [9]. Interesting to note, before the second world war in 1933, the Nazi government accepted a law that enforced sterilization to prevent such “hereditary diseases” [8].

The first mention of the word “neurodegenerative” was in 1965 by J.F. Bray, much later than the first record of Parkinson’s (1817 by James Parkinson in an essay “An Essay on the Shaking Palsy”) [10] and Alzheimer’s (1906 by Alois Alzheimer describing “arteriosclerotic brain atrophy”) [11] diseases (PD and AD). One of the more profound and interesting cases was the first prion disease called Kuru, reported by Gajdusek and Vincent Zigas in 1957. The disease was described as transmissible and even caused by slow unconventional viruses. Following that, scientists discovered that the disease was spread through the cannibalism of the dead by eating contaminated human tissue [12].

1.1.2. Alzheimer’s disease

Alzheimer’s disease is currently the most prevalent type of dementia that can be described as a progressive neurodegenerative disease. AD worsens the life quality and causes memory loss, insomnia, poor judgement, lost track of dates, difficulty completing daily life tasks and more [13]. The pathological hallmark of this disease is characterized by the accumulation of senile plaques (also known as dendritic, neuritic or amyloid plaques) and neurofibrillary tangles (NFTs) [14]. The amyloid plaques are composed of protein aggregates that are formed by the accumulation and aggregation of 40-42 amino acid

peptide called amyloid β ($A\beta$). This peptide derives from a large transmembrane amyloid precursor protein (APP) that is cleaved by enzymes called β - and γ -secretases [15]. In healthy individuals, during the normal protein lifecycle, APP is cleaved by α -secretase (the most dominating process) and then γ -secretase, resulting in soluble peptides that are further broken down and recycled in neurons (called non-amyloidogenic pathway) [16]. However, under disease conditions, APP is proteolytically processed by β - and γ -secretases, leading to a generation of $A\beta$ to extracellular space or APP is internalized into endosomes (acidic compartment), where the precursor protein is cleaved by the same proteases resulting in the generation of $A\beta$ [17]. In neurons, a large fraction of this peptide is degraded by endothelin-converting enzyme, while the rest of its fraction is degraded in the lysosome, recycled to the cell surface or via other known pathways such as matrix metalloproteinase-9, insulin-degrading enzyme and neprilysin. If $A\beta$ escapes the degradation processes, the formation of $A\beta$ oligomers and senile plaques in the extracellular space can occur due to an increasing concentration of the peptide [18]. It is thought that $A\beta$ oligomers may cause multiple harmful changes in the brain, such as disrupted Ca^{2+} homeostasis, plasticity dysfunction, aberrant Tau (microtubule associated protein) phosphorylation, oxidative stress, insulin resistance, inhibition of axonal transport and other critical processes [19]. In addition to that, $A\beta_{42}$ oligomers can interact with various cell surface receptors and enter the cell, causing endoplasmic-reticulum stress and mitochondrial-mediated activation of caspases. This abnormal event prompts the release of Tau and its aggregation into neurofibrillary tangles [20].

Increased production of $A\beta$ is thought to be the main trigger of AD. It is important to note that $A\beta$ peptide is generated into several isoforms. The most common are 40- and 42-amino acid long peptides ($A\beta_{40}$ and $A\beta_{42}$, respectively). While $A\beta_{40}$ is the most abundant of all the isoforms, it is less prone to aggregation than $A\beta_{42}$. It was noted that decreased concentration of both peptides and a ratio of $A\beta_{42}/40$ in CSF is an indicator that the peptide is accumulated into oligomeric and toxic species in the brain. This could be a beneficial biomarker to diagnose AD before the first symptoms [21,22].

1.1.3. Parkinson's disease

The second most common type of neurodegenerative disorders is Parkinson's disease. Most of PD cases are considered to be related to aging, with the typical symptoms being resting tremor, stiffness, slowness of movement, sleep disorders, depression and cognitive changes, however, each

individual may have a unique set of traits [23]. The pathological hallmark of PD is recognised to be the accumulation of abnormal protein deposits called Lewy bodies (LBs) and Lewy neuritis (LNs) [24]. The main component in these inclusions is aggregated α -synuclein (aSyn) [25]. While the exact function of aSyn is not entirely understood, the protein and its mutations are direct links to the onset of the disease [26]. In addition to the aSyn aggregation, the dysfunction of lysosomes, mitochondria, neuroinflammation and synaptic transport issues collectively cause the death of dopaminergic neurons in basal ganglia in the brain [27]. Even though it was thought that the loss of dopaminergic neurons is the direct cause of motor dysfunction, the researches show that spreading aggregation of aSyn affects central and peripheral nervous systems, thus resulting in the development of both motor and non-motor symptoms [28].

1.2. Therapy of neurodegenerative diseases

While neurodegenerative disorders are life-threatening diseases that are diagnosed with increasing numbers of new patients every year [29,30], disease-modifying drugs are extremely needed to treat these conditions. The search for potential drugs has led to many different trials, evaluating possible candidates and their therapy targets, including production, misfolding and aggregation of disease-related peptide/protein, neurotoxicity, inflammation and others [31,32]. However, despite an urgent need for medication and 143 agents being assessed in clinical trials for AD alone (2022) [33], the success rate in approving the medication is low, with many candidates unable to pass the second or third clinical phases [34–38].

1.2.1. Medications on AD

AD currently has six formulations that are FDA-approved [39]. Four are used for symptomatic treatment, while the last two are thought to provide disease-modifying effects (Table 2).

Table 2. Currently available drugs against AD (based on [39–41])

Name	Type	Treatment type
Donepezil	Cholinesterase inhibitor	Symptomatic
Galantamine	Cholinesterase inhibitor	Symptomatic
Rivastigmine	Cholinesterase inhibitor	Symptomatic

Memantine	N-methyl-D-aspartate (NMDA) receptor antagonist	Symptomatic
Aducanumab	Anti-amyloid antibody	Disease-modifying
Lecanemab	Anti-amyloid antibody	Disease-modifying

Cholinesterase inhibitors (Donepezil, Galantamine, Rivastigmine) and NMDA contribute to symptom management. Former reduces the breakdown of acetylcholin by inhibiting butylcholin- and acetylcholinesterase, this way prolonging signals between nerve cells. NMDA receptor antagonist (memantine), blocks the NMDA receptor by preventing the excessive influx of extracellular calcium that leads to cell rapture and death [39].

There is a substantial amount of controversy on the approval of aducanumab. The drug was approved in 2021 by the FDA, however, there are two issues with the medication pointed out after the accelerated admission. The drug (1) did not show enough evidence of efficacy in Phase III trials, and (2) there was a noticeable amount of reporting bias in the publications where aducanumab was reported [41].

Lecanemab was approved recently (6th of January, 2023). The medication showed a reduced amount of both soluble and insoluble A β in the brain. Unfortunately, with the positive anti-amyloid traits, Lecanemab has severe side effects such as brain swelling and bleeding [40].

1.2.2. Future medications on AD

Due to the lack of efficacy of the current disease-modifying medications, a vast number of attempts are made in order to create new formulations to slow or stop the progression of AD or even reverse effects that were developed during the onset of this disease [42]. The ongoing research and development for new medications include therapies targeting two main pathological aspects of AD – A β peptide and tau protein [43].

The therapy against A β pathology [16,39,42,44–50]:

- The production of A β may be explicitly targeted by inhibiting β - and γ -secretases that cleave APP-producing aggregation-prone particles.
- Anti-amyloid agents may inhibit A β aggregation. Ideally, such molecules would bind to A β , preventing the peptide from oligomerization and aggregation, resulting in neurotoxic effects to neurons.

- Active and passive immunotherapy that induces the production of antibodies specifically targeting A β particles. This includes vaccines or direct injection of monoclonal antibodies that bind to A β monomers, oligomers and/or aggregates.

The therapy against Tau pathology [39,42,45–48,50,51]:

- Tau protein aggregates after it undergoes abnormal phosphorylation. Inhibition of this process by targeting glycogen-synthase-kinase-3 β that has the prominent role in hyperphosphorylation of Tau (p-Tau) and should prevent Tau aggregation and its neurotoxicity.
- Molecules that stabilize and prevent tau aggregation.
- Stabilizing microtubules that are destabilized after the abnormal phosphorylation of tau could reduce the number of released hyperphosphorylated Tau.
- Active and passive immunotherapy against pathogenic forms of tau protein.

1.2.3. Polyphenols as anti-amyloid compounds

Natural compounds were always thought to have the upper hand in providing health benefits and potentially curing diseases [52–54]. One of such categories is a group of polyphenolic compounds (Figure 1). They are abundant in nature and found in various fruits, vegetables, spices, herbs, and drinks. They also are shown to have anti-amyloid characteristics by being able to inhibit various protein aggregation processes [55]. Out of all polyphenols, the most known is epigallocatechin-3-gallate (EGCG) that is found in various teas. This catechin inhibits A β , aSyn and other protein aggregation and is also thought to disaggregate already formed amyloid fibrils [56–59]. In addition, gallic acid (GA), which is the direct product of EGCG hydrolysis, is also known to possess similar characteristics [60–62]. However, despite the remarkably well results of *in vitro* studies with EGCG, the polyphenol did not pass clinical trials [63,64]. Other polyphenols that entered clinical trials were curcumin, luteolin, quercetin and resveratrol [63].

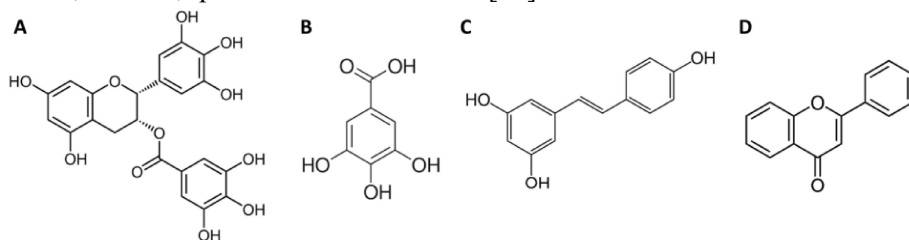


Figure 1. Structures of several polyphenolic compounds. A – epigallocatechin-3-gallate, B – gallic acid, C – resveratrol, D – flavone.

It was shown that EGCG undergoes autoxidation at neutral or higher pH. Šneideris et al. have shown that EGCG does not possess anti-amyloid properties against insulin aggregation at low pH (where the polyphenol is stable), but if the molecule is incubated at physiological pH (7.4), the resulting mixture acquires a strong inhibitory effect [56]. While these chemical modifications happen during *in vitro* assay, there are no exact studies showing whether these essential modifications occur *in vivo* (in humans). This means that there is no guarantee that the medication will work and it may be why clinical trials for polyphenols have failed.

1.3. Protein aggregation

The aggregation process of peptides and proteins in neurodegenerative diseases is complex. Each protein differs by the polypeptide sequence, size, and conformation. This should lead to distinct aggregation mechanisms for each type of molecule. However, the main differences between these processes are related to the initial structure or conformation (intrinsically disordered, globular/functional peptides/proteins), while a further process is comparative and can be simplified to describe overall aggregation process [65], because the resulting form of aggregates exhibit similar structural motifs of highly dense β -structures [66].

1.3.1. Protein aggregation mechanism

The association of peptides or proteins into fibrillar aggregates follows a distinct process that can be described by several main steps (Figure 2). Besides amyloidogenic intrinsically disordered peptide/protein, in the initial phase, molecules transition from the native to the aggregation-prone conformation. This step includes molecule modifications (e.g. phosphorylation of tau protein) [20], proteolytic cleavage (e.g. processing of APP) [17], conformational changes (e.g. dissociation of transthyretin tetramers) [67,68], structure conformation changes due to environment or mutations (e.g. prion protein) [69,70] and other transitions that are found in different diseases [66]. This step may be reversible depending on the peptide/protein [65].

The second step of the mechanism involves the accumulation of aggregation-prone particles into the aggregation nucleus. This process is commonly known as nucleation and is regarded as the aggregation limiting

step. During this course, aggregation-prone molecules (further referred to as monomers) interact with each other and undergo structural changes forming hydrophobic regions that possess cross-molecular β -sheets. With the number of monomers accumulated, the nucleus becomes stable; hence the term nucleus is considered to be the smallest form of aggregate for which the inclusion of monomers is more likely to happen than the loss of monomers [71]. The number of monomers in the nucleus may vary based on the protein/peptide that aggregates; however, can start from one to multiple monomers [72,73]. It is essential to mention that the accumulation of monomers may lead to a secondary pathway that concludes with amorphous aggregates.

The nucleation process is limited by the number of molecule interactions and the reaction time that is needed to form nuclei. The aggregation assay *in vitro* can be altered by various factors affecting the aforementioned processes to speed up the aggregation. Interactions between molecules can be increased by increasing diffusion (e.g. increased temperature), the concentration of monomers in the sample and affecting mechanically (e.g. agitation) [66]. At the same time, reaction speed is controlled by the energy of molecules in the sample (e.g. controlled by the temperature), the concentration of electrolytes (e.g. electrolytes cover the surface of peptide/protein) and has a direct correlation with ligand concentration (e.g. heparin induces tau aggregation) [74].

Once the nucleus is formed, the further aggregation step is called elongation, which also has a reverse counter-process – dissociation. During this reversible reaction, the nucleus binds monomers while converting them into identical conformation. This way, the nucleus linearly grows into fibrils, meaning that the fibril attaches monomers only at the fibril ends. There may be exceptions to this process if mutations or co-aggregation are viable [66,74,75].

Besides the primary aggregation mechanism, the secondary processes can happen during the elongation phase that involves fibril fragmentation and surface-catalyzed nucleation. Fragmentation covers the step where the fibril breaks into shorter fragments, increasing the number of fibrils ends. Surface-catalyzed nucleation (referred to as secondary nucleation), happens at the surface of fibrils and initiates the formation of toxic nuclei/oligomers during the progression of dementia or other protein aggregation related diseases [66,76].

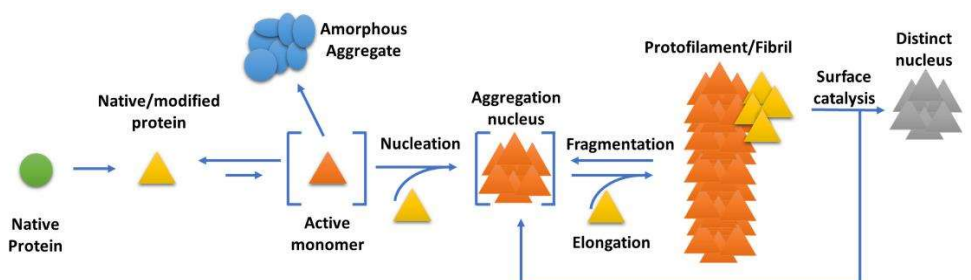


Figure 2. Simplified protein or peptide aggregation mechanism.

1.3.2. Protein aggregation polymorphism

Aggregation of a peptide/protein with an identical amino acid sequence may lead to the formation of different fibrils types due to a distinct β -structure conformation in the final aggregate form [77]. The polymorphism may occur in the presence of different environmental factors or even under identical reaction conditions [78]. Typically, the formation of a specific conformation is linked with the nucleation process, which is followed by a much faster process of elongation. Elongation is recognised to be a templating process during which the monomer inherits the same secondary structure as the fibril. However, there is probability for the formation of two or more distinct nuclei that leads to heterogenous mixture of fibrils [79].

Most fibrils have the ability to template its structure via elongation if the monomer is present in the reaction mixture. However, at very low fibril concentrations and with reduced elongation due to the reaction environment, surface-catalysed nucleation will not mirror the pattern of the fibril, instead leading to the formation of a unique secondary structure fibrils. This means that secondary nucleation is not the templating process, but rather a catalysis process that may influence the formation of distinct fibril conformations [80,81].

1.3.3. Inhibition mechanism

The protein aggregation mechanism is very important when searching for anti-amyloid drugs that may change the aggregation pathway. These are the primary questions that typically arise when assessing the inhibitor: (1) what does the inhibitor target, (2) what is the mechanism of inhibition, and (3) how does the inhibitor affect the toxicity to cells exerted by aggregates? A part of these former questions can be answered using aggregation kinetics data from a range of monomer/inhibitor concentrations. The inhibitor can interact with monomer (e.g. stabilize the monomer), oligomer (e.g. stabilize oligomer),

nucleus (e.g. limit elongation, surface catalysis) and fibril (e.g. limit elongation, surface catalysis and fragmentation) [71,82]. If a monomer or oligomer is the target, then primarily the nucleation process might be affected, resulting in an increased nucleation time. The opposite effect is seen when the inhibitor interacts with nuclei or fibrils. Then, the elongation, secondary nucleation and fragmentation processes are altered, which can only be understood by applying a mathematical fit [82].

1.4. Protein aggregation *in vitro*

1.4.1. Aggregation monitoring

Protein fibrillation is distinct based on various factors, but also brings up information that can help to understand the speed of aggregation, its mechanism and how the inhibitor affects the fibrillation process [71,83]. Initially, monitoring the aggregation by looking at the reaction with the naked eye is very complicated. This is why spectroscopic techniques were adapted in order to track the aggregation process [84]. The most basic approach is to measure the light scattering due to the formation of insoluble particles (fibrils) through the course of the reaction. The scattering is typically measured at distinct absorbance wavelengths [85]. This means that the more aggregates are in the sample, the higher the scattering value should be, yet this method has limitations [84,86,87]:

- Saturation of the detector - reaching maximum trusted value rendering the detection inaccurate.
- Heterogeneity in scattering – other components that precipitate may disrupt the values of scattering.
- The absorbance of molecules at the detection wavelength – during an inhibition assay, an inhibitor may absorb waves, limiting the signal and disrupting real-time aggregation studies.
- Very low signal – fibrils may scatter the light less due to their physical appearance and concentration, leading to low detection levels.

The second option is to use an amyloidophilic dye molecule that possesses an increased fluorescence intensity in the presence of fibrils. Molecules such as thioflavin-t (ThT), dapoxy, Congo red, ANS (anilinonaphtalene-8-sulfonic acid) [88–90] and commercial dyes, such as Amytracker, Amylo-Glo, IRI-1 [91–93] are known to be in use for amyloid staining. Nonetheless, fluorescent markers also have flaws [84,94,95]:

- The dye may interfere with the fibrillation process, slowing down or accelerating the process and changing the interpretation of data. The dye could change the aggregation mechanism, which would be an even worse scenario for the aggregation study.
- The absorbance of molecules at the excitation or emission wavelength of the dye molecule – tested molecules (potential inhibitors) may absorb the excitation or emission wavelength, quenching the fluorescence intensity and leading to false data interpretation.
- Molecular competition – the inhibitor may possess similar affinity to the fibrils as the dye molecule, competing for the binding sites with the dye and reducing the fluorescence intensity.
- Molecular affinity – inhibitor could react with the dye molecule. This way, lower amounts of inhibitor would affect the aggregation process, additionally changing fluorescence intensity due to the reduced amount of dye molecules available to bind to the aggregates.

Despite the drawbacks mentioned above, fluorescence measurements using a dye molecule are one of the most common tool for monitoring the aggregation process *in vitro* [84,96]. Nonetheless, more advanced strategies could be used. Time dependant secondary structure measurement using Fourier-transform infrared spectroscopy (FTIR) or circular dichroism could be applied [97,98]. In addition, high-speed atomic force microscopy (AFM) may bring the morphology data together with tracking the fibrillation process [99]. Besides these methods, dynamic light scattering [100], microfluidics [101], liquid cell electron microscopy [102], fluorescent labelling [103], quantum-dot nanoprobe [104] and other techniques are applied for probing the protein assembly, however, instrumentation and need for expert knowledge makes these approaches less attractive.

1.4.2. Protein aggregation kinetics

Protein aggregation kinetics *in vitro* are typically followed in a sigmoidal trend that is described by three steps - lag, exponential and plateau phases (Figure 3). Nucleation occurs during the lag phase and is the main limiting step of this process. Elongation, fragmentation and surface catalysis is considered to happen simultaneously during the exponential phase that is concluded by the plateau when the ratio between monomers/oligomers and fibrils becomes constant [71,72,74,105].

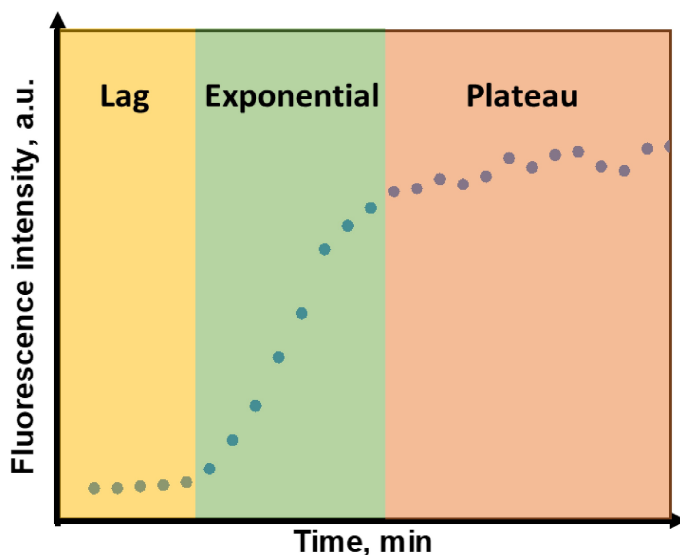


Figure 3. Protein aggregation kinetics curve indicating three aggregation phases.

During seeded aggregation experiments, addition of fibrils alters the aforementioned pathway by removing the lag phase from the process. Added fibrils act as nuclei that initiate the elongation of fibrils resulting in immediate exponential phase. This way the final fibril conformation is related to the seed, not the environment where the aggregation did occur [79].

1.4.3. Fibril morphology and secondary structure

A valid morphological and secondary structure assessment of the fibrils formed helps to explain the effect of the environment, inhibitor or other parameters that had an impact on the fibril formation process [106,107].

For fibril morphology analysis, AFM and electron microscopy (transmission -TEM, scanning - SEM and transmission cryogenic - cryo-EM) can be used [108,109]. Besides stationary scanning, AFM is applicable to measure the fibril assembly in real-time [99]. These scanning techniques are used to confirm the formation of fibrils. Images can be used to identify differences between fibril morphology as well as their structure (e.g. using detailed analysis from data gathered with cryo-EM) [110]. Fibrils may differ by height, length and width distribution, fibril twist periodicity, clustering and thinning/splitting [111]. This, in fact, may provide valuable information on the assembly pathway, count of the filaments in the fibril, maximum length of

the fibril, influence of the inhibitor on the fibril formation process and more characteristics [72]. Furthermore, fibril morphology assessment helps to understand the polymorphism of the fibrils within the same sample, which can help to explain the secondary structure and kinetic differences [112].

Theoretically, each fibril may have a specific intermolecular structure with beta-structures in the core. This means that the same protein can obtain diverse fibril structures. Structural differences may lead to distinct toxicity to cells, morphology, and seeding propensity (aggregate's ability to replicate). In fact, these differences may appear due to a different aggregation mechanism influenced by the reaction environment [113,114]. This is why assessing the secondary structure and understanding these changes is necessary. The analysis uses conventional methods such as Fourier transform infrared (FTIR) spectroscopy, nuclear magnetic resonance, Raman spectroscopy and circular dichroism [115–119]. The data collected using these approaches differ but may complement conclusions drawn using other methods [120].

1.5. Proteins used in this thesis

1.5.1. Amyloid- β

A β aggregation in humans is known to be the initiator of Alzheimer's disease. 40 – 42 amino acid peptide derives from amyloid precursor protein and aggregates in the interstitial fluid [121]. A β can accumulate into multiple assemblies that include oligomers, protofibrils and fibrils. This intrinsically disordered peptide can form amyloid aggregates with “cross β ” structures that can be parallel or anti-parallel, suggesting the existence of various conformations (so called strains) [122]. The most common forms of A β peptide that is used during *in vitro* studies contains 40 or 42 amino acids. A β ₄₀ is more stable than its isoform (A β ₄₂) and aggregates slower but it is also used in various drug screening and fibrilization experiments [49,123,124].

There are two main sources for production of the A β peptide isoforms: synthetic and recombinant. Synthetic source seems to be a more convenient approach (the main source to purchase), however its preparation for the aggregation experiments includes using high pH solutions (1% NH₄OH [125], 10 mM NaOH [126]) or organic solvents (1,1,1,3,3,3-hexafluoro-2-propanol [125]) for the pre-treatment in order to dissolve any possible oligomers [127]. The recombinant synthesis and purification involve a few steps of chromatographic procedures as well as treatment with high concentration of denaturant before the size-exclusion chromatography. This method yields to a high reproducible data without the possibility of leaving detergents attached

to the protein [128,129]. Recombinant A β ₄₂ is known to aggregate rapidly at 37°C forming fibrils within an hour even at very low peptide concentrations [76].

1.5.2. α -synuclein

aSyn is identified as the most abundant protein in the pathology of Parkinson's disease. It forms variety of distinct aggregate forms due to the environment factors or different mutations in its gene SNCA. These aggregates are found in various morphological and secondary structure conformations that possess distinct toxic effect to cells [130]. *In vitro*, aSyn aggregates much slower than the A β , thus for a higher protein concentration and often agitation is used for its assay. It has been reported that aSyn is capable of forming various fibril conformations under the same reaction conditions, especially at lower concentration (50 – 100 μ M) and at lower buffer ionic strength [131].

1.5.3. Insulin

Insulin is a natural hormone that plays a significant role in the regulation of sugars and fats. It contains three alpha-helix regions and is made of two peptide chains that are connected via disulphide bonds [132]. Due to its high availability and relatively low cost, insulin is one of the most well-studied proteins in biology and has been used as a model in various scientific disciplines, including protein aggregation studies [133–135]. It is also used to study mechanisms of protein aggregation as well as to develop new approaches to treat or prevent related diseases to its aggregation in humans [56,96,136,137]. For instance, this protein has been used to explore the role of different factors in aggregation, such as temperature, pH and other solvent conditions [114].

Besides many different conditions used to study insulin aggregation, the most well-known is insulin fibrillation at low pH [114]. The high robustness of kinetic experiments under these acidic reaction conditions allows to simplify the search for inhibitory molecules against protein aggregation [71]. One option for inhibiting insulin aggregation is using small molecules, such as short peptides, chemically synthesised compounds and even antioxidants, that can interact with insulin and prevent its aggregation [120,138]. In addition, this protein can be used to study the inhibitory effect of molecules that are not stable in neutral or physiological conditions [56]. For example, if the molecule autoxidizes or breaks down into different structures in an

environment with a high concentration of hydroxyl ions, it is possible to prevent further conversion by using low pH conditions [139]. This way, it is probable to understand the effect of initial, intermediate, and final products on aggregation. The information gathered can be used to build new, stable molecules that may be involved in the inhibitory process of insulin and modulators in neurodegenerative diseases [140].

2. METHOD OVERVIEW

2.1. Protein purification

Due to the relatively high price of commercially available peptides/proteins and need for high reproducibility between different batches, the biosynthesis and purification of recombinant peptides/proteins is considered to be the best option when working with protein aggregation and their inhibition studies. In the experiments described in this thesis, A β ₄₂ and aSyn were expressed in BL21-star cells using expression vectors as described previously [141].

A β ₄₂ was purified using ion-exchange and size-exclusion chromatography (SEC) methods. The essential part for robust experimental procedure was to avoid peptide aggregation during the purification process and separate any potential oligomeric forms from monomer before kinetic studies. This is why SEC was repeated twice, requiring the lyophilized peptide powder to be dissolved in a high denaturant concentration (5 M of GuSCN) before injecting it into the column. Second SEC was used to gather the peptide, quickly dilute it with a reaction mixture (within 30 minutes) and start the kinetic experiment to reduce the possibility of peptide aggregation during the sample preparation stage.

aSyn is thermostable, thus, it was initially purified using a high-temperature water bath (80 degrees Celsius) to denature a large fraction of proteins. Later, the protein was precipitated using 42% of saturated ammonium sulphate concentration. This was done to reduce the number of nucleic acids in the sample. Then, ion exchange and size exclusion chromatography were performed. The protein was lyophilized after dialyzing it in the volatile ammonium bicarbonate buffer solution. Before the kinetic experiments, the aSyn powder was dissolved in the reaction buffer.

2.2. Protein aggregation studies

Protein aggregation was monitored using fluorescent dye thioflavin-T (ThT) assay. ThT has a distinct absorbance maximum ($\lambda = 412$ nm), but when it binds to fibrillar aggregates, its absorbance maximum redshifts to 440 nm - 450 nm range. In addition, by binding to fibrillar aggregates, ThT has a high increase in the fluorescence intensity ($\lambda = 480$ nm – 490 nm) due to increased quantum yield of stabilized ThT molecule on the surface of the fibril [84]. This allowed for monitoring the formation and growth of amyloid fibrils over time.

The protein aggregation studies were done separately based on the protein/peptide that was used. Insulin aggregation was performed under acidic pH (in 20% acetic acid) at 60 °C, where the protein tends to accumulate into fibrillar aggregates quickly, with high data reproducibility. A β_{42} , on the other hand, was aggregated at near-physiological conditions – under 20 mM sodium phosphate (pH 7.0), PBS and in a medium mimicking the basic composition of cerebrospinal fluid. The last protein covered in the thesis is aSyn. This protein aggregated slower than insulin and A β_{42} under the selected conditions. That is why agitation and glass beads were used to accelerate the fibril formation process.

The aggregation reactions for all proteins used in this thesis were done in a microplate reader using low protein binding 96-well plates.

2.3. Kinetic data analysis

Kinetic data analysis is an important procedure that helps to understand the protein aggregation process in more depth. In this thesis, the data were analysed using Origin software, where the Boltzmann equation function was used to fit kinetic curves determining aggregation half-time values [142]. This parameter allowed to compare how effectively inhibitors affect the aggregation process.

Further analysis of aggregation was done by applying a global fit (Figure 4). This mathematical procedure allows to acquire more details about the mechanism of aggregation. For this to happen, it is necessary to collect aggregation data of different protein concentrations and apply appropriate model steps. The resulting fit provides constants for primary nucleation, elongation, fragmentation, and secondary nucleation. However, it is not possible to draw conclusions only from these constants. Each step (primary and secondary nucleation, fragmentation) generates fibril ends that affect the speed of elongation, thus the multiplication of each constant with elongation

is needed in order to compare the processes between different aggregation mechanisms. In the end, important information about the aggregation mechanism is in the form of combined rate constants (primary nucleation – elongation, elongation – secondary nucleation and elongation – fragmentation) that allow to compare primary and secondary nucleation, and fragmentation speed of different aggregation mechanisms [71,136].

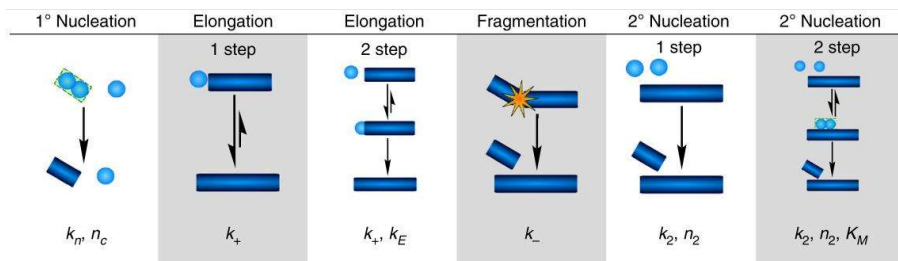


Figure 4. Global fit modelling steps of protein aggregation and their constants (adapted from [71]).

2.4. Protein inhibition studies

The inhibition of protein aggregation can be evaluated by several factors, such as determining the kinetic parameters of protein aggregation with and without the inhibitor, secondary structure and morphology differences of fibrils formed after these studies. However, it is also essential to determine the stability of an inhibitory molecule to avoid secondary processes that may disrupt monitoring the kinetic or structural information. In this work, different inhibitory molecules, including gallic acid, multiple hydroxy-flavones and fluorinated benzenesulfonamide (VR16-09), were used to understand their impact on the protein aggregation process.

2.5. Autoxidation and separation of polyphenolic molecules

The polyphenolic molecules that were used in this work exhibited the potential to autoxidize in neutral and basic pH. Besides EGCG that is known to autoxidize [56], there are plenty of other polyphenolic molecules that may undergo similar pathway of autoxidation that alters their initial chemical structure [139]. To determine which polyphenolic molecules can autoxidize, the process was monitored by measuring absorbance spectra in time and assessing their spectral changes.

The result of autoxidation may be a single molecule or a mixture of components of various chemical structures [143,144]. To identify this

instance, high-performance liquid chromatography was used, which allowed for determining the composition of molecules present in the autoxidation mixture. During this work, large molecules were isolated by concentrating the sample using membrane concentrators (3 kDa cut-off).

2.6. Atomic force microscopy

AFM is an imaging technique that is employed to visualize protein aggregates [145]. This method is known for its high-resolution scale that allows for determining different characteristics of fibrillar aggregates and other structures found on mica (Figure 5). AFM uses a probe (cantilever) to interact with the surface of the protein physically and closely measure the morphology of the fibrillar aggregates [146]. The initial characteristics such as height, width, length and especially fibril twist periodicity can be used to distinguish different types of molecules within the same or different samples. AFM is a great tool to measure the effect of the inhibitor on the formed fibrils. In fact, it grants options for studying single molecules in the same sample, which helps to determine the sample polydispersity and polymorphism [99].

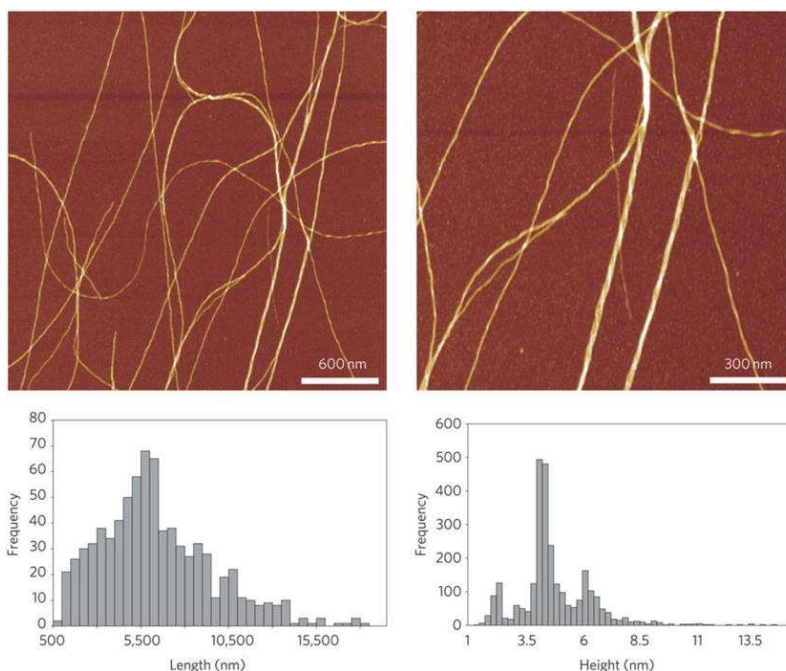


Figure 5. AFM image of different β -lactoglobulin fibrils, their lengths and heights frequencies (adapted from [72]).

2.7. Fourier-transform infrared spectroscopy

FTIR spectroscopy is a powerful tool for the analysis of protein structure. This method measures the absorption of infrared light by a sample and provides information on its molecular structure, including the types and arrangement of bonds in the polypeptide. Protein secondary structure elements are assessed by detecting characteristic vibrational modes by analysing the amide bands. The most common and well-studied band is Amide I/II, which absorption spectrum ranges approximately from 1600 cm^{-1} to 1700 cm^{-1} [147]. In this region, the spectrum provides information about the configuration of hydrogen bonds that reflect the protein secondary structure motifs, such as parallel and anti-parallel beta-sheets, alpha-helices, and unstructured peptide regions. However, FTIR spectroscopy does not allow distinguishing single molecule structures but rather provides structural information of the average molecule in the sample [147,148]. This allows to compare structural similarities and differences in fibrils between separate samples.

3. RESULT OVERVIEW

3.1. Article 1

Gallic Acid Oxidation Products Alter the Formation Pathway of Insulin Amyloid Fibrils

Aim of this study – to determine the inhibitory effect of gallic acid and its oxidation mixture on the insulin aggregation process.

Methods – due to the potential autoxidation of gallic acid (GA) at neutral or higher pH, the compound was dissolved in sodium phosphate (pH 7.4) and incubated till the oxidation process was over (termed as oxidized gallic acid (GAO)). Then insulin aggregation was performed under a range of protein concentrations (0.2 to 1.0 mM) with and without GA or GAO at acidic pH. Global fit of this dataset allowed to understand the effect of these inhibitors on the insulin aggregation microscopic processes (primary and secondary nucleation, and fragmentation). The final samples were collected and further analysed using FTIR and AFM.

Results - Initial experiments were done with gallic acid and its autoxidized form (GAO) that provided valuable data and showed that incubating gallic acid at neutral pH for an extended period of time changes the colour of the sample and inhibitory properties against insulin. GA had no significant impact on the half-time, nor to mechanism of insulin aggregation. The inhibitory effect was seen with GAO, that increased half-time at all added concentrations. The combined rate constant of primary nucleation-elongation and elongation-fragmentation directly correlated with the amount of GAO in the reaction mixture. However, the combined elongation-secondary nucleation constant had undergone minimal changes by both inhibitors.

The addition of GAO altered the aggregation pathway of insulin fibrils. This was particularly visible with increased ThT fluorescence intensity of fibrillation kinetic curves and from the structural assessment of fibrils' FTIR spectra. The shift of the insulin aggregation pathway when it was aggregated in an acetic acid solution was in a concentration-dependent manner. AFM and FTIR revealed that GAO prevented the formation of low-concentration fibrils (LCF) and instead turns the aggregation pathway to the formation of high-concentration fibrils (HCF) (See section 3.2).

Conclusions – Gallic acid does not possess an inhibitory effect against insulin aggregation at low pH. However, if gallic acid is pre-oxidized, it affects the primary nucleation and fragmentation of the insulin aggregation

process while possessing no impact on the fibril secondary nucleation, resulting in the formation of a single fibril type (Figure 6).

3.2. Article 2

Concentration-Dependent Polymorphism of Insulin Amyloid Fibrils

Aim of this study – to understand the concentration-dependant polymorphism of insulin at acidic reaction conditions.

Methods – recombinant human insulin was aggregated in 20% acetic acid in range of concentrations from 0.2 mM to 1.0 mM. In order to test strain self-replication, homogenized fibrils (termed as seed) were added to the reaction mixture (from 5% to 10^{-6} % of monomer mass). Fibril morphology and secondary structure analysis of final samples was done using AFM and FTIR.

Results – At 200 - 400 μ M concentration, insulin forms fibrils that possess low ThT fluorescence intensity, while at 800 – 1000 μ M – the ThT fluorescence intensity is much higher (~10 fold). Two distinct fibril species were termed as low-concentration and high-concentration fibrils. These fibrils were able to propagate their conformation when at least 1% of seed was added.

LCF forms smaller, more dispersed fibrils than HCF. Their secondary structure was able to self-replicate when high amounts of preformed fibrils were added to the reaction mixture. However, at small seed concentrations, fibrils did not replicate sufficiently, resulting in FTIR spectra that is similar to the unseeded fibrils conformation at that reaction environment.

Conclusions – Two distinct insulin fibril conformations LCF and HCF are capable of templating their structure via elongation (when higher amount of seed is added). This process does not happen at lower seed concentration leading to formation of environment-dependent aggregates (Figure 6).

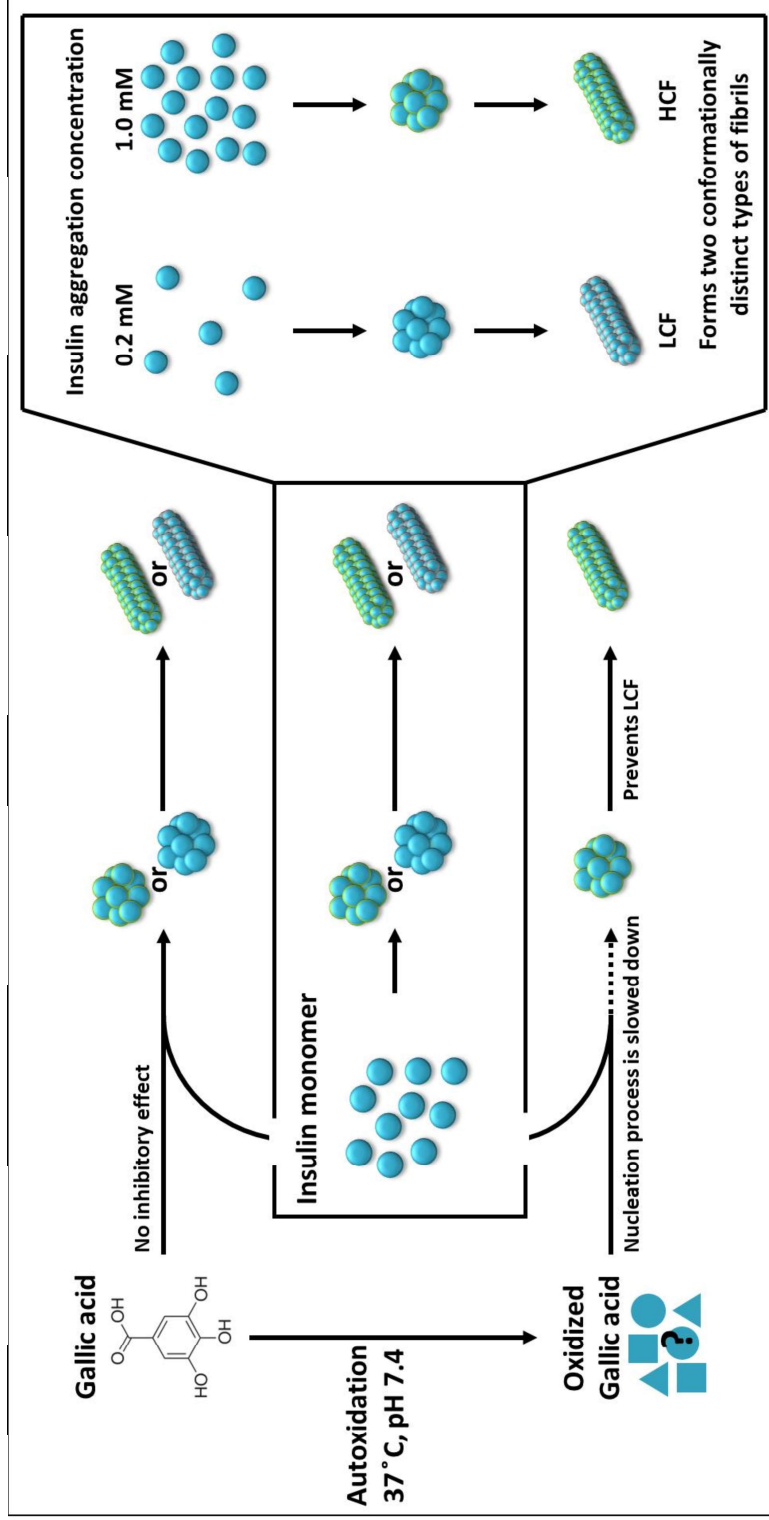


Figure 6. Brief representation of articles 1 and 2.

3.3. Article 3

Autoxidation Enhances Anti-Amyloid Potential of Flavone Derivatives

Aim of this study – to examine the autoxidation pattern of mono- and polyhydroxylated flavones and determine their effect on the fibrillation process of amyloid-beta and insulin.

Methods – to examine the autoxidation pattern of flavones, 64 hydroxylated flavones were incubated at 37°C in 100 mM sodium phosphate buffer containing 10% DMSO (pH 8). The time-dependent UV-vis spectra changes were monitored to inspect any absorbance transitions within an incubation period of 100 hours. All incubated flavones were then used in insulin and A β ₄₂ aggregation experiments, while non-incubated flavones were only applied to insulin aggregation at low pH. Then, aggregated samples with the most potent inhibitors were taken for AFM and FTIR analysis.

Results - the incubation of flavones at pH 8 allowed to categorize the autoxidized flavones into two parts: (1) those that contain neighbouring hydroxyl groups and (2) flavonols (3-hydroxyflavone) derivatives without neighbouring hydroxyl groups with some exceptions such as most of 3,6-dihydroxyflavone, 6,7-dihydroxyflavone and 2',4'-dihydroxyflavone derivatives.

Insulin aggregation can be monitored at low pH where flavones are stable, the A β ₄₂ aggregation process was performed with only incubated flavones due to their potency to autoxidize in the reaction conditions. One out of 64 tested non-incubated flavones did show an inhibitory effect towards insulin aggregation, while after incubation, this number was 23. All these cases showed a relationship with the flavone autoxidation process, meaning that the autoxidation process impacted the inhibitory potential of flavone derivatives. However, flavonols did not have any effect to insulin aggregation process if they lack neighbouring hydroxyl groups. In case of A β ₄₂, a similar result was seen, linking the inhibitory effect with the autoxidation process. Nevertheless, the number of inhibitors was lower, with only 13 autoxidised flavones that slowed the halftime of the A β ₄₂ aggregation process.

AFM images revealed that the most potent inhibitors initiate the formation of fibril clumps with round oligomeric structures attached to them. The height distribution of structures found on the mica indicated that both oligomeric structures and fibrils are higher than the fibrils observed in the control sample.

FTIR data suggests possible difference between secondary structure of A β ₄₂ aggregates formed with and without oxidized 2',3'-dihydroxyflavone.

Conclusions – the autoxidation of flavones is the major factor that enables their potential to inhibit insulin and A β ₄₂ aggregation. The most potent inhibitor was oxidized 2',3'-dihydroxyflavone, which slowed fibrillation processes of each tested protein at least two-fold. AFM data showed that oxidated flavones were bound to the surface of A β ₄₂ oligomers and fibrils (Figure 7).

3.4. Article 4

Exploring the Formation of Polymers with Anti-Amyloid Properties within the 2',3'-Dihydroxyflavone Autoxidation Process

Aim of this study – to study the autoxidation process of 2',3'-dihydroxyflavone and to understand what particles within the sample interfere with the protein aggregation process.

Methods – previously established 2',3'-dihydroxyflavone autoxidation mixture was considered to be the most potent inhibitor amongst various tested hydroxylated flavones. The flavone autoxidation product (oDHF) sample was separated into two fractions that contained high and low molecular weight components (oDHF_{HW} and oDHF_{LW}, respectively) using concentrators with 3 kDa cut-off. Then the samples were analysed using HPLC and compared. These fractions were then used in aggregation experiments of A β ₄₂ and aSyn to determine how they affect A β ₄₂ and aSyn aggregation half-time values. oDHF_{HW} was further analysed using MALDI-TOF and NMR. The cell viability assay was performed to understand how the oDHF_{HW} changed toxicity of fibrils on SH-SY5Y cells. AFM imaging was used to assess changes in morphology of aggregates.

Results - The HPLC chromatogram of non-oxidized 2',3'-dihydroxyflavone contained one sharp peak, while after autoxidation, multiple distinct peaks were found. After separating the sample into oDHF_{LW} and oDHF_{HW} fractions, the latter contained only a few peaks from the original autoxidation mixture, with one of them being very shallow and broad, resembling the dispersity of polymeric molecules.

Aggregation of aSyn was inhibited by both fractions, however, a much stronger impact on relative aggregation half-time was visible when the protein was aggregated with oDHF_{HW}. In the case of A β ₄₂, oDHF_{LW} did not have any influence on this peptide aggregation, while oDHF_{HW} delayed the fibrillation half-time at least two-fold. The mass spectrum showed a series of different

mass-to-charge ratio values that ranged from 400 to 2000 with a constant repeat of ~ 246.51 m/z. NMR spectra additionally contributed to the revelation of polydispersity in the sample, suggesting that the mixture contains polymers of various lengths and dispersity.

The cell viability increased compared to the control sample when aSyn fibrils were formed in the presence of oDHF_{HW} . However, the impact on cell viability of $\text{A}\beta_{42}$ in the presence of oDHF_{HW} did not correlate throughout the whole range of the inhibitor concentration. Smaller amount of inhibitor reduced toxic effect of fibrils, however a larger amount of inhibitor decreased cell viability below the control level ($\text{A}\beta_{42}$ aggregates alone).

AFM images indicated the formation of $\text{A}\beta_{42}$ fibrils with round-shaped structures bound to them. The addition of the inhibitor increased the width and height of the structures on the mica. Interestingly, the oDHF_{HW} sample alone had particles up to 15 nm height, proving the existence of polymers.

Conclusions – Autoxidation of 2',3'-dihydroxyflavone leads to the formation of different molecules. Polydisperse polymeric molecules found in this mixture showed the most substantial inhibitory potential against both $\text{A}\beta_{42}$ and aSyn aggregation (Figure 7).

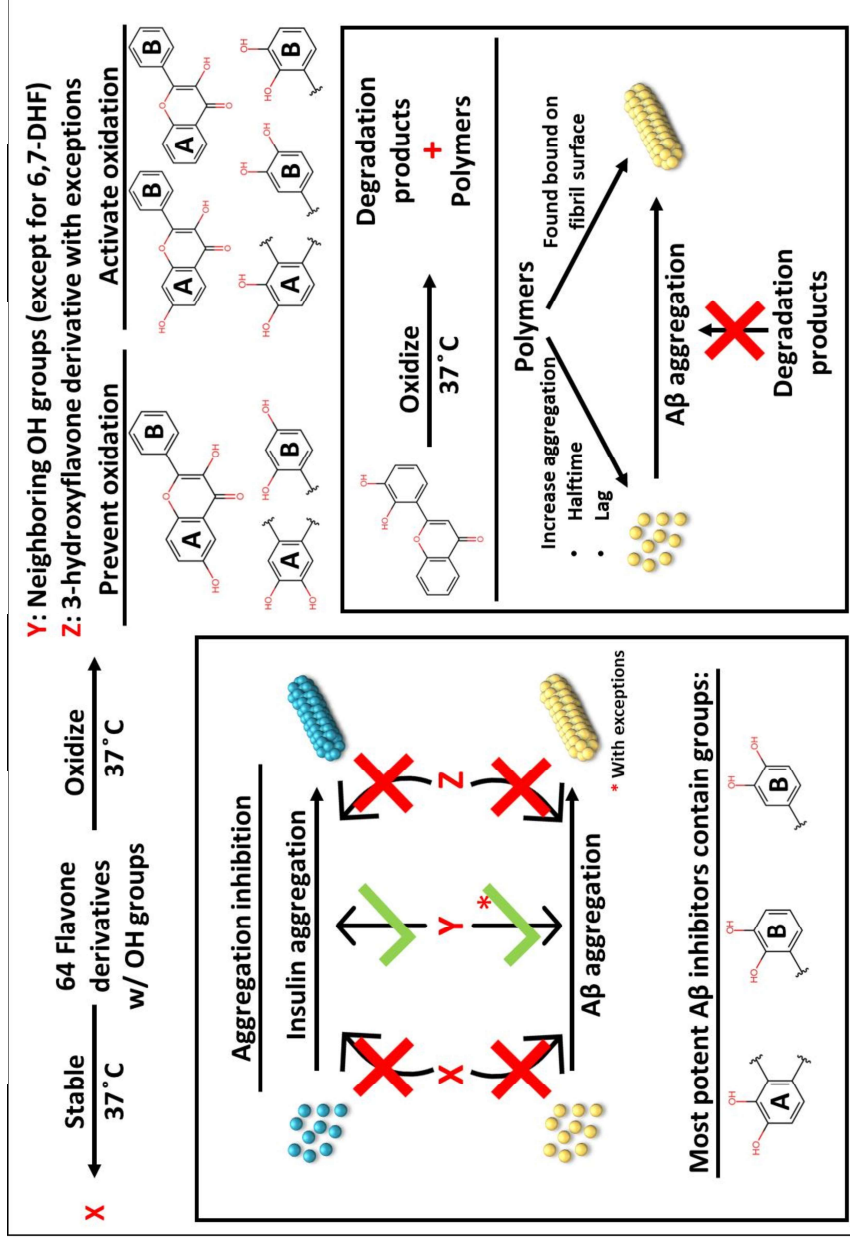


Figure 7. Brief representation of articles 3 and 4.

The Major Components of Cerebrospinal Fluid Dictate the Characteristics of Inhibitors against Amyloid-Beta Aggregation

Aim of this study – to compare how epigallocatechin-3-gallate and VR16-09 affects A β ₄₂ aggregation in PBS and artificial mixture mimicking CSF.

Methods – in order to perform experiments in CSF mimicking environment, artificial cerebrospinal fluid was composed of the main components found in CSF, such as human serum albumin (HSA), glutamine, urea, glucose, cholesterol, lactate, Ca²⁺ and Mg²⁺ ions. A β ₄₂ was aggregated in PBS and aCSF with and without the addition of VR16-09 or oxidized EGCG. AFM images were recorded of each sample to evaluate the differences in aggregates formed during the fibrillation process in both mediums with and without the inhibitor. Evaluation of a single component impact on the inhibitory effect of VR16-09 to A β ₄₂ fibrillation was done. Global fitting of A β ₄₂ in aCSF and in aCSF without HSA with and without VR16-09 was done by acquiring the data of aggregation experiments using a range of A β ₄₂ concentrations (0.75 to 2.0 μ M).

Results - In PBS, oxidized EGCG increased the aggregation halftime (t_{50}) of A β ₄₂ by \sim 2-fold, while VR16-09 did not have any visible effect on this parameter. In aCSF, EGCG accelerated the process, while VR16-09 increased t_{50} more than twice. Longer fibrils were found when A β ₄₂ was aggregated in aCSF. In addition, significantly higher ($p > 0.01$) fibrils were found in PBS compared to aCSF when VR16-09 was present in the reaction mixture.

The aggregation of A β ₄₂ in aCSF was enhanced by Ca²⁺ and Mg²⁺ ions and was inhibited by HSA and glutamine. All components have increased the inhibitory effect of VR16-09, except for glutamine, which had the opposite impact.

Global fit data suggested that VR16-09 decreased primary nucleation and that this effect was strengthened by the presence of HSA. Also, VR16-09 increased secondary nucleation while HSA was seen to reduce this impact. HSA had pronounced influence on fragmentation reducing the process with or without the presence of inhibitor.

Conclusions – A β ₄₂ aggregated slower in aCSF than in PBS. This effect was due to the combination of aCSF components. Both inhibitors impact on A β ₄₂ aggregation was different in these reaction mixtures. EGCG lost the inhibitory potential, at the same time, VR16-09 had a pronounced effect against the A β ₄₂ aggregation process. Based on global fit data, HSA reduced

fragmentation and secondary nucleation (when VR16-09 was present), while VR16-09 decreased primary nucleation and increased secondary nucleation processes (Figure 8).

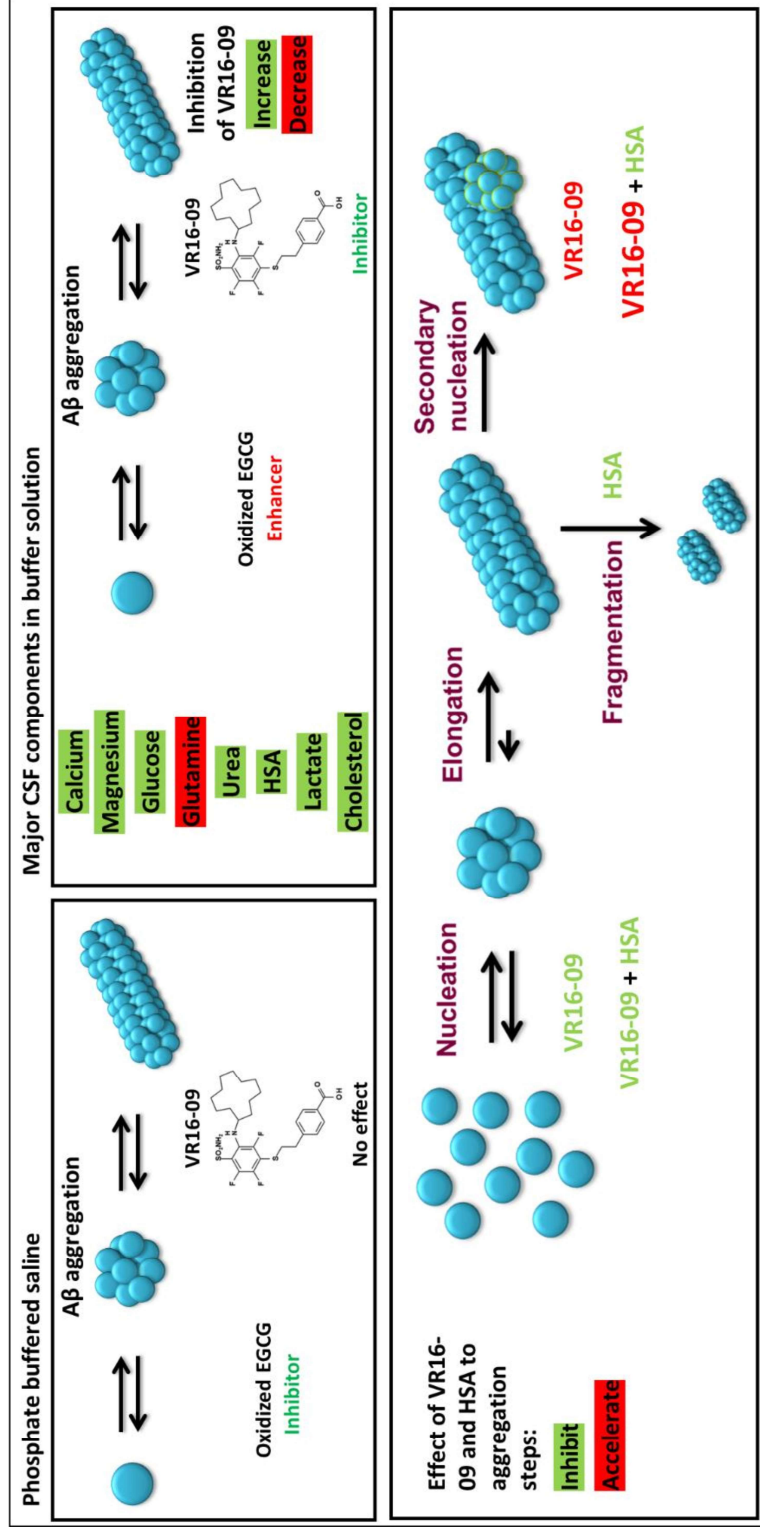


Figure 8. Brief representation of article 5.

4. DISCUSSION

4.1. Autoxidation of polyphenols

Polyphenolic compounds are found to be very applicable within the field of medicine due to their potential to act against oxidation, inflammation, allergies, cancer, HIV, mutagens and the formation of platelet [149–152]. Due to their natural origin and high availability (e.g. in various herbs, spices, and edibles such as vegetables and fruits), they are a great source to be used in therapies [153]. This is why they were also used in research with neurodegenerative diseases [154]. Research shows that EGCG, gallic acid, curcumin, and various flavones such as quercetin, and luteolin had anti-amyloid properties [61,140,154–158], even reporting the possibility of fibril disaggregation [57,159]. This seems as a positive trait of these molecules that may help create an effective drug against neurodegeneration. However, the matters are more complicated than it may seem, and this is why it required a more thorough analysis that answered questions about their inhibitory characteristics and its relationship to the polyphenols structure.

4.1.1. Gallic acid autoxidation

Autoxidation of natural molecules under neutral or higher pH (could be induced by metal ions at lower pH) leads to a loss of the initial structure that results in the formation of different components within the sample that may be very dispersed [139,144,160]. Thus, it was essential to study how such molecule act against protein aggregation before and after it autoxidizes. For this particular purpose, insulin was an ideal protein that aggregates at low pH where polyphenols do not autoxidize and retain initial structure [139]. The sample colour change during the autoxidation process was an indicator of the process. However, the ThT fluorescence spectrum overlaps with spectra of oxidized flavones. Thus monitoring ThT fluorescence intensity in time was confusing as newly formed oxidation derivatives led to fluorescence quenching effect (reducing the intensity over time) which was previously thought to be the result of fibrils dissociation [161]. This study of gallic acid oxidation and its link with the inhibition of insulin aggregation proved that inhibition studies require more thorough analysis of the inhibitor stability.

4.1.2. Flavone autoxidation

Autoxidation process was linked to inhibitory effect of polyphenols against aggregation, thus it was necessary to study this matter using a larger array of different polyphenolic molecules. For this reason, multiple mono- and polyhydroxy flavones were taken. Absorbance measurements allowed to track the autoxidation process, understand how long it takes and also use the resulting sample for inhibition studies. Because not all flavones did autoxidize (their absorbance spectra did not change) during their incubation time (100 hours), it was decided to study the effect of autoxidation on the inhibitory properties of flavones and analyse the specific structural motifs that lead to the autoxidation. By having both autoxidized and non-autoxidized molecules, it was possible to compare their effect to protein aggregation.

Spectral parameters change of flavones during incubation led to the assumption that there could be structural changes in the flavone backbone that disrupts the aromatic system. These differences during the inhibition experiments could disrupt the ThT fluorescence intensity assay and lead to false interpretations of data. To avoid the autoxidation process of unincubated flavones, insulin was used to study their inhibitory characteristics at low pH. While it was discovered that only oxidized flavones were capable to inhibit insulin aggregation, there were a few of them that did not possess any inhibitory characteristics. By looking at the findings of Bijlsma et al. [139], who tracked iron-mediated oxidation of flavones (iron initiates the autoxidation at lower pH), these molecules (3-hydroxyflavone derivatives) are shown to undergo degradation pathway forming various benzoic acids. On the other hand, this structure dependant autoxidation process (formation of degradation and oxidation coupling products) suggests the formation of polymers in the mixture of flavones that were considered as inhibitors. Similar findings with A β ₄₂ confirmed that there is a strong link between the flavone structure, its autoxidation process and inhibitory potential. Sato et al., suggested that catechol-type flavones form o-quinones that may bind to the lysine or arginine residues [162]. However, this only correlates partly with the data present in this thesis – 5,6-dihydroxyflavone and 7,8-dihydroxyflavone did inhibit insulin aggregation while they do not have catechol moiety.

The AFM imaging was complicated because of the low A β ₄₂ concentration and the characteristics of inhibitors. Initially, many round-shape structures were found on the mica, suggesting that the formation of fibrils is turned to the arrangement of oligomeric structures [146]. However, a deeper investigation of samples revealed that most of the fibrils (formed with inhibitors) were clumped together, besides a few that were found dispersed on the mica. These round-shaped structures were bound on the fibrils or fibril clumps, revealing a peculiar affinity between A β ₄₂ oligomers and fibrils. On

the other hand, FTIR spectra of a sample with 2'3'-dihydroxyflavone showed that there could be higher amount of turns or different types of β -sheets (1629 cm^{-1} , 1675 cm^{-1}). This could happen due to the formation of o-quinone capable of covalently binding to lysine residues within A β ₄₂ and stabilising the peptide reported in (+)-taxifolin studies [162]. However, it does not answer why the surface of fibrils is clustered together into very large clumps.

4.1.3. Scavenging the inhibitor within the flavone autoxidation mixture

The unclear view of the clumps of fibrils and round-shape structures and interest in finding the inhibitory molecule within the autoxidation sample initiated further analysis of the most potent inhibitor (2'3'-dihydroxyflavone) out of previously studied incubated flavones. Separation of small and large molecular weight fractions could be identical to the membrane (3 kDa cut-off), however it was enough to separate small molecules from larger components in the autoxidation sample. While the major inhibitory potential was seen to be retained in the sample with larger molecular weight components, it was evident that possible formation of o-quinones is not the main character that leads to inhibition. Polymers that were confirmed with MALDI-TOF, NMR and AFM images (15 μm) seem to be the key component that slows down the aggregation of A β ₄₂ and aSyn. In fact, round shape oligomers (from inhibitor) found on the mica could be confused with the oligomers of the specific protein or peptide. In addition to that, clumped round-shaped structures on the fibril surface are the same components from the inhibitor sample that may be confused with the disaggregation or shifted aggregation pathway towards amorphous aggregates.

Despite the good solubility in water, these polymeric molecules were eluting at the higher MeOH concentration, comparing to the retention times of the initial molecule. Combining this information with the results from NMR and MALDI-TOF, the polymerization may be activated via the formation of ortho quinone structures. Then the ring of o-quinone could bind to amine [162], acid or alcohol groups. While there was strict correlation between structures that lead to active oxidation products against protein aggregation, the degradation of the flavone backbone may not be the limiting factor, if it does not affect the formation of o-quinone. However, if the ring has no possibility to form a bond at the reactive carbon in para position (tertiary carbon, presence of OH group), then no such polymerization was seen. This, in fact, explains why 6',7'-dihydroxyflavone did not oxidize, while 7',8'-dihydroxyflavone did. Although this information is evident, there may other factors involved in this process.

Another important aspect to cover is the limitations to the applicability of autoxidized flavones as potential medications against neurological disorders. In this case, polymeric molecules break Lipinski's rule of five. This rule indicates that in order to pass brain-blood-barrier, molecule should be smaller than 500 Daltons, should not contain more than 5 hydrogen donors and 10 hydrogen acceptors [163,164]. Many polyphenols were thought to be ideal inhibitors due to their unique molecular structure that allows passing through the brain-blood barrier, however, the resulting inhibitor does not possess such characteristics. Nonetheless, autoxidation products should not be ruled out as studies are showing a potential link between the aggregation of proteins in the gut and the onset of PD [165], which could be an ideal case for using such polymeric molecules.

4.2. Insulin polymorphism

One of the more interesting discoveries via inhibitory effect was the insulin polymorphism. Our group previously summarized two possible conformations of insulin fibrils at low pH that forms based on the equilibriums between monomers and oligomers of insulin [114]. Despite that, a third strain was discovered when insulin was aggregated under a range of protein concentrations that showed a concentration-dependant polymorphism and the formation of two distinct conformations. It appears, that GAO prevented formation of LCF strain, effectively inhibited primary nucleation while virtually not affecting secondary nucleation or elongation. It could be that GAO suppressed the nucleation of LCF, instead allowing the formation of HCF nuclei.

HFC has a distinct characteristic of increasing the ThT fluorescence intensity 10-fold compared to the LFC. This distinct aggregation pathway change with higher ThT fluorescence intensity was visible when insulin was inhibited with incubated flavones. Perhaps flavones and gallic acid impede insulin fibrillation via similar inhibitory mechanisms.

4.3. Altering the *in vitro* screening

In vitro screening is an essential part of finding the potential molecule, nonetheless, different environments where the aggregation reaction occurs may lead to distinct results [56]. This is why mimicking cerebrospinal fluid led to perceiving different inhibitory characteristics of both EGCG and VR16-09. Such results could be linked to two possible factors: (1) changed A β ₄₂

aggregation pathway by the component(s) in aCSF and (2) affinity between the inhibitor and components of aCSF.

The first point is covered more in literature, however, only in the forms of one or two aCSF components. There are records of Ca^{2+} ions [124], HSA [166], HSA with cholesterol [167] and other components affecting the aggregation of $\text{A}\beta_{42}$. While the contribution of other components is not well studied, there are significant data about $\text{A}\beta_{42}$ aggregation in CSF from human patients that show similarly slowed aggregation as in the case of aCSF [168]. The second point emphasizes the complex bridge between *in vitro* screening and the results of the inhibitor *in vivo*. Each component would need to be tested with an inhibitor to understand whether they have a specific affinity. However, this does not provide full information about extra factors that could happen in physiological conditions.

The complex struggle to account for the differences between the experiments *in vitro* and *in vivo* may emerge due to the complexity of CSF and nanomolar amounts of components found in the fluid [169–172] that may be critical in shifting both $\text{A}\beta_{42}$ aggregation and its inhibition process. However, an altered medium must be used during the initial search for the inhibitor as it lowers the possibility of getting false-positive and false-negative results. Aggregation and its inhibition comparison between CSF and aCSF could lead to finding a reaction mixture that would closely match the results of aggregation in CSF and lead to substituting artificial screening medium for the initial pH 8.0, TBS or PBS. It could potentially reduce the number of falsely discovered/undiscovered inhibitors. This is especially important as the drug discovery process gets more expensive when advancing through development steps, and it would be best to allocate money investments “correctly”.

CONCLUDING REMARKS AND FUTURE PROSPECTS

A thorough analysis of protein aggregation inhibition studies using polyphenolic molecules led to several conclusions. First, hydroxyflavones autoxidation is limited to its structure, which involves having neighbouring hydroxyl groups or the backbone of the flavonol. Second, gallic acid and hydroxyflavones do not have any inhibitory effect on insulin and A β ₄₂ if they are unaffected by autoxidation. Nonetheless, there are a few exceptions, such as flavonols without neighbouring hydroxyl groups and some outliers - 3,3',4'-trihydroxyflavone and 6,7,3',4'-tetrahydroxyflavone. Last, the autoxidation of 2',3'-dihydroxyflavone leads to generation of multiple different molecules, however, the polymeric molecules in the sample possess a significant part of the inhibitory features of the mixture.

Exploring A β ₄₂ aggregation and inhibition in PBS and aCSF revealed that *in vitro* molecule screening is very sensitive to the reaction mixture where effects of oxidized EGCG and VR16-09 changed. Oxidized EGCG being ineffective and VR16-09 increasing inhibitory potential in aCSF. Let alone HSA being one component in aCSF that enables the activity of VR16-09 against A β ₄₂ aggregation. This result enables to propose a screening protocol that is closer to *in vivo* conditions, avoiding unnecessary and ineffective research funding application.

Taking all results into account, it is evident that inhibitory studies of protein aggregation require analysis not only for the phase transition of the studied protein, but also for the state of inhibitor and how it behaves at near physiological conditions (at least including the main components found *in vivo*). These findings will allow to shape our current research and contribute this knowledge into future studies.

Conclusions:

1. Gallic acid does not inhibit insulin aggregation, while its oxidized form slows down this process significantly altering the fibril formation pathway.
2. Hydroxyflavones do not inhibit aggregation of A β ₄₂ and insulin unless they possess neighbouring hydroxyl groups and undergo autoxidation.
3. 2',3'-dihydroxyflavone autoxidize forming degradation and polymerization products, where the latter are the only capable species in the mixture to inhibit A β ₄₂ and α -synuclein aggregation process.

4. The inhibitory potential of oxidized epigallocatechin-3-gallate and fluorinated benzenesulfonamide against $A\beta_{42}$ is notably influenced by the main components of cerebrospinal fluid, particularly by HSA.

SUMMARY IN LITHUANIAN LANGUAGE

SANTRUMPOS

A β ₄₀	Amiloidas beta (1-40)
A β ₄₂	Amiloidas beta (1-42)
aCSF	Dirbtinis smegenų skystis
AJM	Atominės jėgos mikroskopija
AL	Alzheimerio liga
APP	Amiloido beta prekursorius / pirmtakas
DMSO	Dimetil sulfoksidai
EGCG	Epigalokatechin-3-galatas
FTIR	Fourier-transformacijos infraraudonoji spektroskopija
GA	Galo rūgštis
GAO	Oksiduota galo rūgštis
HCF	Fibrilės suformuotos, esant didelei baltymo koncentracijai
HPLC	Aukšto efektyvumo chromatografijos sistema
LCF	Fibrilės suformuotos, esant mažai baltymo koncentracijai
PBS	Fosfatų buferinis tirpalas atitinkantis fiziologinę druskų koncentraciją
oDHF	Oksiduotas 2'3'-dihidroksiflavonas
oDHF _{HW}	Didelės molekulinės masės komponentai oDHF mišinyje
oDHF _{LW}	Mažos molekulinės masės komponentai oDHF mišinyje
PL	Parkinsono liga
TBS	Tris buferinis tirpalas atitinkantis fiziologinę druskų koncentraciją
ThT	Tioflavinas-T

SANTRAUKA

Neurodegeneracinės ligos, tokios kaip Parkinsono ar Alzheimerio, ženkliai blogina gyvenimo kokybę ir yra laikomos nepagydomomis. Prognozuojama, kad ilgėjant gyvenimo trukmei, neurodegeneracinių ligų atvejų skaičius eksponentiškai didės. Manoma, kad šių ligų atsiradimą ir progresavimą lemia baltymų kaupimasis į fibrilinius agregatus, kuriems būdinga beta-klosčių struktūra. Jau kelis dešimtmečius ieškoma vaistų gydyti šiems neurologiniams susirgimams, tačiau dauguma klinikinių bandymų baigiasi nesėkmingai. Tam kuriami ir pasitelkiami įvairūs metodai, iš kurių vienas yra baltymų agregacijos slopinimo tyrimai. Šiuo metu yra sukurti ir patvirtinti keli simptomus lengvinantys ar ligos eigą modifikuojantys preparatai, kurie sulėtina neurodegeneracinės ligos progresavimą, tačiau taip pat turi ir reikšmingų šalutinių poveikių. Dėl šios priežasties, labai svarbu tęsti naujų potencialių vaistų tyrimus, skiriant daug dėmesio pirminiams kandidatų kūrimo etapams, kurie galėtų padėti išvengti brangių tolimesnių išlaidų. Siekiant paspartinti vaistų kūrimo procesus ir padidinti jų veiksmingumą, svarbu tobulinti *in vitro* atrankos procedūras ir potencialių vaistų ikiklinikinių tyrimų analizę.

Visų pirma, šiame darbe daugiausiai dėmesio buvo skirta tirti polifenolinės prigimties junginius ir jų gebėjimą slopinti baltymų agregacijos procesą. Kadangi daugelis šių junginių klinikinių tyrimų buvo nesėkmingi (pvz., epigalokatechin-3-galatas, kurkuminas, resveratrolis) buvo atlikta išsamesnė jų stabilumo ir poveikio baltymų agregacijai analizė *in vitro*. Rezultatai parodė, kad šios molekulės, esant neutraliam ar aukštesniam pH, atitinkančiam fiziologines sąlygas, yra nestabilios. Dalis šių tirtų molekulių yra paveikiamos sudėtingo proceso, vadinamo autoksidacija, kuris labai svarbus slopinant $A\beta_{42}$ ir insulino agregaciją. Įdomu tai, jog stipriausias $A\beta_{42}$ ir insulino fibriliacijos inhibitorius - 2',3'-dihidroksiflavonas - autoksiduojasi, sudarydamas skirtingus molekulinis junginius (mažas molekules ir polimerus), iš kurių tik polimerinės molekulės dalyvauja slopinimo procese.

Antroji šio tyrimo dalis buvo skirta *in vitro* atrankos procedūrai tobulinti. Paprastai baltymų agregacijos tyrimas *in vitro* atliekamas naudojant PBS, TBS ar net buferinius tirpalus, kurie buvo naudoti galutiniame gryninimo etape. Nors ši metodika leidžia lengviau įvertinti gautus duomenis, agregacijos mechanizmas ir slopinamasis junginių poveikis gali skirtis nuo proceso, vykstančio smegenyse. Todėl buvo sukurta terpė, imituojanti smegenų skysčio sudėtį, kuri leido įvertinti, kaip pagrindiniai smegenų skysčio komponentai veikia $A\beta_{42}$ agregacijos slopinimą naudojant

epigalokatechino-3-galatą ir fluorintą benzensulfonamidą VR16-09. Rezultatai visiškai skyrėsi nuo gautų naudojant PBS, todėl *in vitro* vaistų atrankos eksperimentų metu yra svarbu taikyti terpę, kurioje stebimų procesų poveikis būtų kuo panašesnis į vykstantį smegenyse fiziologinėmis sąlygomis. Dirbtinis smegenų skystis (aCSF) galėtų būti nauja terpė, naudojama anti-amiloidiniams junginiams tirti. Šis mišinys galėtų pakeisti šiuo metu populiarias PBS arba TBS bei sumažinti skirtumą tarp *in vitro* ir *in vivo* tyrimų.

Tikslas: Ištirti skirtingų polifenolinių junginių poveikį baltymų amiloidinės agregacijos procesui.

Uždaviniai:

1. Nustatyti galo rūgšties ir jos oksiduotos formos slopinamąjį poveikį insulino agregacijos procesui ir jo mechanizmui.
2. Nustatyti ryšį tarp hidroksiflavonų autoksidacijos proceso ir jo poveikio $A\beta_{42}$ ir insulino agregacijai.
3. Ištirti 2'3'-dihidroksiflavono autoksidacijos produktus ir išskirti molekules, dalyvaujančias slopinant $A\beta_{42}$ ir α -sinukleino agregaciją.
4. Įvertinti smegenų skysčio komponentų įtaką/poveikį Ab_{42} agregacijos slopinimo efektyvumui, naudojant epigalokatechin-3-galatą ir fluorinuatą benzensulfonamidą - VR16-09.

Mokslinis naujumas: Šis tyrimas parodė, kad ryšys tarp polifenolinių junginių ir jų antiamiloidinių savybių yra susijęs su šių molekulių autoksidacija, dėl kurios pasikeičia jų cheminės savybės. Šis procesas vyksta esant neutraliam ar aukštesniam pH, dėl kurio pasikeičia polifenolinių junginių poveikis amiloidinei agregacijai, o tai gali lemti neteisingą duomenų interpretaciją. Šiame darbe atlikti eksperimentai leido išanalizuoti polifenolių antiagregacines savybes prieš jų autoksidacijos procesą ir jam pasibaigus. Atlikta analizė leido suprasti, kodėl tam tikromis reakcijos sąlygomis slopinamasis poveikis nėra matomas. Buvo įrodyta, kad pati galo rūgštis nepasižymi anti-amiloidinėmis savybėmis, priešingai nei jos oksiduota forma. Be to, baltymų agregacijos slopinimo galo rūgštimi tyrimas leido rasti naują insulino agregato konformaciją, kuri priklauso nuo šio peptido koncentracijos.

Flavonų autoksidacijos procesas yra labai sudėtingas ir nėra nuodugnai išanalizuotas. Šio proceso metu susidaro daugybė molekulių. Todėl tiesioginio ryšio tarp gautame mišinyje susidariusių polimerų ir šiame darbe aptartų polifenolių slopinamųjų savybių prieš tai nebuvo nustatyta. Be to,

ištirus molekulių anti-amiloidines savybes skirtingomis reakcijos sąlygomis, paaiškėjo, kad įprastai naudojama terpė, atliekant *in vitro* potencialių slopiklių atranką, gali lemti neteisingą duomenų interpretaciją. Tai leido sukurti atskirą dirbtinę smegenų skysčio terpę, kuri galėtų sumažinti prarają tarp *in vitro* ir *in vivo* eksperimentų.

Ginamieji teiginiai:

1. Polifenolinių junginių autoksidacija yra esminis veiksnys, lemiantis baltymų amiloidinės agregacijos slopinimą.
2. Flavonų autoksidacijos metu susidaro polimerinės molekulės, kurios yra pagrindinis susidariusių junginių mišinio slopinamojo poveikio A β ₄₂ agregacijai veiksnys.
3. Smegenų skysčio komponentai keičia anti-amiloidinių junginių slopinamąjį poveikį.

LITERATŪROS APŽVALGA

1. Neurodegeneracinės ligos

Atrodytų, kad terminas „neurodegeneracija“ yra visuotinai suprantamas. Tačiau nėra vieno tikslaus apibrėžimo, kuris tilptų į sakinių ir apimtų daugybę tame dalyvaujančių procesų. Šis terminas yra žodžių „neuro“, reiškiančio nervines ląsteles arba neuronus, ir „degeneracija“, nurodančio ląstelių funkcijos ar struktūros praradimą arba „išsigimimą“, derinys. Taigi, neurodegeneracija reikštų pirminių nervinių ląstelių funkcijos praradimą. Tačiau iš tikrųjų šiuo žodžiu apibūdinama daugybė skirtingų mechanizmų, siejamų su įvairiomis neurologinėmis ligomis, kurios pasireiškia skirtingose nugaros ar galvos smegenų srityse ir pasižymi tam tikrais patologiniais požymiais. [1].

Skirtingais istorijos laikotarpiais neurodegeneracinės ligos buvo apibrėžiamos pagal jų sukeltus simptomus ir tuo metu vyravusius visuomenės įsitikinimus. Dažniausiai tokių susirgimų etiologija buvo aiškinama, kaip antgamtinė (pvz., sukelta dievų, demonų ar net vaiduoklių), sukelta reprodukcinę organų (pvz., pasislinkusi gimda trukdo kitų organų funkcijoms), trauminių išgyvenimų ir kognityvinių išankstinių nusistatymų dėl kūno simptomų [5]. Tačiau jau 2000 m. pr. m. e. egiptiečiai aprašė, kad vyresnio amžiaus žmonėms būdingas atminties pablogėjimas. Vėliau Pitagoras senatvę įvardijo kaip laiką, kai protas sumenksta iki kūdikio lygio.

Panašius pastebėjimus taip pat įvardijo Hipokratas, Platonas ir Markas Tulijus Ciceronas, o mūsų eros laikotarpiu Viljamas Šekspyras savo veikaluose, tikėtina, aprašė tam tikros rūšies demencijos simptomus [6].

Pirmą kartą terminą „neurodegeneracija“ 1965 m. paminėjo J. F. Bray, t. y. gerokai vėliau nei buvo pirmą kartą aprašytos Parkinsono (1817 m. Jameso Parkinsono esė „Esė apie drebėjimo paralyžių“) [10] ir Alzheimerio ligos (1906 m. Aloizas Alzheimeris aprašė „arteriosklerozinę smegenų atrofiją“) [11]. 1957 m. Gajdusekas ir Vincentas Zigas aprašė pirmąją prioninę ligą, vadinamą Kuru, kuri buvo įvardinta kaip užkrečiama ir sukelta netradicinių virusų. Tik vėliau mokslininkai išsiaiškino, kad liga plito kanibalizmo būdu, žmonėms valgant užkrėstus mirusių gentainių audinius [12].

1.1. Alzheimerio liga

Alzheimerio liga (AL) šiuo metu yra labiausiai paplitusi demencijos rūšis, kurią galima apibūdinti kaip ilgai progresuojančią neurodegeneracinę ligą. – Ji yra gyvenimo kokybę bloginantis sutrikimas, dėl kurio suprastėja atmintis, kamuoja nemiga, sutrinka orientacija, sunku atlikti kasdienes užduotis [13]. Šiai ligai būdingas patologinis požymis - senilinių plokštelių (dar vadinamų dendritinėmis, neuritinėmis arba amiloidinėmis plokštelėmis) ir neurofibrilinių raizginių (NFT) kaupimasis smegenyse [14]. Amiloidinės plokštelės sudarytos iš 40-42 aminorūgščių peptido, vadinamo amiloidu β ($A\beta$), agregatų. Šis peptidas gaunamas iš didelio transmembraninio amiloido pirmtako baltymo (APP), kurį skaldo fermentai, vadinami β - ir γ -sekretazėmis [15]. Jei $A\beta$ išvengia proteolitinio skaidymo procesų, tikėtina, kad $A\beta$ oligomerai ir senilinės plokštelės ekstraląstelinėje erdvėje formuojasi dėl didėjančios peptido koncentracijos [18]. Manoma, kad $A\beta$ oligomerai gali sukelti daugybę žalingų pokyčių smegenyse, pavyzdžiui, sutrikusią Ca^{2+} homeostazę, plastiškumo disfunkciją, aberantinį Tau fosforilinimą, oksidacinį stresą, atsparumą insulinui, aksoninio transporto slopinimą ir kitus procesus [19]. Be to, $A\beta_{42}$ oligomerai gali sąveikauti su įvairiais ląstelių paviršiaus receptoriais ir patekti į ląstelę, sukeldami endoplazminio tinklo stresą ir mitochondrijų kaspazių aktyvaciją. Tai paskatina su mikrovamzdeliais susijusio baltymo Tau išsiskyrimą ir jo agregaciją į neurofibrilinius raizginius [20].

Manoma, kad padidėjusi $A\beta$ gamyba yra pagrindinė Alzheimerio ligos priežastis. Svarbu pažymėti, kad $A\beta$ peptidas susidaro iš kelių izoformų. Labiausiai paplitę yra 40 ir 42 aminorūgščių ilgieji peptidai (atitinkamai $A\beta_{40}$ ir $A\beta_{42}$). Nors $A\beta_{40}$ yra gausiausia iš visų izoformų, ji mažiau linkusi agreguoti nei $A\beta_{42}$. Pastebėta, kad sumažėjusi abiejų peptidų koncentracija ir $A\beta_{42}/40$

santykis smegenų minkštyme galėtų būti naudingas biomarkeris diagnozuojant Alzheimerio ligą iki pasireiškiant pirmiesiems simptomams [21,22].

1.2. Parkinsono liga

Antrasis pagal dažnumą neurodegeneracinis sutrikimas yra Parkinsono liga (PL). PL yra susijusi su amžiumi, o jai būdingi simptomai yra tremoras, sustingimas, judesių lėtumas, miego sutrikimai, depresija ir kognityviniai pokyčiai [23]. Patologiniu PL požymiu laikomas nenormalių baltymų sancaupų, vadinamų Lewy kūneliais (angl. Lewy bodies), kaupimasis [24]. Pagrindiniai šių kūnelių komponentai yra α -sinukleino (aSyn) agregatai [25]. Nors tiksli aSyn funkcija nežinoma, šis baltymas ir jo mutacijos yra tiesiogiai susijusios su ligos pradžia [26].

2. Neurodegeneracinių ligų gydymas

Nors neurodegeneraciniai sutrikimai yra gyvybei pavojingos ligos, kasmet diagnozuojamos vis naujiems pacientams [29,30], joms gydyti labai svarbūs ligos eigą modifikuojantys vaistai. Ieškant potencialių preparatų, atlikta daug įvairių tyrimų, vertinant galimus kandidatus ir jų terapijos taikinius, įskaitant su liga susijusių peptidų ir (arba) baltymų gamybą, neteisingą aminorūgščių susilankstymą ir agregaciją, neurotoksiškumą, uždegimą ir kt. [31,32].

Vien 2022 m. klinikiniuose tyrimuose buvo vertinti 143 potencialūs medikamentai AL gydyti [33], tačiau nepaisant neatidėliotino vaistų poreikio, tik labai nedidelė dalis tokių tyrimų yra sėkmingi ir pereina antrąjį ar trečiąjį klinikinių tyrimų etapą [34-38].

2.1. Vaistų kūrimas prieš AL

Dėl nepakankamo dabartinių ligą modifikuojančių vaistų veiksmingumo dedama daug pastangų siekiant sukurti naujus preparatus, kurie sulėtintų ar sustabdytų Alzheimerio ligos progresavimą ar net panaikintų šios ligos pradžioje atsiradusius padarinius [42]. Šiuo metu ieškomi ir kuriami nauji vaistai, įskaitant terapiją, nukreiptą į du pagrindinius patologinius AL aspektus - A β peptidą ir tau baltymą [43].

Gydymas nuo A β patologijos [16,39,42,44-50]:

- A β gamyba gali būti stabdoma slopinant β - ir γ -sekretozes, kurios skaldo APP ir generuoja A β monomerus.
- Anti-amiloidiniai preparatai gali slopinti A β agregaciją. Idealiu atveju tokios molekulės prisijungtų prie A β , neleidamos peptidui formuoti oligomerų ir agreguoti.

- Aktyvioji ir pasyvioji imunoterapija, skatinanti antikūnų, specifiskai nukreiptų prieš A β daleles, gamybą. Tai apima vakcinas arba tiesioginį monokloninių antikūnų, kurie jungiasi su A β monomerais, oligomerais ir (arba) agregatais, patekimą į organizmą.

Gydymas nuo Tau patologijos [39,42,45-48,50,51]:

- Tau baltymas agreguoja po to, kai jis yra hiperfosforilinas. Šio proceso slopinimas, nukreiptas į glikogeno-sintetazės-kinazę-3 β , kuri atlieka svarbų vaidmenį Tau hiperfosforilinimo (p-Tau) procese, turėtų užkirsti kelią tau agregacijai ir jo neurotoksiškumui.
- Molekulės, stabilizuojančios ir užkertančios kelią tau agregacijai.
- Stabilizuojant mikrovamzdelius, kurie yra destabilizuojami po tau fosforilinimo. Taip būtų galima sumažinti išsiskiriančio p-Tau kiekį.
- Aktyvioji ir pasyvioji imunoterapija prieš patogenines tau baltymo formas.

2.2. Polifenolių naudojimas amiloidinių ligų gydymui

Visada buvo manoma, kad natūralūs junginiai turi pranašumą teikiant naudą sveikatai ir gydant ligas [52-54]. Viena iš tokių kategorijų yra polifenolinių junginių grupė. Jų gausu gamtoje ir randama įvairiuose vaisiuose, daržovėse, prieskoniuose, žolelėse ir gėrimuose. Taip pat įrodyta, kad jie pasižymi antiamiloidinėmis savybėmis, nes gali slopinti įvairius baltymų agregacijos procesus [55]. Iš visų polifenolių labiausiai žinomas yra epigalokatechino-3-galatas (EGCG). Šis katechinas slopina A β , aSyn ir kitų baltymų agregaciją, taip pat manoma, kad jis suardo jau susidariusias amiloidines fibriles [56-59]. Be to, pastebėta, kad panašiomis savybėmis pasižymi ir galo rūgštis (GA), kuri yra tiesioginis EGCG hidrolizės produktas [60-62]. Nepaisant nepaprastai gerų EGCG *in vitro* tyrimų rezultatų, šis preparatas nepaėjo klinikinių tyrimų [63,64]. Kiti polifenoliai, kurie naudoti klinikiniuose tyrimuose, buvo kurkuminas, liuteolinas, kvercetas ir resveratrolis [63].

Nustatyta, kad EGCG autoksidacija vyksta esant neutraliam ar aukštesniam pH. Šis procesas yra susijęs su cheminėmis molekulės modifikacijomis. Šneideris ir bendraautorai įrodė, kad EGCG nepasižymi antiamiloidinėmis savybėmis prieš insulino agregaciją esant žemam pH (kai polifenolis yra stabilus), tačiau jei molekulė inkubuojama esant fiziologiniam

pH (7,4), gautas mišinys įgyja stiprų slopinamąjį poveikį [56]. Nors šios cheminės modifikacijos pastebimos *in vitro* tyrimuose, tačiau vis dar nėra tikslių įrodymų, patvirtinančių šių esminių pokyčių atsiradimą *in vivo* (žmonėse). Tai reiškia, kad nėra jokios garantijos, jog vaistas veiks, ir tai gali būti priežastis, kodėl polifenolių klinikiniai tyrimai buvo nesėkmingi.

3. Baltymų agregacija

Neurodegeneracinių ligų atsiradime ir progresavime dalyvaujančių peptidų ir baltymų agregacijos procesas yra sudėtingas. Kiekvienas baltymas skiriasi polipeptidine seka, dydžiu ir konformacija. Tai turėtų lemti skirtingus kiekvieno tipo molekulių agregacijos mechanizmus. Tačiau pagrindiniai šių procesų skirtumai yra susiję su pradine struktūra arba konformacija (netvarkingos struktūros, globuliniai arba funkciniai peptidai ir baltymai), o bendrą agregacijos procesą galima supaprastinti [65]. Didžiosios dalies baltymų agregacijos mechanizmai yra panašūs, dėl to, kad jie formuoja giminingos struktūros fibrilinius agregatus [66].

3.1. Baltymų agregacijos mechanizmas

Peptidų ar baltymų jungimasis į fibrilinius agregatus vyksta keliais pagrindiniais etapais. Pirmajame etape molekulės pereina iš natyvios formos į agregacijai palankią konformaciją (nebent baltymas jau yra netvarkingos struktūros).

Antrasis mechanizmo etapas apima procesą, kurio metu agregacijai linkusios dalelės kaupiasi į agregacijos branduolius. Šis procesas paprastai vadinamas branduolių susidarymu ir laikomas agregaciją ribojančiu etapu. Jo metu agregacijai linkusios molekulės (toliau vadinamos monomerais) sąveikauja tarpusavyje ir patiria struktūrinius pokyčius, suformuodamos hidrofobines sritis, turinčias kryžmines β -klostes. Didėjant monomerų kiekiui, branduolys tampa stabilus; todėl terminas branduolys laikomas mažiausia agregato forma, kai monomerų įtraukimas yra labiau tikėtinas nei monomerų praradimas [71]. Monomerų skaičius branduolyje gali skirtis priklausomai nuo agreguojančio baltymo / peptido; ir gali prasidėti nuo vieno ar tik kelių monomerų [72,73]. Labai svarbu paminėti, kad monomerų kaupimasis gali lemti antrinį kelią, kuris baigiasi amorfinių agregatų susidarymu.

Branduolių susidarymo procesą riboja molekulių sąveikų skaičius ir reakcijos laikas, kurio reikia branduoliams susidaryti. Agregacijos tyrimas *in vitro* gali būti pagreitintas įvairiais veiksniais, turinčiais įtakos minėtiems

procesams. Sąveiką tarp molekulių (susidūrimų skaičių) galima padidinti veikiant difuzijos procesą (pvz., keliant temperatūrą), didinant monomerų koncentraciją mėginyje ir paveikiant mišinį mechaniškai (pvz., maišant) [66]. Kartu reakcijos greitį kontroliuoja molekulių energija mėginyje (pvz., reguliuojama temperatūra), elektrolitų koncentracija (pvz., elektrolitai padengia peptido / baltymo paviršių) ir turi tiesioginę priklausomybę nuo ligando koncentracijos (pvz., heparinas skatina tau agregaciją) [74].

Susidarius branduoliui, vyksta tolesnis agregacijos etapas, vadinamas ilgėjimu, kurio metu yra stebimas ir jam atvirkštinis procesas – disociacija. Vykstant šiai grįžtamajai reakcijai, branduolys prisijungia monomeras, tuo pat metu paversdamas juos identiškais branduolio konformacijai. Taip branduolys linijiniu būdu auga į fibriles, o tai reiškia, kad fibrilė prisijungia monomeras tik jos galuose [66,74,75].

Be minėto pirminio agregacijos mechanizmo, antriniai procesai gali vykti ilgėjimo fazėje, kai vyksta fibrilių fragmentacija ir paviršiaus katalizuojamas branduolių susidarymas. Fragmentacija įvyksta, kai fibrilė suskyla į trumpesnius fragmentus, todėl padidėja galų skaičius. Paviršiaus katalizuojamas branduolių susidarymas (kartais vadinamas antrine nukleacija) vyksta fibrilių paviršiuje ir inicijuoja toksiškų branduolių ir (arba) oligomerų susidarymą demencijos progresavimo metu [66,76].

3.2. Baltymų agregatų polimorfizmas

Identišką aminorūgščių seką turinčio polipeptido agregacija gali lemti skirtingų fibrilių susidarymą, kurios pasižymi savita β struktūros konformacija galutinėje agregato formoje [77]. Polimorfizmo poveikis gali pasireikšti esant skirtingiems aplinkos veiksniams arba net esant vienodoms reakcijos sąlygoms [78]. Paprastai specifinės konformacijos susidarymas yra susijęs su branduolių susidarymo procesu, po kurio seka daug greitesnis ilgėjimo procesas. Ilgėjimas laikomas šabloniniu procesu, kurio metu monomeras paveldi tą pačią antrinę struktūrą kaip ir fibrilė. Tačiau yra tikimybė, kad agregacijos metu susidarys du ar daugiau skirtingi branduolių tipai, dėl kurių mišinys taps heterogenišku [79].

Dauguma fibrilių geba šablonizuoti savo struktūrą, jei reakcijos mišinyje yra monomero. Tačiau esant labai mažai fibrilių koncentracijai ir dėl reakcijos aplinkos sulėtėjus ilgėjimo procesui, paviršiaus katalizuojamas antrinis branduolių susidarymas gali lemti unikalios antrinės struktūros fibrilių

susidarymą. Tai reiškia, kad antrinė nukleacija yra ne šabloninis procesas, o veikiau katalizė, kuri gali turėti įtakos skirtingų konformacijų fibrilių formavimuisi [80,81].

3.3.Slopinimo mechanizmas

Baltymų agregacijos mechanizmas yra labai svarbus ieškant vaistų neurodegeneracinių ligų gydymui, nes slopiklio molekulės gali ne tik sustabdyti procesą, bet ir pakeisti baltymo agregacijos kelią. Todėl kyla keletas klausimų, kai vertinami inhibitoriai: 1) kas yra slopiklio taikiny (monomeras, oligomeras, fibrilė), 2) koks yra slopinimo mechanizmas ir 3) kaip slopiklis veikia agregatų sukeliama toksiškumą ląstelėms? Į dalį minėtų klausimų galima atsakyti remiantis agregacijos kinetikos duomenimis, gautais analizuojant skirtingas monomero ir inhibitoriaus koncentracijas. Inhibitorius gali sąveikauti su monomeru (pvz., stabilizuoti monomerą), oligomeru (pvz., stabilizuoti oligomerą), branduoliu (pvz., riboti ilgėjimą, paviršiaus katalizę) ir fibrile (pvz., riboti ilgėjimą, paviršiaus katalizę ir fragmentaciją) [71,82]. Jei taikiny yra monomeras arba oligomeras, gali būti paveiktas nukleacijos procesas, sulėtinant pirminį branduolių formavimą. Tuo tarpu, jeigu inhibitorius sąveikauja su branduoliais arba fibrilėmis, pakinta ilgėjimo, antrinės nukleacijos ir fragmentacijos procesai, kuriuos galima suprasti tik taikant matematinius modelius [82].

4. Šiame darbe naudoti baltymai

4.1.Amiloidas- β

A β agregacija žmonių organizme sukelia Alzheimerio ligą. 40-42 aminorūgščių peptidas atsiranda iš amiloido pirmtako baltymo ir agreguoja tarpląsteliniam skystyje [121]. A β gali formuoti skirtingo tipo sankaupas – oligomeras, protofibriles ir fibrilinius agregatus. Šis peptidas sudaro agregatus, pasižyminčius tiek paralelinėmis, tiek anti-paralelinėmis beta klostėmis. Dėl to yra randami skirtingos struktūros (konformacijos) baltymo agregatai [122]. Dažniausios A β peptido formos, kurios naudojamos atliekant *in vitro* tyrimus, turi 40 ir 42 aminorūgštis.

Šio peptido izoformų sintezė gali būti sintetinė arba bakterijose (rekombinantinė). Kiekviena iš jų turi teigiamų ir neigiamų aspektų. Nors sintetinį A β galima išgryninti aukšto grynumo, prieš tolimesnius tyrimus peptidą reikia paveikti 1% NH₄OH [126], 10 mM NaOH [126] ar net

organiniais junginiais (1,1,1,3,3,3-heksafluoro-2-propanoliu)[125]. Tai yra daroma tam, kad išvengti bet kokių užsilikusių A β oligomerinių formų pradiniame mėginyje. Nors tokia metodika yra gera, bet yra tikimybė, kad šarmais ar organiniais junginiais paveiktas peptidas gali būti pakitęs [128]. Tam, kad išvengti tokių problemų, yra naudojama dydžio atskyrimo chromatografija (tipiškai rekombinantinio baltymo gryninimo metu). Baltymas yra tirpinamas didelės koncentracijos denatūrantu tirpale ir tada yra atskiriamas pagal dydį nuo bet kokių užsilikusių oligomerinių formų [129]. Yra žinoma, kad A β_{42} rekombinantinė forma greitai agreguoja 37°C temperatūroje, per valandą suformuojant fibriles net ir esant labai mažai peptido koncentracijai [76].

4.2. α -sinukleinas

aSyn yra labiausiai paplitęs baltymas Parkinsono ligos patogenezėje. Dėl aplinkos veiksnių arba skirtingų jį koduojančio geno *SNCA* mutacijų, šis baltymas sudaro įvairius agregatus, kurie pasižymi skirtingomis morfologinėmis savybėmis, antrinės struktūros konformacijomis ir toksišku poveikiu ląstelėms [130]. *In vitro* aSyn agreguoja daug lėčiau nei A β , todėl jis agreguojamas daug didesnėmis koncentracijomis ir dažnai maišant. Nustatyta, kad aSyn gali sudaryti skirtingas fibrilių konformacijas tomis pačiomis reakcijos sąlygomis, ypač esant mažesnei baltymo koncentracijai (50-100 μ M) ir mažesnei buferinio tirpalo joninei jėgai [131].

4.3. Insulinas

Insulinas yra natūralus hormonas, kuris atlieka svarbų vaidmenį reguliuojant cukraus ir riebalų kiekį. Jį sudaro trys alfa spiralės sritys ir dvi peptidinės grandinės, sujungtos disulfidinėmis jungtimis [132]. Dėl didelio prieinamumo ir santykinai nedidelės kainos insulinas yra vienas iš geriausiai ištirtų baltymų biologijoje ir naudojamas kaip modelis įvairiose mokslo disciplinose, įskaitant baltymų agregacijos tyrimus [133-135]. Jis taip pat naudojamas baltymų agregacijos mechanizms tirti bei siekiant atrasti slopiklius prieš insulino sukeltas amiloidozes [56,96,136,137]. Pavyzdžiui, šis baltymas buvo naudojamas tiriant įvairių agregacijos veiksnių, tokių kaip temperatūra, pH ir kitos reakcijos mišinio sąlygos, vaidmenį [114].

Iš daugybės skirtingų sąlygų, kurios yra naudojamos insulino agregacijai tirti, geriausiai žinomas yra insulino fibrilių formavimasis esant žemam pH [114]. Didelis kinetinių eksperimentų patikimumas ir sigmoidinės formos

kreivės tokiomis rūgščiomis reakcijos sąlygomis leidžia supaprastinti baltymų agregaciją ir slopinančių molekulių paiešką [71]. Viena iš insulino agregacijos slopinimo galimybių - naudoti mažas molekules, pavyzdžiui, trumpus peptidus, chemiškai susintetintus junginius ir net antioksidantus, galinčius sąveikauti su insulinu ir užkirsti kelią jo agregacijai [120,138]. Be to, šis baltymas gali būti naudojamas tiriant slopinamąjį poveikį molekulių, kurios nėra stabilios neutraliomis ar fiziologinėmis sąlygomis [56]. Pavyzdžiui, jei molekulė autoksiduojasi arba skyla į skirtingas struktūras aplinkoje, kurioje yra didelė hidroksilo jonų koncentracija, galima užkirsti kelią tolesnei konversijai naudojant žemo pH sąlygas [139]. Taip galima suprasti pradinių, tarpinių ir galutinių produktų poveikį agregacijai. Surinkta informacija gali būti panaudota kuriant naujas, stabilias molekules, kurios gali dalyvauti insulino slopinimo procese [140].

METODAI

5.1. Baltymų gryninimas

Dėl santykinai didelės komerciškai prieinamų peptidų/baltymų kainos ir būtinybės užtikrinti aukštą eksperimentų atkartojamumą, rekombinantinių peptidų/baltymų biosintezė ir gryninimas laikomi geriausiu pasirinkimu, atliekant baltymų agregacijos ir jų slopinimo tyrimus. Šiame darbe aprašytuose eksperimentuose $A\beta_{42}$ ir aSyn buvo sintetinami BL21-star ląstelėse, naudojant ekspresijos vektorius, kaip aprašyta anksčiau išleistame straipsnyje [141].

$A\beta_{42}$ buvo išgrynintas naudojant jonų mainų chromatografijos ir gelfiltracijos metodus. Siekiant užtikrinti patikimą eksperimentinę procedūrą, buvo labai svarbu išvengti peptido agregacijos gryninimo proceso metu ir prieš atliekant kinetinius tyrimus atskirti bet kokias galimas oligomeres formas nuo monomero. Dėl šios priežasties gelfiltracijos procesas buvo pakartotas du kartus.

aSyn yra termostabilus, todėl iš pradžių buvo gryninamas naudojant aukštos temperatūros vandens vonelę (80 laipsnių Celsijaus), kad būtų denatūruota didelė baltymų dalis. Vėliau baltymas nusodintas naudojant 42 % sotųjį amonio sulfato tirpalą. Tai buvo padaryta siekiant sumažinti nukleorūgščių kiekį mėginyje. Tada buvo atlikta jonų mainų ir dydžio išskyrimo chromatografija. Po dializės baltymai buvo liofilizuoti lakiamame amonio bikarbonato buferiniame tirpale. Prieš kinetinius eksperimentus aSyn milteliai buvo ištirpinti reakcijos buferiniame tirpale ir nufiltruoti.

5.2. Baltymų agregacija

Baltymų agregacija buvo stebima naudojant fluorescencinį dažą tioflaviną-T (ThT). ThT turi aiškų sugerties maksimumą ($\lambda = 412$ nm), bet kai jis prisijungia prie fibrilinių agregatų, jo sugerties maksimumas pasislenka į 440-450 nm bangos ilgio diapazoną. Be to, ThT prisijungus prie fibrilinių agregatų, molekulė yra stabilizuojama ir dėl to padidėja jos fluorescencijos intensyvumas ($\lambda = 480$ -490 nm) [84]. Tai leidžia stebėti amiloidinių fibrilių formavimąsi ir augimą laike.

5.3. Kinetinių duomenų analizė

Kinetinių duomenų analizė yra labai svarbi procedūra, padedanti geriau suprasti baltymų agregacijos procesą. Šiame darbe duomenys buvo analizuojami naudojant Origin programinę įrangą, kurioje Boltzmanno lygties funkcija buvo naudojama kinetinėms kreivėms sulyginti ir nustatyti agregacijos puslaikio vertes [142]. Šie parametrai leido palyginti, kaip inhibitoriai veikia agregacijos procesą.

Tolesnė agregacijos analizė atlikta taikant globalią aproksimaciją. Ši matematinė procedūra leidžia apskaičiuoti agregacijos mechanizmo parametrus. Tam pasiekti yra būtina atlikti agregacijos kinetikos tyrimus, esant skirtingoms baltymo koncentracijoms ir taikyti atitinkamus modelio žingsnius. Gautas modelis suteikia informaciją apie pirminį branduolių susidarymą, fibrilių ilgėjimą, fragmentaciją ir antrinę nukleaciją. Tačiau iš gaunamų konstantų negalima daryti išvadų. Kiekviename žingsnyje susidaro fibrilių galai (pirminė ir antrinė nukleacija, fragmentacija), kurie turi įtakos ilgėjimo greičiui, todėl, norint palyginti skirtingus agregacijos mechanizmų procesus, reikia kiekvieną konstantą padauginti iš elongacijos. Galiausiai, sudauginus konstantas, gaunamos kombinuotos greičio konstantos (pirminė nukleacija - elongacija, elongacija - antrinė nukleacija ir elongacija - fragmentacija), kurios leidžia palyginti skirtingų agregacijos mechanizmų pirminės ir antrinės nukleacijos bei fragmentacijos greičius [71,136].

5.4. Baltymų slopinimo tyrimai

Baltymų agregacijos slopinimo efektas yra įvertinamas keliais skirtingais būdais. Pavyzdžiui, galima nustatyti baltymų agregacijos kinetinius parametrus, fibrilių antrinės struktūros ir morfologijos skirtumus, baltymą

agreguojant su inhibitoriumi ir be jo. Tačiau taip pat labai svarbu nustatyti inhibitoriaus stabilumą reakcijos tirpale tam, kad būtų išvengta antrinių procesų, kurie gali pakeisti agregacijos kinetinius parametrus ar susidarantių fibrilių struktūrą. Šiame darbe, baltymų slopinimo tyrimuose buvo naudojamos skirtingos inhibitorių molekules, įskaitant galo rūgštį, EGCG, 64 hidroksiflavonus ir fluorintą benzensulfonamidą (VR16-09).

5.5. Polifenolinių molekulių autoksidacija ir atskyrimas

Dalis šiame darbe naudotų polifenolinių molekulių savaime oksidavosi, jas inkubuojant neutraliame ir baziniame pH. Be EGCG, kuris, kaip žinoma, autoksiduojasi [56], buvo pasirinkti galo rūgštis ir įvairūs hidroksiflavonai, kurie taip pat gali autoksidotis [139]. Siekiant nustatyti, kurios polifenolinės molekules gali modifikuotis reakcijos sąlygomis, procesas buvo stebimas matuojant kiekvieno iš jų sugerties spektrą laike ir vertinant jų spektrų pokyčius.

Autoksidacijos proceso rezultatas gali lemti vienos ar įvairių molekulių susidarymą [143,144]. Tam nustatyti buvo naudojama didelio efektyvumo skysčių chromatografija, kuri leido įvertinti autoksidacijos mišinio kompleksiskumą. Šio darbo metu didelės molekulinės masės molekules buvo išskirtos iš 2',3'-dihidroksiflavono oksidacijos mišinio koncentruojant mėginį membraniniais koncentratoriais (3 kDa riba).

5.6. Atominės jėgos mikroskopija

AJM yra vaizdavimo metodas, naudojamas baltymų agregatams vizualizuoti [145]. Šis metodas žinomas dėl didelės skiriamosios gebos, leidžiančios nustatyti įvairias fibrilinių agregatų ir kitų struktūrų, randamų ant žėručio, charakteristikas. Pradinės morfologinės savybės, tokios kaip aukštis, plotis, ilgis ir fibrilių susisukimo periodiškumas, gali būti naudojamos atskirti skirtingų tipų molekules tame pačiame arba skirtinguose mėginiuose [146]. AJM yra puiki priemonė matuoti inhibitoriaus poveikį susidariusiems agregatams. Ši metodika suteikia galimybę tirti pavienes molekules tame pačiame mėginyje, o tai padeda nustatyti polidispersiskumą ir susidariusių fibrilių polimorfizmą [99].

5.7. Infraraudonųjų spindulių spektroskopija

FTIR spektroskopija yra galinga baltymų struktūros analizės priemonė. Šiuo metodu matuojama mėginio infraraudonųjų spindulių šviesos sugertis ir gaunama informacija apie molekulės antrinę struktūrą. Baltymų antrinės struktūros elementai įvertinami nustatant būdingus baltymo virpesių režimus, analizuojant amidų regionus. Labiausiai naudojamas yra amido I/II regionas, kurio sugerties spektras yra maždaug nuo 1600 cm^{-1} iki 1700 cm^{-1} [147]. Šioje srityje spektras suteikia informacijos apie vandenilinių ryšių konfigūraciją, atspindinčią baltymų antrinės struktūros motyvus, pavyzdžiui, paralelines arba anti-paralelines β -klostes, alfa spirales ir nestruktūrizuotas peptidų sritis. Deja, FTIR spektroskopija neleidžia išskirti pavienių molekulių struktūrų, o veikia suteikia molekulių konformacijų vidurkį [147,148]. Todėl FTIR spektroskopija yra naudojama palyginti atskirų mėginių fibrilių struktūrinius panašumus ir skirtumus.

REZULTATŲ APŽVALGA

6.1. Publikacija 1

Galo rūgšties oksidacijos produktai keičia insulino amiloidinės agregacijos mechanizmą

Tyrimo tikslas - nustatyti galo rūgšties ir jos oksidacijos mišinio slopinamąjį poveikį insulino agregacijos procesui.

Rezultatai - atlikus eksperimentus su galo rūgštimi (GA) ir jos autoksiduota forma (GAO), paaiškėjo, kad ilgesnį laiką inkubuojant galo rūgštį neutraliame pH, pasikeičia mėginio spalva ir poveikis insulino agregacijai. GA neturėjo reikšmingos įtakos agregacijos puslaikiui ir insulino agregacijos mechanizmui. Vis dėlto slopinimo poveikis pasireiškė naudojant GAO, kuri pailgino agregacijos puslajį, naudojant skirtingas slopiklio koncentracijas. Kinetinės konstantos gautos iš globalios aproksimacijos (pirminės branduolių susidarymo-ilgėjimo ir ilgėjimo-fragmentacijos) turėjo atvirkščią priklausomybę nuo GAO kiekio reakcijos mišinyje (kuo didesnė GAO koncentracija, tuo lėtesni nukleacijos ir fragmentacijos procesai). Abu junginiai (GA ir GAO) neturėjo įtakos kombinuotai ilgėjimo – antrinės nukleacijos greičio konstantai.

Pridėjus GAO, pasikeitė insulino fibrilių agregacijos mechanizmas. Tai lėmė stipriai padidėjusį ThT fluorescencijos intensyvumą ir kitokią susidariusių fibrilių struktūrą, nustatytą FTIR metodu. AJM ir FTIR parodė, kad GAO neleidžia susidaryti LCF ir vietoje to pakeičia agregacijos mechanizmą susidarant HCF (žr. 3.2 skyrelį).

Išvados - galo rūgštis neslopina insulino agregacijos žemame pH. Tačiau jei galo rūgštis yra iš anksto oksiduota, ji lėtina insulino agregacijos procesą, slopinant pirminį branduolių susidarymą ir fragmentaciją.

6.2. Publikacija 2

Nuo koncentracijos priklausomas insulino amiloidinės agregacijos polimorfizmas

Tyrimo tikslas - išsiaiškinti nuo koncentracijos priklausantį insulino agregatų polimorfizmą rūgštinės reakcijos sąlygomis.

Rezultatai - esant 200 - 400 μ M koncentracijai, insulinas suformuoja fibriles, kurių ThT fluorescencijos intensyvumas yra santykinai mažas, o esant

800 - 1000 μM koncentracijai, ThT fluorescencijos intensyvumas yra daug didesnis (~ 10 kartų). Tai lemia susidariusios skirtingos konformacijos agregatai, kurie buvo pavadinti mažos koncentracijos (LCF) ir didelės koncentracijos (HCF) fibrilėmis. Šios fibrilės galėjo replikuoti savo konformaciją, kai buvo pridėta bent 1 % prieš tai suformuotų agregatų. Tačiau esant mažesnei pridėtų fibrilių koncentracijai, fibrilės nereplikavo struktūros, todėl šių agregatų FTIR spektras buvo panašus į susidariusių fibrilių konformaciją toje reakcijos aplinkoje. Naudojant AJM buvo pastebėta, kad LCF fibrilės yra mažesnės ir labiau išsibarsčiusios nei HCF.

Išvados - dvi skirtingos insulino fibrilių konformacijos - LCF ir HCF - gali replikuoti savo struktūrą vykstant fibrilių ilgėjimo procesui (pridėjus didesnę kiekį prieš tai suformuotų fibrilių). Šis procesas nevyksta esant mažesnei agregatų koncentracijai, todėl formuojasi nuo aplinkos priklausomi agregatai.

6.3. Publikacija 3

Autoksidacija pakeičia flavonų anti-amiloidines savybes

Tyrimo tikslas - ištirti mono- ir polihidroksilintų flavonų autoksidacijos procesą ir nustatyti jų poveikį amiloido beta ir insulino fibrilizacijai.

Rezultatai – inkubuojant flavonus pH 8 dalis jų oksidavosi. Pastarieji buvo suskirstyti į dvi dalis: (1) flavonus, turinčius gretimas hidroksilo grupes ir (2) flavonolius (3-hidroksiflavonus) be gretimų hidroksilo grupių.

Insulino agregacija buvo stebima žemame pH, kai flavonai yra stabilūs, o $\text{A}\beta_{42}$ agregacijos procesas buvo atliekamas tik su inkubuotais flavonais, tam kad išvengti šių junginių oksidacijos proceso agregacijos metu. Tik vienas iš 64 tirtų neinkubuotų flavonų turėjo slopinantį poveikį insulino fibrilizacijos procesui, o po inkubacijos šis skaičius išaugo iki 23. Autoksidacijos procesas turėjo įtakos flavonų poveikiui insulino agregacijai, tačiau ne visi autoksidavę junginiai slopino šį procesą. Pavyzdžiui flavonoliai neslopino insulino fibrilizacijos proceso, jei jų struktūroje nebuvo gretimų hidroksilo grupių. $\text{A}\beta_{42}$ atveju, gautas panašus rezultatas, susiejantis slopinamąjį poveikį su jų oksidacijos procesu. Vis dėlto inhibitorių skaičius buvo mažesnis - tik 13 oksiduotų flavonų sulėtino $\text{A}\beta_{42}$ agregacijos puslaidį.

AJM vaizdai parodė, kad stipriausi inhibitoriai limpa prie fibrilių ir inicijuoja šių fibrilių sulipimą tarpusavyje. Ant žėručio rastų struktūrų aukščio pasiskirstymas parodė, kad tiek oligomerinės struktūros, tiek ir fibriliniai dariniai yra aukštesni už kontroliniame mėginyje stebėtas fibriles. FTIR

duomenys parodė galimą $A\beta_{42}$ agregatų, susidariusių su oksiduotu 2',3'-dihidroksiflavonu ir be jo, antrinės struktūros skirtumą.

Išvados - flavonų autoksidacija yra pagrindinis veiksnys, dėl kurio jie slopina insulino ir $A\beta_{42}$ agregaciją. Stipriausias inhibitorius buvo oksiduotas 2',3'-dihidroksiflavonas, kuris abiejų baltymų agregacijos procesus sulėtino mažiausiai du kartus. AJM duomenys parodė, kad oksiduoti flavonai buvo prisijungę prie $A\beta_{42}$ oligomerų ir fibrilių paviršiaus.

6.4. Publikacija 4

Polimerų, turinčių anti-amiloidinių savybių 2',3'-dihidroksiflavono autoksidacijos mišinyje tyrimas

Tyrimo tikslas - ištirti 2'3'-dihidroksiflavono autoksidaciją ir išsiaiškinti, kokios dalelės mėginyje veikia baltymų agregacijos procesą.

Rezultatai - Neoksiduoto 2'3'-dihidroksiflavono HPLC chromatogramoje buvo viena aštri smailė (pradinis junginys), o po autoksidacijos – daug smailių, kurios parodė įvairių skirtingas struktūras turinčių molekulių susidarymą. Atskyrus mėginį į $oDHF_{LW}$ ir $oDHF_{HW}$ frakcijas, pastarosiose buvo tik kelios smailės iš pradinio autoksidacijos mišinio, o viena iš jų buvo labai plati, primenanti eliuojančias įvairias polimerines molekules.

ASyn fibrilizaciją slopino abi frakcijos, tačiau didesnis poveikis santykiniam agregacijos puslaikiui buvo stebimas, kai baltymas buvo agreguojamas su $oDHF_{HW}$. $A\beta_{42}$ atveju $oDHF_{LW}$ neturėjo jokios įtakos šio peptido fibrilizacijos procesui, o $oDHF_{HW}$ pailgino agregacijos puslaikį mažiausiai du kartus. Masių spektrometrijos tyrimai parodė keletą skirtingų masės ir krūvio santykio verčių, kurios svyravo nuo 400 iki 2000, o pastovus jų pasikartojimas buvo $\sim 246,51$ m/z. BMR spektrai papildomai padėjo atskleisti mėginio polidispersiškumą, o tai rodo, kad mišinyje yra įvairaus ilgio ir dispersiškumo polimerų.

AJM vaizduose nustatytos suformuotos $A\beta_{42}$ fibrilės. Esant slopikliui, agregatai matomi su prie jų prisijungusiomis apvalios formos struktūromis. Vien tik inhibitoriaus ($oDHF_{HW}$) mėginio vaizdinyje buvo stebimos dalelės, kurių aukštis siekė iki 15 nm, o tai įrodo polimerų egzistavimą slopiklio mėginyje.

Išvados - 2',3'-dihidroksiflavono autoksidacijos metu susidaro skirtingos molekulinės masės molekulės. $oDHF_{HW}$ frakcijoje rastos polidispersinės polimerinės molekulės pasižymėjo didžiausiu poveikiu $A\beta_{42}$ ir aSyn agregacijos procesui.

6.5. Publikacija 5

Pagrindiniai smegenų skysčio komponentai keičia amiloido beta agregacijos inhibitorių savybes

Tyrimo tikslas - palyginti, kaip epigalokatechin-3-galatas ir VR16-09 veikia $A\beta_{42}$ agregaciją PBS ir dirbtiniame smegenų skysčio mišinyje (aCSF).

Rezultatai - PBS tirpale oksiduotas EGCG padidino $A\beta_{42}$ agregacijos puslaikį ~2 kartus, o VR16-09 neturėjo jokio pastebimo poveikio šiam parametrai. aCSF tirpale, oksiduotas EGCG pagreitino procesą, o VR16-09 padidino agregacijos puslaikį daugiau nei du kartus. $A\beta_{42}$ agreguojant aCSF, nustatytos ilgesnės fibrilės. Be to, aukštesnės fibrilės buvo rastos PBS ($P > 0,01$), lyginant su aCSF, kai reakcijos mišinyje buvo VR16-09 slopiklis.

$A\beta_{42}$ agregaciją pagreitino Ca^{2+} ir Mg^{2+} jonai, bet slopino žmogaus serumo albuminas (HSA) ir glutaminas. Visi aCSF komponentai didino VR16-09 poveikį agregacijai, išskyrus glutaminą. Globalaus matematinio modelio duomenys rodo, kad VR16-09 lėtina pirminio branduolių susidarymo procesą ir kad ši poveikį dar sustiprina tirpale esantis HSA. Be to, VR16-09 pagreitino antrinę nukleaciją, o HSA šį poveikį sumažino. Taip pat, HSA mažino fibrilių fragmentaciją, esant inhibitoriui arba be jo.

Išvados - $A\beta_{42}$ agregacija aCSF tirpale vyksta lėčiau nei PBS buferiniame tirpale. Šį poveikį lemia aCSF komponentų derinys. Abiejų inhibitorių poveikis $A\beta_{42}$ agregacijai šiuose reakcijos mišiniuose buvo skirtingas. aCSF tirpale EGCG neturėjo slopinamojo poveikio, tuo pat metu, VR16-09 turėjo ryškų poveikį $A\beta_{42}$ agregacijos procesui. Remiantis globalios aproksimacijos duomenimis, HSA sulėtino fragmentaciją ir antrinę nukleaciją (kai yra VR16-09), o VR16-09 lėtino pirminės nukleacijos ir greitino antrinės nukleacijos procesus.

IŠVADOS IR ATEITIES PERSPEKTYVOS

Atlikus išsamią baltymų agregacijos slopinimo tyrimų analizę naudojant polifenolines molekules, padarytos kelios išvados. Pirma, hidroksiflavonų autoksidaciją apibrėžia jų struktūra – oksiduojasi tik tie hidroksiflavonai, kurių struktūroje yra gretimos hidroksilo grupės arba hidroksilo grupė 3 pozicijoje (3-hidroksiflavonai). Antra, galo rūgštis ir hidroksiflavonai neturi jokio slopinamojo poveikio insulinui ir $A\beta_{42}$, jeigu jie nėra oksiduoti. Vis dėlto yra keletas išimčių, pavyzdžiui, flavonoliai, neturintys gretimų hidroksilo grupių, 3,3',4'-trihidroksiflavonas, bei 6,7,3',4'-tetrahidroksiflavonas. Galiausiai, vykstant 2',3'-dihidroksiflavono autoksidacijai, susidaro daugybė skirtingų molekulių, iš kurių polimerai yra pagrindiniai agregaciją slopinantys junginiai.

Tiriant $A\beta_{42}$ agregaciją ir šio proceso slopinimą PBS ir aCSF tirpaluose, paaiškėjo, kad slopinančių molekulių atranka *in vitro* yra labai jautri reakcijos mišiniui. Oksiduoto EGCG ir VR16-09 poveikis buvo skirtingas PBS ir aCSF. Oksiduotas EGCG prarado slopinimo poveikį, o VR16-09 tapo geresniu slopikliu vykdant reakciją aCSF. Taip pat, didžioji dalis aCSF komponentų padidino VR16-09 poveikį $A\beta_{42}$ agregacijos procesui.

Atsižvelgiant į visus rezultatus, akivaizdu, kad baltymų agregacijos slopinimo tyrimų metu reikia analizuoti ne tik tiriamojo baltymo fibrilizacijos procesą, bet kartu ir inhibitorių būseną bei jų elgseną artimose fiziologijai sąlygose. Šios išvados leis tinkamai formuoti mūsų dabartinius tyrimus ir panaudoti šias žinias ateities studijoms.

Išvados:

1. Galo rūgštis neturi poveikio insulino agregacijai, tuo tarpu, jos oksiduota forma slopina insulino fibrilizaciją ir pakeičia šio proceso mechanizmą.
2. Hidroksiflavonai neslopina $A\beta_{42}$ ir insulino agregacijos, nebent šie junginiai turi gretimas hidroksigrupes ir autoksiduojasi.
3. 2'3'-dihidroksiflavono audoksidacijos proceso metu formuojasi degradacijos ir polimerizacijos produktai, iš kurių polimeriniai dariniai slopina $A\beta_{42}$ ir α -sinukleino agregacijos procesus.
4. Epigalokatechin-3-galato ir fluorinuoto benzensulfonamido poveikis $A\beta_{42}$ agregacijos procesui yra reikšmingai paveikiamas pagrindinių smegenų skysčio komponentų, iš kurių didžiausią poveikį turi žmogaus serumo albuminas.

REFERENCES/BIBLIOGRAFIJA

1. Przedborski, S.; Vila, M.; Jackson-Lewis, V. Neurodegeneration: What is it and where are we? *J. Clin. Invest.* **2003**, *111*, 3–10, doi:10.1172/JCI200317522.
2. Saberi, S.; Stauffer, J.E.; Schulte, D.J.; Ravits, J. Neuropathology of Amyotrophic Lateral Sclerosis and Its Variants. *Neurol. Clin.* **2015**, *33*, 855–876, doi:10.1016/j.ncl.2015.07.012.
3. Spires-Jones, T.L.; Attems, J.; Thal, D.R. Interactions of pathological proteins in neurodegenerative diseases. *Acta Neuropathol.* **2017**, *134*, 187–205, doi:10.1007/s00401-017-1709-7.
4. Dugger, B.N.; Dickson, D.W. Pathology of neurodegenerative diseases. *Cold Spring Harb. Perspect. Biol.* **2017**, *9*, doi:10.1101/cshperspect.a028035.
5. Raynor, G.; Baslet, G. A historical review of functional neurological disorder and comparison to contemporary models. *Epilepsy Behav. Reports* **2021**, *16*, 100489, doi:10.1016/j.ebr.2021.100489.
6. Yang, H.D.; Kim, D.H.; Lee, S.B.; Young, L.D. History of Alzheimer ' s Disease. **2016**, *15*, 115–121.
7. Gulliver, G. On Fatty Degeneration of the Arteries, with a Note on Some other Fatty Degenerations. *J. R. Soc. Med.* **1843**, *MCT-26*, 86–99, doi:10.1177/095952874302600107.
8. Jennekens, F.G.I. A short history of the notion of neurodegenerative disease. *J. Hist. Neurosci.* **2014**, *23*, 85–94, doi:10.1080/0964704X.2013.809297.
9. Gillham, N.W. Sir Francis Galton and the Birth of Eugenics. *Annu. Rev. Genet.* **2001**, *35*, 83–101, doi:10.1146/annurev.genet.35.102401.090055.
10. Goetz, C.G. The History of Parkinson's Disease: Early Clinical Descriptions and Neurological Therapies. *Cold Spring Harb. Perspect. Med.* **2011**, *1*, a008862–a008862, doi:10.1101/cshperspect.a008862.
11. Drouin, E.; Drouin, G. The first report of Alzheimer's disease. *Lancet Neurol.* **2017**, *16*, 687, doi:10.1016/S1474-4422(17)30258-2.
12. Liberski, P.P.; Gajos, A.; Sikorska, B.; Lindenbaum, S. Kuru, the first human prion disease. *Viruses* **2019**, *11*, doi:10.3390/v11030232.
13. Merriam, A.E.; Aronson, M.K.; Gaston, P.; Wey, S. -L; Katz, I. The Psychiatric Symptoms of Alzheimer's Disease. *J. Am. Geriatr. Soc.* **1988**, *36*, 7–22, doi:10.1111/j.1532-5415.1988.tb03427.x.
14. Breijjeh, Z.; Karaman, R. Comprehensive Review on Alzheimer's Disease: Causes and Treatment. *Molecules* **2020**, *25*, 5789, doi:10.3390/molecules25245789.
15. Selkoe, D.J. Alzheimer's Disease: Genes, Proteins, and Therapy. *Physiol. Rev.* **2001**, *81*, 741–766, doi:10.1152/physrev.2001.81.2.741.
16. Castellani, R.J.; Plascencia-Villa, G.; Perry, G. The amyloid cascade and Alzheimer's disease therapeutics: theory versus observation. *Lab. Investig.* **2019**, doi:10.1038/s41374-019-0231-z.
17. Ehehalt, R.; Keller, P.; Haass, C.; Thiele, C.; Simons, K. Amyloidogenic processing of the Alzheimer β -amyloid precursor protein depends on lipid rafts. *J. Cell Biol.* **2003**, *160*, 113–123, doi:10.1083/jcb.200207113.
18. Baranello, R.J.; Bharani, K.L.; Padmaraju, V.; Chopra, N.; Lahiri, D.K.; Greig, N.H.; Pappolla, M.A.; Sambamurti, K. Amyloid-beta protein clearance and degradation (ABCD) pathways and their role in Alzheimer's disease. *Curr. Alzheimer Res.* **2015**, *12*, 32–46.
19. Viola, K.L.; Klein, W.L. Amyloid β oligomers in Alzheimer's disease pathogenesis, treatment, and diagnosis. *Acta Neuropathol.* **2015**, *129*, 183–206, doi:10.1007/s00401-015-1386-3.
20. Lim, S.; Haque, M.M.; Kim, D.; Kim, D.J.; Kim, Y.K. Cell-based models to investigate Tau aggregation. *Comput. Struct. Biotechnol. J.* **2014**, *12*, 7–13, doi:10.1016/j.csbj.2014.09.011.
21. Pérez-Grijalba, V.; Romero, J.; Pesini, P.; Sarasa, L.; Monleón, I.; San-José, I.; Arbizu,

- J.; Martínez-Lage, P.; Munuera, J.; Ruiz, A.; et al. Plasma A β 42/40 Ratio Detects Early Stages of Alzheimer's Disease and Correlates with CSF and Neuroimaging Biomarkers in the AB25 Study. *J. Prev. Alzheimer's Dis.* **2019**, *6*, 34–41, doi:10.14283/jpad.2018.41.
22. Dumurgier, J.; Schraen, S.; Gabelle, A.; Vercruyse, O.; Bombois, S.; Laplanche, J.L.; Peoc'h, K.; Sablonnière, B.; Kastanenka, K. V.; Delaby, C.; et al. Cerebrospinal fluid amyloid- β 42/40 ratio in clinical setting of memory centers: A multicentric study. *Alzheimer's Res. Ther.* **2015**, *7*, 1–9, doi:10.1186/s13195-015-0114-5.
 23. Hughes, R.C. Parkinson's Disease and its Management. *Bmj* **1994**, *308*, 281, doi:10.1136/bmj.308.6923.281.
 24. Stefanis, L. α -Synuclein in Parkinson's Disease. **2012**, 1–24.
 25. Breydo, L.; Wu, J.W.; Uversky, V.N. α -Synuclein misfolding and Parkinson's disease. *Biochim. Biophys. Acta - Mol. Basis Dis.* **2012**, *1822*, 261–285, doi:10.1016/j.bbadis.2011.10.002.
 26. Blauwendraat, C.; Nalls, M.A.; Singleton, A.B. The genetic architecture of Parkinson's disease. *Lancet Neurol.* **2020**, *19*, 170–178, doi:10.1016/S1474-4422(19)30287-X.
 27. Bloem, B.R.; Okun, M.S.; Klein, C. Parkinson's disease. *Lancet* **2021**, *397*, 2284–2303, doi:10.1016/S0140-6736(21)00218-X.
 28. Marinus, J.; Zhu, K.; Marras, C.; Aarsland, D.; van Hilten, J.J. Risk factors for non-motor symptoms in Parkinson's disease. *Lancet Neurol.* **2018**, *17*, 559–568, doi:10.1016/S1474-4422(18)30127-3.
 29. Anand, A.; Patience, A.A.; Sharma, N.; Khurana, N. The present and future of pharmacotherapy of Alzheimer's disease: A comprehensive review. *Eur. J. Pharmacol.* **2017**, *815*, 364–375, doi:10.1016/j.ejphar.2017.09.043.
 30. Reikatsina, M.; Paladini, A.; Piroli, A.; Zis, P.; Pergolizzi, J. V.; Varrassi, G. Pathophysiology and Therapeutic Perspectives of Oxidative Stress and Neurodegenerative Diseases: A Narrative Review. *Adv. Ther.* **2020**, *37*, 113–139, doi:10.1007/s12325-019-01148-5.
 31. Sweeney, P.; Park, H.; Baumann, M.; Dunlop, J.; Frydman, J.; Kopito, R.; McCampbell, A.; Leblanc, G.; Venkateswaran, A.; Nurmi, A.; et al. Protein misfolding in neurodegenerative diseases: Implications and strategies. *Transl. Neurodegener.* **2017**, *6*, 1–13, doi:10.1186/s40035-017-0077-5.
 32. Mallucci, G.R.; Klenerman, D.; Rubinsztein, D.C. Developing Therapies for Neurodegenerative Disorders: Insights from Protein Aggregation and Cellular Stress Responses. *Annu. Rev. Cell Dev. Biol.* **2020**, *36*, 165–189, doi:10.1146/annurev-cellbio-040320-120625.
 33. Cummings, J.; Lee, G.; Nahed, P.; Kambar, M.E.Z.N.; Zhong, K.; Fonseca, J.; Taghva, K. Alzheimer's disease drug development pipeline: 2022. *Alzheimer's Dement. Transl. Res. Clin. Interv.* **2022**, *8*, doi:10.1002/trc2.12295.
 34. Mehta, D.; Jackson, R.; Paul, G.; Shi, J.; Sabbagh, M. Why do trials for Alzheimer's disease drugs keep failing? A discontinued drug perspective for 2010–2015. *Expert Opin. Investig. Drugs* **2017**, *26*, 735–739, doi:10.1080/13543784.2017.1323868.
 35. Cummings, J. Lessons Learned from Alzheimer Disease: Clinical Trials with Negative Outcomes. *Clin. Transl. Sci.* **2018**, *11*, 147–152, doi:10.1111/cts.12491.
 36. Cheng, B.; Gong, H.; Xiao, H.; Petersen, R.B.; Zheng, L.; Huang, K. Inhibiting toxic aggregation of amyloidogenic proteins: A therapeutic strategy for protein misfolding diseases. *Biochim. Biophys. Acta - Gen. Subj.* **2013**, *1830*, 4860–4871, doi:10.1016/j.bbagen.2013.06.029.
 37. Mathur, S.; Dewitte, S.; Robledo, I.; Isaacs, T.; Stamford, J. Rising to the challenges of clinical trial improvement in Parkinson's disease. *J. Parkinsons. Dis.* **2015**, *5*, 263–268, doi:10.3233/JPD-150541.
 38. Söderbom, G. Status and future directions of clinical trials in Parkinson's disease. *Int. Rev. Neurobiol.* **2020**, *154*, 153–188, doi:10.1016/bs.irm.2020.02.009.
 39. Vaz, M.; Silvestre, S. Alzheimer's disease: Recent treatment strategies. *Eur. J. Pharmacol.* **2020**, *887*, 173554, doi:10.1016/j.ejphar.2020.173554.

40. Couzin-Frankel, J. Alzheimer's drug approval gets a mixed reception. *Science* (80-.). **2023**, *379*, 126–127, doi:10.1126/science.adg6275.
41. Yeo-Teh, N.S.L.; Tang, B.L. A Review of Scientific Ethics Issues Associated with the Recently Approved Drugs for Alzheimer's Disease. *Sci. Eng. Ethics* **2023**, *29*, 1–18, doi:10.1007/s11948-022-00422-0.
42. Srivastava, S.; Ahmad, R.; Khare, S.K. Alzheimer's disease and its treatment by different approaches: A review. *Eur. J. Med. Chem.* **2021**, *216*, 113320, doi:10.1016/j.ejmech.2021.113320.
43. Huang, L.K.; Chao, S.P.; Hu, C.J. Clinical trials of new drugs for Alzheimer disease. *J. Biomed. Sci.* **2020**, *27*, 1–13, doi:10.1186/s12929-019-0609-7.
44. Mangialasche, F.; Solomon, A.; Winblad, B.; Mecocci, P.; Kivipelto, M. Alzheimer's disease: clinical trials and drug development. *Lancet Neurol.* **2010**, *9*, 702–716, doi:10.1016/S1474-4422(10)70119-8.
45. Piton, M.; Hirtz, C.; Desmetz, C.; Milhau, J.; Lajoix, A.D.; Bennys, K.; Lehmann, S.; Gabelle, A. Alzheimer's disease: Advances in drug development. *J. Alzheimer's Dis.* **2018**, *65*, 3–13, doi:10.3233/JAD-180145.
46. Abeysinghe, A.A.D.T.; Deshapriya, R.D.U.S.; Udawatte, C. Alzheimer's disease; a review of the pathophysiological basis and therapeutic interventions. *Life Sci.* **2020**, *256*, 117996, doi:10.1016/j.lfs.2020.117996.
47. Athar, T.; Al Balushi, K.; Khan, S.A. Recent advances on drug development and emerging therapeutic agents for Alzheimer's disease. *Mol. Biol. Rep.* **2021**, *48*, 5629–5645, doi:10.1007/s11033-021-06512-9.
48. Cummings, J.; Ritter, A.; Zhong, K. Clinical Trials for Disease-Modifying Therapies in Alzheimer's Disease: A Primer, Lessons Learned, and a Blueprint for the Future. *J. Alzheimer's Dis.* **2018**, *64*, S3–S22, doi:10.3233/JAD-179901.
49. Panza, F.; Lozupone, M.; Logroscino, G.; Imbimbo, B.P. A critical appraisal of amyloid- β -targeting therapies for Alzheimer disease. *Nat. Rev. Neurol.* **2019**, *15*, 73–88, doi:10.1038/s41582-018-0116-6.
50. Cummings, J.; Lee, G.; Ritter, A.; Sabbagh, M.; Zhong, K. Alzheimer's disease drug development pipeline: 2020. *Alzheimer's Dement. Transl. Res. Clin. Interv.* **2020**, *6*, 1–29, doi:10.1002/trc2.12050.
51. Ji, C.; Sigurdsson, E.M. Current Status of Clinical Trials on Tau Immunotherapies. *Drugs* **2021**, *81*, 1135–1152, doi:10.1007/s40265-021-01546-6.
52. Singh, M.; Kaur, M.; Silakari, O. Flavones: An important scaffold for medicinal chemistry. *Eur. J. Med. Chem.* **2014**, *84*, 206–239, doi:10.1016/j.ejmech.2014.07.013.
53. Rigacci, S.; Stefani, M. Nutraceuticals and amyloid neurodegenerative diseases: A focus on natural phenols. *Expert Rev. Neurother.* **2014**, *15*, 41–52, doi:10.1586/14737175.2015.986101.
54. Doig, A.J.; Derreumaux, P. Inhibition of protein aggregation and amyloid formation by small molecules. *Curr. Opin. Struct. Biol.* **2015**, *30*, 50–56, doi:10.1016/j.sbi.2014.12.004.
55. Pagano, K.; Tomaselli, S.; Molinari, H.; Ragona, L. Natural Compounds as Inhibitors of A β Peptide Aggregation: Chemical Requirements and Molecular Mechanisms. *Front. Neurosci.* **2020**, *14*, 1–18, doi:10.3389/fnins.2020.619667.
56. Sneideris, T.; Sakalauskas, A.; Sternke-Hoffmann, R.; Peduzzo, A.; Ziaunys, M.; Buell, A.K.; Smirnovas, V. The Environment Is a Key Factor in Determining the Anti-Amyloid Efficacy of EGCG. *Biomolecules* **2019**, *9*, 855, doi:10.3390/biom9120855.
57. Zhao, J.; Liang, Q.; Sun, Q.; Chen, C.; Xu, L.; Ding, Y.; Zhou, P. (-)-Epigallocatechin-3-gallate (EGCG) inhibits fibrillation, disaggregates amyloid fibrils of α -synuclein, and protects PC12 cells against α -synuclein-induced toxicity. *RSC Adv.* **2017**, *7*, 32508–32517, doi:10.1039/c7ra03752j.
58. Caruana, M.; Vassallo, N. *Natural Compounds as Therapeutic Agents for Amyloidogenic Diseases*; Vassallo, N., Ed.; Advances in Experimental Medicine and Biology; Springer International Publishing: Cham, 2015; Vol. 863; ISBN 978-3-319-18364-0.
59. Ardah, M.T.; Paleologou, K.E.; Lv, G.; Khair, S.B.A.; Kendi, A.K. Al; Minhas, S.T.;

- Al-Tel, T.H.; Al-Hayani, A.A.; Haque, M.E.; Eliezer, D.; et al. Structure activity relationship of phenolic acid inhibitors of α -synuclein fibril formation and toxicity. *Front. Aging Neurosci.* **2014**, *6*, 1–17, doi:10.3389/fnagi.2014.00197.
60. Liu, Y.; Carver, J.A.; Calabrese, A.N.; Pukala, T.L. Gallic acid interacts with α -synuclein to prevent the structural collapse necessary for its aggregation. *Biochim. Biophys. Acta - Proteins Proteomics* **2014**, *1844*, 1481–1485, doi:10.1016/j.bbapap.2014.04.013.
61. Konar, M.; Bag, S.; Roy, P.; Dasgupta, S. Gallic acid induced dose dependent inhibition of lysozyme fibrillation. *Int. J. Biol. Macromol.* **2017**, *103*, 1224–1231, doi:10.1016/j.ijbiomac.2017.05.158.
62. Liu, Y.; Pukala, T.L.; Musgrave, I.F.; Williams, D.M.; Dehle, F.C.; Carver, J.A. Gallic acid is the major component of grape seed extract that inhibits amyloid fibril formation. *Bioorganic Med. Chem. Lett.* **2013**, *23*, 6336–6340, doi:10.1016/j.bmcl.2013.09.071.
63. Molino, S.; Dossena, M.; Buonocore, D.; Ferrari, F.; Venturini, L.; Ricevuti, G.; Verri, M. Polyphenols in dementia: From molecular basis to clinical trials. *Life Sci.* **2016**, *161*, 69–77, doi:10.1016/j.lfs.2016.07.021.
64. Mereles, D.; Hunstein, W. Epigallocatechin-3-gallate (EGCG) for clinical trials: More Pitfalls than Promises? *Int. J. Mol. Sci.* **2011**, *12*, 5592–5603, doi:10.3390/ijms12095592.
65. Chiti, F.; Dobson, C.M. Protein Misfolding, Functional Amyloid, and Human Disease. *Annu. Rev. Biochem.* **2006**, *75*, 333–366, doi:10.1146/annurev.biochem.75.101304.123901.
66. Chiti, F.; Dobson, C.M. Protein Misfolding, Amyloid Formation, and Human Disease: A Summary of Progress Over the Last Decade. *Annu. Rev. Biochem.* **2017**, *86*, 27–68, doi:10.1146/annurev-biochem-061516-045115.
67. Maurer, M.S.; Schwartz, J.H.; Gundapaneni, B.; Elliott, P.M.; Merlini, G.; Waddington-Cruz, M.; Kristen, A. V.; Grogan, M.; Witteles, R.; Damy, T.; et al. Tafamidis Treatment for Patients with Transthyretin Amyloid Cardiomyopathy. *N. Engl. J. Med.* **2018**, *379*, 1007–1016, doi:10.1056/NEJMoa1805689.
68. Elliott, P.; Drachman, B.M.; Gottlieb, S.S.; Hoffman, J.E.; Hummel, S.L.; Lenihan, D.J.; Ebede, B.; Gundapaneni, B.; Li, B.; Sultan, M.B.; et al. Long-Term Survival With Tafamidis in Patients With Transthyretin Amyloid Cardiomyopathy. *Circ. Hear. Fail.* **2022**, *15*, doi:10.1161/CIRCHEARTFAILURE.120.008193.
69. Ambadi Thody, S.; Mathew, M.K.; Udgaonkar, J.B. Mechanism of aggregation and membrane interactions of mammalian prion protein. *Biochim. Biophys. Acta - Biomembr.* **2018**, *1860*, 1927–1935, doi:10.1016/j.bbamem.2018.02.031.
70. Srivastava, K.R.; Lapidus, L.J. Prion protein dynamics before aggregation. *Proc. Natl. Acad. Sci. U. S. A.* **2017**, *114*, 3572–3577, doi:10.1073/pnas.1620400114.
71. Meisl, G.; Kirkegaard, J.B.; Arosio, P.; Michaels, T.C.T.; Vendruscolo, M.; Dobson, C.M.; Linse, S.; Knowles, T.P.J. Molecular mechanisms of protein aggregation from global fitting of kinetic models. *Nat. Protoc.* **2016**, *11*, 252–72, doi:10.1038/nprot.2016.010.
72. Adamcik, J.; Jung, J.M.; Flakowski, J.; De Los Rios, P.; Dietler, G.; Mezzenga, R. Understanding amyloid aggregation by statistical analysis of atomic force microscopy images. *Nat. Nanotechnol.* **2010**, *5*, 423–428, doi:10.1038/nnano.2010.59.
73. Morozova-roche, L.A. Finke – Watzky Two-Step Nucleation – Autocatalysis Model of S100A9 Amyloid Formation: Protein Misfolding as “Nucleation” Event. *ACS Chem. Neurosci.* **2017**, *5*–11, doi:10.1021/acscchemneuro.7b00251.
74. Almeida, Z.L.; Brito, R.M.M. Structure and aggregation mechanisms in amyloids. *Molecules* **2020**, *25*, doi:10.3390/molecules25051195.
75. Mathieu, C.; Pappu, R. V.; Paul Taylor, J. Beyond aggregation: Pathological phase transitions in neurodegenerative disease. *Science (80-.)*. **2020**, *370*, 56–60, doi:10.1126/science.abb8032.
76. Frankel, R.; Törnquist, M.; Meisl, G.; Hansson, O.; Andreasson, U.; Zetterberg, H.; Blennow, K.; Frohm, B.; Cedervall, T.; Knowles, T.P.J.; et al. Autocatalytic

- amplification of Alzheimer-associated A β 42 peptide aggregation in human cerebrospinal fluid. *Commun. Biol.* **2019**, *2*, 365, doi:10.1038/s42003-019-0612-2.
77. Fändrich, M.; Nyström, S.; Nilsson, K.P.R.; Böckmann, A.; LeVine, H.; Hammarström, P. Amyloid fibril polymorphism: a challenge for molecular imaging and therapy. *J. Intern. Med.* **2018**, *283*, 218–237, doi:10.1111/joim.12732.
 78. Zhou, J.; Venturelli, L.; Keiser, L.; Sekatskii, S.K.; Gallaire, F.; Kasas, S.; Longo, G.; Knowles, T.P.J.; Ruggeri, F.S.; Dietler, G. Environmental Control of Amyloid Polymorphism by Modulation of Hydrodynamic Stress. *ACS Nano* **2021**, *15*, 944–953, doi:10.1021/acsnano.0c07570.
 79. Meisl, G.; Xu, C.K.; Taylor, J.D.; Michaels, T.C.T.; Levin, A.; Otzen, D.; Klenerman, D.; Matthews, S.; Linse, S.; Andreasen, M.; et al. Uncovering the universality of self-replication in protein aggregation and its link to disease. *Sci. Adv.* **2022**, *8*, doi:10.1126/sciadv.abn6831.
 80. Törnquist, M.; Michaels, T.C.T.; Sanagavarapu, K.; Yang, X.; Meisl, G.; Cohen, S.I.A.; Knowles, T.P.J.; Linse, S. Secondary nucleation in amyloid formation. *Chem. Commun.* **2018**, *54*, 8667–8684, doi:10.1039/c8cc02204f.
 81. Auer, S. Nucleation of polymorphic amyloid fibrils. *Biophys. J.* **2015**, *108*, 1176–1186, doi:10.1016/j.bpj.2015.01.013.
 82. Arosio, P.; Vendruscolo, M.; Dobson, C.M.; Knowles, T.P.J. Chemical kinetics for drug discovery to combat protein aggregation diseases. *Trends Pharmacol. Sci.* **2014**, *35*, 127–135, doi:10.1016/j.tips.2013.12.005.
 83. Housmans, J.A.J.; Wu, G.; Schymkowitz, J.; Rousseau, F. A guide to studying protein aggregation. *FEBS J.* **2021**, *290*, 554–583, doi:10.1111/febs.16312.
 84. Ziaunys, M.; Mikalauskaite, K.; Smirnovas, V. Amyloidophilic Molecule Interactions on the Surface of Insulin Fibrils: Cooperative Binding and Fluorescence Quenching. *Sci. Rep.* **2019**, *9*, 1–10, doi:10.1038/s41598-019-56788-y.
 85. Streets, A.M.; Sourigues, Y.; Kopito, R.R.; Melki, R.; Quake, S.R. Simultaneous Measurement of Amyloid Fibril Formation by Dynamic Light Scattering and Fluorescence Reveals Complex Aggregation Kinetics. *PLoS One* **2013**, *8*, 1–10, doi:10.1371/journal.pone.0054541.
 86. Zhao, R.; So, M.; Maat, H.; Ray, N.J.; Arisaka, F.; Goto, Y.; Carver, J.A.; Hall, D. Measurement of amyloid formation by turbidity assay—seeing through the cloud. *Biophys. Rev.* **2016**, *8*, 445–471, doi:10.1007/s12551-016-0233-7.
 87. Huang, Y.; Bai, Y.; Jin, W.; Shen, D.; Lyu, H.; Zeng, L.; Wang, M.; Liu, Y. Common Pitfalls and Recommendations for Using a Turbidity Assay to Study Protein Phase Separation. *Biochemistry* **2021**, *60*, 2447–2456, doi:10.1021/acs.biochem.1c00386.
 88. Taylor, C.G.; Meisl, G.; Horrocks, M.H.; Zetterberg, H.; Knowles, T.P.J.; Klenerman, D. Extrinsic Amyloid-Binding Dyes for Detection of Individual Protein Aggregates in Solution. *Anal. Chem.* **2018**, *90*, 10385–10393, doi:10.1021/acs.analchem.8b02226.
 89. Celej, M.S.; Jares-Erijman, E.A.; Jovin, T.M. Fluorescent N-arylaminothalene sulfonate probes for amyloid aggregation of α -synuclein. *Biophys. J.* **2008**, *94*, 4867–4879, doi:10.1529/biophysj.107.125211.
 90. Yakupova, E.I.; Bobyleva, L.G.; Vikhlyantsev, I.M.; Bobylev, A.G. Congo Red and amyloids: History and relationship. *Biosci. Rep.* **2019**, *39*, doi:10.1042/BSR20181415.
 91. Pretorius, E.; Page, M.J.; Hendricks, L.; Nkosi, N.B.; Benson, S.R.; Kell, D.B. Both lipopolysaccharide and lipoteichoic acids potently induce anomalous fibrin amyloid formation: Assessment with novel Amytracker TM stains. *J. R. Soc. Interface* **2018**, *15*, doi:10.1098/rsif.2017.0941.
 92. Schmued, L.; Raymick, J.; Sarkar, S. High Contrast and Resolution Labeling of Amyloid Plaques in Tissue Sections from APP-PS1 Mice and Humans with Alzheimer’s Disease with the Zinc Chelator HQ-O: Practical and Theoretical Considerations. *Curr. Alzheimer Res.* **2019**, *16*, 577–586, doi:10.2174/1567205016666190725155038.
 93. Shin, J.; Verwilt, P.; Choi, H.; Kang, S.; Han, J.; Kim, N.H.; Choi, J.G.; Oh, M.S.; Hwang, J.S.; Kim, D.; et al. Harnessing Intramolecular Rotation To Enhance Two-photon Imaging of A β Plaques through Minimizing Background Fluorescence. *Angew.*

- Chemie* **2019**, *131*, 5704–5708, doi:10.1002/ange.201900549.
94. Buell, A.K.; Dobson, C.M.; Knowles, T.P.J.; Welland, M.E. Interactions between Amyloidophilic dyes and their relevance to studies of amyloid inhibitors. *Biophys. J.* **2010**, *99*, 3492–3497, doi:10.1016/j.bpj.2010.08.074.
 95. Hudson, S.A.; Ecroyd, H.; Kee, T.W.; Carver, J.A. The thioflavin T fluorescence assay for amyloid fibril detection can be biased by the presence of exogenous compounds. *FEBS J.* **2009**, *276*, 5960–5972, doi:10.1111/j.1742-4658.2009.07307.x.
 96. Lindgren, M.; Sörgjerd, K.; Hammarström, P. Detection and Characterization of Aggregates, Prefibrillar Amyloidogenic Oligomers, and Protofibrils Using Fluorescence Spectroscopy. *Biophys. J.* **2005**, *88*, 4200–4212, doi:10.1529/biophysj.104.049700.
 97. Chun, S.Y.; Son, M.K.; Park, C.R.; Lim, C.; Kim, H.I.; Kwak, K.; Cho, M. Direct observation of protein structural transitions through entire amyloid aggregation processes in water using 2D-IR spectroscopy. *Chem. Sci.* **2022**, *13*, doi:10.1039/d1sc06047c.
 98. Martial, B.; Lefèvre, T.; Buffeteau, T.; Auger, M. Vibrational Circular Dichroism Reveals Supramolecular Chirality Inversion of α -Synuclein Peptide Assemblies upon Interactions with Anionic Membranes. *ACS Nano* **2019**, *13*, 3232–3242, doi:10.1021/acsnano.8b08932.
 99. Ruggeri, F.S.; Šneideris, T.; Vendruscolo, M.; Knowles, T.P.J. Atomic force microscopy for single molecule characterisation of protein aggregation. *Arch. Biochem. Biophys.* **2019**, *664*, 134–148, doi:10.1016/j.abb.2019.02.001.
 100. Yu, Z.; Reid, J.C.; Yang, Y.P. Utilizing dynamic light scattering as a process analytical technology for protein folding and aggregation monitoring in vaccine manufacturing. *J. Pharm. Sci.* **2013**, *102*, 4284–4290, doi:10.1002/jps.23746.
 101. Herling, T.W.; Levin, A.; Saar, K.L.; Dobson, C.M.; Knowles, T.P.J. Microfluidic approaches for probing amyloid assembly and behaviour. *Lab Chip* **2018**, *18*, 999–1016, doi:10.1039/C7LC01241A.
 102. DiMemmo, L.M.; Cameron Varano, A.; Haulenbeek, J.; Liang, Y.; Patel, K.; Dukes, M.J.; Zheng, S.; Hubert, M.; Piccoli, S.P.; Kelly, D.F. Real-time observation of protein aggregates in pharmaceutical formulations using liquid cell electron microscopy. *Lab Chip* **2017**, *17*, 315–322, doi:10.1039/C6LC01160H.
 103. Ignatova, Z.; Gierasch, L.M. Monitoring protein stability and aggregation in vivo by real-time fluorescent labeling. *Proc. Natl. Acad. Sci. U. S. A.* **2004**, *101*, 523–528, doi:10.1073/pnas.0304533101.
 104. Sasaki, R.; Tainaka, R.; Ando, Y.; Hashi, Y.; Deepak, H. V.; Suga, Y.; Murai, Y.; Anetai, M.; Monde, K.; Ohta, K.; et al. An automated microliter-scale high-throughput screening system (MSHTS) for real-time monitoring of protein aggregation using quantum-dot nanoprobes. *Sci. Rep.* **2019**, *9*, 1–9, doi:10.1038/s41598-019-38958-0.
 105. Hora, M.; Carballo-Pacheco, M.; Weber, B.; Morris, V.K.; Wittkopf, A.; Buchner, J.; Strodel, B.; Reif, B. Epigallocatechin-3-gallate preferentially induces aggregation of amyloidogenic immunoglobulin light chains. *Sci. Rep.* **2017**, *7*, 1–12, doi:10.1038/srep41515.
 106. Ami, D.; Mereghetti, P.; Natalello, A. Contribution of Infrared Spectroscopy to the Understanding of Amyloid Protein Aggregation in Complex Systems. *Front. Mol. Biosci.* **2022**, *9*, 1–7, doi:10.3389/fmolb.2022.822852.
 107. Szulc, N.; Burdukiewicz, M.; Gašior-Głogowska, M.; Wojciechowski, J.W.; Chilimoniuk, J.; Mackiewicz, P.; Šneideris, T.; Smirnovas, V.; Kotulska, M. Bioinformatics methods for identification of amyloidogenic peptides show robustness to misannotated training data. *Sci. Rep.* **2021**, *11*, 8934, doi:10.1038/s41598-021-86530-6.
 108. Lutter, L.; Al-Hilaly, Y.K.; Serpell, C.J.; Tuite, M.F.; Wischik, C.M.; Serpell, L.C.; Xue, W.F. Structural Identification of Individual Helical Amyloid Filaments by Integration of Cryo-Electron Microscopy-Derived Maps in Comparative Morphometric Atomic Force Microscopy Image Analysis. *J. Mol. Biol.* **2022**, *434*, 167466, doi:10.1016/j.jmb.2022.167466.

109. Heise, H.; Hoyer, W.; Becker, S.; Andronesi, O.C.; Riedel, D.; Baldus, M. Molecular-level secondary structure, polymorphism, and dynamics of full-length α -synuclein fibrils studied by solid-state NMR. *Proc. Natl. Acad. Sci. U. S. A.* **2005**, *102*, 15871–15876, doi:10.1073/pnas.0506109102.
110. Ragonis-Bachar, P.; Landau, M. Functional and pathological amyloid structures in the eyes of 2020 cryo-EM. *Curr. Opin. Struct. Biol.* **2021**, *68*, 184–193, doi:10.1016/j.sbi.2021.01.006.
111. Mastrangelo, I.A.; Ahmed, M.; Sato, T.; Liu, W.; Wang, C.; Hough, P.; Smith, S.O. High-resolution atomic force microscopy of soluble A β 42 oligomers. *J. Mol. Biol.* **2006**, *358*, 106–119, doi:10.1016/j.jmb.2006.01.042.
112. Krasnoslobodtsev, A. V.; Deckert-Gaudig, T.; Zhang, Y.; Deckert, V.; Lyubchenko, Y.L. Polymorphism of amyloid fibrils formed by a peptide from the yeast prion protein Sup35: AFM and Tip-Enhanced Raman Scattering studies. *Ultramicroscopy* **2016**, *165*, 26–33, doi:10.1016/j.ultramic.2016.03.011.
113. Moran, S.D.; Zanni, M.T. How to Get Insight into Amyloid Structure and Formation from Infrared Spectroscopy. *J. Phys. Chem. Lett.* **2014**, *5*, 1984–1993, doi:10.1021/jz500794d.
114. Sneideris, T.; Darguzis, D.; Botyriute, A.; Grigaliunas, M.; Winter, R.; Smirnovas, V. PH-driven polymorphism of insulin amyloid-like fibrils. *PLoS One* **2015**, *10*, e0136602, doi:10.1371/journal.pone.0136602.
115. Stuart, B. *Infrared Spectroscopy: Fundamentals and applications*; 2005;
116. Hume, S.; Hithell, G.; Greetham, G.M.; Donaldson, P.M.; Towrie, M.; Parker, A.W.; Baker, M.J.; Hunt, N.T. Measuring proteins in H₂O with 2D-IR spectroscopy. *Chem. Sci.* **2019**, *10*, 6448–6456, doi:10.1039/C9SC01590F.
117. Gauglitz, G.; Moore, D.S. *Handbook of spectroscopy; 2nd ed.*; 2014; ISBN 9783527330041.
118. Iconomidou, V.A.; Chryssikos, D.G.; Gionis, V.; Pavlidis, M.A.; Paipetis, A.; Hamodrakas, S.J. Secondary structure of chorion proteins of the teleostean fish Dentex dentex by ATR FT-IR and FT-Raman spectroscopy. *J. Struct. Biol.* **2000**, *132*, 112–122, doi:10.1006/jbsi.2000.4307.
119. Requena, J.R.; Wille, H. The structure of the infectious prion protein: experimental data and molecular models. *Prion* **2014**, *8*, 60–6, doi:10.4161/pri.28368.
120. Hadi Ali Janvand, S.; Ladefoged, L.K.; Zubrienė, A.; Sakalauskas, A.; Christiansen, G.; Dudutienė, V.; Schiøtt, B.; Matulis, D.; Smirnovas, V.; Otzen, D.E. Inhibitory effects of fluorinated benzenesulfonamides on insulin fibrillation. *Int. J. Biol. Macromol.* **2023**, *227*, 590–600, doi:10.1016/j.ijbiomac.2022.12.105.
121. Gouras, G.K.; Tampellini, D.; Takahashi, R.H.; Capetillo-Zarate, E. Intraneuronal β -amyloid accumulation and synapse pathology in Alzheimer's disease. *Acta Neuropathol.* **2010**, *119*, 523–541, doi:10.1007/s00401-010-0679-9.
122. Shim, G.; Kim, D.; Park, G.T.; Jin, H.; Suh, S.-K.; Oh, Y.-K. Therapeutic gene editing: delivery and regulatory perspectives. *Acta Pharmacol. Sin.* **2017**, *38*, 738–753, doi:10.1038/aps.2017.2.
123. Kodali, R.; Williams, A.D.; Chemuru, S.; Wetzell, R. A β (1–40) Forms Five Distinct Amyloid Structures whose β -Sheet Contents and Fibril Stabilities Are Correlated. *J. Mol. Biol.* **2010**, *401*, 503–517, doi:10.1016/j.jmb.2010.06.023.
124. Itkin, A.; Dupres, V.; Dufrière, Y.F.; Bechinger, B.; Ruyschaert, J.-M.; Raussens, V. Calcium Ions Promote Formation of Amyloid β -Peptide (1–40) Oligomers Causally Implicated in Neuronal Toxicity of Alzheimer's Disease. *PLoS One* **2011**, *6*, e18250, doi:10.1371/journal.pone.0018250.
125. Ryan, T.M.; Caine, J.; Mertens, H.D.T.; Kirby, N.; Nigro, J.; Breheney, K.; Waddington, L.J.; Streltsov, V.A.; Curtain, C.; Masters, C.L.; et al. Ammonium hydroxide treatment of A β produces an aggregate free solution suitable for biophysical and cell culture characterization. *PeerJ* **2013**, *1*, e73, doi:10.7717/peerj.73.
126. Fezoui, Y.; Hartley, D.M.; Harper, J.D.; Khurana, R.; Walsh, D.M.; Condron, M.M.; Selkoe, D.J.; Lansbury, P.T.; Fink, A.L.; Teplow, D.B. An improved method of preparing the amyloid β -protein for fibrillogenesis and neurotoxicity experiments.

- Amyloid* **2000**, *7*, 166–178, doi:10.3109/13506120009146831.
127. Stine, W.B.; Jungbauer, L.; Yu, C.; LaDu, M.J. Preparing Synthetic A β in Different Aggregation States. In; 2010; pp. 13–32.
 128. Fallor, P.; Hureau, C. Reproducibility Problems of Amyloid- β Self-Assembly and How to Deal With Them. *Front. Chem.* **2021**, *8*, doi:10.3389/fchem.2020.611227.
 129. Walsh, D.M.; Thulin, E.; Minogue, A.M.; Gustavsson, N.; Pang, E.; Teplow, D.B.; Linse, S. A facile method for expression and purification of the Alzheimer's disease-associated amyloid β -peptide. *FEBS J.* **2009**, *276*, 1266–1281, doi:10.1111/j.1742-4658.2008.06862.x.
 130. Kalia, L. V.; Lang, A.E. Parkinson's disease. *Lancet* **2015**, *386*, 896–912, doi:10.1016/S0140-6736(14)61393-3.
 131. Ziaunys, M.; Sakalauskas, A.; Mikalauskaite, K.; Smirnovas, V. Polymorphism of Alpha-Synuclein Amyloid Fibrils Depends on Ionic Strength and Protein Concentration. *Int. J. Mol. Sci.* **2021**, *22*, 12382, doi:10.3390/ijms222212382.
 132. Weiss, M.A. Chapter 2 The Structure and Function of Insulin. Decoding the TR Transition. In *Vitamins and Hormones*; Elsevier Inc., 2009; Vol. 80, pp. 33–49 ISBN 9780123744081.
 133. Gong, H.; He, Z.; Peng, A.; Zhang, X.; Cheng, B.; Sun, Y.; Zheng, L.; Huang, K. Effects of several quinones on insulin aggregation. *Sci. Rep.* **2014**, *4*, 1–8, doi:10.1038/srep05648.
 134. Jayamani, J.; Shanmugam, G. Gallic acid, one of the components in many plant tissues, is a potential inhibitor for insulin amyloid fibril formation. *Eur. J. Med. Chem.* **2014**, *85*, 352–358, doi:10.1016/j.ejmech.2014.07.111.
 135. Malisauskas, R.; Botyriute, A.; Cannon, J.G.; Smirnovas, V. Flavone derivatives as inhibitors of insulin amyloid-like fibril formation. *PLoS One* **2015**, *10*, e0121231, doi:10.1371/journal.pone.0121231.
 136. Ziaunys, M.; Sneideris, T.; Smirnovas, V. Self-inhibition of insulin amyloid-like aggregation. *Phys. Chem. Chem. Phys.* **2018**, *20*, 27638–27645, doi:10.1039/c8cp04838j.
 137. Ziaunys, M.; Mikalauskaite, K.; Sakalauskas, A.; Smirnovas, V. Interplay between epigallocatechin-3-gallate and ionic strength during amyloid aggregation. *PeerJ* **2021**, *9*, e12381, doi:10.7717/peerj.12381.
 138. Hong, Y.; Meng, L.; Chen, S.; Leung, C.W.T.; Da, L.T.; Faisal, M.; Silva, D.A.; Liu, J.; Lam, J.W.Y.; Huang, X.; et al. Monitoring and inhibition of insulin fibrillation by a small organic fluorogen with aggregation-induced emission characteristics. *J. Am. Chem. Soc.* **2012**, *134*, 1680–1689, doi:10.1021/ja208720a.
 139. Bijlsma, J.; de Bruijn, W.J.C.; Velikov, K.P.; Vincken, J.P. Unravelling discolouration caused by iron-flavonoid interactions: Complexation, oxidation, and formation of networks. *Food Chem.* **2022**, *370*, 131292, doi:10.1016/j.foodchem.2021.131292.
 140. Matos, A.M.; Cristóvão, J.S.; Yashunsky, D. V.; Nifantiev, N.E.; Viana, A.S.; Gomes, C.M.; Rauter, A.P. Synthesis and effects of flavonoid structure variation on amyloid- β aggregation. *Pure Appl. Chem.* **2017**, *89*, 1305–1320, doi:10.1515/pac-2017-0201.
 141. Šneideris, T.; Baranauskienė, L.; Cannon, J.G.; Rutkienė, R.; Meškys, R.; Smirnovas, V. Looking for a generic inhibitor of amyloid-like fibril formation among flavone derivatives. *PeerJ* **2015**, *2015*, 1–17, doi:10.7717/peerj.1271.
 142. Walz, D.; Caplan, S.R. *Nonequilibrium Thermodynamics and Fluctuation Kinetics*; Brenig, L., Brilliantov, N., Tlidi, M., Eds.; Fundamental Theories of Physics; Springer International Publishing: Cham, 2022; Vol. 208; ISBN 978-3-031-04457-1.
 143. Ishii, T.; Mori, T.; Tanaka, T.; Mizuno, D.; Yamaji, R.; Kumazawa, S.; Nakayama, T.; Akagawa, M. Covalent modification of proteins by green tea polyphenol (-)-epigallocatechin-3-gallate through autoxidation. *Free Radic. Biol. Med.* **2008**, *45*, 1384–1394, doi:10.1016/j.freeradbiomed.2008.07.023.
 144. Tulyathan, V.; Boulton, R.B.; Singleton, V.L. Oxygen Uptake by Gallic Acid as a Model for Similar Reactions in Wines. *J. Agric. Food Chem.* **1989**, *37*, 844–849, doi:10.1021/jf00088a002.
 145. Simone Ruggeri, F.; Habchi, J.; Cerreta, A.; Dietler, G. AFM-Based Single Molecule

- Techniques: Unraveling the Amyloid Pathogenic Species. *Curr. Pharm. Des.* **2016**, *22*, 3950–3970, doi:10.2174/1381612822666160518141911.
146. Banerjee, S.; Sun, Z.; Hayden, E.Y.; Teplow, D.B.; Lyubchenko, Y.L. Nanoscale Dynamics of Amyloid β -42 Oligomers As Revealed by High-Speed Atomic Force Microscopy. *ACS Nano* **2017**, *11*, 12202–12209, doi:10.1021/acsnano.7b05434.
 147. Barth, A. Infrared spectroscopy of proteins. *Biochim. Biophys. Acta - Bioenerg.* **2007**, *1767*, 1073–1101, doi:10.1016/j.bbabi.2007.06.004.
 148. KONG, J.; YU, S. Fourier Transform Infrared Spectroscopic Analysis of Protein Secondary Structures. *Acta Biochim. Biophys. Sin. (Shanghai)*. **2007**, *39*, 549–559, doi:10.1111/j.1745-7270.2007.00320.x.
 149. Galanakis, M.C. *Polyphenols: Properties, Recovery, and Applications*; 2018;
 150. Zhang, H.; Tsao, R. Dietary polyphenols, oxidative stress and antioxidant and anti-inflammatory effects. *Curr. Opin. Food Sci.* **2016**, *8*, 33–42, doi:10.1016/j.cofs.2016.02.002.
 151. Singh, M.; Silakari, O. *Flavone: An Important Scaffold for Medicinal Chemistry*; Elsevier Ltd, 2018; ISBN 9780081020838.
 152. Es-Safi, N.E.; Ghidouche, S.; Ducrot, P.H. Flavonoids: Hemisynthesis, reactivity, characterization and free radical scavenging activity. *Molecules* **2007**, *12*, 2228–2258, doi:10.3390/12092228.
 153. Costa, C.; Tsatsakis, A.; Mamoulakis, C.; Teodoro, M.; Briguglio, G.; Caruso, E.; Tsoukalas, D.; Margina, D.; Dardiotis, E.; Kouretas, D.; et al. Current evidence on the effect of dietary polyphenols intake on chronic diseases. *Food Chem. Toxicol.* **2017**, *110*, 286–299, doi:10.1016/j.fct.2017.10.023.
 154. Bhullar, K.S.; Rupasinghe, H.P.V. Polyphenols: Multipotent Therapeutic Agents in Neurodegenerative Diseases. *Oxid. Med. Cell. Longev.* **2013**, *2013*, 1–18, doi:10.1155/2013/891748.
 155. Porat, Y.; Abramowitz, A.; Gazit, E. Inhibition of amyloid fibril formation by polyphenols: Structural similarity and aromatic interactions as a common inhibition mechanism. *Chem. Biol. Drug Des.* **2006**, *67*, 27–37, doi:10.1111/j.1747-0285.2005.00318.x.
 156. Molino, S.; Dossena, M.; Buonocore, D.; Ferrari, F.; Venturini, L.; Ricevuti, G.; Verri, M. Polyphenols in dementia: From molecular basis to clinical trials. *Life Sci.* **2016**, *161*, 69–77, doi:10.1016/j.lfs.2016.07.021.
 157. Squillaro, T.; Schettino, C.; Sampaolo, S.; Galderisi, U.; Di Iorio, G.; Giordano, A.; Melone, M.A.B. Adult-onset brain tumors and neurodegeneration: Are polyphenols protective? *J. Cell. Physiol.* **2018**, *233*, 3955–3967, doi:10.1002/jcp.26170.
 158. Phan, H.T.T.; Samarat, K.; Takamur, Y.; Azo-Oussou, A.F.; Nakazono, Y.; Vestergaard, M.C. Polyphenols modulate alzheimer’s amyloid beta aggregation in a structure-dependent manner. *Nutrients* **2019**, *11*, doi:10.3390/nu11040756.
 159. Yu, K.H.; Lee, C.I. Quercetin disaggregates prion fibrils and decreases fibril-induced cytotoxicity and oxidative stress. *Pharmaceutics* **2020**, *12*, 1–10, doi:10.3390/pharmaceutics12111081.
 160. Tan, J.; De Bruijn, W.J.C.; Van Zadelhoff, A.; Lin, Z.; Vincken, J.P. Browning of Epicatechin (EC) and Epigallocatechin (EGC) by Auto-Oxidation. *J. Agric. Food Chem.* **2020**, *68*, 13879–13887, doi:10.1021/acs.jafc.0c05716.
 161. Franko, A.; Rodriguez Camargo, D.C.; Böddrich, A.; Garg, D.; Rodriguez Camargo, A.; Rathkolb, B.; Janik, D.; Aichler, M.; Feuchtinger, A.; Neff, F.; et al. Epigallocatechin gallate (EGCG) reduces the intensity of pancreatic amyloid fibrils in human islet amyloid polypeptide (hIAPP) transgenic mice. *Sci. Rep.* **2018**, *8*, 1116, doi:10.1038/s41598-017-18807-8.
 162. Sato, M.; Murakami, K.; Uno, M.; Nakagawa, Y.; Katayama, S.; Akagi, K.I.; Masuda, Y.; Takegoshi, K.; Irie, K. Site-specific inhibitory mechanism for amyloid β 42 aggregation by catechol-type flavonoids targeting the lys residues. *J. Biol. Chem.* **2013**, *288*, 23212–23224, doi:10.1074/jbc.M113.464222.
 163. Shahinozzaman, M.; Taira, N.; Ishii, T.; Halim, M.A.; Hossain, M.A.; Tawata, S. Anti-inflammatory, anti-diabetic, and anti-Alzheimer’s effects of prenylated flavonoids

- from Okinawa propolis: An investigation by experimental and computational studies. *Molecules* **2018**, *23*, 1–18, doi:10.3390/molecules23102479.
164. Lipinski, C.A. Lead- and drug-like compounds: The rule-of-five revolution. *Drug Discov. Today Technol.* **2004**, *1*, 337–341, doi:10.1016/j.ddtec.2004.11.007.
165. Kim, S.; Kwon, S.; Kam, T.; Panicker, N.; Karuppagounder, S.S.; Lee, S.; Lee, J.H.; Kim, W.R.; Kook, M.; Foss, C.A.; et al. Transneuronal Propagation of Pathologic α -Synuclein from the Gut to the Brain Models Parkinson's Disease. *Neuron* **2019**, *103*, 627–641.e7, doi:10.1016/j.neuron.2019.05.035.
166. Stanyon, H.F.; Viles, J.H. Human Serum Albumin Can Regulate Amyloid- β Peptide Fiber Growth in the Brain Interstitium. *J. Biol. Chem.* **2012**, *287*, 28163–28168, doi:10.1074/jbc.C112.360800.
167. Bode, D.C.; Stanyon, H.F.; Hirani, T.; Baker, M.D.; Nield, J.; Viles, J.H. Serum Albumin's Protective Inhibition of Amyloid- β Fiber Formation Is Suppressed by Cholesterol, Fatty Acids and Warfarin. *J. Mol. Biol.* **2018**, *430*, 919–934, doi:10.1016/j.jmb.2018.01.008.
168. Padayachee, E.R.; Zetterberg, H.; Portelius, E.; Borén, J.; Molinuevo, J.L.; Andreasen, N.; Cukalevski, R.; Linse, S.; Blennow, K.; Andreasson, U. Cerebrospinal fluid-induced retardation of amyloid β aggregation correlates with Alzheimer's disease and the APOE ϵ 4 allele. *Brain Res.* **2016**, *1651*, 11–16, doi:10.1016/j.brainres.2016.09.022.
169. Ashok K., S.; Gabriele, Z. The Interstitial System of the Brain in Health and Disease. *Aging Dis.* **2020**, *11*, 200, doi:10.14336/AD.2020.0103.
170. Serot, J.M.; Christmann, D.; Dubost, T.; Couturier, M. Cerebrospinal fluid transthyretin: Aging and late onset Alzheimer's disease. *J. Neurol. Neurosurg. Psychiatry* **1997**, *63*, 506–508, doi:10.1136/jnnp.63.4.506.
171. Rainesalo, S.; Keränen, T.; Palmio, J.; Peltola, J.; Oja, S.S.; Saransaari, P. Plasma and Cerebrospinal Fluid Amino Acids in Epileptic Patients. *Neurochem. Res.* **2004**, *29*, 319–324, doi:10.1023/B:NERE.0000010461.34920.0c.
172. Di Terlizzi, R.; Platt, S. The function, composition and analysis of cerebrospinal fluid in companion animals: Part I – Function and composition. *Vet. J.* **2006**, *172*, 422–431, doi:10.1016/j.tvjl.2005.07.021.

CURRICULUM VITAE

EDUCATION:

2013 - 2017: Bachelor's degree in Bioengineering, Vilnius Gediminas Technical University, Vilnius, Lithuania.

2017 - 2019: Master's degree in Biochemistry, Vilnius University, Vilnius, Lithuania.

2019 – 2023: PhD studies in Chemical Engineering, Vilnius University, Vilnius, Lithuania

WORK EXPERIENCE:

2016 – now: Sales manager at SIA HPLC Solutions, Marupe, Latvia.

2016 – 2019: Intern at Department of Biothermodynamics and Drug Design, Institute of Biotechnology, Vilnius University, Vilnius, Lithuania.

2017 – now: Product manager at ChromSword, Marupe, Latvia.

2019 – 2020: Senior laboratory assistant at Department of Biothermodynamics and Drug Design, Institute of Biotechnology, Vilnius University, Vilnius, Lithuania.

2020 – now: Junior researcher at Amyloid Research Sector, Institute of Biotechnology, Vilnius University, Vilnius, Lithuania.

PARTICIPATION IN RESEARCH PROJECTS:

2020 – 2021: RCL National Research Programme „Healthy Ageing“ „Cross-interactions in amyloid fibril formation: from mechanisms to inhibition“ (S-SEN-20-3)

2020 – 2023: European Social Fund project operated by Central Project Management Agency „Exploring drug candidates for cancer and neurodegenerative diseases“ (01.2.2-CPVA-K-703-03-0006)

2020 – 2023: European Social Fund project operated by Central Project Management Agency „Exploring drug candidates for cancer and neurodegenerative diseases“ (01.2.2-CPVA-K-703-03-0006)

2020 – 2023: European Structural Fund project „Design of anti-Alzheimer's Drug Candidates that Inhibit BACE1 Enzymatic Activity and Aggregation of A β Peptide“ (01.2.2-LMT-K-718-03-0003)

2022 – 2025: RCL National Research Programme. Research group project
“Protein interactions in amyloid fibril formation: role of the proinflammatory
protein S100A9” (S-MIP-22-115)

LIST OF PUBLICATIONS INCLUDED IN THE DISSERTATION

1. **Sakalauskas, A.**; Ziaunys, M.; Smirnovas, V. Concentration-Dependent Polymorphism of Insulin Amyloid Fibrils. *PeerJ* **2019**, 7, e8208. <https://doi.org/10.7717/peerj.8208>.

Author contribution – I have devised the idea, planned the experiments, performed aggregation kinetic, AFM imaging experiments, scanned FTIR spectra and prepared the methodology sections.

2. **Sakalauskas, A.**; Ziaunys, M.; Smirnovas, V. Gallic Acid Oxidation Products Alter the Formation Pathway of Insulin Amyloid Fibrils. *Sci. Rep.* **2020**, 1–9. <https://doi.org/10.1038/s41598-020-70982-3>.

Author contribution – I have devised the idea, planned the experiments, performed aggregation kinetic and inhibition, AFM imaging experiments, scanned FTIR spectra and prepared the methodology sections.

3. **Sakalauskas, A.**; Ziaunys, M.; Snieckute, R.; Smirnovas, V. Autoxidation Enhances Anti-Amyloid Potential of Flavone Derivatives. *Antioxidants* **2021**, 10, 1428. <https://doi.org/10.3390/antiox10091428>

Author contribution – I have devised the idea, planned the experiments, performed flavone oxidation in time, aggregation kinetic and inhibition, AFM imaging experiments, scanned FTIR spectra. I prepared the initial draft of the publication.

4. **Sakalauskas, A.**; Janoniene, A.; Zvinys, G.; Mikalauskaite, K.; Ziaunys, M.; Smirnovas, V. Exploring the Formation of Polymers with Anti-Amyloid Properties within the 2'3'-Dihydroxyflavone Autoxidation Process. *Antioxidants* **2022**, 11, 1711, [doi:10.3390/antiox11091711](https://doi.org/10.3390/antiox11091711).

Author contribution - I have devised the idea, planned the

experiments, performed aggregation kinetic and inhibition, AFM imaging, performed HPLC separation and inhibitor isolation experiments, scanned FTIR spectra. I prepared the initial draft of the publication.

5. **Sakalauskas, A.**; Ziaunys, M.; Snieckute, R.; Janoniene, A.; Veiveris, D.; Zvirblis, M.; Dudutiene, V.; Smirnovas, V. The Major Components of Cerebrospinal Fluid Dictate the Characteristics of Inhibitors against Amyloid-Beta Aggregation. *Int. J. Mol. Sci.* **2023**, *24*, 5991, doi:10.3390/ijms24065991.

Author contribution – I have decided the idea, planned the experiments, performed aggregation kinetic and inhibition, AFM imaging experiments, formulated the aCSF reaction mixture. I prepared the initial draft of the publication.

LIST OF PUBLICATIONS NOT INCLUDED IN THE
DISSERTATION

1. Sneideris, T.; **Sakalauskas, A.**; Sternke-Hoffmann, R.; Peduzzo, A.; Ziaunys, M.; Buell, A. K.; Smirnovas, V. The Environment Is a Key Factor in Determining the Anti-Amyloid Efficacy of EGCG. *Biomolecules* **2019**, *9* (12), 855. <https://doi.org/10.3390/biom9120855>.
2. Ziaunys, M.; **Sakalauskas, A.**; Smirnovas, V. Identifying Insulin Fibril Conformational Differences by Thioflavin-T Binding Characteristics. *Biomacromolecules* **2020**, *21* (12), 4989–4997. <https://doi.org/10.1021/acs.biomac.0c01178>.
3. Ziaunys, M.; **Sakalauskas, A.**; Sneideris, T.; Smirnovas, V. Lysozyme Fibrils Alter the Mechanism of Insulin Amyloid Aggregation. *Int. J. Mol. Sci.* **2021**, *22* (4), 1775. <https://doi.org/10.3390/ijms22041775>.
4. Jurgelevičiūtė, J.; Bičkovas, N.; **Sakalauskas, A.**; Novickij, V.; Smirnovas, V.; Lastauskienė, E. Effects of Pulsed Electric Fields on Yeast with Prions and the Structure of Amyloid Fibrils. *Appl. Sci.* **2021**, *11* (6), 2684. <https://doi.org/10.3390/app11062684>.
5. Ziaunys, M.; **Sakalauskas, A.**; Mikalauskaite, K.; Smirnovas, V. Exploring the Occurrence of Thioflavin-T-Positive Insulin Amyloid Aggregation Intermediates. *PeerJ* **2021**, *9*, e10918. <https://doi.org/10.7717/peerj.10918>.
6. Ziaunys, M.; **Sakalauskas, A.**; Mikalauskaite, K.; Snieckute, R.; Smirnovas, V. Temperature-Dependent Structural Variability of Prion Protein Amyloid Fibrils. *Int. J. Mol. Sci.* **2021**, *22*, 5075. <https://doi.org/10.3390/ijms22105075>
7. Ziaunys, M.; Mikalauskaite K.; **Sakalauskas, A.**; Smirnovas, V. Using lysozyme amyloid fibrils as a means of scavenging

- aggregation-inhibiting compounds. *Biotechnol J.* **2021**, 2100138, doi: 10.1002/biot.202100138
8. Ziaunys, M.; **Sakalauskas, A.**; Mikalauskaite, K.; Smirnovas, V. Polymorphism of Alpha-Synuclein Amyloid Fibrils Depends on Ionic Strength and Protein Concentration. *Int. J. Mol. Sci.* **2021**, *22*, 12382, doi:10.3390/ijms222212382.
 9. Ziaunys, M.; Mikalauskaite, K.; **Sakalauskas, A.**; Smirnovas, V. Interplay between epigallocatechin-3-gallate and ionic strength during amyloid aggregation. *PeerJ* **2021**, *9*, e12381, doi:10.7717/peerj.12381.
 10. Strazdaite, S.; Roeters, S.J.; **Sakalauskas, A.**; Sneideris, T.; Kirschner, J.; Pedersen, K.B.; Schiøtt, B.; Jensen, F.; Weidner, T.; Smirnovas, V.; et al. Interaction of Amyloid- β -(1–42) Peptide and Its Aggregates with Lipid/Water Interfaces Probed by Vibrational Sum-Frequency Generation Spectroscopy. *J. Phys. Chem. B* **2021**, *125*, 11208–11218, doi:10.1021/acs.jpcc.1c04882.
 11. Zakšauskas, A.; Čapkauskaitė, E.; Paketurytė-Latvė, V.; Smirnov, A.; Leitans, J.; Kazaks, A.; Dvinskis, E.; Stančaitis, L.; Mickevičiūtė, A.; Jachno, J.; **et al.** Methyl 2-halo-4-substituted-5-sulfamoyl-benzoates as high affinity and selective inhibitors of carbonic anhydrase ix. *Int. J. Mol. Sci.* **2022**, *23*, doi:10.3390/ijms23010130.
 12. Ziaunys, M.; Mikalauskaite, K.; Veiveris, D.; **Sakalauskas, A.**; Smirnovas, V. Superoxide dismutase-1 alters the rate of prion protein aggregation and resulting fibril conformation. *Arch. Biochem. Biophys.* **2022**, *715*, 109096, doi:10.1016/j.abb.2021.109096.
 13. Hadi-Alijanvand, S.; Ladefoged, L.K.; Zubrienė, A.; **Sakalauskas, A.**; Christiansen, G.; Dudutiene, V.; Schiott, B.; Matulis, D.; Smirnovas, V.; Otzen, D.E. Inhibitory effects of

Fluorinated Benzenesulfonamides on insulin fibrillation. *Int. J. Biol. Macromol.* 2023, 227, 590–600;
10.1016/j.ijbiomac.2022.12.105

LIST OF SCIENTIFIC EVENTS

Oral presentations:

1. Sakalauskas, A.; Janonienė, A.; Žiaunys, M.; Zvinys, G.; Smirnovas, V. Autoxidation Increases Anti-Amyloid Characteristics of Flavones. amyloid Diseases and Amyloid Mechanisms. Riga, Latvia, 2022

Poster presentations:

2. Andrius Sakalauskas, Mantas Žiaunys, Vytautas Smirnovas. Gallic acid oxidation products possess anti-amyloid properties. International Conference Vita Scientia, Vilnius, Lietuva, 2020;
3. Andrius Sakalauskas, Mantas Žiaunys, Vytautas Smirnovas. Gallic acid oxidation products possess anti-amyloid properties. The Coins, Vilnius, Lietuva, 2020;
4. Andrius Sakalauskas, Vytautas Smirnovas. Autoxidation enhances anti-amyloid potential of flavone derivatives. International Conference on Alzheimer's Drug Discovery, NY, USA, 2021;
5. Andrius Sakalauskas, Vytautas Smirnovas. Flavone oxidation derivatives act as inhibitors of Amyloidbeta aggregation. Open Readings, Vilnius, Lietuva, 2021;
6. Andrius Sakalauskas, Vytautas Smirnovas. Flavone oxidation derivatives act as inhibitors of Amyloidbeta aggregation. The Coins 2021, Vilnius, Lietuva, 2021;
7. Andrius Sakalauskas, Mantas Žiaunys, Gediminas Zvinys, Vytautas Smirnovas. Autoxidation Increases Anti-Amyloid Characteristics of Flavones. Protein phase transitions in ageing and age-related diseases: from atomic resolution to cellular solutions. Roscoff, France, 2022;

8. Andrius Sakalauskas, Mantas Ziaunys, Vytautas Smirnovas. Isolation and characterization of Flavone Oxidation Products Prone to Inhibit Ab and aSyn Aggregation. HPLC 2022, San Diego, CA, USA, 2022 (Laimėtas apdovanojimas už geriausią stendinį pranešimą).

COPIES OF PUBLICATIONS/PUBLIKACIJŲ KOPIJOS



OPEN

Gallic acid oxidation products alter the formation pathway of insulin amyloid fibrils

Andrius Sakalauskas, Mantas Ziaunys & Vytautas Smirnovas[✉]

Amyloidogenic protein assembly into insoluble fibrillar aggregates is linked with several neurodegenerative disorders, such as Alzheimer's or Parkinson's disease, affecting millions of people worldwide. The search for a potential anti-amyloid drug has led to the discovery of hundreds of compounds, none of which have passed all clinical trials. Gallic acid has been shown to both modulate factors leading to the onset of neurodegenerative disorders, as well as directly inhibit amyloid formation. However, the conditions under which this effect is seen could lead to oxidation of this polyphenol, likely changing its properties. Here we examine the effect of gallic acid and its oxidised form on the aggregation of a model amyloidogenic protein—insulin at low pH conditions. We show a vastly higher inhibitory potential of the oxidised form, as well as an alteration in the aggregation pathway, leading to the formation of a specific fibril conformation.

Protein aggregation into highly-structured, beta-sheet rich fibrils is associated with multiple neurodegenerative disorders, such as Alzheimer's, Parkinson's or prion diseases^{1,2}. The prevalence of these diseases is of utmost concern, as there is currently no available drug or effective treatment³. As of right now, there are various potential antibodies, peptides, naturally occurring polyphenolic molecules and other compounds with either direct or indirect anti-amyloid activity^{4–5}. However, a large portion of them are either in initial trials or do not work in vivo and most have not passed the third clinical trial stage⁶.

Tea extracts are known for their beneficial effects on health and a wide variety of compounds present in them have been shown to possess anti-amyloid properties, with one of them being gallic acid (GA)^{7,8}. This simple polyphenol is considered to be able to not only mediate the factors leading to neurodegenerative diseases, such as oxidative stress or inflammation, but also to directly inhibit the formation of amyloid fibrils^{9–22}.

In these experiments, one of the methods used to track the existence or formation of amyloids is an amyloidophilic dye molecule—thioflavin-T (ThT), which fluorescence emission intensity increases significantly when it binds to the beta-sheet grooves on the surface of amyloid fibrils²³. In some cases, where GA or other polyphenolic compounds displayed a reduction in ThT fluorescence, additional examinations by alternative methods, such as transmission electron microscopy, revealed that such a fluorescence inhibition may be related to interference between the dye and inhibitor²⁴. This could be the result of either fluorescence quenching due to molecule interactions or as an inner filter effect, because of the absorbance of ThT emissions by the inhibitor²⁵. Despite this, multiple reports consider the reduction of ThT fluorescence as inhibition of aggregation^{10–12,14,16,17,19,22,26}.

The effect of GA is also usually determined in neutral pH both in vitro and in vivo^{11,12,16,17,19,20,26}. And it is known that it is capable of undergoing oxidation at neutral and higher pH^{26–29}. One report demonstrated that when this process is carried out at pH 7.4, a *o*-quinone is produced and changes in the solution's absorbance spectra can be observed²⁶. In another instance, incubation of GA at neutral pH lead to the formation of a gallic acid dimer³⁰. Oxidation at highly basic conditions was shown to yield ellagic acid³¹. The varying reports make it highly likely that when GA is incubated under neutral conditions, the product may be a mixture of two or more different compounds.

It was shown for other natural polyphenolic compounds, such as EGCG, that oxidation alters their anti-amyloid effects in a positive way^{32,33}. The appearance of new oxidised GA forms could result in the modulation of different aggregation pathways, as well as have higher or lower aggregation inhibition or fibril disassembly potential. In addition, it was shown that during auto-oxidation, some of the reactions could lead to the formation of hydrogen peroxide³⁴. This could, in turn, result in the hydroxylation of ThT and cause the previously

Life Sciences Center, Institute of Biotechnology, Vilnius University, Sauletekio al. 7, 10257 Vilnius, Lithuania. ✉email: vytautas.smirnovas@bti.vu.lt

mentioned reduction in fluorescence intensity³⁵. All of these factors may lead to a false interpretation of the inhibitory potential of GA; therefore, its effect requires further analysis.

A commonly used model protein to examine anti-amyloid compound activity is insulin³⁶. The majority of insulin aggregation studies are carried out at low pH conditions^{14,37–40}, with some being conducted at neutral pH^{41,42}. Depending on the acidity of the solution, insulin can exist as a monomer, dimer, tetramer or hexamer⁴³. This greatly complicates matters when attempting to fit experimental data to an aggregation model, as it needs to account for the formation and existence of these non-monomeric assemblies, which can even directly affect the aggregation process⁴⁴. It is known that insulin exists as a monomer in a 20% acetic acid solution⁴³, which negates the need for the model to account for any oligomeric forms and it can be broken down into four basic steps, which include primary nucleation, fibril elongation, secondary nucleation on the surface of fibrils and fragmentation of aggregates⁴⁵. We have also recently reported that when insulin is aggregated in a 20% acetic acid solution, it forms two distinct fibril conformations, based on the initial concentration of the protein⁴⁶. Fibrils, formed at low protein concentration (further referred as low concentration fibrils or LCF) are short, dispersed and result in a low fluorescence intensity of fibril-bound-ThT, while fibrils formed at high protein concentration (high concentration fibrils or HCF) are longer, clumped together and result in a high fluorescence intensity of fibril-bound-ThT. This creates an additional opportunity to examine whether the effect of GA is dependent on the conformation of aggregates. Such a low pH solution should also prevent or minimize the oxidation of GA, which allows to explore its inhibitory effect without the appearance of any of its oxidised forms.

In this work we examine the effect of GA and how it modulates the mechanism of insulin amyloid aggregation. We show that its oxidation products have a significantly higher inhibitory effect on the formation of primary nuclei and favour a specific insulin fibril conformation.

Methods

Insulin sample preparation. Human recombinant insulin powder (Sigma-Aldrich cat. No. 91077C) was dissolved in a 20% acetic acid solution (prepared from 100% acetic acid; Carl-Roth, cat. No. 3738.1) containing 100 mM NaCl (Fisher cat. No. 10316943, purity > 99.5%), which is further referenced as the reaction solution, to a final concentration of 2 mM (11.6 mg/ml). Samples for unseeded aggregation kinetic measurements were prepared by diluting the 2 mM stock solution to a range of concentrations from 0.2 to 1.0 mM by using the reaction solution, as well as 10 mM ThT (Sigma-Aldrich, cat. No. T3516) and 10 mM gallic acid (TCI Chemicals, cat. No. G0011, purity > 98%) stock solutions (final ThT concentration was 100 μ M in all cases, gallic acid concentration was in the range from 0 to 200 μ M). For seeded aggregation, insulin fibrils, prepared from the 0.2 mM sample (which did not contain gallic acid), were sonicated for 10 min using Sonopuls 3,100 (Bandelin) ultrasonic homogenizer equipped with a MS73 tip (40% power, 30 s sonication/30 s rest intervals). The homogenized fibrils were then mixed with the insulin, gallic acid and ThT stock solutions to yield 0.2 and 1.0 mM unaggregated protein concentration samples containing 100 μ M ThT, and a range of fibril concentrations (from 1 to 10⁻⁶% of total protein mass) with and without 200 μ M gallic acid.

Gallic acid solution preparation. Non-oxidised gallic acid (GA) stock solution was prepared by dissolving 10 mM gallic acid in the reaction solution. Oxidised gallic acid (GAO) stock solution was prepared by dissolving 10 mM gallic acid in a 100 mM sodium phosphate (Carl-Roth, cat. No. P030.3 and T879.2, purity > 99%) buffer (pH 7.4). Oxidation was achieved by incubating the solution at 37 °C for 15 days. Absorbance spectra of GA at the start and end of the reaction were scanned in the range from 250 to 800 nm to confirm changes to its structure (Fig. S1).

Aggregation kinetics. Insulin aggregation kinetics were monitored in non-binding 96-well plates (sample volume was 100 μ L) at 60 °C without agitation by measuring ThT fluorescence emission intensity (excitation wavelength—440 nm, emission—480 nm) through the bottom of the plate, using Synergy H4 Hybrid Multi-Mode (Biotek) microplate reader (readouts were taken every 10 min). For every condition 3 independent measurements were performed. In order to rule out any possible effect ThT may have on the aggregation measurements, the aggregation was simultaneously tracked by ThT fluorescence and sample optical density at 600 nm (Fig. S2). The ThT fluorescence intensity was normalized and the aggregation half-time (t_{50}) values were calculated by applying a linear fit to the data points ranging from 40 to 60% of normalised intensity values and interpolating the time at which 50% of intensity is reached. The increase in t_{50} was used as a main hallmark of inhibition.

Atomic force microscopy (AFM). After kinetic measurements, the sample AFM images were scanned as previously described⁴⁶. In short, 20 μ L of each sample was deposited on freshly cleaved mica and incubated for 1 min. Then the samples were rinsed with MilliQ water and dried under airflow. AFM images were scanned using a Dimension Icon (Bruker) atomic force microscope. The 1,024 × 1,024 pixel resolution images were analysed using Gwyddion 2.55. Fibril length, height and width were determined by tracing parallel and perpendicular to each fibril's axis.

Fourier-transform infrared (FTIR) spectroscopy. Insulin fibrils were separated from solution by centrifugation at 10,000 g for 30 min and subsequently resuspended in 1 mL of D₂O, the procedure was repeated 3 times. After the last centrifugation the fibrils were resuspended in 0.25 mL of D₂O and sonicated for 1 min using a MS72 tip (with 50% power and constant sonication). FTIR spectra were recorded and analysed as previously described⁴⁶.

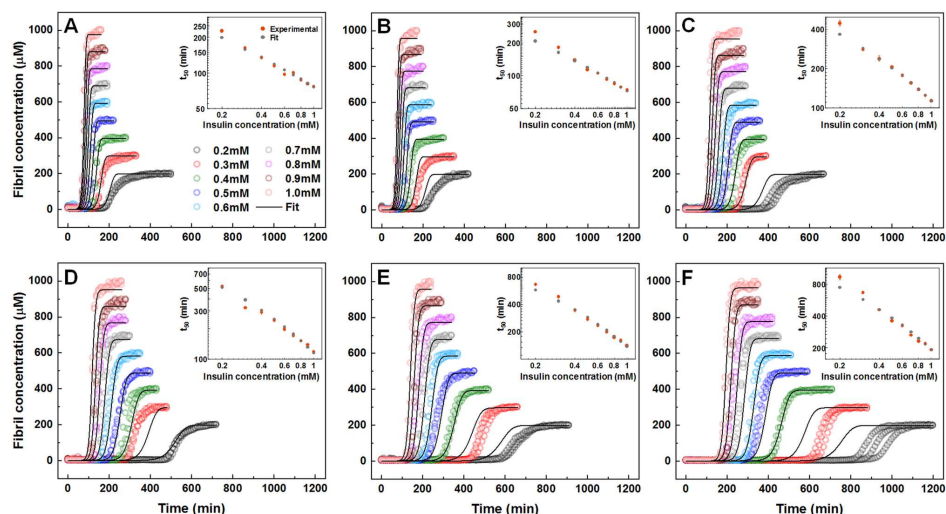


Figure 1. Unseeded aggregation kinetics of insulin without GA (A), with 200 μM GA (B), 25 μM GAO (C), 50 μM GAO (D), 100 μM GAO (E) and 200 μM GAO (F). For each condition, global-fitting was applied using a four-step aggregation model. Inserts show a comparison between t_{50} values obtained from both experimental and global-fit data.

Analysis of aggregation kinetics. Experimental data fitting was done using rModeler (Ubical Software) as described previously⁴⁴ and the model's mathematical framework is provided as supplementary information. In short, a "classic" model comprised of four aggregation steps, including primary nucleation, elongation, secondary nucleation and fragmentation, was applied to fit the kinetic data. Three combined rate constants (primary nucleation-elongation, elongation-secondary nucleation and elongation-fragmentation)^{44,47,48} were obtained for every condition. Each set of kinetic constants is the average of 3 data set fits (insulin concentration is in micromoles; nuclei size is set to 2).

Results

Aggregation kinetics. The aggregation of insulin was performed under a range of protein concentrations from 0.2 to 1.0 mM in a 20% acetic acid solution, containing no GAO or GA (Fig. 1A), with 200 μM GA (Fig. 1B) and with a range of GAO concentrations (Fig. 1C–F). GA had nearly no visible influence on the aggregation half-times, apart from a small effect on the lowest insulin concentrations (Fig. 1A,B). However, when GA was oxidised, the inhibitory effect became much more potent, with larger t_{50} values seen even at low GAO concentrations (Fig. 1C). Double logarithmic plots of the aggregation half-times versus insulin concentrations are linear under all GAO conditions (Fig. 1A–F insets), suggesting that the overall aggregation mechanism remains the same and there are no saturation or competition effects present⁴⁹.

The ThT fluorescence intensity and fibril concentration ratios (sample fluorescence intensity divided by its protein concentration) at the end of the reaction were compared in order to determine if there are any differences (Fig. 2A) when insulin is aggregated in the absence or presence of 200 μM GA or GAO (Fig. S3). GAO leads to a tenfold higher ratio when insulin is aggregated at 0.2 mM concentration, while GA has no effect. In the case of 1.0 mM insulin, the ratio is similar between samples containing no additives or GA and they are only slightly lower when compared to the sample with GAO. In all four cases, the FTIR spectra (Fig. 2B) exhibit a maximum at 1628 cm^{-1} with a shoulder at 1641 cm^{-1} in the amide I/I' region. Three of the four spectra look nearly identical, with 0.2 mM without GAO being the odd one out with the more pronounced shoulder. It is reflected in the second derivative FTIR spectra (Fig. 2C) in a more pronounced minimum and displays a minor shoulder at 1641 cm^{-1} . Moreover, the shoulder at 1620 cm^{-1} is visible in all second order derivative spectra, except the case of 0.2 mM insulin fibrils prepared without GAO. All of this suggests differences in the secondary structure of fibrils. This is in line with the ThT intensity-fibril concentration ratio distribution, which shows that the 0.2 mM sample without GAO is distinct from the rest.

Global fitting of the kinetic curves resulting from a range of protein concentrations at different GAO concentrations reveals that there is a sizeable decrease in the combined primary nucleation-elongation rate constant and a considerable decrease in the combined elongation-fragmentation rate constant, while the combined elongation-secondary nucleation constant experiences minimal changes (Fig. 3, Table S1). In some cases, the

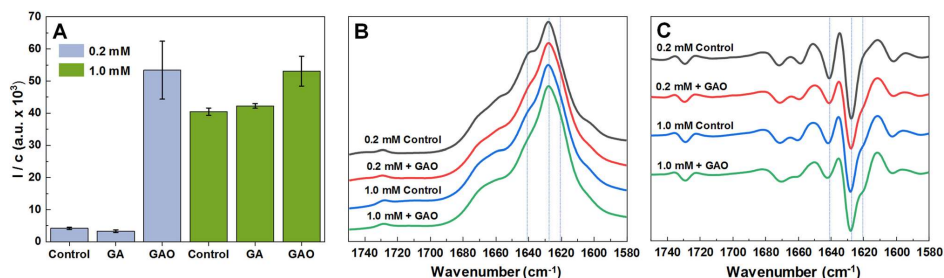


Figure 2. Fluorescence emission intensity and fibril concentration ratios calculated by dividing the sample's fluorescence intensity by its protein concentration (A), FTIR (B) and second derivative spectra (C) of insulin fibrils formed from 0.2 mM and 1.0 mM insulin with or without 200 μ M GAO.

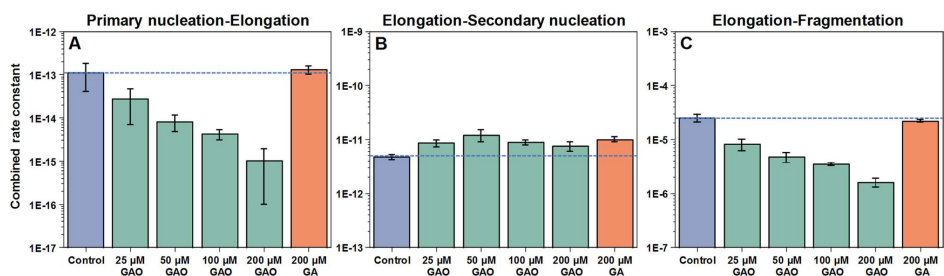


Figure 3. Insulin aggregation primary nucleation-elongation (A), elongation-secondary nucleation (B) and elongation-fragmentation (C) combined rate constants when there is 200 μ M GA or different GAO concentrations present in solution. Rate constants were obtained by global-fitting the entire concentration range (0.2–1.0 mM) of insulin aggregation kinetic data at a specific GA or GAO concentration.

fit is not ideal at low concentrations due to the stochastic nature of insulin aggregation⁵⁰. Non-oxidised GA had nearly no effect on any of the combined rate constants.

Seeded aggregation. To determine whether GAO has an effect on fibril elongation, seeded aggregation (Fig. 4A,B) was performed using fibrils prepared from a 0.2 mM insulin solution (aggregates that possess a relatively low bound-ThT fluorescence). When the amount of seed present in solution is high, GAO has almost no effect on the reaction t_{50} values (Fig. 4C) or the resulting ThT fluorescence intensity (Fig. 4D). This indicates that the seed replicates its structure via elongation and GAO has virtually no influence on this process. However, when the seed concentration is low (10^{-3} – $10^{-6}\%$) and nucleation events have a substantial contribution to the aggregation process, GAO causes a significant increase in both the t_{50} values, as well as bound-ThT fluorescence intensity. This higher intensity is attributed to fibrils formed at 1.0 mM insulin concentration or when GAO is present during spontaneous aggregation. This suggests that the presence of GAO affects predominantly nucleation events and induces the formation of a different fibril conformation.

Fibril morphology. The morphology of insulin fibrils formed at different protein and GA or GAO concentrations was compared using AFM (Fig. 5). In the case of 0.2 mM insulin without GAO (Fig. 5A and Fig. S4) or with 200 μ M GA (Fig. 5B and Fig. S4), the fibrils are mostly dispersed and short. When there is 200 μ M GAO present in the sample (Fig. 5C and Fig. S4), the formed aggregates are longer (Fig. 5G), wider (Fig. 5I) and more prone to self-association, while their average height (Fig. 5H) remains relatively even. In the case of 1.0 mM insulin, all conditions lead to longer fibrils that are prone to self-association (Fig. 5D–F and Fig. S5). There is also a slight increase in their average length (Fig. 5G and Fig. S6). While in both cases length and width experience a GAO concentration-dependent change, there appears to be almost no effect on fibril height (Fig. S6). These GAO-induced changes in morphology further support the hypothesis that GAO alters the pathway of fibril formation, which is especially visible in the case of 0.2 mM insulin.

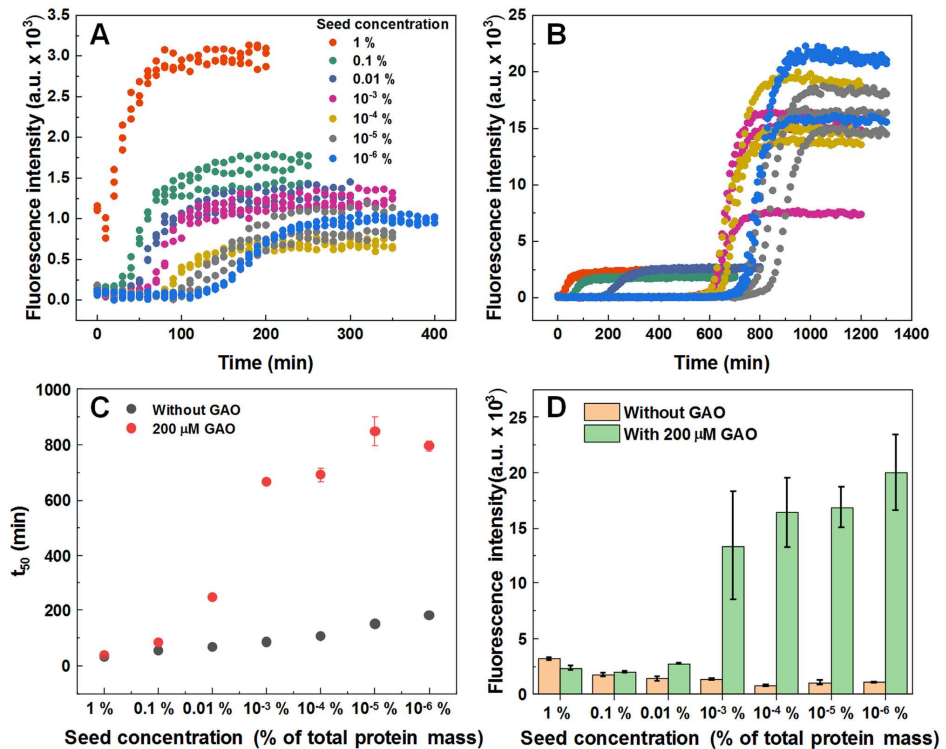


Figure 4. Seeded aggregation kinetic curves of insulin without (A) and with (B) 200 μ M GAO and their t_{50} values (C). The fluorescence intensity of fibrils formed during seeded aggregation with and without 200 μ M GAO (D).

Discussion

The unseeded aggregation kinetic data shows that at low pH values, GA has virtually no effect on insulin aggregation, while GAO inhibits it quite effectively (Fig. 1). This could be the reason why experiments conducted at neutral pH, where GA can undergo oxidation, show an effective inhibition of amyloid formation. Due to this factor, the inhibitory effect can be best analysed using pre-oxidised gallic acid at low pH values, where it no longer experiences any further oxidation.

Fitting the spontaneous aggregation kinetic data with the “classic” aggregation model reveals that GAO most effectively inhibits primary nucleation (Fig. 3A), as 200 μ M GAO results in a 100-fold decrease in the rate of nuclei formation. There is also a considerable decrease in fragmentation rates (Fig. 3C). Despite the massive effect on primary nuclei formation, secondary nucleation appears to be almost unaffected, even at the highest GAO concentrations (Fig. 3B).

A previous report demonstrated that distinct fibril conformations can be formed at 0.2 mM and 1 mM insulin concentrations, termed LCF (low concentration fibrils) and HCF (high concentration fibrils), respectively⁴⁶. When 0.2 mM insulin aggregates in the presence of GAO, the fibril-bound-ThT fluorescence intensity is much higher than typically observed for the LCF conformation, and the intensity-concentration ratio is similar to the HCF conformation (Fig. 2A). It is likely that GAO induces formation of HCF, which is further supported by the differences in secondary structure, as examined by FTIR (Fig. 2B,C), where fibrils formed with GAO possess a similar secondary structure as HCF (Fig. 6A). Interestingly, even the HCF sample ratio experiences a slight increase with the addition of GAO, suggesting that without GAO it likely contains some LCF as well.

Seeded aggregation data shows that at high initial LCF concentrations, GAO has virtually no effect on the t_{50} value (Fig. 4A–C), indicating that it does not affect the rate of elongation (Fig. 6B). At high concentrations, the LCF seed replicates its conformation and we observe no differences in ThT fluorescence intensity between samples with and without GAO (Fig. 4D). However, once the amount of seed reaches a low enough value, there

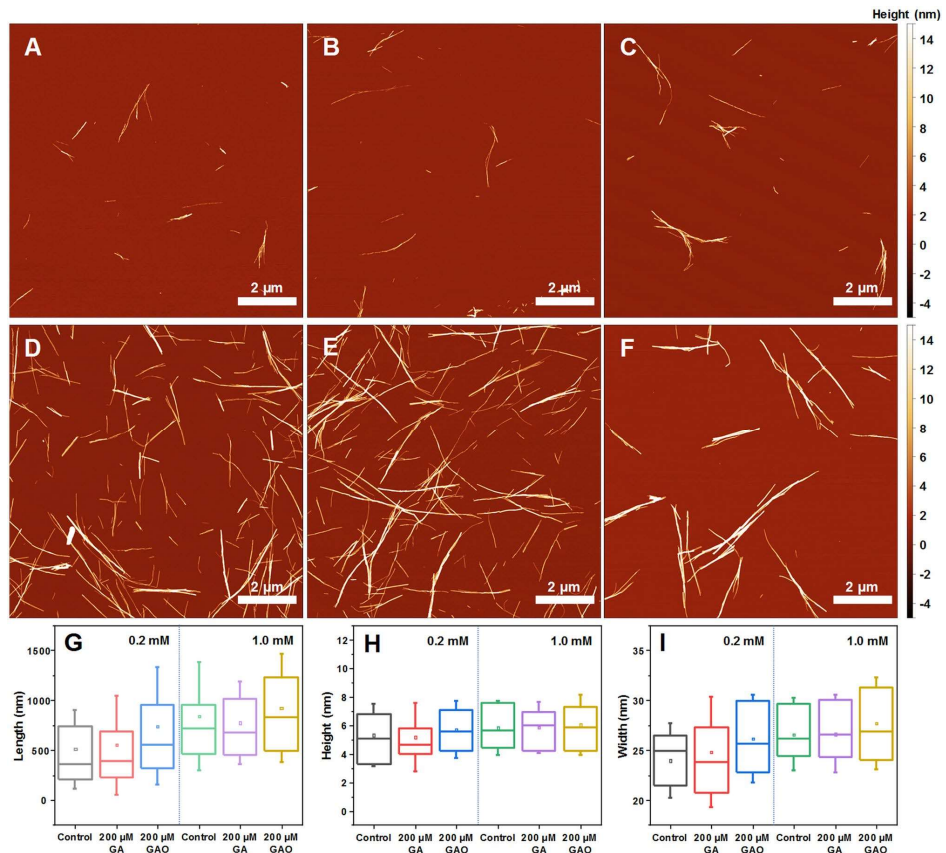


Figure 5. AFM images of insulin fibrils formed without (A, D) and with 200 μM of GA (B, E) or GAO (C, F) at 0.2 mM and 1.0 mM protein concentration respectively. Fibril length (G), height (H) and width (I) distribution, where box plots indicate the interquartile range and errors bars are for 1 standard deviation (n = 50).

is a drastic change in t_{50} values and ThT fluorescence intensities between both conditions, indicating that GAO causes the formation of HCF.

When GAO is present, the dependence of t_{50} on initial seed concentration is not linear on a logarithmic scale. This suggests that the process is more complex and involves not just inhibition of primary nucleation. Since the concentration of seed appears to factor into this effect, it is possible that GAO affects the rate of secondary nucleation on the surface of fibrils (Fig. 6B). However, fitting the data of spontaneous aggregation does not display any significant differences in the combined elongation-secondary nucleation rate constants (Fig. 3B). Considering that the fit model is comprised of four basic aggregation steps, it would be unable to account for any additional processes or inhibitor-fibril interactions. One possible explanation for this effect is that GAO does inhibit secondary nucleation by hiding the accessible surface of fibrils, but its affinity towards the fibril's surface is so low that only a small amount of fibrils can be effectively covered. When more aggregates are present, it is simply incapable of effectively covering the fibril surface area. Seeing as its effect on secondary nucleation diminishes at around 0.01% fibril concentration (Fig. 4C), such a tiny amount of aggregates would likely not be detected in the spontaneous aggregation experiments, which is why fitting their kinetic data shows virtually no effect on secondary nucleation.

If we consider the effect of GAO based on the spontaneous and seeded aggregation kinetic data, it seems that it is potent at inhibiting the formation of nuclei and has no influence on the elongation process. Based on the differences in bound-ThT fluorescence data, as well as AFM images and FTIR spectra, it appears that GAO is also capable of altering the aggregation pathway of these nuclei. Even under conditions which would favour

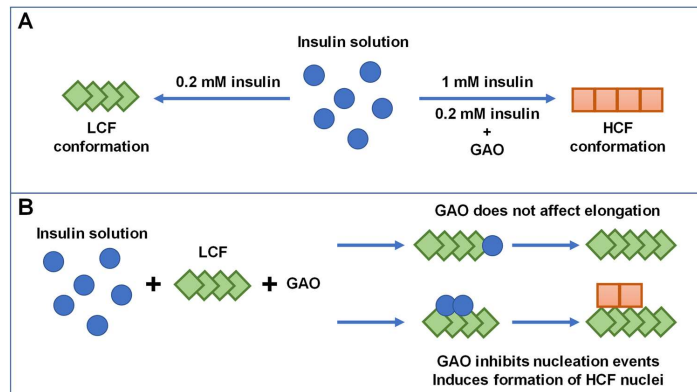


Figure 6. Formation of distinct insulin fibril conformations based on protein concentration and the absence or presence of GAO (A). Effect of GAO on LCF elongation, as well as nucleation events.

the formation of the LCF conformation, GAO manages to alter the fibrillization process towards HCF. The non-oxidised form of GA, on the other hand, has no visible effect on the aggregation kinetics, nor does it change the resulting fibril type.

Conclusions

Gallic acid does not affect the aggregation of insulin at low pH and it only gains its inhibitory potential after undergoing oxidation. The oxidized form is highly effective at inhibiting primary nuclei formation, while having no effect on fibril elongation. It also appears to alter the formation pathway of insulin amyloid aggregation, resulting in HCF even at low protein concentrations.

Data availability

The datasets generated and/or analysed during the current study are available from the corresponding author on reasonable request.

Received: 19 February 2020; Accepted: 5 August 2020

Published online: 02 September 2020

References

- Chiti, F. & Dobson, C. M. Protein misfolding, amyloid formation, and human disease: a summary of progress over the last decade. *Annu. Rev. Biochem.* **86**, 27–68 (2017).
- Knowles, T. P. J., Vendruscolo, M. & Dobson, C. M. The amyloid state and its association with protein misfolding diseases. *Nat. Rev. Mol. Cell Biol.* **15**, 384–396 (2014).
- Cummings, J., Lee, G., Ritter, A., Sabbagh, M. & Zhong, K. Alzheimer's disease drug development pipeline: 2019. *Alzheimer's Dement. Transl. Res. Clin. Interv.* **5**, 272–293 (2019).
- Porat, Y., Abramowitz, A. & Gazit, E. Inhibition of amyloid fibril formation by polyphenols: structural similarity and aromatic interactions as a common inhibition mechanism. *Chem. Biol. Drug Des.* **67**, 27–37 (2006).
- Goyal, D., Shuaib, S., Mann, S. & Goyal, B. Rationally designed peptides and peptidomimetics as inhibitors of amyloid- β (A β) aggregation: potential therapeutics of Alzheimer's disease. *ACS Comb. Sci.* **19**, 55–80 (2017).
- Mehta, D., Jackson, R., Paul, G., Shi, J. & Sabbagh, M. Why do trials for Alzheimer's disease drugs keep failing? A discontinued drug perspective for 2010–2015. *Expert Opin. Investig. Drugs* **26**, 735–739 (2017).
- Fernando, W. *et al.* Diabetes and Alzheimer's disease: can tea phytochemicals play a role in prevention?. *J. Alzheimer's Dis.* **59**, 481–501 (2017).
- Omar, S. H., Scott, C. J., Hamlin, A. S. & Obied, H. K. The protective role of plant biophenols in mechanisms of Alzheimer's disease. *J. Nutr. Biochem.* **47**, 1–20 (2017).
- Hajjipour, S. *et al.* Effect of gallic acid on dementia type of Alzheimer disease in rats: electrophysiological and histological studies. *Basic Clin. Neurosci. J.* **7**, 97–106 (2016).
- Yu, M. *et al.* Gallic acid disruption of A β 1–42 aggregation rescues cognitive decline of APP/PS1 double transgenic mouse. *Neurobiol. Dis.* **124**, 67–80 (2019).
- Liu, Y., Carver, J. A., Calabrese, A. N. & Pukala, T. L. Gallic acid interacts with α -synuclein to prevent the structural collapse necessary for its aggregation. *Biochim. Biophys. Acta Proteins Proteomics* **1844**, 1481–1485 (2014).
- Liu, Y. *et al.* Gallic acid is the major component of grape seed extract that inhibits amyloid fibril formation. *Bioorg. Med. Chem. Lett.* **23**, 6336–6340 (2013).
- Kim, M.-J. *et al.* Gallic acid, a histone acetyltransferase inhibitor, suppresses β -amyloid neurotoxicity by inhibiting microglial-mediated neuroinflammation. *Mol. Nutr. Food Res.* **55**, 1798–1808 (2011).
- Jayamani, J. & Shanmugam, G. Gallic acid, one of the components in many plant tissues, is a potential inhibitor for insulin amyloid fibril formation. *Eur. J. Med. Chem.* **85**, 352–358 (2014).

15. Youn, K. & Jun, M. Inhibitory effects of key compounds isolated from Corni fructus on BACE1 activity. *Phyther. Res.* **26**, 1714–1718 (2012).
16. Chan, S. *et al.* Metal chelation, radical scavenging and inhibition of A β 2 fibrillation by food constituents in relation to Alzheimer's disease. *Food Chem.* **199**, 185–194 (2016).
17. Bastianetto, S., Yao, Z.-X., Papadopoulos, V. & Quirion, R. Neuroprotective effects of green and black teas and their catechin gallate esters against β -amyloid-induced toxicity. *Eur. J. Neurosci.* **23**, 55–64 (2006).
18. Ban, J. Y. *et al.* Neuroprotective properties of gallic acid from sanguisorbae radix on amyloid β protein (25–35)-induced toxicity in cultured rat cortical neurons. *Biol. Pharm. Bull.* **31**, 149–153 (2008).
19. Konar, M., Ghosh, D., Roy, P. & Dasgupta, S. Probing the role of ortho-dihydroxy groups on lysozyme fibrillation. *Int. J. Biol. Macromol.* **109**, 619–628 (2018).
20. Ardah, M. T. *et al.* Structure activity relationship of phenolic acid inhibitors of α -synuclein fibril formation and toxicity. *Front. Aging Neurosci.* **6**, 1–17 (2014).
21. Visentin, C. *et al.* Epigallocatechin-3-gallate and related phenol compounds redirect the amyloidogenic aggregation pathway of ataxin-3 towards non-toxic aggregates and prevent toxicity in neural cells and caenorhabditis elegans animal model. *Hum. Mol. Genet.* **26**, 3271–3284 (2017).
22. Nesi, G. *et al.* Nature-based molecules combined with rivastigmine: a symbiotic approach for the synthesis of new agents against Alzheimer's disease. *Eur. J. Med. Chem.* **141**, 232–239 (2017).
23. Biancalana, M. & Koide, S. Molecular mechanism of Thioflavin-T binding to amyloid fibrils. *Biochim. Biophys. Acta Proteomics Proteomics* **1804**, 1405–1412 (2010).
24. Wong, D. Y. S., Musgrave, I. F., Harvey, B. S. & Smid, S. D. A β 1 (Euterpe oleraceae Mart.) berry extract exerts neuroprotective effects against β -amyloid exposure in vitro. *Neurosci. Lett.* **556**, 221–226 (2013).
25. Ziaunys, M., Mikalauskaitė, K. & Smirnovas, V. Amyloidophilic molecule interactions on the surface of insulin fibrils: cooperative binding and fluorescence quenching. *Sci. Rep.* **9**, 1–10 (2019).
26. Konar, M., Bag, S., Roy, P. & Dasgupta, S. Gallic acid induced dose dependent inhibition of lysozyme fibrillation. *Int. J. Biol. Macromol.* **103**, 1224–1231 (2017).
27. Eslami, A. C., Pasanphan, W., Wagner, B. A. & Buettner, G. R. Free radicals produced by the oxidation of gallic acid: an electron paramagnetic resonance study. *Chem. Cent. J.* **4**, 15 (2010).
28. Vijayalakshmi, G., Adinarayana, M. & Rao, P. J. Kinetics and mechanisms of oxidation of some antioxidants with photochemically generated tert-butoxyl radicals. *Indian J. Biochem. Biophys.* **47**, 292–297 (2010).
29. Caregnato, P. *et al.* Theoretical and experimental investigation on the oxidation of gallic acid by sulfate radical anions. *J. Phys. Chem. A* **112**, 1188–1194 (2008).
30. Honda, S., Ishida, R., Hidaka, K. & Masuda, T. Stability of polyphenols under alkaline conditions and the formation of a xanthine oxidase inhibitor from gallic acid in a solution at pH 7.4. *Food Sci. Technol. Res.* **25**, 123–129 (2019).
31. Tulyathan, V., Boulton, R. B. & Singleton, V. L. Oxygen uptake by gallic acid as a model for similar reactions in wines. *J. Agric. Food Chem.* **37**, 844–849 (1989).
32. An, T.-T., Feng, S. & Zeng, C.-M. Oxidized epigallocatechin gallate inhibited lysozyme fibrillation more strongly than the native form. *Redox Biol.* **11**, 315–321 (2017).
33. Sneideris, T. *et al.* The environment is a key factor in determining the anti-amyloid efficacy of EGCG. *Biomolecules* **9**, 1–17 (2019).
34. Akagawa, M., Shigemitsu, T. & Suyama, K. Production of hydrogen peroxide by polyphenols and polyphenol-rich beverages under quasi-physiological conditions. *Biosci. Biotechnol. Biochem.* **67**, 2632–2640 (2003).
35. Fodera, V. *et al.* Thioflavin T hydroxylation at basic pH and its effect on amyloid fibril detection. *J. Phys. Chem. B* **112**, 15174–15181 (2008).
36. Brange, J., Andersen, L., Laursen, E. D., Meyn, G. & Rasmussen, E. Toward understanding insulin fibrillation. *J. Pharm. Sci.* **86**, 517–525 (1997).
37. Kuroski, D. *et al.* Disulfide bridges remain intact while native insulin converts into amyloid fibrils. *PLoS ONE* **7**, e36989 (2012).
38. Malisaukas, R., Botyriute, A., Cannon, J. G. & Smirnovas, V. Flavone derivatives as inhibitors of insulin amyloid-like fibril formation. *PLoS ONE* **10**, e0121231 (2015).
39. Whittingham, J. L. *et al.* Insulin at pH 2: structural analysis of the conditions promoting insulin fibre formation. *J. Mol. Biol.* **318**, 479–490 (2002).
40. Nie, R., Zhu, W., Peng, J., Ge, Z. & Li, C. Comparison of disaggregative effect of A-type EGCG dimer and EGCG monomer on the preformed bovine insulin amyloid fibrils. *Biophys. Chem.* **230**, 1–9 (2017).
41. Wang, S.-H., Dong, X.-Y. & Sun, Y. Effect of (–)-epigallocatechin-3-gallate on human insulin fibrillation/aggregation kinetics. *Biochem. Eng. J.* **63**, 38–49 (2012).
42. Gong, H. *et al.* Effects of several quinones on insulin aggregation. *Sci. Rep.* **4**, 5648 (2015).
43. Uversky, V. N. *et al.* Prediction of the association state of insulin using spectral parameters. *J. Pharm. Sci.* **92**, 847–858 (2003).
44. Ziaunys, M., Sneideris, T. & Smirnovas, V. Self-inhibition of insulin amyloid-like aggregation. *Phys. Chem. Chem. Phys.* **20**, 27638–27645 (2018).
45. Meisl, G. *et al.* Scaling behaviour and rate-determining steps in filamentous self-assembly. *Chem. Sci.* **8**, 7087–7097 (2017).
46. Sakalauskas, A., Ziaunys, M. & Smirnovas, V. Concentration-dependent polymorphism of insulin amyloid fibrils. *PeerJ* **7**, e8208 (2019).
47. Meisl, G. *et al.* Differences in nucleation behavior underlie the contrasting aggregation kinetics of the A β 40 and A β 42 peptides. *Proc. Natl. Acad. Sci.* **111**, 9384–9389 (2014).
48. Cohen, S. I. A. *et al.* Distinct thermodynamic signatures of oligomer generation in the aggregation of the amyloid- β peptide. *Nat. Chem.* **10**, 523–531 (2018).
49. Meisl, G. *et al.* Molecular mechanisms of protein aggregation from global fitting of kinetic models. *Nat. Protoc.* **11**, 252–272 (2016).
50. Fodera, V., Librizzi, F., Groenning, M., Van De Weert, M. & Leone, M. Secondary nucleation and accessible surface in insulin amyloid fibril formation. *J. Phys. Chem. B* **112**, 3853–3858 (2008).

Acknowledgements

A.S. was supported by a PhD fellowship from European Social Fund (Project No. KD-19076) under Grant agreement with the Research Council of Lithuania.

Author contributions

A.S., M.Z., and V.S. designed the studies. A.S. and M.Z. undertook the experimental work. A.S., M.Z., and V.S. analyzed the data and prepared the manuscript.

Competing interests

The authors declare no competing interests.

Additional information

Supplementary information is available for this paper at <https://doi.org/10.1038/s41598-020-70982-3>.

Correspondence and requests for materials should be addressed to V.S.

Reprints and permissions information is available at www.nature.com/reprints.

Publisher's note Springer Nature remains neutral with regard to jurisdictional claims in published maps and institutional affiliations.



Open Access This article is licensed under a Creative Commons Attribution 4.0 International License, which permits use, sharing, adaptation, distribution and reproduction in any medium or format, as long as you give appropriate credit to the original author(s) and the source, provide a link to the Creative Commons license, and indicate if changes were made. The images or other third party material in this article are included in the article's Creative Commons license, unless indicated otherwise in a credit line to the material. If material is not included in the article's Creative Commons license and your intended use is not permitted by statutory regulation or exceeds the permitted use, you will need to obtain permission directly from the copyright holder. To view a copy of this license, visit <http://creativecommons.org/licenses/by/4.0/>.

© The Author(s) 2020

Concentration-dependent polymorphism of insulin amyloid fibrils

Andrius Sakalauskas, Mantas Ziaunys and Vytautas Smirnovas

Institute of Biotechnology, Life Sciences Center, Vilnius University, Vilnius, Lithuania

ABSTRACT

Protein aggregation into highly structured fibrils has long been associated with several neurodegenerative disorders, such as Alzheimer's or Parkinson's disease. Polymorphism of amyloid fibrils increases the complexity of disease mechanisms and may be one of the reasons for the slow progress in drug research. Here we report protein concentration as another factor leading to polymorphism of insulin amyloid fibrils. Moreover, our data suggests that insulin amyloid conformation can self-replicate only via elongation, while seed-induced nucleation will lead to environment-defined conformation of fibrils. As similar observations were already described for a couple of other amyloid proteins, we suggest it to be a generic mechanism for self-replication of different amyloid fibril conformations.

Subjects Biochemistry, Biophysics

Keywords Amyloid, Insulin, Polymorphism, Fibril, Protein aggregation

INTRODUCTION

Protein aggregation into amyloid fibrils has been linked to multiple neurodegenerative disorders, including Alzheimer's, Parkinson's and infectious prion diseases (*Chiti & Dobson, 2017; Knowles, Vendruscolo & Dobson, 2014*), which affect tens of millions of people worldwide and is predicted to become even more prominent as the average human lifespan continues to increase (*Isik, 2010*). Matters are further complicated by the fact that very few drugs have reached stage four of clinical trials and no efficient treatment or cure is available (*Cummings et al., 2019; Mehta et al., 2017*). One of the main reasons for such limited progress in the development of potential cures may be the complexity of fibril formation mechanisms (*Meisl et al., 2017; Doig et al., 2017; Nasica-Labouze et al., 2015*), as well as polymorphism of amyloid aggregates (*Stein & True, 2014*).

The ability of the same protein to adopt distinct pathogenic conformations was first reported in studies of infectious prions and such conformations were referred to as strains (*Safar et al., 1998; Collinge & Clarke, 2007*). Recently strain-like polymorphism was reported for a number of amyloid proteins in vivo (*Lu et al., 2013; Watts et al., 2014; Fändrich et al., 2018; Yamasaki et al., 2019*), in vitro (*Heise et al., 2005; Paravastu et al., 2008; Debelouchina et al., 2010; Dinkel et al., 2011; Bousset et al., 2013*), and in silico (*Pellarin et al., 2010*). A number of environmental factors including pH (*Sneideris et al., 2015*), temperature (*Tanaka et al., 2006; Colby et al., 2009*), concentration of co-solvents (*Dzvolak et al., 2004; Chatani et al., 2012*), denaturants (*Colby et al., 2009; Cobb et al., 2014*) or salts (*Morel et al., 2010; Bousset et al., 2013*), as well as agitation (*Petkova et al.,*

Submitted 27 September 2019

Accepted 13 November 2019

Published 10 December 2019

Corresponding author
Vytautas Smirnovas,
vytautas@smirnovas.info

Academic editor
Bettina Böttcher

Additional Information and
Declarations can be found on
page 9

DOI 10.7717/peerj.8208

© Copyright
2019 Sakalauskas et al.

Distributed under
Creative Commons CC-BY 4.0

OPEN ACCESS

2005; Ostapchenko et al., 2010) can lead to different conformations of amyloid fibrils. Enormous amounts of data must be collected and analyzed in order to understand the complex effects of the environment on polymorphism of amyloids.

Due to its relatively low cost, wide availability and simple aggregation protocols, insulin became one of the most common proteins used to study amyloid fibril formation. Several years ago, we summarized available data on polymorphism of insulin amyloid fibrils and came with the hypothesis that the number of insulin amyloid conformations may be limited to two and the major factor which determines formation of different strains is a shift of the equilibrium between insulin monomers and dimers (oligomers) (Sneideris et al., 2015). Our current data supports the existence of a third conformation of insulin amyloid fibrils and suggests that polymorphism of insulin amyloid fibrils is more complex.

MATERIALS AND METHODS

Insulin sample preparation

Human recombinant insulin powder (Sigma-Aldrich cat. No. 91077C) was dissolved in a 20% acetic acid solution containing 100 mM NaCl (reaction solution) to a final concentration of 2 mM (11.6 mg/ml). Insulin concentration was determined by measuring the sample's absorbance at 280 nm $\epsilon=6,335 \text{ M}^{-1}\text{cm}^{-1}$, $M = 5808 \text{ Da}$. Samples for unseeded aggregation kinetic measurements were prepared by diluting the 2 mM stock solution using the reaction solution and 10 mM ThT stock solution to a range of concentrations from 0.2 mM to 1.0 mM (which contained 100 μM of ThT). For seeded aggregation, insulin fibrils prepared from the 0.2 mM and 1.0 mM samples were sonicated for 10 min using Sonopuls 3100 (Bandelin) ultrasonic homogenizer equipped with a MS73 tip (40% power, 30 s sonication/ 30 s rest intervals). The homogenized fibrils were then diluted with the reaction solution and mixed with the 2 mM insulin and 10 mM ThT stock solutions to yield 0.2 mM and 1.0 mM concentration samples containing 100 μM ThT and a range of fibril concentrations (from 5% to 10^{-6} % of monomer mass).

Aggregation kinetics

Insulin aggregation kinetics were monitored at 60 °C without agitation by measuring ThT fluorescence emission intensity (excitation wavelength—440 nm, emission—480 nm) through the bottom of a 96 well non-binding surface plate using Synergy H4 Hybrid Multi-Mode (Biotek) plate reader (readouts were taken every 10 min to minimize plate agitation). For every condition, four independent measurements were performed. Aggregation half-times (t_{50}) were calculated as the time needed to reach 50% of signal intensity. The full concentration range of aggregated insulin samples were centrifuged at 10 000 g for 30 min and the residual unaggregated insulin in the supernatant was determined to be less than 1% of initial protein concentration.

Atomic Force Microscopy (AFM)

After kinetic measurements, samples were diluted with the reaction solution to a 50 μM concentration and 20 μL of each was deposited on freshly cleaved mica and incubated for 1 min. Subsequently, samples were rinsed with one mL of MilliQ water and dried under

gentle airflow. Three-dimensional AFM maps were acquired using a Dimension Icon (Bruker) atomic force microscope operating in tapping mode and equipped with a silicon cantilever Tap300AI-G (40 N m^{-1} ; Budget Sensors) with a typical tip radius of curvature of 8 nm. High-resolution ($1,024 \times 1,024$ pixels) images were acquired. The scan rate was 1 Hz. AFM images were flattened and analyzed using SPIP (Image Metrology).

Fourier-Transform Infrared (FTIR) Spectroscopy

Insulin fibrils were separated from solution by centrifugation at 10 000 g for 30 min and subsequently resuspended in one mL of D_2O , the procedure was repeated three times. Then the fibrils were resuspended in 0.2 mL of D_2O and sonicated for 1 min using a MS72 tip (with 20% power and constant sonication). Samples were deposited between two CaF_2 transmission windows separated by 0.05 mm teflon spacers. The FTIR spectra were recorded using Vertex 80v (Bruker) IR spectrometer equipped with a mercury cadmium telluride detector, at room temperature under vacuum (~ 2 mBar) conditions. 256 interferograms of two cm^{-1} resolution were averaged for each spectrum. Spectrum of D_2O was subtracted from the spectrum of each sample. All spectra were normalized to the same area of amide I/I' band ($1,700\text{--}1,595 \text{ cm}^{-1}$). All data processing was performed using GRAMS software.

RESULTS

Fibril formation at different concentrations

Aggregating a range of insulin concentrations in 20% acetic acid with 100 mM NaCl at 60°C without agitation reveals a typical kinetic curve pattern, where an increasing insulin concentration leads to shorter aggregation times (Fig. 1A). However, we observe an uneven ratio distribution between ThT fluorescence emission intensities and final fibril concentrations (Fig. 1B). As the concentration of insulin in the sample increases, this ratio shifts ten-fold, indicating either a higher quantum yield or considerably more bound ThT molecules.

The FTIR spectra of aggregated samples exhibit maxima in the amide I/I' region at $\sim 1,628 \text{ cm}^{-1}$ with the shoulder at $\sim 1,641 \text{ cm}^{-1}$, and a small band outside of the amide I/I' region at $\sim 1,729 \text{ cm}^{-1}$ (Fig. 1C), which is very similar to previously reported insulin fibrils formed in phosphate buffer at $\text{pH} \leq 2$ (Sneideris et al., 2015). However, minor concentration-dependent differences can be observed (Figs. 1C and 1D). The spectra of fibrils, formed at lower insulin concentrations, have a pronounced shoulder at $1,641 \text{ cm}^{-1}$, while a minor band at $1,620 \text{ cm}^{-1}$ appears in the second derivative spectra (Fig. 1D) of samples aggregated at higher protein concentrations. The 1.0 mM and 0.8 mM fibril spectra are nearly identical, while 0.6 mM and 0.4 mM spectra appear to be intermediates between 0.8 mM and 0.2 mM, suggesting the existence of two distinct conformations.

Fibril morphology

The morphology of insulin fibrils formed at different concentrations was compared using AFM. We can see far more small and separated aggregates in samples formed at lower insulin concentration (Figs. 2A–2E). Analysis of variance (ANOVA) reveals that there is a statistically relevant fibril height difference ($p = 0.01$, $n = 50$) between the low and high

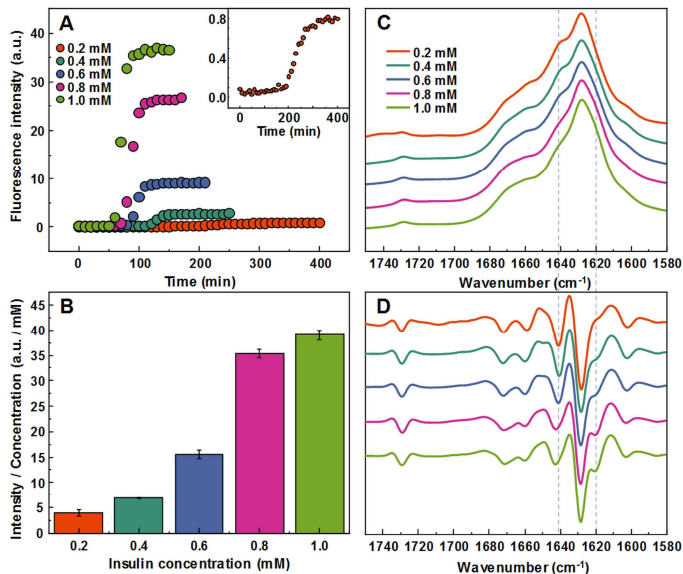


Figure 1 Concentration-dependent differences of insulin aggregation. Aggregation kinetics of unseeded insulin in 20% acetic acid with 100 mM NaCl at 60 °C without agitation followed by ThT fluorescence (A), insert shows aggregation kinetics of 0.2 mM insulin. Each kinetic data point is the average of 4 repeats. ThT fluorescence intensity and fibril concentration ratios (B). FTIR absorption (C) and second derivative (D) spectra of insulin fibrils.

Full-size [DOI: 10.7717/peerj.8208/fig-1](https://doi.org/10.7717/peerj.8208/fig-1)

concentration samples (Fig. 2F). Additional AFM images of these conditions are available as Fig. S1.

Seeded aggregation

In order to determine whether observed different fibril templates can propagate at unfavorable conditions, a set of seeded aggregation reactions were performed (Figs. 3A–3D, Fig. S2). In all four cases we observe a fibril-concentration-dependent seeding propensity (Fig. 3E), however, there is an interesting ThT fluorescence distribution, based on the amount and type of seed added (Fig. 3F). When the low concentration fibrils (0.2 mM, further on referred as LCF) are added to 0.2 mM insulin solutions, there are relatively no major differences in the fluorescence intensity at the end of each reaction. The same can be said in the case when the high concentration fibrils (1.0 mM, further on referred as HCF) are added to 1.0 mM insulin solutions. However, when the LCF are added to 1.0 mM insulin solutions, high seed concentrations yield a low fluorescence intensity, which then rises with decreased amount of seeds, eventually resulting in an intensity comparable to HCF. The opposite is observed when HCF are added to 0.2 mM insulin solutions, where

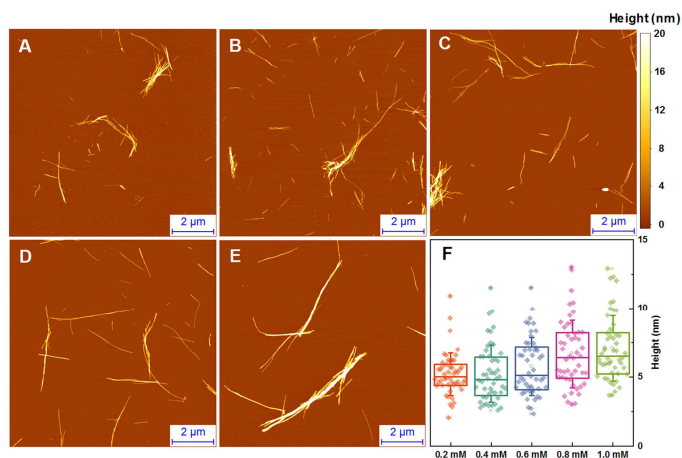


Figure 2 AFM analysis of insulin fibrils. Insulin fibrils formed at 0.2 mM (A), 0.4 mM (B), 0.6 mM (C), 0.8 mM (D) and 1.0 mM (E) concentrations. Insulin fibril height distribution with box plots indicating the interquartile range and errors bars are for one standard deviation (F). Sample size for each ANOVA test was 50.

Full-size [DOI: 10.7717/peerj.8208/fig-2](https://doi.org/10.7717/peerj.8208/fig-2)

high initial fibril concentrations yield an intensity comparable to the seed conformation (when accounted for fibril concentration at the end of the reaction) and an intensity similar to LCF when the seed concentration becomes minimal.

In order to further confirm the self-replication ability of both conformations, fibrils formed during seeded aggregation were examined by FTIR and their spectra were compared to the unseeded aggregation fibril spectra (Figs. 4A–4D). The results show that when a large concentration of preformed fibrils is added to either 0.2 mM or 1.0 mM insulin solutions, the seed self-replicates and maintains its initial secondary structure. On the other hand, when a low concentration of seed is added, the resulting FTIR spectra are similar to their respective environment conformations, rather than the seed.

Seeded fibril morphology

When large amounts of sonicated aggregates are used, there is minimal difference in the length and distribution of fibrils (Figs. 5A–5D), likely due to the large amount of aggregation centers. When the amount of seed used is low, the fibril length and distribution is similar to unseeded aggregation (Figs. 5E–5H). Fibril height distribution reveals a similarity between almost all conditions, except for when 1.0 mM insulin is seeded with low concentrations of either conformation (Fig. 5I), where the height distribution is comparable to unseeded nucleation. Additional AFM images of these conditions are available as supplementary information (Fig. S3).

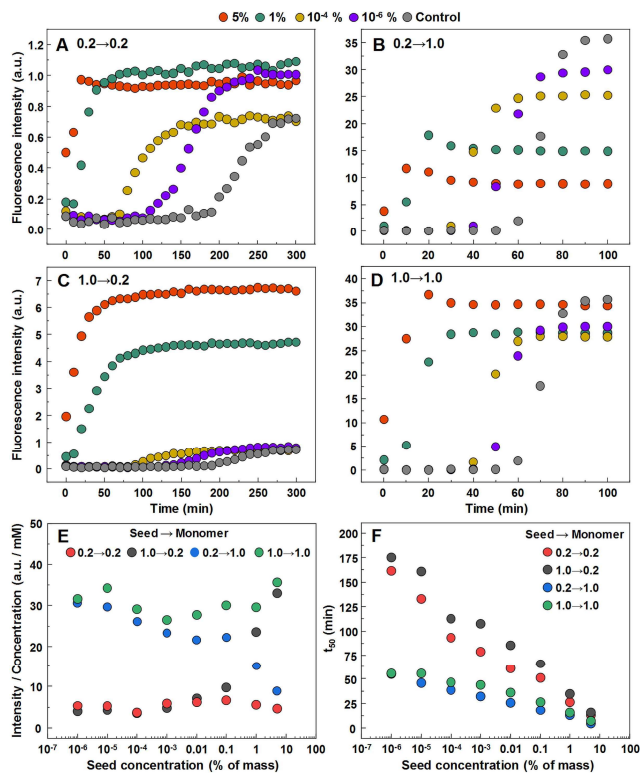


Figure 3 Seeded aggregation of insulin with a range of preformed fibrils. Aggregation kinetics of insulin where the LCF are added to 0.2 mM insulin solutions (A), LCF to 1.0 mM (B), HCF to 0.2 mM (C) and HCF to 1.0 mM (D). Aggregation half-time (t_{50}) dependence on concentration and type of seed added (E). ThT fluorescence intensity and fibril concentration ratio dependence on added seed concentration (F). Each data point is the average of four repeats.

Full-size [DOI: 10.7717/peerj.8208/fig-3](https://doi.org/10.7717/peerj.8208/fig-3)

DISCUSSION

The first and most apparent difference between the samples, aggregated at different protein concentrations is their ability to enhance ThT fluorescence. A very similar effect was reported in case of protein-concentration-dependent polymorphism of glucagon amyloid fibrils (Pedersen *et al.*, 2006). A 10-fold increase in ThT binding positions is highly improbable and slightly different fibril size distribution seen in AFM images could not strongly affect the number of binding positions, so a more appropriate explanation could be changes in the fibril's surface, facilitating a different ThT binding mode, as insulin

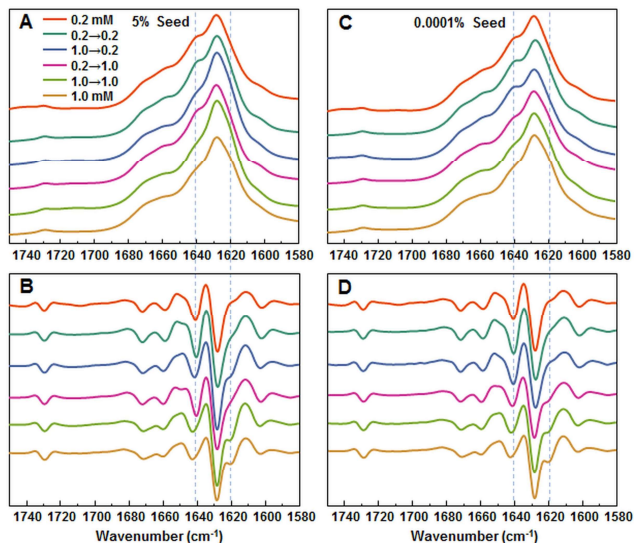


Figure 4 FTIR analysis of seeded aggregates. Absorption and second derivate spectra of insulin fibrils when 5% (A and B, respectively) and 0.0001% (C and D, respectively) preformed fibrils are added.

Full-size [DOI: 10.7717/peerj.8208/fig-4](https://doi.org/10.7717/peerj.8208/fig-4)

fibrils have been shown to possess more than one way of incorporating ThT molecules (Groenning *et al.*, 2007). Similar differences in ThT fluorescence were observed with different conformations of alpha-synuclein fibrils and attributed to the different binding of ThT molecules (Sidhu *et al.*, 2018), so we can hypothesize that a low protein concentration leads to a different conformation of insulin amyloid fibrils.

Protein-concentration-dependent polymorphism of insulin amyloid fibrils is supported also by different FTIR spectra. In fact, spectral differences are rather minor in comparison to the ones observed between spectra of previously reported insulin conformations (Dzwolak *et al.*, 2004; Sneideris *et al.*, 2015), but the hallmark of each spectrum is conserved in seeding experiments (Figs. 4A and 4B), which supports the hypothesis of different amyloid conformations. Comparison of FTIR spectra to the previously reported data (Sneideris *et al.*, 2015) suggests that the fibril conformation formed at higher insulin concentrations is the same as previously reported, while the one formed at lower concentrations falls out of the previously proposed scheme (Sneideris *et al.*, 2015).

Atomic force microscopy data does not add much of information. It seems that average size of spontaneously formed fibrils slightly increases with higher protein concentration (Fig. 2), but this effect does not depend on the type of seeds (Fig. 5).

Currently we are aware of two mechanisms of seed-induced aggregation. One is amyloid fibril elongation via attachment and refolding of protein molecules at seed fibril ends,

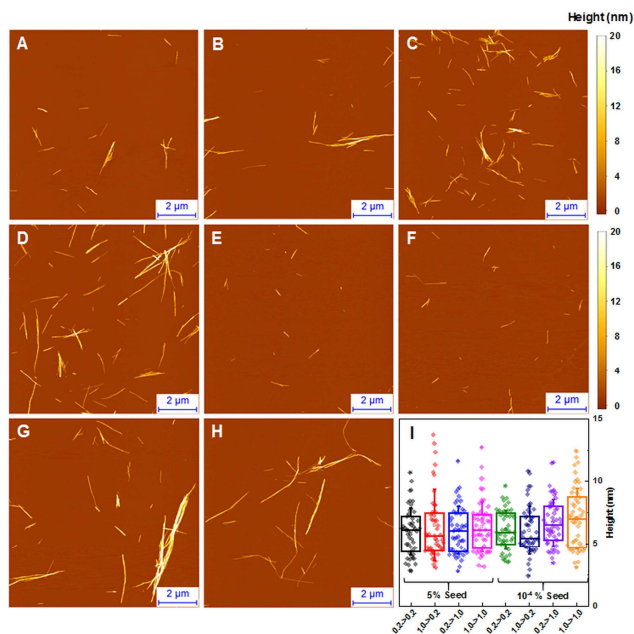


Figure 5 AFM analysis of seeded insulin fibrils. Insulin fibrils resulting from seeding 0.2 mM insulin with LCF (A, E), 0.2 mM with HCF (B, F), 1.0 mM with LCF (C, G), 1.0 mM with HCF (D, H) using 5% or 10⁻⁴ % of preformed fibrils respectively. Insulin fibril height distribution with box plots indicating the interquartile range and errors bars are for one standard deviation. Sample size for each ANOVA test was 50.

Full-size [DOI: 10.7717/peerj.8208/fig-5](https://doi.org/10.7717/peerj.8208/fig-5)

another one is formation of new aggregation nuclei catalyzed by the surface of seeds (often referred as secondary nucleation (Meisl et al., 2016; Foderà et al., 2008; Scheidt et al., 2019; Törnquist et al., 2018; Bunce et al., 2019)). Previously we have demonstrated that in case of cross-seeding of different environment-induced conformations of prion protein amyloid fibrils, the conformational template can self-propagate only via elongation mechanism, while surface induced nucleation only speeds up the aggregation process, but the conformation is defined by the environment conditions (Sneideris, Milto & Smirnovas, 2015). Recently similar observations were reported on amyloid beta (Brännström et al., 2018) and alpha synuclein (Peduzzo, Linse & Buell, 2019). Our cross-environment seeding data on insulin follows the same path. With higher amount of seeds, the aggregation kinetic curves are exponential, which means that the majority of the protein is aggregated via elongation of seeds—in such case the final relative ThT fluorescence intensity and FTIR spectra of seeds and final aggregates are very similar. Lowering the amount of seeds

leads to sigmoid kinetic curves which means that the majority of the protein is aggregated via new-formed nuclei and seeds are mainly employed as catalyzers—in such case the final relative ThT fluorescence intensity and FTIR spectra of seeds and final aggregates are different.

CONCLUSIONS

Generally, in the seeded growth experiment of amyloid fibrils one expects self-replication of seed conformation. Here we showed that such expectations are valid only at certain circumstances—amyloid fibrils self-replicate their conformation only via elongation, or else the conformation of aggregates is environment-dependent. As similar conclusions were previously derived in studies of prion protein, amyloid beta, and alpha-synuclein, there may be enough data to consider it as a general way for self-replication of different amyloid fibril conformations.

ACKNOWLEDGEMENTS

The authors acknowledge Prof. G. Niaura from the Center of Physical Sciences and Technology for the access to FTIR.

ADDITIONAL INFORMATION AND DECLARATIONS

Funding

The authors received no funding for this work.

Competing Interests

The authors declare there are no competing interests.

Author Contributions

- Andrius Sakalauskas and Mantas Ziaunys conceived and designed the experiments, performed the experiments, analyzed the data, prepared figures and/or tables, authored or reviewed drafts of the paper, approved the final draft.
- Vytautas Smirnovas conceived and designed the experiments, analyzed the data, contributed reagents/materials/analysis tools, authored or reviewed drafts of the paper, approved the final draft.

Data Availability

The following information was supplied regarding data availability:

The raw data are available as [Supplementary Files](#).

Supplemental Information

Supplemental information for this article can be found online at <http://dx.doi.org/10.7717/peerj.8208#supplemental-information>.

REFERENCES

- Bousset L, Pieri L, Ruiz-Arlandis G, Gath J, Jensen PH, Habenstein B, Madiona K, Olieric V, Böckmann A, Meier BH, Melki R. 2013. Structural and functional characterization of two alpha-synuclein strains. *Nature Communications* 4:2575 DOI 10.1038/ncomms3575.
- Brännström K, Islam T, Gharibyan AL, Iakovleva I, Nilsson L, Lee CC, Sandblad L, Pamrén A, Olofsson A. 2018. The properties of amyloid- β fibrils are determined by their path of formation. *Journal of Molecular Biology* 430(13):1940–1949 DOI 10.1016/j.jmb.2018.05.001.
- Bunce SJ, Wang Y, Stewart KL, Ashcroft AE, Radford SE, Hall CK, Wilson AJ. 2019. Molecular insights into the surface-catalyzed secondary nucleation of amyloid- β 40 (A β 40) by the peptide fragment A β 16–22. *Science Advances* 5(6):eaav8216 DOI 10.1126/sciadv.aav8216.
- Chatani E, Yagi H, Naiki H, Goto Y. 2012. Polymorphism of β 2-microglobulin amyloid fibrils manifested by ultrasonication-enhanced fibril formation in trifluoroethanol. *Journal of Biological Chemistry* 287(27):22827–22837 DOI 10.1074/jbc.M111.333310.
- Chiti F, Dobson CM. 2017. Protein misfolding, amyloid formation, and human disease: a summary of progress over the last decade. *Annual Review of Biochemistry* 86(1):27–68 DOI 10.1146/annurev-biochem-061516-045115.
- Cobb NJ, Apostol MI, Chen S, Smirnovas V, Surewicz WK. 2014. Conformational stability of mammalian prion protein amyloid fibrils is dictated by a packing polymorphism within the core region. *Journal of Biological Chemistry* 289(5):2643–2650 DOI 10.1016/j.jmb.2010.05.051.
- Colby DW, Giles K, Legname G, Wille H, Baskakov IV, DeArmond SJ, Prusiner SB. 2009. Design and construction of diverse mammalian prion strains. *Proceedings of the National Academy of Sciences of the United States of America* 106(48):20417–20422 DOI 10.1073/pnas.0910350106.
- Collinge J, Clarke AR. 2007. A general model of prion strains and their pathogenicity. *Science* 318(5852):930–936 DOI 10.1126/science.1138718.
- Cummings J, Lee G, Ritter A, Sabbagh M, Zhong K. 2019. Alzheimer’s disease drug development pipeline: 2019. *Alzheimer’s & Dementia: Translational Research & Clinical Interventions* 5:272–293 DOI 10.1016/j.trci.2019.05.008.
- Debelouchina GT, Platt GW, Bayro MJ, Radford SE, Griffin RG. 2010. Magic angle spinning NMR analysis of β 2-microglobulin amyloid fibrils in two distinct morphologies. *Journal of the American Chemical Society* 132(30):10414–10423 DOI 10.1021/ja102775u.
- Dinkel PD, Siddiqua A, Huynh H, Shah M, Margittai M. 2011. Variations in filament conformation dictate seeding barrier between three- and four-repeat Tau. *Biochemistry* 50(20):4330–4336 DOI 10.1021/bi2004685.
- Doig AJ, Del Castillo-Frias MP, Berthoumieu O, Tarus B, Nasica-Labouze J, Sterpone F, Nguyen PH, Hooper NM, Faller P, Derreumaux P. 2017. Why is research

- on amyloid- β failing to give new drugs for Alzheimer's disease? *ACS Chemical Neuroscience* 8(7):1435–1437 DOI 10.1021/acschemneuro.7b00188.
- Dzwolak W, Smirnovas V, Jansen R, Winter R. 2004.** Insulin forms amyloid in a strain-dependent manner: an FT-IR spectroscopic study. *Protein Science* 13(7):1927–1932 DOI 10.1110/ps.03607204.
- Fändrich M, Nyström S, Nilsson KPR, Böckmann A, LeVine H, Hammarström P. 2018.** Amyloid fibril polymorphism: a challenge for molecular imaging and therapy. *Journal of Internal Medicine* 283(3):218–237 DOI 10.1111/joim.12732.
- Foderà V, Librizzi F, Groenning M, van de Weert M, Leone M. 2008.** Secondary nucleation and accessible surface in insulin amyloid fibril formation. *The Journal of Physical Chemistry B* 112(12):3853–3858 DOI 10.1021/jp710131u.
- Groenning M, Norrman M, Flink JM, Van de Weert M, Bukrinsky JT, Schluckebier G, Frokjaer S. 2007.** Binding mode of thioflavin T in insulin amyloid fibrils. *Journal of Structural Biology* 159(3):483–497 DOI 10.1016/j.jsb.2007.06.004.
- Heise H, Hoyer W, Becker S, Andronesi OC, Riedel D, Baldus M. 2005.** Molecular-level secondary structure, polymorphism, and dynamics of full-length β -synuclein fibrils studied by solid-state NMR. *Proceedings of the National Academy of Sciences of the United States of America* 102(44):15871–15876 DOI 10.1073/pnas.0506109102.
- Isik AT. 2010.** Late onset Alzheimer's disease in older people. *Clinical Interventions in Aging* 5(October):307–311 DOI 10.2147/CIA.S11718.
- Knowles TPJ, Vendruscolo M, Dobson CM. 2014.** The Amyloid state and its association with protein misfolding diseases. *Nature Reviews Molecular Cell Biology* 15(6):384–396 DOI 10.1038/nrm3810.
- Lu J-X, Qiang W, Yau W-M, Schwieters CD, Meredith SC, Tycko R. 2013.** Molecular structure of β -amyloid fibrils in Alzheimer's disease brain tissue. *Cell* 154(6):1257–1268 DOI 10.1016/j.cell.2013.08.035.
- Mehta D, Jackson R, Paul G, Shi J, Sabbagh M. 2017.** Why do trials for Alzheimer's disease drugs keep failing? A discontinued drug perspective for 2010–2015. *Expert Opinion on Investigational Drugs* 26(6):735–739 DOI 10.1080/13543784.2017.1323868.
- Meisl G, Kirkegaard JB, Arosio P, Michaels TCT, Vendruscolo M, Dobson CM, Linse S, Knowles TPJ. 2016.** Molecular mechanisms of protein aggregation from global fitting of kinetic models. *Nature Protocols* 11(2):252–272 DOI 10.1038/nprot.2016.010.
- Meisl G, Rajah L, Cohen SAI, Pfammatter M, Šarić A, Hellstrand E, Buell AK, Aguzzi A, Linse S, Vendruscolo M, Dobson CM, Knowles TPJ. 2017.** Scaling behaviour and rate-determining steps in filamentous self-assembly. *Chemical Science* 8(10):7087–7097 DOI 10.1039/C7SC01965C.
- Morel B, Varela L, Azuaga AI, Conejero-Lara F. 2010.** Environmental conditions affect the kinetics of nucleation of amyloid fibrils and determine their morphology. *Biophysical Journal* 99(11):3801–3810 DOI 10.1016/j.bpj.2010.10.039.
- Nasica-Labouze J, Nguyen PH, Sterpone F, Berthoumieu O, Buchete N-V, Coté S, De Simone A, Doig AJ, Faller P, Garcia A, Laio A, Suan Li M, Melchionna S, Mousseau N, Mu Y, Paravastu A, Pasquali S, Rosenman DJ, Strodel B, Tarus B, Viles JH, Zhang T, Wang C, Derreumaux P. 2015.** Amyloid β protein and

- Alzheimer's disease: when computer simulations complement experimental studies. *Chemical Reviews* **115**(9):3518–3563 DOI [10.1021/cr500638n](https://doi.org/10.1021/cr500638n).
- Ostapchenko VG, Sawaya MR, Makarava N, Savtchenko R, Nilsson KPR, Eisenberg D, Baskakov IV. 2010.** Two amyloid states of the prion protein display significantly different folding patterns. *Journal of Molecular Biology* **400**(4):908–921 DOI [10.1016/j.jmb.2010.05.051](https://doi.org/10.1016/j.jmb.2010.05.051).
- Paravastu AK, Leapman RD, Yau W-M, Tycko R. 2008.** Molecular structural basis for polymorphism in Alzheimer's α -amyloid fibrils. *Proceedings of the National Academy of Sciences of the United States of America* **105**(47):18349–18354 DOI [10.1073/pnas.0806270105](https://doi.org/10.1073/pnas.0806270105).
- Pedersen JS, Dikov D, Flink JL, Hjuler HA, Christiansen G, Otzen DE. 2006.** The changing face of glucagon fibrillation: structural polymorphism and conformational imprinting. *Journal of Molecular Biology* **355**(3):501–523 DOI [10.1016/j.jmb.2005.09.100](https://doi.org/10.1016/j.jmb.2005.09.100).
- Peduzzo A, Linse S, Buell A. 2019.** The properties of α -synuclein secondary nuclei are dominated by the solution conditions rather than the seed fibril strain. *ChemRxiv*. DOI [10.26434/chemrxiv.9757778.v1](https://doi.org/10.26434/chemrxiv.9757778.v1).
- Pellarin R, Schuetz P, Guarnera E, Caflich A. 2010.** Amyloid fibril polymorphism is under kinetic control. *Journal of the American Chemical Society* **132**(42):14960–14970 DOI [10.1021/ja106044u](https://doi.org/10.1021/ja106044u).
- Petkova AT, Leapman RD, Guo Z, Yau W-M, Mattson MP, Tycko R. 2005.** Self-propagating, molecular-level polymorphism in Alzheimer's beta-amyloid fibrils. *Science* **307**(5707):262–265 DOI [10.1126/science.1105850](https://doi.org/10.1126/science.1105850).
- Safar J, Wille H, Itri V, Groth D, Serban H, Torchia M, Cohen FE, Prusiner SB. 1998.** Eight prion strains have prpsc molecules with different conformations. *Nature Medicine* **4**(10):1157–1165 DOI [10.1038/2654](https://doi.org/10.1038/2654).
- Scheidt T, Łapińska U, Kumita JR, Whiten DR, Klenerman D, Wilson MR, Cohen SIA, Linse S, Vendruscolo M, Dobson CM, Knowles TPJ, Arosio P. 2019.** Secondary nucleation and elongation occur at different sites on Alzheimer's amyloid- β aggregates. *Science Advances* **5**(4):eaau3112 DOI [10.1126/sciadv.aau3112](https://doi.org/10.1126/sciadv.aau3112).
- Sidhu A, Vaneyck J, Blum C, Segers-Nolten I, Subramaniam V. 2018.** Polymorph-specific distribution of binding sites determines thioflavin-T fluorescence intensity in α -synuclein fibrils. *Amyloid* **25**(3):189–196 DOI [10.1080/13506129.2018.1517736](https://doi.org/10.1080/13506129.2018.1517736).
- Sneideris T, Darguzis D, Botyriute A, Grigaliunas M, Winter R, Smirnovas V. 2015.** pH-Driven polymorphism of insulin amyloid-like fibrils. *PLOS ONE* **10**(8):e0136602 DOI [10.1371/journal.pone.0136602](https://doi.org/10.1371/journal.pone.0136602).
- Sneideris T, Milto K, Smirnovas V. 2015.** Polymorphism of amyloid-like fibrils can be defined by the concentration of seeds. *PeerJ* **3**(August):e1207 DOI [10.7717/peerj.1207](https://doi.org/10.7717/peerj.1207).
- Stein KC, True HL. 2014.** Prion strains and amyloid polymorphism influence phenotypic variation. *PLOS Pathogens* **10**(9):e1004328 DOI [10.1371/journal.ppat.1004328](https://doi.org/10.1371/journal.ppat.1004328).

- Tanaka M, Collins SR, Toyama BH, Weissman JS. 2006.** The physical basis of how prion conformations determine strain phenotypes. *Nature* **442(7102)**:585–589 DOI [10.1038/nature04922](https://doi.org/10.1038/nature04922).
- Törnquist M, Michaels TCT, Sanagavarapu K, Yang X, Meisl G, Cohen SIA, Knowles TPJ, Linse S. 2018.** Secondary nucleation in amyloid formation. *Chemical Communications* **54(63)**:8667–8684 DOI [10.1039/C8CC02204F](https://doi.org/10.1039/C8CC02204F).
- Watts JC, Condello C, Stohr J, Oehler A, Lee J, DeArmond SJ, Lannfelt L, Ingelsson M, Giles K, Prusiner SB. 2014.** Serial propagation of distinct strains of a prions from Alzheimer's disease patients. *Proceedings of the National Academy of Sciences of the United States of America* **111(28)**:10323–10328 DOI [10.1073/pnas.1408900111](https://doi.org/10.1073/pnas.1408900111).
- Yamasaki TR, Holmes BB, Furman JL, Dhavale DD, Su BW, Song E-S, Cairns NJ, Kotzbauer PT, Diamond MI. 2019.** Parkinson's disease and multiple system atrophy have distinct α -synuclein seed characteristics. *Journal of Biological Chemistry* **294(3)**:1045–1058 DOI [10.1074/jbc.RA118.004471](https://doi.org/10.1074/jbc.RA118.004471).



Article

Autoxidation Enhances Anti-Amyloid Potential of Flavone Derivatives

Andrius Sakalauskas , Mantas Ziaunys, Ruta Snieckute and Vytautas Smirnovas *

Life Sciences Center, Institute of Biotechnology, Vilnius University, LT-10257 Vilnius, Lithuania; andrius.sakalauskas@gmc.vu.lt (A.S.); mantas.ziaunys@gmail.com (M.Z.); r.snieckute@gmail.com (R.S.)

* Correspondence: vytautas.smirnovas@bti.vu.lt

Abstract: The increasing prevalence of amyloid-related disorders, such as Alzheimer's or Parkinson's disease, raises the need for effective anti-amyloid drugs. It has been shown on numerous occasions that flavones, a group of naturally occurring anti-oxidants, can impact the aggregation process of several amyloidogenic proteins and peptides, including amyloid-beta. Due to flavone autoxidation at neutral pH, it is uncertain if the effective inhibitor is the initial molecule or a product of this reaction, as many anti-amyloid assays attempt to mimic physiological conditions. In this work, we examine the aggregation-inhibiting properties of flavones before and after they are oxidized. The oxidation of flavones was monitored by measuring the UV-vis absorbance spectrum change over time. The protein aggregation kinetics were followed by measuring the amyloidophilic dye thioflavin-T (ThT) fluorescence intensity change. Atomic force microscopy was employed to image the aggregates formed with the most prominent inhibitors. We demonstrate that flavones, which undergo autoxidation, have a far greater potency at inhibiting the aggregation of both the disease-related amyloid-beta, as well as a model amyloidogenic protein—insulin. Oxidized 6,2',3'-trihydroxyflavone was the most potent inhibitor affecting both insulin (7-fold inhibition) and amyloid-beta (2-fold inhibition). We also show that this tendency to autoxidize is related to the positions of the flavone hydroxyl groups.

Keywords: aggregation; amyloid-beta; insulin; flavones; inhibition; autoxidation



Citation: Sakalauskas, A.; Ziaunys, M.; Snieckute, R.; Smirnovas, V. Autoxidation Enhances Anti-Amyloid Potential of Flavone Derivatives. *Antioxidants* **2021**, *10*, 1428. <https://doi.org/10.3390/antiox10091428>

Academic Editors: Rui F. M. Silva and Lea Pogačnik

Received: 9 August 2021

Accepted: 1 September 2021

Published: 7 September 2021

Publisher's Note: MDPI stays neutral with regard to jurisdictional claims in published maps and institutional affiliations.



Copyright: © 2021 by the authors. Licensee MDPI, Basel, Switzerland. This article is an open access article distributed under the terms and conditions of the Creative Commons Attribution (CC BY) license (<https://creativecommons.org/licenses/by/4.0/>).

1. Introduction

Protein aggregation into highly structured aggregates is associated with various amyloidoses, such as Alzheimer's disease (AD) and Parkinson's disease (PD) [1]. AD alone is recognized to be the most common cause of dementia (60–80%) [2] that affects more than 50 million people worldwide and, according to the World Alzheimer's Report, is set to increase up to 152 million by 2050. The cause of this forecast is that the onset of AD mostly occurs after 60 years of age, and the increasing life expectancy leads to more people suffering from dementia. The pathological hallmark of this disease is the increased concentration of the 42 amino acid peptide—amyloid-beta ($A\beta_{42}$) that prompts the formation of its oligomeric and fibrillar species [3].

The increasing focus on anti-amyloid- β compounds has led to many different in vitro studies showing positive effects against protein aggregation [4]. Despite this fact, many suggested disease-modifying compounds, ranging from small organic molecules to large monoclonal antibodies, have not led to an effective cure, leaving 99.5% of clinical trials unsuccessful [5,6]. Several potential problems with the very low clinical trial success rate are linked to targeting the wrong pathological substrates, concerns with drug development, and problems with methodologies [7,8]. Subsequently, it is of utmost importance to take into consideration the gap between the initial drug screening and human physiology [4,9].

The aggregation process of the $A\beta_{42}$ peptide is exceptionally complicated; however, the mechanism is rather well described [10,11]. The process of several steps involves

primary nucleation, elongation, fibril surface-catalyzed nucleation (often referred to as secondary nucleation), and fragmentation [12]. While primary nucleation causes the formation of nuclei that eventually grow into fibril aggregates, secondary nucleation is shown to be the main source of more cytotoxic oligomeric species that cause direct neurotoxicity [13–15]. For that reason, it is beneficial to find an anti-amyloidogenic compound that prevents primary and secondary nucleation as well as elongation processes [16].

Flavones are abundant in nature and found in a variety of herbs, fruits, vegetables, and spices [17]. This group of natural anti-oxidants has been reported to possess anti-amyloid characteristics, exhibit neuroprotective, anti-inflammatory, and anti-microbial properties [16,18]. In addition, flavone derivatives have shown positive effects when treating diabetes, cancer, malaria, asthma, and cardiovascular system diseases [19]. Studies have also shown that a variety of flavonoids function as acetylcholinesterase inhibitors (AChEI) [20,21]. AChEI is currently one of the most prominent options for symptomatic treatment of AD, mostly by increasing neurotransmitter acetylcholine concentrations in synaptic gaps of the nervous system [22,23]. If the same compound would also inhibit amyloid formation, it could be an ultimate anti-amyloid drug. Moreover, the small molecular weight and widely abundant flavonoids could be a better option for drug development. Compared to the large monoclonal antibody-based drugs, such molecules do pass Lipinski's rule of 5, have high availability and stability, and could potentially be used for less expensive prevention against the onset of neurodegenerative diseases [24].

Studies with flavones demonstrated properties against A β ₄₂ aggregation in vitro [25,26]. In many cases, the anti-aggregation potential is evaluated via measurement of amyloidophilic dye thioflavin-T (ThT) fluorescence intensity [27,28], assuming that relatively lower fluorescence intensity correlates with fewer fibrils formed. While this hypothesis is quite prominent, various counterfactors exist. Typically, A β ₄₂ aggregation is examined at neutral pH without evaluating the characteristics of the potential inhibitor in question. Numerous flavones have light absorbance properties in the same range as typically used fluorescent amyloid-dyes [29]. In addition, flavones could potentially bind to either the dye molecule itself or the formed aggregates, preventing its interaction with the fibril [30].

Many polyphenolic compounds, including flavones, are reported to undergo autoxidation at neutral or higher pH [31,32]. One particular study shows the oxidation mechanism of quercetin, suggesting that the process involves the breakdown of the flavone C ring, enabling different structure formations [32]. In another report, the A β ₄₂ inhibitory effect is based on the autoxidation of (+)-taxifolin [28]. This leads to an assumption that molecule autoxidation could be the main cause of the inhibitory effect in vitro. Furthermore, several reports demonstrate low mono- and polyhydroxylated flavone oral bioavailability due to direct metabolism [33]. In addition, human cytochrome P450 enzymes oxidize the 5-hydroxyflavone to specific di- or trihydroxyflavones [34]. These aforementioned aspects raise questions about whether the tested molecule or its oxidized species inhibit amyloid formation in vitro.

In this work, we examined the oxidation potential of 64 mono- and polyhydroxylated flavones and tested their inhibitory effect on the aggregation of amyloid-beta and a commonly used model amyloid protein—insulin. We show that the positions of flavone hydroxy groups have a remarkably high impact on autoxidation which enables the inhibitory effect on both proteins under the tested conditions.

2. Materials and Methods

2.1. Flavone Solution Preparation

Each non-oxidized flavone stock solution was prepared by dissolving the flavones (Indofine Chemical Company, Inc., Hillsborough, NJ, USA) in dimethylsulfoxide (DMSO, Carl Roth, Karlsruhe, Germany) to a final concentration of 10 mM. The oxidation solution of each flavone was prepared by diluting 10 mM flavone stock solution with 10 mM sodium phosphate buffer (pH 8.0) and DMSO to yield a final flavone concentration of 0.2 mM in

9 mM sodium phosphate buffer solution containing 10% DMSO. The 10% DMSO buffer solution was used to increase the solubility of flavones.

2.2. Absorbance Measurements

The autoxidation of flavones was monitored by measuring UV-Vis absorbance spectrum changes over time using a ClarioStar Plus plate reader (BMG Labtech, Ortenberg, Germany). Each flavone oxidation solution was stored as 100 μ L samples in a UV-clear 96-well plate (Thermo Fisher Scientific, Inc., Waltham, MA, USA, cat. No. 11670352) and incubated at 37 $^{\circ}$ C, while the measuring absorbance spectra were in the range from 240 nm to 800 nm. Data were collected each hour for a total of 100 h. Spectra was baseline corrected at 800 nm. The resulting samples, which are later referred to as “incubated” or “oxidized” flavones, were then used in aggregation kinetic experiments.

Samples for the measurement of ThT and flavone interaction were prepared by mixing 0.5 mM incubated flavone, 10 mM ThT stock solution, and 20 mM phosphate buffer solution (pH 7.0), yielding either separate 50 μ M flavone and 20 μ M ThT or combined 50 μ M flavone and 20 μ M ThT solutions in 20 mM phosphate buffer (pH 7.0). Samples were scanned using a Shimadzu UV-1800 spectrophotometer (1 nm steps). Separate 50 μ M flavone and 20 μ M ThT spectra were added together for comparison with their mixture. Each sample was scanned three times and averaged; the baseline was corrected at 800 nm.

2.3. Fluorescence Measurements

Samples for the fluorescence measurements were prepared by mixing 0.5 mM incubated flavone, 10 mM ThT stock solution, 2 μ M of A β ₄₂ aggregates, and 20 mM phosphate buffer solution (pH 7.0), yielding 1 μ M of A β ₄₂ fibril samples with either 20 μ M ThT or 50 μ M flavone samples with both ThT and flavone. The fluorescence intensity was scanned using a Varian Cary Eclipse fluorescence spectrophotometer, with excitation and emission wavelengths being 440 nm and 480 nm, respectively (5 nm excitation and 2.5 nm emission slit widths). The intrinsic fluorescence emission intensity, occurring from non-fibril-bound ThT or flavones, was subtracted from their respective fibril-compound sample intensities. This was done by acquiring fluorescence emission intensity values of ThT or flavone samples in the absence of A β ₄₂ aggregates.

2.4. Purification of Recombinant A β ₄₂

The expression vector of A β ₄₂ was described previously [35]. The peptide was expressed in *E. coli* BL-21StarTM (DE3) (Invitrogen, Carlsbad, CA, USA) and purified as described previously [36]. In brief, the transformed cells were incubated on LB agar plates containing ampicillin (100 μ g/mL) overnight at 37 $^{\circ}$ C. The next day, the overnight cultures were prepared from single colonies and grown in LB medium with ampicillin (100 μ g/mL). The 1 mL of the culture was transferred to 400 mL of auto-inductive ZYM-5052 medium [37] containing ampicillin (100 μ g/mL) and grown for 15 h. The collected cell pellet was washed 3 times to remove all soluble proteins. The procedure involves pellet homogenization, sonication, and centrifugation. After removing soluble proteins, the cell pellet was resuspended in 50 mL of 20 mM Tris/HCL pH 8.0 buffer solution containing 8 M urea and 1 mM EDTA, homogenized, and centrifuged as in the previous steps. The collected supernatant was diluted with 150 mL of 20 mM Tris/HCL (pH 8.0) buffer containing 1 mM EDTA, mixed with 60 mL DEAE-sepharose and agitated at 80 rpm for 30 min at 4 $^{\circ}$ C. The chromatography procedure was performed using a Buchner funnel with Fisherbrand glass microfiber paper on a vacuum glass bottle. The resin with bound proteins was washed with 20 mM Tris/HCL pH 8.0 buffer containing 1 mM EDTA in increasing NaCl concentrations in a step-gradient (0, 20, 150, 500 mM). The target protein fractions were collected by washing the resin with a 50 mL buffer solution (containing 150 mM NaCl) four times. Collected fractions were mixed together, lyophilized, and stored at -20 $^{\circ}$ C.

The A β ₄₂ peptide powder was dissolved in a 20 mM sodium phosphate buffer solution (pH 8.0) containing 5 M guanidine thiocyanate (GuSCN, Carl Roth). The dissolved sample

was loaded on a Tricorn 10/300 column (packed with Superdex 75) and eluted at 1 mL/min using a 20 mM sodium phosphate buffer solution (pH 8.0) containing 0.2 mM EDTA and 0.02% NaN₃. Collected fractions were mixed together, lyophilized, and stored at −20 °C. Before aggregation experiments, the purification procedure was repeated, but this time the collected fraction (0.75 mL) was purified Aβ₄₂ was stored on ice for 5 min. The concentration was determined by calculating the integrated chromatographic UV absorbance peak ($\epsilon_{280} = 1\,490\text{ M}^{-1}\text{ cm}^{-1}$). Afterward, it was diluted and immediately used for aggregation experiments.

2.5. Aggregation Kinetics of Aβ₄₂ Peptide

The purified peptide fraction (1.5 mL, pH 8.0) was mixed with 3 mL of 20 mM sodium phosphate buffer solution (pH 6.33) to yield a 3-fold diluted peptide solution (pH 7.0). The peptide and each oxidized or incubated flavone solution was mixed together with 20 mM sodium phosphate buffer solution (pH 7.0), 10 mM ThT stock solution, and DMSO to a final reaction mixture, containing 1 μM Aβ₄₂, 20 μM ThT, 50 μM of selected flavone compound and 1% DMSO. The kinetic aggregation measurements were performed in non-binding 96-well plates (Fisher, Waltham, MA, USA, cat. No. 10438082) (sample volume was 80 μL) at 37 °C by measuring ThT fluorescence using 440 nm excitation and 480 emission wavelengths in a ClarioStar Plus (BMG Labtech, Ortenberg, Germany).

2.6. Aggregation Kinetics of Insulin

Human recombinant insulin powder (Sigma-Aldrich, St. Louis, MO, USA, cat. No. 91077C) was dissolved in a 20% acetic acid solution (prepared from 100% acetic acid; Carl-Roth) containing 100 mM NaCl (Fisher) to a protein concentration of 400 μM. This insulin stock solution was mixed with non-oxidized/incubated or oxidized/incubated flavone solutions and 10 mM ThT stock solution to a final insulin concentration of 200 μM, 100 μM ThT, and 20 μM of each flavone. The aggregation kinetic measurements were performed similarly as in the case of Aβ₄₂, but at 60 °C.

2.7. Kinetic Data Analysis

After reaching the plateau, kinetic aggregation curves were fit using Boltzmann's sigmoidal equation:

$$y = \frac{(A_1 - A_2)}{\left(1 + e^{\frac{x-x_0}{dx}}\right)} + A_2 \quad (1)$$

where, A_1 is the starting fluorescence intensity, A_2 —final fluorescence intensity, x_0 —aggregation half-time. The relative half-time and relative ThT fluorescence intensity values were calculated based on the control sample in their specific microplate. These values were calculated by dividing each sample's average value by the average control value. Data were processed using Origin software (OriginLab, Northampton, MA, USA).

2.8. Atomic Force Microscopy (AFM)

The samples for AFM images were collected after kinetic measurements and scanned similarly as previously described [31,38]. In short, 40 μL of 1% (v/v) APTES (Sigma-Aldrich, cat. No. 440140) in MilliQ water was deposited on freshly cleaved mica and incubated for 5 min. Then, mica was rinsed with 2 mL of MilliQ water and dried under gentle airflow. Each sample was deposited (40 μL) on the functionalized surface and incubated for another 5 min. Prepared samples were rinsed with 2 mL of MilliQ water and dried under gentle airflow. AFM imaging was performed using a Dimension Icon (Bruker, Billerica, MA, USA) atomic force microscope. Images were 1024 × 1024 pixel resolution and were analyzed using Gwyddion 2.5.5 software. Fibril heights were determined by tracing perpendicular to each fibril's axis.

2.9. FTIR

A β_{42} fibrils were separated from the buffer solution by placing the mixture in the 0.5 mL 10 kDa concentrators (Fisher, cat. No. 88513) and spinning at 10,000 g for 10 min. Then 0.5 mL of D₂O was added, and the process of buffer exchange to D₂O was repeated 3 times. After the last spinning step, fibrils were resuspended in 0.1 mL of D₂O. FTIR spectra were recorded using an Invenio S IR spectrophotometer equipped with an MCT detector. The sample was placed in the CaF₂ transmission windows with 0.05 mm Teflon spacers, 256 interferograms of 2 cm⁻¹ resolution were averaged per spectrum. All spectra were normalized in the 1705–1595 cm⁻¹ region, and baseline corrected after subtracting the D₂O and water vapor spectrums. The data were processed using GRAMS software (Thermo Fisher Scientific, Inc., Waltham, MA, USA).

3. Results

We first incubated flavones at 37 °C in order to evaluate potential structural transitions that occur due to autoxidation. The time-dependent changes in the UV-vis spectra of flavones were recorded over a period of 100 h, comparing the absorbance in the 240–800 nm region. At the start of the experiment, each flavone spectrum (Figure 1) exhibited two characteristic maxima that are associated with the $\pi \rightarrow \pi^*$ transitions within rings A and C, referred to as benzoyl system, band II (~240–290 nm), and ring B that is conjugated with the carbonyl of ring C, referred to as cinnamoyl system, band I (~300–415 nm) [39] (Figure S1). A decrease in the magnitude of these bands was observed in all displayed spectra that led to no characteristic maxima (No. 11, 22, 31, 38, 44, 46, 48, 51–52, 57, 59, 64) or appearance of new maxima peaks in other cases. The absorbance spectra changes and reduced characteristics of the band I indicate structural changes, loss of conjugation in a chromophore, and development of different intra- and intermolecular interactions [40]. A few trihydroxyflavones (THF) (No. 38, 46), tetrahydroxyflavones (TeHF) (51–52), and most of penta- and hexahydroxyflavones (PHF and HHF) (No. 59, 61, 63, 64) had major spectrum changes within the first 5 h. Most of the other flavones, including dihydroxyflavones (DHF), THF, and TeHF (No.10, 11, 22, 31, 38, 42, 44, 46, 48, 53, 55, 57), had significant absorbance changes within a 5–40 h period, while only a few (No. 1, 32, 37, 58) exhibited most of their spectrum transitions only after > 40 h of incubation. The rest of the flavones had minor spectra changes during incubation that are reflected in slight transitions of the maxima positions (No. 30, 45, 54, 56, 60, 62) or a decrease in the magnitude of the maxima in the 380–420 nm region (No. 21, 43).

Examining the effect of non-oxidized flavones reveals that only the presence of luteolin (Figure 2A,B No. 56) slightly increased the aggregation halftime of insulin (Table S1) while not affecting the fluorescence intensity. Other flavone relative halftime and ThT fluorescence intensity did not change, except for a few cases, where they even decreased the aggregation halftime (Figure 2A No. 10, 21–22, 48, 53, 54, 59, 61–63). However, once flavones were oxidized, many of them displayed substantial inhibitory potential. Some flavones (Figure 2A,B No. 31, 59, 63) increased the aggregation halftime more than five-fold, which correlates with the ten-fold elevated fluorescence intensity (compared to the control sample). In most cases, oxidized flavones inhibited insulin aggregation, except for a few (Figure 2A,B No. 1, 30, 32, 37, 46, 54–55, 58) that did not possess such properties, as neither ThT fluorescence intensity nor halftime changed compared to the previously tested non-oxidized forms. A completely different effect was seen on A β_{42} aggregation. Here, the fluorescence intensity (Figure 2D) was diminished in all cases, except for four flavones (Figure 2D No. 1, 30, 32, 37) which seem to have had no impact on either protein aggregation process, while several oxidized compounds (Figure 2D No. 22, 31, 52, 59) showed reduced intensity values ranging from 93% to 98%, which also reduced the aggregation rate. Despite the fact that most oxidized flavones inhibited insulin aggregation, only thirteen (Figure 2C No. 22, 31, 38, 43, 46, 48, 51, 52, 56–57, 59–60, 63) appeared to increase A β_{42} relative halftime and only three (Figure 2C No. 22, 31, 52) slowed the aggregation by at least 50%.

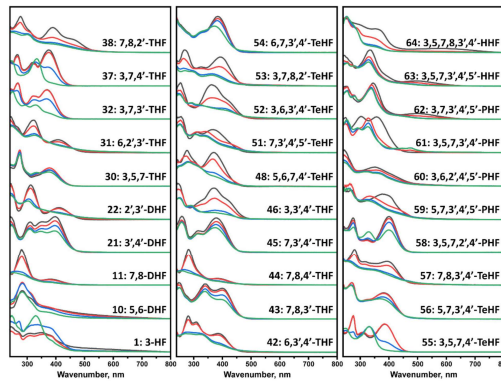


Figure 1. UV-visible absorbance spectra of flavones, recorded at 0 h (black), 5 h (red), 40 h (blue) and 100 h (green). Spectra were baseline corrected at 800 nm. Most of the flavone spectra experienced a significant change in the 250–450 nm region. In contrast, 21, 30, 43, 45, 54, 56, 60, and 62 experienced only a slight transition of maxima or decrease in the magnitude of the initial absorbance spectrum.

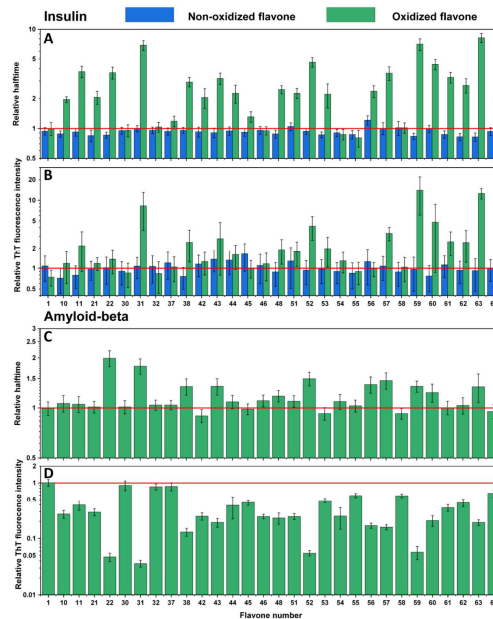


Figure 2. Effects of non-oxidized and oxidized flavones on insulin aggregation kinetics (A) and relative ThT fluorescence intensity (B). Effect of oxidized flavones on $A\beta_{42}$ aggregation kinetics (C) and relative ThT fluorescence intensity (D). Error bars are for one standard deviation ($n = 4$). None of the non-oxidized flavones, except 56, inhibited insulin aggregation; after the oxidation, more than half of the flavones showed an inhibitory effect, with 31, 59, and 63 having the most significant impact. Oxidized flavones 22, 31, 52, and 59 increased the relative halflife of $A\beta_{42}$ the most, while 1, 30, 32, 37 did not affect the relative halflife nor the relative ThT fluorescence intensity.

The flavone autoxidation experiment described above allowed us to evaluate the effect of oxidized flavones on protein aggregation. Nevertheless, not all compounds may undergo structural changes in the reaction mixture; thus, an additional number of flavones were incubated at the experimental conditions to evaluate whether UV-vis spectrum changes occur. Every tested flavone maintained the absorbance of Band I and Band II, with no major changes in the tested region (Figure 3). However, spectra of many compounds exhibited intensity changes with no shape or maximum transitions (No. 3, 6, 8, 9, 12, 13, 14, 19, 23, 26, 33, 47) that may be related to the solubility of each molecule, especially when the change occurred between the first two scans.

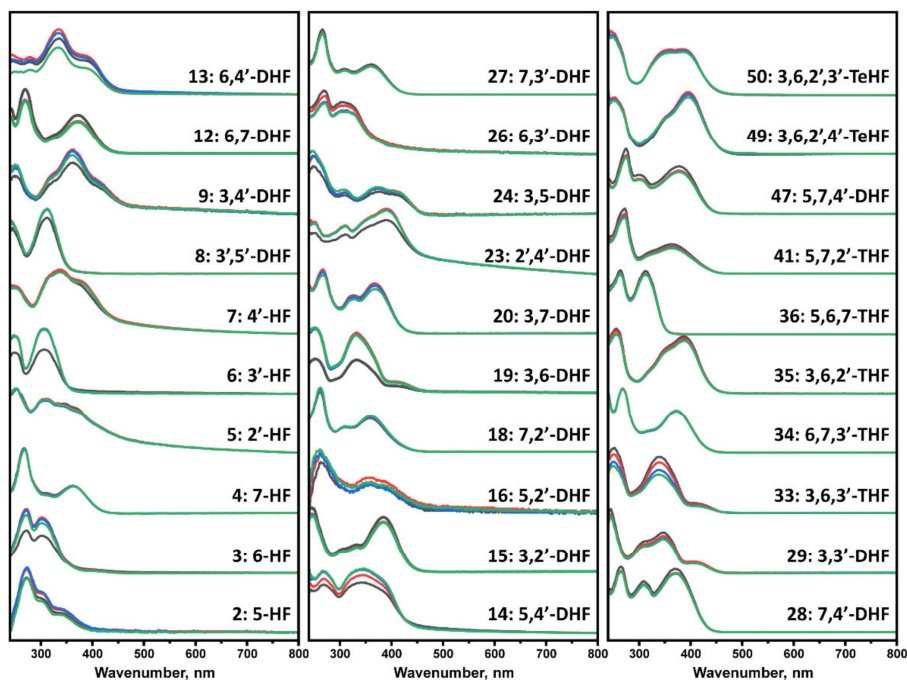


Figure 3. UV-visible absorbance spectra of flavones, recorded at 0 h (black), 5 h (red), 40 h (blue), and 100 h (green). Spectra were baseline corrected at 800 nm. Numbers 3, 6, 13, 14, 19, 23, 33 experienced the most significant decrease in the magnitude of the spectrum, while 4, 18, 27, 34, 36 had no notable change over the course of the experiment.

An identical experiment was conducted with the second set of flavones to evaluate their influence on insulin (Figure 4A,B) and $A\beta_{42}$ (Figure 4C,D) aggregation processes. Here, similar results were observed, where most of the non-incubated and incubated flavones did not inhibit insulin aggregation, yet some increased its rate (Figure 4A No. 2, 3, 7, 8, 9, 12, 13, 15, 16, 18, 19, 20, 49, 50). The majority of flavones did not affect $A\beta_{42}$ aggregation as well. However, a significant decrease in ThT fluorescence intensity was mostly evident for flavones with a higher number (Figure 4D No. 34–35, 41, 49–50), which represents THF and TeHF. In addition, dihydroxyflavones did not reduce the intensity value, except for no. 15. Three flavones (Figure 4C,D No. 5, 14, 16) that stand out appear to have altered the aggregation process by increasing the ThT fluorescence intensity and decreasing $A\beta_{42}$ aggregation halftime.

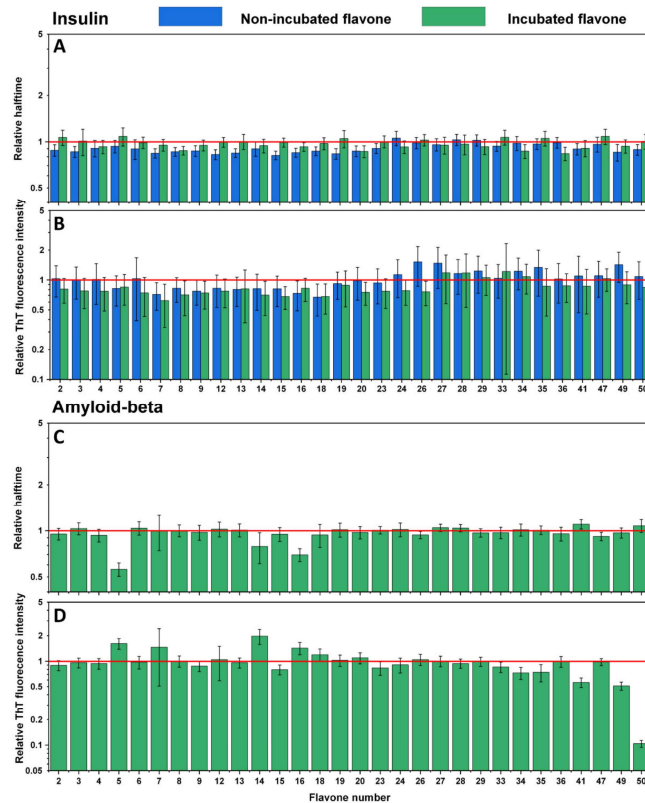


Figure 4. Effects of non-incubated and incubated flavones on insulin aggregation kinetics (A) and relative ThT fluorescence intensity (B). Effect of incubated flavones on Aβ₄₂ aggregation kinetics (C) and relative ThT fluorescence intensity (D). Error bars are for one standard deviation ($n = 4$). The non-incubated and incubated flavones did not impact insulin and Aβ₄₂ relative half-time, while incubated flavones 34, 35, 41, and 50 had the most significant impact on the relative ThT fluorescence intensity of Aβ₄₂.

Atomic force microscopy imaging was employed to observe whether fibrils were formed at the end of the Aβ₄₂ aggregation experiment (when plateau was reached). Five samples were tested that represented the control sample (Figure 5A,B) and Aβ₄₂ with incubated 2',3'-DHF (Figure 5C,D), 6,2',3'-THF (Figure 5E,F), 3,6,2',3'-TeHF (Figure 5G,H), 3,6,3',4'-TeHF (Figure 5I,J), 5,7,3',4',5'-PHF (Figure 5K,L). These particular compounds were selected due to their high impact on Aβ₄₂ aggregation rate and bound-ThT. All samples with flavones revealed Aβ₄₂ fibrillar aggregates on the mica, despite the fact that the surface was mostly covered by round-shaped oligomeric, very short fibrillar structures. Samples with flavones revealed Aβ₄₂ fibrillar aggregates on the mica, despite the fact that the surface was mostly covered by round-shaped oligomeric, very short fibrillar structures. Samples with 2',3'-DHF, 6,2',3'-THF, 3,6,2',3'-TeHF, and 5,7,3',4',5'-PHF (Figure 5C,F,G,K) appeared to have clumps of fibrils with round-shaped oligomeric structures attached to them, leaving the area empty around this structure. This suggests that inhibition requires the binding of an active molecule to the protein or its oligomeric/fibrillar species. In order to further analyze AFM images, we measured the height of a hundred oligomeric structures or fibrils and compared their height distribution (Figure 5M). Structures formed with inhibitors

had a dispersed height distribution, revealing that oligomeric structures may resemble clumped protofibrils. To understand this aspect more, the FTIR spectra of control $A\beta_{42}$ fibrils and the sample with 2',3'-DHF (when both samples reached a plateau in the ThT intensity) were recorded (Figure 5N). Samples for this experiment were prepared by using 10 kDa concentrator tubes that aided in changing the reaction solution to D_2O . This method also eliminated monomeric species of amyloid- β . Notably, the FTIR spectrum of control fibrils exhibited the only major maximum at 1630 cm^{-1} , typical for β -sheet structures, commonly found in amyloid fibrils, while the spectrum of $A\beta_{42} + 2',3'$ -DHF sample, had a less expressed β -sheet-related band at 1629 cm^{-1} , and another broad peak at 1675 cm^{-1} , which can mean the presence of substantial amounts of turns or different types of β -sheets. Unfortunately, the FTIR spectra could not be analyzed deeper; due to very low signal intensity, the signal-to-noise ratio was too high. It is necessary to note that, before spectra were normalized, the area of the amide I band of the sample with inhibitor was almost twice as small as the area of the amide I band of the control sample, leading to an assumption that less oligomeric and fibrillar species were present.

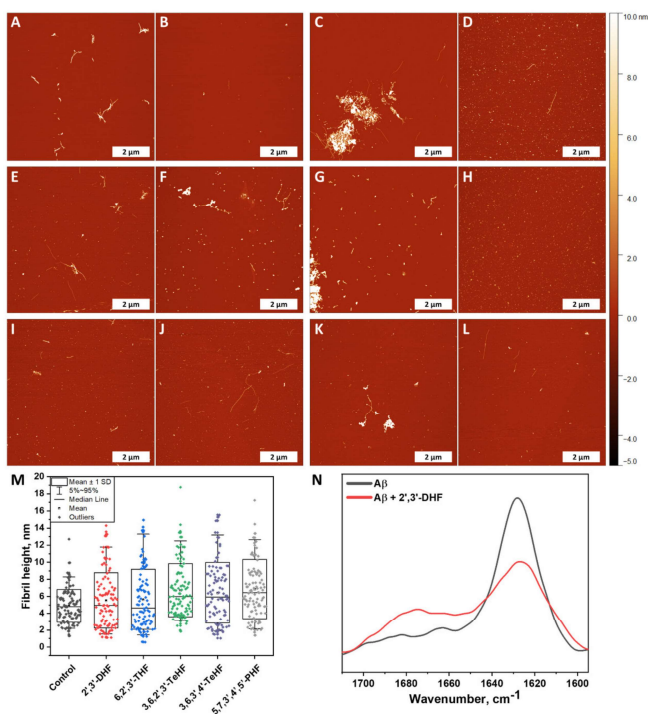


Figure 5. Atomic force microscopy images of $A\beta_{42}$ formed without (A,B) and with 50 μM of oxidized 2',3'-DHF (C,D), 6,2',3'-THF (E,F), 3,6,2',3'-TeHF (G,H), 3,6,3',4'-TeHF (I,J) and 5,7,3',4',5'-PHF (K,L) flavones. Fibril and oligomeric species height distribution (M), where box plots indicate mean \pm SD and error bars are in the 5%–95% range ($n = 100$). FTIR spectra (N) of $A\beta_{42}$ fibrils formed alone and with 50 μM of 2',3'-DHF. The AFM images of $A\beta_{42}$ aggregates formed with all inhibitors showed a similar distribution in height and revealed round shape structures that were not present in the image of the control sample. The FTIR spectrum of the sample with 2',3'-DHF had less expressed β -sheet-related band at 1629 cm^{-1} than the control sample.

4. Discussion

The characteristics of insulin aggregation kinetic data show that 63 out of 64 tested non-oxidized flavones possess no anti-amyloid properties under the tested conditions (Table S1), while most flavones that undergo the autoxidation process slow down insulin fibril formation. This is expressed in altered relative aggregation half-time. However, compounds also change the ThT fluorescence intensity (Figure 2A,B), which can be explained based on our previous report, where we show that insulin is capable of forming distinct fibril conformations in 20% acetic acid solution, with one exhibiting ~10-fold higher bound-ThT intensity values [41]. Increased fluorescence intensity is also observed using oxidized gallic acid [38], leading to a hypothesis that oxidized flavones redirect insulin amyloid formation.

Contrary results are seen during the A β ₄₂ aggregation process. Here, oxidized flavones led to a reduced ThT fluorescence intensity (Figures 2D and 4D), and only 14 oxidized flavones (Figures 2C and 4C) affected the aggregation rate. These diverse results introduce several potential explanations which may act simultaneously during the kinetic experiment. First, molecules that act as inhibiting agents should bind to monomers, intermediate oligomeric species, or aggregation nuclei to prevent the aggregation process [42]. Matos et al. revealed that quercetin, luteolin, and (+)-dihydroxyquercetin non-covalently bind to A β ₄₂ lysine residues [27] and Sato et al. displayed the mechanism where catechol-type flavonoids, namely (+)-taxifolin, autoxidize forming an o-quinone on the B-ring that covalently binds to the amino group of lysine [28]. Second, the fluorescence quenching is unavoidable when using ThT as the excitation and emission wavelengths overlap with the majority of oxidized flavones absorbance region (Figures 1 and 3) and appear to form oxidized flavone-ThT interactions (as seen from differences in absorbance spectra, when the compounds are separate or together, Figure S2) that may lead to less bound-ThT on the fibril surface, reducing the fluorescence intensity even further (Figure S3). Therefore, most of the oxidized flavones (especially with more OH groups) suppress the fluorescence intensity in A β ₄₂ aggregation experiments. This effect has been observed when two dye molecules interact alone or in the presence of fibrils [30].

Taking a deeper look into the AFM images, we see a tendency for the formation of major clumps when A β ₄₂ aggregates with oxidized flavones, especially with 2',3'-DHF (Figure 5C) and 3,6,2',3'-TeHF (Figure 5G). This indicates that flavone derivatives bind to the surface of higher-level oligomeric particles as well as fibrils. While most of the mica is covered by oligomeric species, the AFM images may be analyzed, and it can be concluded that inhibitors redirect the aggregation pathway towards the arrangement of different structures. However, this explanation is just the tip of the iceberg, and a more revealing image is seen after a larger-scale analysis. The fibrillar clumps, which appear to be a combination of oligomeric structures and fibrils, consist mostly of aggregates present on the mica that is hardly found. Despite this, some oligomeric species that are found around these clusters led to the assumption that aggregation was partially stopped.

The main objective of this work was to understand the variety of flavones that may act as inhibiting molecules. There is a distinct correlation between the positions of hydroxyl groups, flavone oxidation, and inhibition of the insulin and the A β ₄₂ aggregation process. Adjacent OH groups have a tendency to increase the solubility compared to other flavones and enable the autoxidation process, which was seen via UV-vis absorbance spectral data (Figures 1 and 3). Taking into consideration dihydroxyflavones, only four (5,6-DHF, 7,8-DHF, 2',3'-DHF and 3',4'-DHF) had an influence on the protein aggregation process. Surprisingly, 6,7-DHF does not autoxidize or affect protein aggregation. Despite this, the majority of hydroxyflavones that have neighboring hydroxy groups undergo oxidation leading to an enhanced inhibitory potential. This structural aspect is similar for 6,7,3'-THF and 5,6,7'-THF, while 5,6,7,4'-TeHF and 6,7,3',4'-TeHF tend to oxidize, potentially due to the additional hydroxy groups on the flavone B ring. 2',3'-DHF appears to have the highest inhibition potential out of all tested flavones, which is then followed by 6,2',3'-THF. This may resemble a close connection between structures and the autoxidation end products.

Surprisingly, some of the flavonol derivatives that do not have neighboring hydroxyl groups (3-hydroxyflavone, 3,5,7-THF, 3,7,3'-THF, 3,7,4'-THF, 3,5,7,4'-TeHF and 3,5,7,2',4'-PHF) undergo autoxidation; however, these autoxidized molecules do not increase the $A\beta_{42}$ aggregation time. This finding suggests a distinct autoxidation mechanism as well as different cinnamoyl system characteristics that are decisive for the developed anti-amyloid properties. Further, flavones with a higher number of hydroxyl groups that contain the aforementioned neighboring OH groups do autoxidize and inhibit insulin aggregation, but only some extend the $A\beta_{42}$ aggregation time. These flavones can be categorized into two groups: 7,8-DHF derivatives (7,8,2'-THF, 7,8,3'-THF, and 7,8,3',4'-TeHF) and flavones that have at least two hydroxyl groups on ring B (3,6,3',4'-TeHF, 5,7,3',4'-TeHF, 5,7,3',4',5'-PHF, 3,6,2',4',5'-PHF and 3,5,7,3',4',5'-PHF). Even though the number of effective inhibitors directly correlates with the number of OH groups on the molecule, the penta- and hexahydroxyflavone groups are far more complex. One probable scenario is that the flavone inhibitory effect is enabled by the appearance of particular molecular structures that form during the autoxidation process. These molecules should be structurally related, as the positions of OH groups on the molecule repeat, potentially leading to similar autoxidation mechanisms and products. While this study shows that the autoxidation of flavones leads to the formation of different structures, it is essential to note that due to this process, flavones may lose their initial characteristics, such as being inhibitors of AChE or anti-oxidants.

5. Conclusions

Taking everything into account, non-oxidized flavones do not inhibit the aggregation process of insulin or amyloid-beta, while their oxidized forms show potential against fibril formation. We also show that flavone autoxidation and inhibition are strictly related to the structure of the molecule and depend highly on the position of hydroxyl groups.

Supplementary Materials: The following are available online at <https://www.mdpi.com/article/10.3390/antiox10091428/s1>, Figure S1: Flavone structure; Figure S2: Absorbance spectra of incubated flavone mixed with ThT (red) and combined spectra of incubated flavone and ThT when they are scanned separately (black); Figure S3: Fluorescence intensity values of preformed $A\beta_{42}$ aggregates mixed with incubated flavone (red), ThT (blue) and incubated flavone with ThT (green); Table S1: Relative half-time and ThT fluorescence intensity values of Insulin and Amyloid- β aggregation.

Author Contributions: A.S. and V.S. designed the experiments; A.S., M.Z., and R.S. performed the experiments; A.S., M.Z., and V.S. analyzed the data and prepared the manuscript. All authors have read and agreed to the published version of the manuscript.

Funding: This research was funded by grant no. S-SEN-20-3 from the Research Council of Lithuania.

Institutional Review Board Statement: Not applicable.

Informed Consent Statement: Not applicable.

Data Availability Statement: The data presented in this study are available in this manuscript.

Conflicts of Interest: The authors declare no conflict of interest.

References



1. Chiti, F.; Dobson, C.M. Protein Misfolding, Amyloid Formation, and Human Disease: A Summary of Progress Over the Last Decade. *Annu. Rev. Biochem.* **2017**, *86*, 27–68. [CrossRef]
2. Anand, A.; Patience, A.A.; Sharma, N.; Khurana, N. The present and future of pharmacotherapy of Alzheimer's disease: A comprehensive review. *Eur. J. Pharmacol.* **2017**, *815*, 364–375. [CrossRef] [PubMed]
3. Gouras, G.K.; Tampellini, D.; Takahashi, R.H.; Capetillo-Zarate, E. Intraneuronal β -amyloid accumulation and synapse pathology in Alzheimer's disease. *Acta Neuropathol.* **2010**, *119*, 523–541. [CrossRef]
4. Mallucci, G.R.; Klenerman, D.; Rubinsztein, D.C. Developing Therapies for Neurodegenerative Disorders: Insights from Protein Aggregation and Cellular Stress Responses. *Annu. Rev. Cell Dev. Biol.* **2020**, *36*, 165–189. [CrossRef] [PubMed]
5. Mehta, D.; Jackson, R.; Paul, G.; Shi, J.; Sabbagh, M. Why do trials for Alzheimer's disease drugs keep failing? A discontinued drug perspective for 2010–2015. *Expert Opin. Investig. Drugs* **2017**, *26*, 735–739. [CrossRef] [PubMed]

6. Mathur, S.; Dewitte, S.; Robledo, I.; Isaacs, T.; Stamford, J. Rising to the challenges of clinical trial improvement in Parkinson's disease. *J. Parkinson's Dis.* **2015**, *5*, 263–268. [[CrossRef](#)] [[PubMed](#)]
7. Huang, L.K.; Chao, S.P.; Hu, C.J. Clinical trials of new drugs for Alzheimer disease. *J. Biomed. Sci.* **2020**, *27*, 18. [[CrossRef](#)]
8. Cummings, J.; Ritter, A.; Zhong, K. Clinical Trials for Disease-Modifying Therapies in Alzheimer's Disease: A Primer, Lessons Learned, and a Blueprint for the Future. *J. Alzheimer's Dis.* **2018**, *64*, S3–S22. [[CrossRef](#)]
9. Rekasina, M.; Paladini, A.; Piroli, A.; Zis, P.; Pergolizzi, J.V.; Varrassi, G. Pathophysiology and Therapeutic Perspectives of Oxidative Stress and Neurodegenerative Diseases: A Narrative Review. *Adv. Ther.* **2020**, *37*, 113–139. [[CrossRef](#)]
10. Frankel, R.; Törnquist, M.; Meisl, G.; Hansson, O.; Andreasson, U.; Zetterberg, H.; Blennow, K.; Frohm, B.; Cedervall, T.; Knowles, T.P.J.; et al. Autocatalytic amplification of Alzheimer-associated A β 42 peptide aggregation in human cerebrospinal fluid. *Commun. Biol.* **2019**, *2*, 365. [[CrossRef](#)] [[PubMed](#)]
11. Chaturvedi, S.K.; Siddiqi, M.K.; Alam, P.; Khan, R.H. Protein misfolding and aggregation: Mechanism, factors and detection. *Process Biochem.* **2016**, *51*, 1183–1192. [[CrossRef](#)]
12. Morris, A.M.; Watzky, M.A.; Finke, R.G. Protein aggregation kinetics, mechanism, and curve-fitting: A review of the literature. *Biochim. Biophys. Acta—Proteins Proteom.* **2009**, *1794*, 375–397. [[CrossRef](#)]
13. Mucke, L.; Selkoe, D.J. Neurotoxicity of amyloid β -protein: Synaptic and network dysfunction. *Cold Spring Harb. Perspect. Med.* **2012**, *2*, a006338. [[CrossRef](#)] [[PubMed](#)]
14. Tanokashira, D.; Mamada, N.; Yamamoto, F.; Taniguchi, K.; Tamaoka, A.; Lakshmana, M.K.; Araki, W. The neurotoxicity of amyloid β -protein oligomers is reversible in a primary neuron model. *Mol. Brain* **2017**, *10*, 4. [[CrossRef](#)] [[PubMed](#)]
15. Lee, S.J.C.; Nam, E.; Lee, H.J.; Savellieff, M.G.; Lim, M.H. Towards an understanding of amyloid- β oligomers: Characterization, toxicity mechanisms, and inhibitors. *Chem. Soc. Rev.* **2017**, *46*, 310–323. [[CrossRef](#)]
16. Pagano, K.; Tomaselli, S.; Molinari, H.; Ragona, L. Natural Compounds as Inhibitors of A β Peptide Aggregation: Chemical Requirements and Molecular Mechanisms. *Front. Neurosci.* **2020**, *14*, 619667. [[CrossRef](#)] [[PubMed](#)]
17. Herrmann, K. Flavonols and flavones in food plants: A review. *Int. J. Food Sci. Technol.* **1976**, *11*, 433–448. [[CrossRef](#)]
18. Phan, H.T.T.; Samarut, K.; Takamaru, Y.; Azo-Oussou, A.F.; Nakazono, Y.; Vestergaard, M.C. Polyphenols modulate alzheimer's amyloid beta aggregation in a structure-dependent manner. *Nutrients* **2019**, *11*, 756. [[CrossRef](#)] [[PubMed](#)]
19. Singh, M.; Kaur, M.; Silakari, O. Flavones: An important scaffold for medicinal chemistry. *Eur. J. Med. Chem.* **2014**, *84*, 206–239. [[CrossRef](#)]
20. Yiannopoulou, K.G.; Papageorgiou, S.G. Current and Future Treatments in Alzheimer Disease: An Update. *J. Cent. Nerv. Syst. Dis.* **2020**, *12*, 1–12. [[CrossRef](#)]
21. Khan, H.; Marya, A.; Amin, S.; Kamal, M.A.; Patel, S. Flavonoids as acetylcholinesterase inhibitors: Current therapeutic standing and future prospects. *Biomed. Pharmacother.* **2018**, *101*, 860–870. [[CrossRef](#)]
22. Uriarte-Pueyo, I.; Calvo, M.I. Flavonoids as Acetylcholinesterase Inhibitors. *Curr. Med. Chem.* **2011**, *18*, 5289–5302. [[CrossRef](#)]
23. Abeyasinghe, A.A.D.T.; Deshapriya, R.D.U.S.; Udawatte, C. Alzheimer's disease; a review of the pathophysiological basis and therapeutic interventions. *Life Sci.* **2020**, *256*, 117996. [[CrossRef](#)]
24. Youdim, K.A.; Shukitt-Hale, B.; Joseph, J.A. Flavonoids and the brain: Interactions at the blood–brain barrier and their physiological effects on the central nervous system. *Free Radic. Biol. Med.* **2004**, *37*, 1683–1693. [[CrossRef](#)] [[PubMed](#)]
25. Yu, K.H.; Lee, C.I. Quercetin disaggregates prion fibrils and decreases fibril-induced cytotoxicity and oxidative stress. *Pharmaceutics* **2020**, *12*, 1081. [[CrossRef](#)]
26. Sonawane, S.K.; Balmik, A.A.; Boral, D.; Ramasamy, S.; Chinnathambi, S. Baicalein suppresses Repeat Tau fibrillization by sequestering oligomers. *Arch. Biochem. Biophys.* **2019**, *675*, 108119. [[CrossRef](#)] [[PubMed](#)]
27. Matos, A.M.; Cristóvão, J.S.; Yashunsky, D.V.; Nifantiev, N.E.; Viana, A.S.; Gomes, C.M.; Rauter, A.P. Synthesis and effects of flavonoid structure variation on amyloid- β aggregation. *Pure Appl. Chem.* **2017**, *89*, 1305–1320. [[CrossRef](#)]
28. Sato, M.; Murakami, K.; Uno, M.; Nakagawa, Y.; Katayama, S.; Akagi, K.I.; Masuda, Y.; Takegoshi, K.; Irie, K. Site-specific inhibitory mechanism for amyloid β 42 aggregation by catechol-type flavonoids targeting the lys residues. *J. Biol. Chem.* **2013**, *288*, 23212–23224. [[CrossRef](#)] [[PubMed](#)]
29. Hudson, S.A.; Ecroyd, H.; Kee, T.W.; Carver, J.A. The thioflavin T fluorescence assay for amyloid fibril detection can be biased by the presence of exogenous compounds. *FEBS J.* **2009**, *276*, 5960–5972. [[CrossRef](#)]
30. Ziaunys, M.; Mikalauskaite, K.; Smirnovas, V. Amyloidophilic Molecule Interactions on the Surface of Insulin Fibrils: Cooperative Binding and Fluorescence Quenching. *Sci. Rep.* **2019**, *9*, 20303. [[CrossRef](#)]
31. Sneideris, T.; Sakalauskas, A.; Sternke-Hoffmann, R.; Peduzzo, A.; Ziaunys, M.; Buell, A.K.; Smirnovas, V. The Environment Is a Key Factor in Determining the Anti-Amyloid Efficacy of EGCG. *Biomolecules* **2019**, *9*, 855. [[CrossRef](#)] [[PubMed](#)]
32. Sokolová, R.; Ramešová, Š.; Degano, I.; Hromadová, M.; Žabka, J. The oxidation of natural flavonoid quercetin. *Chem. Commun.* **2012**, *48*, 3433–3435. [[CrossRef](#)] [[PubMed](#)]
33. Walle, T. Methylation of Dietary Flavones Greatly Improves Their Hepatic Metabolic Stability and Intestinal Absorption. *Mol. Pharm.* **2007**, *4*, 826–832. [[CrossRef](#)]
34. Nagayoshi, H.; Murayama, N.; Kakimoto, K.; Tsujino, M.; Takenaka, S.; Katahira, J.; Lim, Y.R.; Kim, D.; Yamazaki, H.; Komori, M.; et al. Oxidation of Flavone, 5-Hydroxyflavone, and 5,7-Dihydroxyflavone to Mono-, Di-, and Tri-Hydroxyflavones by Human Cytochrome P450 Enzymes. *Chem. Res. Toxicol.* **2019**, *32*, 1268–1280. [[CrossRef](#)] [[PubMed](#)]

35. Walsh, D.M.; Thulin, E.; Minogue, A.M.; Gustavsson, N.; Pang, E.; Teplow, D.B.; Linse, S. A facile method for expression and purification of the Alzheimer's disease-associated amyloid β -peptide. *FEBS J.* **2009**, *276*, 1266–1281. [[CrossRef](#)]
36. Vignaud, H.; Bobo, C.; Lascu, I.; Sörgjerd, K.M.; Zako, T.; Maeda, M.; Salin, B.; Lecomte, S.; Cullin, C. A structure-toxicity study of A β 42 reveals a new anti-parallel aggregation pathway. *PLoS ONE* **2013**, *8*, e80262. [[CrossRef](#)]
37. Studier, F.W. Protein production by auto-induction in high-density shaking cultures. *Protein Expr. Purif.* **2005**, *41*, 207–234. [[CrossRef](#)]
38. Sakalauskas, A.; Ziaunys, M.; Smirnovas, V. Gallic acid oxidation products alter the formation pathway of insulin amyloid fibrils. *Sci. Rep.* **2020**, *10*, 14466. [[CrossRef](#)]
39. Jomová, K.; Hudcová, L.; Lauro, P.; Simunková, M.; Alwasel, S.H.; Alhazza, I.M.; Valko, M. A Switch between Antioxidant and Prooxidant Properties of the Phenolic Compounds Myricetin, Morin, 3',4'-Dihydroxyflavone, Taxifolin and 4-Hydroxy-Coumarin in the Presence of Copper(II) Ions: A Spectroscopic, Absorption Titration and DNA Damage Study. *Molecules* **2019**, *24*, 4335. [[CrossRef](#)]
40. Wormell, P.; Rodger, A. Absorption Spectroscopy: Relationship of Transition Type to Molecular Structure. In *Encyclopedia of Biophysics*; Roberts, G.C.K., Ed.; Springer: Berlin/Heidelberg, Germany, 2013; pp. 35–38. ISBN 978-3-642-16711-9.
41. Sakalauskas, A.; Ziaunys, M.; Smirnovas, V. Concentration-dependent polymorphism of insulin amyloid fibrils. *PeerJ* **2019**, *7*, e8208. [[CrossRef](#)]
42. Ma, L.; Yang, C.; Zheng, J.; Chen, Y.; Xiao, Y.; Huang, K. Non-polyphenolic natural inhibitors of amyloid aggregation. *Eur. J. Med. Chem.* **2020**, *192*, 112197. [[CrossRef](#)] [[PubMed](#)]

Article

Exploring the Formation of Polymers with Anti-Amyloid Properties within the 2′3′-Dihydroxyflavone Autoxidation Process

Andrius Sakalauskas , Agne Janoniene, Gediminas Zvinys, Kamile Mikalauskaite, Mantas Ziaunys and Vytautas Smirnovas * 

Institute of Biotechnology, Life Sciences Center, Vilnius University, LT-10257 Vilnius, Lithuania

* Correspondence: vytautas.smirnovas@bti.vu.lt

Abstract: Amyloid- β and α -synuclein aggregation into amyloid fibrils is linked to the onset and progression of Alzheimer's and Parkinson's diseases. While there are only a few disease-modifying drugs, it is essential to search for new, more effective ways to encounter these neurodegenerative diseases. Multiple research articles have shown that the autoxidation of flavone is a critical factor for activating the inhibitory potential against the protein aggregation. Despite this, the structure of the newly-formed inhibitors is unknown. In this research, we examined the autoxidation products of 2′,3′-dihydroxyflavone that were previously shown to possess one of the most prominent inhibitory effects against amyloid- β aggregation. Their analysis using HPLC suggested the formation of polymeric molecules that were isolated using a 3 kDa cut-off. These polymeric structures were indicated as the most potent inhibitors based on protein aggregation kinetics and AFM studies. This revelation was confirmed using MALDI-TOF and NMR. We also show that active molecules have a tendency to reduce the Amyloid- β and α -synuclein aggregates toxicity to SH-SY5Y cells.

Keywords: aggregation; amyloid-beta; alpha-synuclein; flavone; inhibition; autoxidation; polymers



Citation: Sakalauskas, A.; Janoniene, A.; Zvinys, G.; Mikalauskaite, K.; Ziaunys, M.; Smirnovas, V. Exploring the Formation of Polymers with Anti-Amyloid Properties within the 2′3′-Dihydroxyflavone Autoxidation Process. *Antioxidants* **2022**, *11*, 1711. <https://doi.org/10.3390/antiox11091711>

Academic Editor: Justyna Godos

Received: 22 July 2022

Accepted: 27 August 2022

Published: 30 August 2022

Publisher's Note: MDPI stays neutral with regard to jurisdictional claims in published maps and institutional affiliations.



Copyright: © 2022 by the authors. Licensee MDPI, Basel, Switzerland. This article is an open access article distributed under the terms and conditions of the Creative Commons Attribution (CC BY) license (<https://creativecommons.org/licenses/by/4.0/>).

1. Introduction

Protein accumulation into insoluble aggregates is linked with neurological disorders, such as Alzheimer's disease (AD) and Parkinson's disease (PD) [1]. AD was recognized as the most prevalent neurological condition affecting over 50 million people worldwide [2] and is projected to increase to 76 million by 2030 [3]. The pathological hallmark of AD is the deposition of extracellular amyloid- β (A β) peptide plaques and Tau neurofibrillary tangles in neuronal cells [4]. PD is known to be the second most common neurodegenerative disease after AD [5]. PD is considered a movement disorder caused by the accumulation of neuronal inclusions (Lewy Bodies) consisting of α -synuclein (aSyn) aggregates [6,7]. While both disorders are associated with aggregation that causes the onset of the disease, it is essential and beneficial to search for a potential treatment that could affect the beginning and progression of AD and PD.

Many possible counters for these neurological disorders involve treatment using anti-amyloid drugs [8–11]. In order to be effective, these compounds should selectively bind to the aggregation-prone peptide or protein, stabilizing them or changing the aggregation pathway to form non-toxic amorphous aggregates [12]. With this knowledge, numerous different compound groups have been screened, sorting out only potential inhibitors. However, this number has been vastly reduced in the clinical trials leaving only a few that can be used in the symptomatic treatment against AD and PD [13,14]. Therefore, it is necessary to fully test and categorize the newly found inhibiting molecules and understand their practical sense as anti-amyloid compounds.

Flavones belong to a group of natural anti-oxidants that are found in nature in fruits, herbs, spices, and vegetables [15,16]. Besides their anti-microbial, anti-HIV, anti-cancer,

anti-platelet, neuroprotective, anti-mutagenic, anti-allergic and anti-inflammatory characteristics [17–19], they were also shown in multiple reports to possess anti-amyloid properties [20–22]. A large number of flavone derivatives are described as acetylcholinesterase (AChE) inhibitors which makes them appealing candidates for the symptomatic treatment of AD [23,24]. In fact, there are twice as many flavone AChE inhibitors than flavanones, meaning that the structural integrity of the C2-C3 bond is essential [25]. However, the stability of flavones is questionable. The derivatives possessing neighboring hydroxyl groups are very likely to autoxidize at neutral or basic pH, completely changing the nature of these molecules [21]. Nevertheless, autoxidation improves the inhibitory effect against A β and insulin aggregation [20,22]. This effect is shown in studies covering different polyphenolic compound groups including flavones. The most famous is EGCG that possesses an inhibitory effect against aggregation of different proteins [26,27]. While the compound autoxidation mixture seems to have anti-amyloid features, it can hold components that have opposite or even cytotoxic effects. Therefore, it is essential to understand which autoxidation products exhibit inhibitory features towards protein aggregation.

The autoxidation of polyphenolic molecules can lead to multiple distinct products obtaining unique structures and features [28,29]. This process involves degradation, oxidative coupling [17,30,31], and polymerization [32]. A recent study shows that the browning of the epicatechin and epigallocatechin samples is related to the oxidative coupling where o-quinone intermediates participate [33]. A similar pattern is observed in the iron-mediated autoxidation of flavonoids that leads to the formation of dehydro-type dimers, while the autoxidative degradation results in the breakdown of the C ring and the formation of HBA, DHBA, THBA, and THPGA derivatives [34].

In order to identify the inhibitory molecules in the flavone oxidation mixture, we selected oxidized 2',3'-dihydroxyflavone, which has previously been shown to possess the highest inhibitory potential among number of tested flavones against A β aggregation [21]. The 2',3'-dihydroxyflavone has a C2-C3 double bond catechol moiety and the absence of 3-hydroxyl group that should favor the stabilization of the o-quinone and the oxidation coupling [30]. In this work, we show that the 2',3'-dihydroxyflavone oxidation products range from small degradation to large oligomeric molecular compounds. The sample molecules were separated using a 3 kDa cut-off and examined using HPLC. The anti-aggregation effects were tested on A β and aSyn aggregation. The fraction containing inhibitor molecules was scanned using MALDI-TOF and NMR.

2. Materials and Methods

2',3'-dihydroxyflavone oxidation. The 2',3'-dihydroxyflavone stock solution was prepared by dissolving 2',3'-dihydroxyflavone (Indofine Chemical Company, Inc., Hillsborough Township, NJ, USA) in dimethylsulfoxide (DMSO, Carl Roth) to a final concentration of 10 mM. The oxidation solution was prepared by diluting 10 mM stock solution with 10 mM sodium phosphate buffer (pH 8.0) and DMSO to yield a final flavone concentration of 0.5 mM in 9 mM sodium phosphate buffer solution containing 10% DMSO. The final 10% DMSO in buffer solution was used to increase the solubility. The autoxidation was carried out by incubating the solution in 37 °C for 100 h.

Separation of oDHF fractions. The oxidized 2',3'-dihydroxyflavone (oDHF) was distributed to the concentrators with a 3 kDa cut-off. The concentrators were spun at 4000 g for 20 min. The flowthrough consisting of <3 kDa molecular weight molecules (oDHF_{LOW}) and a cut-off sample consisting of >3 kDa molecular weight molecules (oDHF_{HIGH}) were separated. The oDHF_{HIGH} fraction was washed using the 9 mM sodium phosphate buffer solution containing 10% DMSO (pH 8.0) (further referred to as oxidation buffer) to remove all low molecular weight compounds from the mixture. The oDHF_{HIGH} was diluted to the original volume of oDHF to retain a comparable concentration of high molecular weight molecules in the sample (Figure S1 displays the sample preparation procedure).

High-performance liquid chromatography. The oDHF and its fractions (oDHF_{LOW} and oDHF_{HIGH}) were separated and analyzed using Shimadzu UFLC system with a CMB-

20A communication module, two LC20AD quaternary and isocratic pumps, a SIL-20AC autosampler, a CTO-20A column compartment and an SPD-M20A DAD detector (Shimadzu Corp., Kyoto, Japan). For the detection of the eluting molecules, the DAD spectra recording was set from 190 nm to 500 nm with a data rate of 12.5 Hz. The ODS-AQ HPLC separation column (15×4.6 , 3 μm , YMC) was used together with a 1 cm guard column. The HPLC grade MeCN (Fisher Scientific) and Milli-Q water ($18.2 \text{ M}\Omega \text{ cm}^{-1}$, Milli-Q Plus system, Millipore Bedford, MA, USA) were used for the RP-HPLC separation.

The samples were separated using a ternary gradient consisting of ultrapure water (eluent A), MeCN (eluent B) and 1% TFA in ultrapure water (eluent C). A constant 10% flow of eluent C was used to maintain 0.1% TFA concentration in the column throughout the separation experiment. The gradient between eluents A and B was 18% (0 min), 81% (20 min), and 81% (28 min). Before each analytical run, the column equilibration (10 column volume) was performed. The column thermostat was set to 40 °C and the flow rate to 1 mL min⁻¹.

Solid state ¹H NMR spectroscopy. ¹H solid-state NMR spectra were recorded on a Bruker spectrometer (400 MHz) (Billerica, MA, USA) in DMSO-D₆ using residual DMSO signals (2.50 ppm) as the internal standard, and proton chemical shifts were expressed in parts per million (ppm).

MALDI-TOF mass analysis. Full scan MALDI-TOF-MS mass spectra were performed on a Bruker Autoflex Speed (Billerica, MA, USA) using a 1 kHz smartbeam™-II laser for MALDI. The mass spectra laser shots were collected for the spectra at a 19.5 kV acceleration voltage. The oDHF_{HW} sample was prepared with 2,5-dihydroxybenzoic acid (2,5-DHB) and sinapinic acid (SA) matrixes.

Preparation of sample with 2,5-DHB matrix: 1 μL of 2,5-DHB solution (20 mg/mL in the 30% ACN [*v/v*] containing 0.1% TFA) and 1 μM of oDHF_{HW} were deposited on the MALDI target plate and dried under vacuum.

Preparation of sample with SA matrix: saturated SA in EtOH was deposited on the MALDI target plate and dried under vacuum. Then 1 μL of SA solution (20 mg/mL in the 30% ACN [*v/v*] containing 0.1% TFA) and 1 μM of oDHF_{HW} were deposited on the MALDI target plate and dried under vacuum.

Purification of recombinant A β 42. The A β 42 peptide was expressed in *E. coli* BL-21Star™ (DE3) (Invitrogen, Carlsbad, CA, USA) and purified similarly as previously described [21]. In brief, the cell culture was grown for 15 h in a ZYM-5052 medium containing ampicillin (100 $\mu\text{g}/\text{mL}$). Then, after collecting the cell pellet, it was homogenized, sonicated, centrifuged and washed using 20 mM Tris/HCL and 1 mM EDTA buffer solution (pH 8.0). The procedure was repeated three times to remove all soluble proteins. Then, the remaining cell pellet was resuspended, homogenized and sonicated in the buffer solution containing 20 mM Tris/HCL, 8 M urea and 1 mM EDTA (pH 8.0). After centrifugation, the supernatant was diluted four times using 20 mM Tris/HCL, 1 mM EDTA buffer solution (pH 8.0) and mixed with 50 mL DEAE-Sepharose (equilibrated in the same buffer solution), and agitated using a magnetic stirrer at 80 rpm for 30 min at 4 °C. For the chromatography procedure, a Buchner funnel with Fisherbrand glass microfiber paper on a vacuum glass bottle was used. The resin was washed with the loading buffer (20 mM Tris/HCL, 1 mM EDTA pH 8.0), increasing NaCl concentration using a step gradient procedure. The steps contained 0, 20, 150, and 500 mM of NaCl in the loading buffer solution. The target protein was collected in the fraction containing 150 mM NaCl. Collected protein sample was flash-frozen, lyophilized and stored at -20 °C.

To separate any impurities from the target peptide, size exclusion chromatography (SEC) was performed. The lyophilized powder was dissolved in a 20 mM sodium phosphate buffer solution containing 5 M GuSCN (pH 8.0). The sample was then loaded on a Tricorn 10/300 column (packed with Superdex 75) and eluted at 1 mL/min using 20 mM sodium phosphate, 0.2 mM EDTA and 0.02% NaN₃ buffer solution (pH 8.0). The target peptide was eluted at around 15 min. The eluted protein fraction was lyophilized and stored at -20 °C. Before each experiment, the SEC procedure was repeated to prepare the fresh

peptide solution (without any oligomeric or fibrillar structures). The protein fraction with purified A β was collected to the maximum recovery microtubes (Corning, New York, NY, USA) and stored on ice for 2 min, while the concentration was determined by integrating the UV absorbance peak ($\epsilon_{280} = 1490 \text{ M}^{-1} \text{ cm}^{-1}$). Then, the peptide sample was diluted and immediately used for the experiments.

Purification of recombinant aSyn. aSyn was purified similarly as previously described [35]. In short, the cells with expressed aSyn were homogenized and then sonicated using a buffer solution containing 20 mM Tris/HCl, 0.5 M NaCl, 1 mM EDTA and 1 mM PMSF (pH 8.0). The supernatant was then heated for 20 min at 80 °C using a water bath. The aggregated proteins were centrifuged at $15,000 \times g$ for 30 min at 4 °C, and then soluble aSyn (collected in the supernatant) was precipitated by adding ammonium sulphate (using ~40% saturation). The precipitated proteins were centrifuged and dissolved in a dialysis buffer solution containing 20 mM Tris/HCl, 1 mM EDTA, 0.5 mM DTT, and were dialyzed and loaded onto the HiScale 26/300 column (packed with DEAE-Sepharose equilibrated in the dialysis buffer). The target peptide was washed using a salt gradient (0.1 M NaCl). The collected fractions with aSyn were concentrated and loaded on HiLoad 26/600 column (packed with Superdex 75 pg) and eluted at 4 mL/min using a 50 mM ammonium bicarbonate buffer solution. The eluted protein was flash-frozen, lyophilized and stored at $-20 \text{ }^{\circ}\text{C}$.

Aggregation kinetics of A β peptide. The purified peptide (1.5 mL, pH 8.0) was mixed with 3 mL 20 mM sodium phosphate buffer solution (pH 6.33) to yield a 3-fold diluted peptide solution (pH 7.0). The peptide was mixed with 20 mM sodium phosphate buffer (pH 7.0), 10 mM thioflavin-T (ThT) (Sigma-Aldrich, cat. No. T3516) stock solution, oxidation buffer and oDHF (or its fraction—oDHF_{LW}, oDHF_{HW}) to the final reaction mixture, containing 1 μM A β , 20 μM ThT, 10% (*v/v*) (percentages in all further cases are in form of *v/v*) of corresponding oDHF sample and 1% DMSO. For the experiments where a range of oDHF_{HW} concentrations were used (0–20%), the initial oDHF_{HW} was diluted using an oxidation buffer. The aggregation kinetics was followed in non-binding 96-well plates (Fisher, Waltham, MA, USA, cat. No. 10438082) (sample volume was 80 μL) at 37 °C by measuring ThT fluorescence using 440 nm excitation and 480 emission wavelengths in a ClarioStar Plus plate reader (BMG Labtech, Ortenberg, Germany).

Aggregation kinetics of aSyn. Lyophilised aSyn powder was dissolved in a 20 mM potassium phosphate buffer (pH 7.4) containing 300 mM NaCl and filtered through a 0.22 μm syringe filter. The protein concentration was determined by measuring the sample absorbance at 280 nm using a Nanodrop 2000 spectrophotometer (Thermo Fisher Scientific, Inc., Waltham, MA, USA) ($\epsilon_{280} = 5960 \text{ M}^{-1} \text{ cm}^{-1}$). Then, the protein sample was mixed with 10 mM ThT stock solution, oxidation buffer and oDHF (or its fraction—oDHF_{LW}, oDHF_{HW}) to a final reaction mixture, containing 100 μM aSyn, 100 μM ThT, 20% of corresponding oDHF sample and 2% DMSO. In case of aSyn fibril samples that were used with SH-SY5Y cells, the range of inhibitor concentration was used (0.1–40%). The kinetic experiments were performed similarly as mentioned above with A β additionally using 600 RPM orbital agitation and each plate well containing a single 3 mm glass bead (sample volume was 100 μL).

Atomic force microscopy (AFM). Samples for AFM images were collected after kinetic measurements (experiment time—1000 min for A β and 2500 min for aSyn) and scanned similarly as previously described [20]. In short, 40 μL of 0.5% (*v/v*) APTES (Sigma-Aldrich, cat. No. 440140) in MilliQ water was deposited on freshly cleaved mica and incubated for 5 min. Then, the mica was carefully washed using 2 mL of MilliQ water and dried under gentle airflow and 40 μL of each sample was deposited on the functionalized surface and incubated for another 5 min. Prepared samples were again washed using 2 mL of MilliQ water and dried under gentle airflow. AFM imaging was performed using a Dimension Icon (Bruker) atomic force microscope in tapping mode using RTESPA-300 probes. The 10 $\mu\text{m} \times 10 \mu\text{m}$ images of the 1024 \times 1024 pixel resolution were analyzed using Gwyddion 2.5.5 software. The heights and widths of the structures found on the mica were determined by tracing perpendicular to each structure axes.

FTIR. aSyn fibrils were pelleted by centrifuging at $16,100\times g$ for 10 min. Then, the supernatant was removed, and 0.5 mL of D₂O was added. This procedure was repeated three times to replace most of the water molecules with the D₂O. After the last centrifugation step, the fibrils were resuspended in 80 μ L of D₂O. The FTIR procedure was performed as previously described [36]. In brief, the spectra were recorded using an Invenio S IR spectrophotometer equipped with a Mercury Cadmium Telluride detector. The sample was placed in the CaF₂ transmission windows with 0.05 mm Teflon spacers, 256 interferograms of 2 cm^{-1} resolution were averaged per spectrum. Before normalizing to the same area of Amide I region (1705–1595 cm^{-1}), the D₂O and water vapor spectrums were subtracted. The data were processed using GRAMS software (Thermo Fisher Scientific, Inc., Waltham, MA, USA).

Cell culturing. SH-SY5Y human neuroblastoma cells were obtained from American Type Culture Collection (ATCC, Manassas, VA, USA). The cells were grown in Dulbecco's Modified Eagle Medium (DMEM) (Gibco, Grand Island, NY, USA), supplemented with 10% Fetal Bovine Serum (FBS) (Sigma-Aldrich, St. Louis, MO, USA), 1% Penicillin-Streptomycin (10,000 U/mL) (Gibco, Grand Island, NY, USA) at 37 °C in a humidified, 5% CO₂ atmosphere in a CO₂ incubator.

MTT assay. SH-SY5Y cells were seeded in a 96-well plate (15,000 cells/well) and were allowed to attach overnight. Then the medium was changed to the one containing A β monomers or fibrils or aSyn fibrils with or without the different amounts of oDHF_{HW} (2% to 20% of the three times concentrated sample) and different amounts of oDHF_{HW} (2% to 20% of the three times concentrated sample) alone. The cell viability was not performed with aSyn monomers due to the aggregation conditions-constant agitation with glass beads which may disrupt the assay. To remove DMSO, the oDHF_{HW} sample was lyophilized and resuspended in a 10 mM phosphate buffer (pH 8.0). Medium, containing buffers (20 mM phosphate buffer solution as A β stock solution and 10 mM phosphate buffer as oDHF_{HW} stock solution), served as a control. After 48 h of incubation 10 μ M of 3-(4,5-dimethylthiazol-2-yl)-2,5-diphenyltetrazolium bromide (MTT) reagent (12.1 mM in PBS) was added to each well and left to incubate for 2 h. Then, 100 μ L of 10% SDS with 0.01 N HCl solution was added to each well to dissolve formazan crystals and, after 2 h, the absorbance at 570 nm and 690 nm (reference wavelength) of each well was measured using a ClarioStar Plus plate reader.

LDH assay. Quantification of LDH release into the medium was assessed using a cytotoxicity detection kit (Roche Applied Science, Germany) under the manufacturer's protocol. Briefly, SH-SY5Y cells were seeded in a 96-well plate (15,000 cells/well) and were allowed to attach overnight. Then the medium inside the wells was aspirated, and 100 μ L of Advanced DMEM (Gibco, Grand Island, NY, USA) was added to each well. Afterwards, A β monomers with different oDHF_{HW} concentrations were suspended in Advanced DMEM and were added to the wells (to reach 200 μ L total medium volume in each well), which resulted in the final 3 μ M A β and range of oDHF_{HW} (2–20%) concentrations. After 24 h of incubation, 100 μ L of the medium from each well was aspirated, centrifuged, and transferred into a TPP 96-well tissue culture test plate (Trasadingen, Switzerland). LDH reagent was added, and after 30 min of incubation at room temperature, the absorbance of wells was measured at 492 nm and 600 nm (reference wavelength) using a ClarioStar Plus plate reader.

Data analysis. The aggregation kinetics were followed at least in triplicate independent samples. The data analysis was performed by fitting the kinetic curves using Boltzmann's sigmoidal equation [36]. The relative half-time values were calculated based on the control sample in their specific microplate. The data were processed using Origin software (OriginLab, Northampton, MA, USA).

All the experiments with SH-SY5Y cells were performed at least in triplicate independent measurements. The obtained values are represented as mean with standard deviation. Student's t-test was used to evaluate statistical significance between the groups with a probability of * $p < 0.05$, ** $p < 0.01$, and *** $p < 0.001$.

3. Results

It is known that the autoxidation of polyphenolic compounds may lead to the formation of the higher mass molecules as a result of oxidation and interflavic coupling reactions [31]. Due to this, we first separated coupling and degradation products of the oxidized 2',3'-dihydroxyflavone (oDHF) mixture using a concentrator (3 kDa cut-off). The 2',3'-dihydroxyflavone, oDHF and its fractions of lower molecular weight (oDHF_{LOW}) and higher molecular weight (oDHF_{HIGH}) components were analyzed using HPLC separation (Figure 1A). The 2',3'-dihydroxyflavone autoxidized to many different components seen in the chromatogram. The shallow and broad peak (12–27 min) resembles the elution of the mixture containing various lengths of oligomeric molecules [37]. Most of the eluting peaks in the oDHF_{LOW} sample separation were within the 2.5–17.5 min range. In the case of oDHF_{HIGH}, the chromatogram mainly contains a shallow peak that is typical for a broad range of oligomeric species (12–27 min). Except for this, the chromatogram contains a few peaks that are also visible in the oDHF_{LOW} chromatogram.

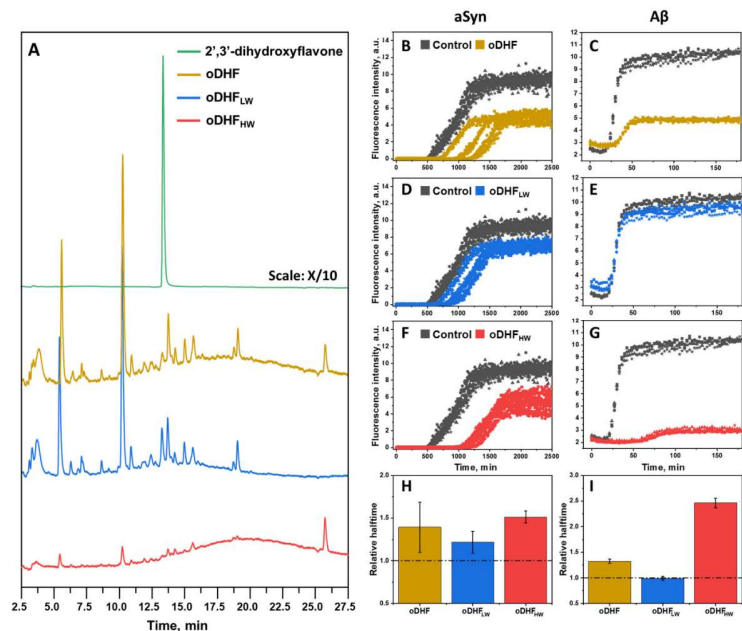


Figure 1. Chromatographic separation of 2',3'-dihydroxyflavone, oDHF and oDHF fractions (oDHF_{LOW} and oDHF_{HIGH}) (A). aSyn (100 μ M) (B,D,F) and A β (1 μ M) (C,E,G) aggregation kinetics in the presence of oDHF, oDHF_{LOW} and oDHF_{HIGH} (20% for aSyn and 10% for A β experiments) and their respective relative half-time values (H,I). The relative half-time values were calculated based on the control sample and error bars are one standard deviation (n = 3).

To further test the inhibitory effect of each sample, the oDHF, oDHF_{LOW} and oDHF_{HIGH} were used in the aSyn (Figure 1B,D,F) aggregation experiment. When using oDHF, the aggregation is stochastic (t_{50} values are highly dispersed) and reaches plateau at twice as low ThT intensity values compared to the control sample. Similar diminished ThT intensity values were seen in the experiments with oDHF_{HIGH}, where the relative half-time was the highest amongst the tested inhibitor samples. However, the oDHF_{LOW} had the lowest effect on aSyn aggregation, only slowing down the aggregation by ~25%. A similar result is seen in the aggregation experiments with A β (Figure 1C,E,G). The oDHF and oDHF_{HIGH}

greatly diminished the ThT intensity, while oDHF_{1W} had no effect. This effect of ThT quenching, which has no impact on or correlation with the number of aggregates formed, was previously assessed in the literature [21]. The relative half-time values (Figure 1H,I) followed the same trend, where the oDHF_{HW} showed a significantly higher inhibitory effect than the oDHF. At the same time, the oDHF_{1W} did not possess any influence on the aggregation time of A β .

Based on the results presented in Figure 1, we have further investigated the oDHF_{HW} sample. First, we measured the mass spectrum with MALDI-TOF using positive ionization and two ionization matrices (Sinapinic acid and 2,5-DHB) (Figure S2). The results revealed a number of different m/z values ranging from 400 m/z to 2000 m/z . The m/z difference between maxima of adjacent peak clusters was measured to be constant ($\sim 246.51 \pm 0.36$ molar mass (the Z value was determined to be equal to one)). The visible pattern of m/z distribution is specific to the polymeric structure. It may be that lower molecular weight compounds did oversaturate the detector, limiting the observation of higher molecular weight polymers. It is worth noting that the lowest m/z values did not match the mass of 2',3'-dihydroxyflavone (254,238), nor the mass difference between different lengths of polymers. In addition, the 2',3'-dihydroxyflavone and oDHF_{HW} NMR spectra display different characteristics (Figure S3). The unoxidized flavone NMR spectrum exhibits intense and narrow peak signals assigned to the initial flavone structure. The opposite spectrum is seen in the case of the oDHF_{HW} sample. A broad multiplet in the aromatic region is observed (between 6.33 and 8.68 ppm), which indicates a formation of potentially branched polydisperse polymers. The high level of polydispersity of oDHF_{HW} was confirmed using DLS measurement data (data not shown). Such findings correlate with eight aromatic protons (atoms 1–3, 6, 9, 13–15) observed in 2',3'-dihydroxyflavone NMR spectra (Figure S2B,C). Protons of hydroxyl groups (18 and 19, 10.00 and 9.57 ppm respectively) were not present in the proton NMR spectra of oDHF_{HW}.

To characterize the inhibitory effect of oDHF_{HW} against A β aggregation, a range of inhibitor concentrations was used (Figure 2A). The ThT fluorescence intensity was diminished with the increasing concentration of oDHF_{HW}. The ThT fluorescence intensity was lowered by half using 1% of oDHF_{HW} and was entirely reduced to the noise level when the oDHF_{HW} concentration was 20% (Figures 2A and S4). However, the A β aggregation relative half-time relationship with the oDHF_{HW} concentration (Figure 2D) followed two different trends that had a point of discontinuity at 2% of oDHF_{HW} concentration. The lower concentrations slightly decrease (up to 10%) the aggregation half-time, enhancing the fibrillization rate. The inhibitory effect, which seems to have affected both nucleation and elongation stages, occurred only when using a 4% or higher inhibitor concentration. The 20% oDHF_{HW} relative aggregation half-time value was excluded from the graph because of the low ThT fluorescence intensity that would result in low-quality fit (Figure S4).

The SH-SY5Y cell viability (Figure 2B) and LDH release (Figure 2E) tests were performed to understand whether the inhibition of A β aggregation also reduces its cytotoxicity to cells. The oDHF_{HW} alone did not significantly affect the cell viability and LDH release at any used concentration. Despite that, when A β monomers and oDHF_{HW} were incubated with cells, the survivability adopted the non-linear correlation. When the oDHF_{HW} concentration was 2%, the cell survivability and LDH release were the same as without the inhibitor. Increasing the concentration to 4% increased the cell viability to a statistically significant ($p < 0.05$). Nonetheless, the higher oDHF_{HW} concentration turned in the opposite direction, where the cell viability was lower than with A β alone.

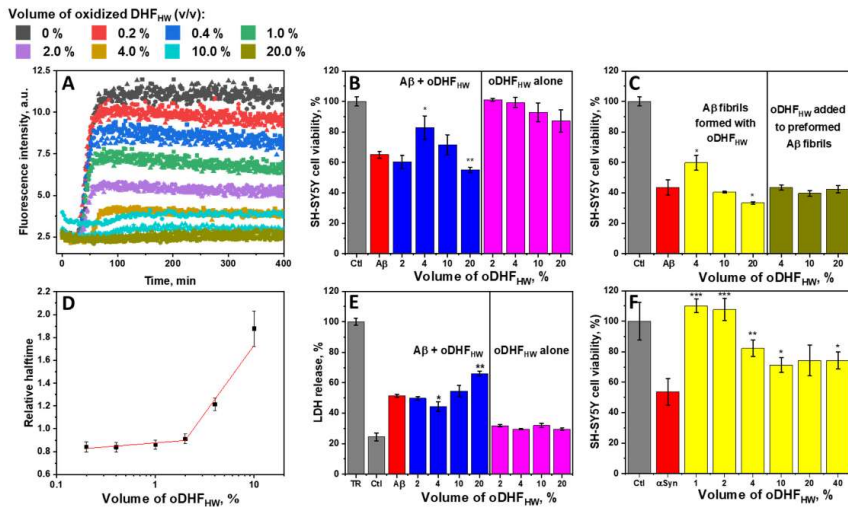


Figure 2. The kinetic curves of 1 μM Aβ aggregation with a range of oDHF_{HW} (0%–20% v/v) (A), and their respective relative half-time values (D) compared to the control sample. SH-SY5Y cell viability (B) and LDH release (E) after incubating (48 and 24 h, respectively) with 3 μM of Aβ and different oDHF_{HW} concentrations (% by v/v). SH-SY5Y cell viability after incubating 48 h with 3 μM Aβ (C) and 100 μM aSyn (F) fibrils formed with or without the oDHF_{HW}. Student’s *t*-test significance values were compared to the Aβ or aSyn controls, * *p* < 0.05, ** *p* < 0.01, and *** *p* < 0.001. Relative aggregation half-time error bars are one standard deviation (n = 3) approximated using a linear fit.

The equal effect is seen when Aβ was aggregated with oDHF_{HW}, and then the pre-formed fibrils were added to the SH-SY5Y cells medium and incubated for 48 h (Figure 2C). At the same time, there was no significant effect on the cell viability if the fibrils were formed without oDHF_{HW} and only then mixed together and incubated (24 h at 37 °Celsius) before pooling them on cells. More favorable results were observed with the preformed fibrils of aSyn in the presence of a different concentration of oDHF_{HW} (Figure 2F). When the oDHF_{HW} concentration was 1% to 2%, a significant reduction (*p* < 0.001) of aSyn cytotoxic effect on SH-SY5Y cells was recorded. The higher concentration of inhibitors had less of an impact, although it significantly increased cell viability.

Atomic force microscopy imaging was employed to observe the structures formed during Aβ aggregation kinetics experiment in the presence of oDHF_{HW} (concentration range 0–20%) (Figure 3A–E). The Aβ alone formed typical short 4–5 nm height fibrils that can be seen in the aggregation experiments using a low peptide concentration (1 μM) [38,39]. Very similar structures were observed with 1% of oDHF_{HW}. However, the height (Figure 3G) and width (Figure 3H) distribution are more dispersed since oDHF_{HW} (as a polymeric structure) (Figure 3F) was found on the mica in the form of round shape structures with height (4–15 nm) and width (20–40 nm) values larger than the Aβ alone. In the sample images where the oDHF_{HW} concentration was higher (4% to 20%), the larger round shape structures were visible, potentially being the product of the Aβ and oDHF_{HW} combination. These structures are statistically seen in the upward shift of maximum height and width mean and median values. No round shape structures, nor significant height or width distributions, were found in the samples of aSyn aggregates formed in the presence of oDHF, oDHF_{LW} and oDHF_{HW} (Figure S5A–F).

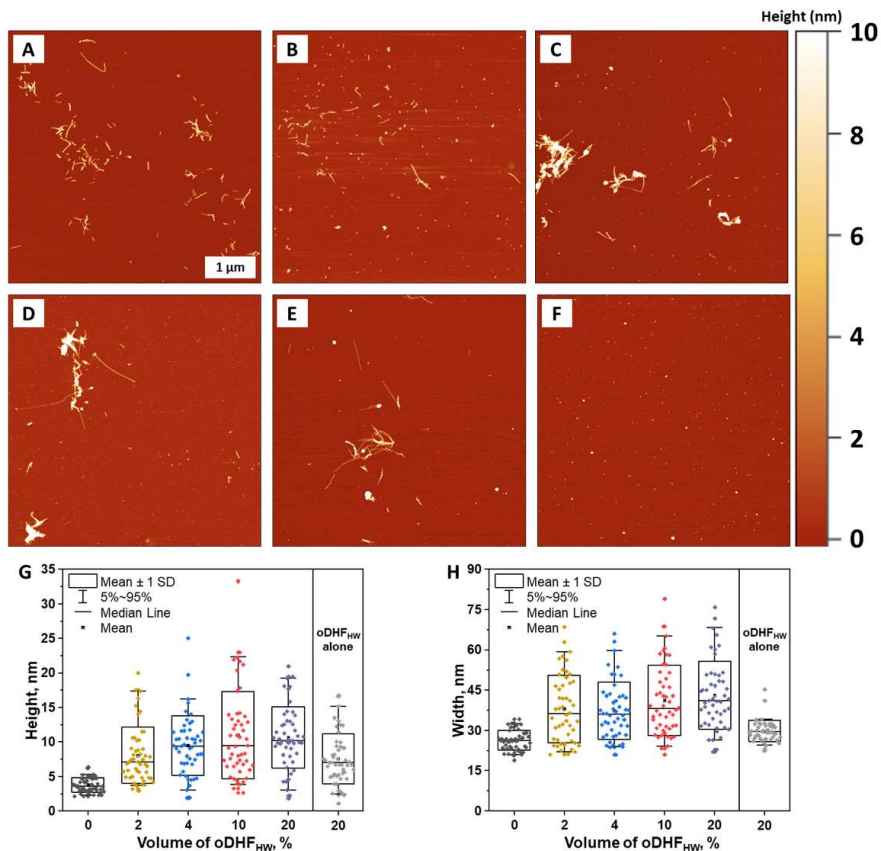


Figure 3. Atomic force microscopy (AFM) images of A β without (A) and with 1% (B), 4% (C), 10% (D) and 20% (E) oDHF_{HW} concentration and the 20% of oDHF_{HW} alone (F). The height (G) and width (H) distribution of structures present on the mica, where box plots indicate mean \pm SD and error bars are in the 5–95% range (n = 50).

4. Discussion

The interest in the autoxidation of polyphenolic molecules in protein aggregation studies is growing because it has been proven that the initial polyphenol does not have an effect against the aggregation process, while the autoxidation mixture possesses anti-amyloid features [20–22,26]. The 2'3'-dihydroxyflavone autoxidation was confirmed in our study (Figure 1A), leading to the scarce amount of the initial compound and a variety of different end-products. These products were possibly formed during the processes of degradation, oxidation coupling and polymerization [30,33,34].

The initial strategy of using membrane concentrators was expected to aid in isolating the larger molecules fraction (considering the formation of polymeric structures) from the rest of the smaller molecules in the autoxidation sample. There is no real evidence about whether all oDHF_{HW} molecules at the time of separation were more than 3 kDa molecular weight. In fact, the smaller molecules (<3 kDa) might not have passed through the membrane (3 kDa cut-off) because of the possible planar aromatic structure that cannot

bend through the multiple pores. Despite this fact, the separated fractions exhibited drastically different inhibition effects against protein aggregation (Figure 1B–I). The oDHF_{HW} had sustained all the inhibitory potential, while oDHF_{LW} only slightly impacted aSyn aggregation, providing the evidence that larger flavone autoxidation products can function as anti-aggregation agents. This may also reflect the idea that a different concentration of inhibitor is necessary for a significant inhibition of distinct protein/peptide aggregation processes. In particular, this inhibitor/protein ratio is significantly lower for aSyn compared to studies with A β [27]. For this reason, the lower amount of inhibitor that may be present in DHF_{LW}, is capable of slowing down the aggregation of aSyn, but not A β . In the case of A β , the molecular mass of the inhibitor must be larger than what passes through the 3 kDa membrane, while for aSyn, smaller polymeric molecules (that do pass through the membrane) also act as inhibitor compounds. This led to the assumption that only larger molecular mass components of the autoxidation sample possess the anti-amyloid features.

The larger mass molecules from the DHF autoxidation sample adopted polydisperse polymeric characteristics, loss of the hydroxyl groups and coordination with sodium ions (the mass of neighboring peaks differ by 23 Da (Figures S2 and S3)). These findings indicate that the autoxidation of 2',3'-dihydroxyflavone (pH 8.0) leads to the polymerization of intermediate products. The literature describes a potential pathway through the formation of quinone moiety in the B ring [30,33]. Such motifs are more likely to form when flavones possess the C2-C3 double bond and absence of 3-OH group. Flavones that contain the aforementioned characteristics and neighboring hydroxyl groups are also shown to oxidize and exhibit anti-amyloid features [21]. However, the MALDI-TOF results suggest that the polymerization mechanism is more complex. The measured monomeric mass difference (246–247 Da) leads to an assumption that the polymerization occurs after further molecular changes or coupling of degradation products.

Since the inhibitor is a polymer, it is necessary to discuss its impact on protein aggregation. The AFM data in this work suggest the formation of higher and wider round-shaped structures. These macromolecules might be the reaction products between the inhibitor and a certain form of A β structure (monomer/oligomer or fibrillar) (Figure 3). The increasing concentration of oDHF_{HW} reduces the aggregation rate; however, this trend does contradict the cell viability assay. This inconsistency between results may be related to ThT fluorescence quenching by the inhibitor molecules, which reduces the signal intensity but not the formation of fibrillar structures. The longer aggregation term may lead to the formation of different A β aggregation intermediate products through a changed aggregation pathway that resulted in different cytotoxic effects on the SH-SY5Y cells (Figure 2B,E). In fact, the preformed fibrils with oDHF_{HW} showed similar cell viability results, meaning that the cytotoxic effect is exhibited by the end products. At the same time, the cytotoxicity tends to be gained during the initial protein aggregation phase as oDHF_{HW} did not change the A β cytotoxicity to cells when the fibrils were preformed without the inhibitor. On a positive note, the lower inhibitor concentrations reveal the reduced cytotoxicity of A β and aSyn. This outcome could probably be related to stabilization of protein monomeric/oligomeric species. Potentially, the 4% concentration of oDHF_{HW} in A β aggregation experiments leads to the formation of longer protofibrils that are covered with the inhibitor molecules, while at higher oDHF_{HW} concentrations, there are more inhibitor molecules that stabilize smaller oligomeric particles that are more toxic. Therefore, the margin of inhibitor concentration that diminishes the cytotoxic effect is narrow (at lower concentrations, there is no effect, while at higher there is decreased cell viability).

5. Conclusions

Taking all these results together, it appears that only part of the autoxidation products of 2',3'-dihydroxyflavone exhibit anti-amyloid effects against A β and aSyn. These molecules appear to be of a polymeric nature and bind to the oligomeric and fibrillar structures of A β increasing the cell viability; however, the effect is reversed at higher concentrations of inhibitor.

Supplementary Materials: The following are available online at <https://www.mdpi.com/article/10.3390/antiox11091711/s1>, Figure S1: Oxidation of 2',3'-dihydroxyflavone and the separation procedure of the oxidation mixture; Figure S2: MALDI-TOF spectrum of oDHF_{HW} prepared using SA (A) and 2,5-DHB (B) as a MALDI matrix material; Figure S3: The ¹H NMR spectra of oDHF_{HW} and 2',3'-dihydroxyflavone recorded in DMSO-d₆ (A). Aromatic region (9.0–6.0 ppm) of oDHF_{HW} (B) and the zoomed spectra (10.5–6.5 ppm) of 2',3'-dihydroxyflavone aromatic and hydroxyl groups region; Figure S4: The kinetic curves of 1 μM Aβ aggregation with 50 μM and 100 μM oDHF_{HW}; Figure S5: Atomic force microscopy (AFM) images of aSyn without (A) and with oDHF (B), oDHF_{LW} (C) and oDHF_{HW} (D). The fibril height (E) and width (F) distribution, where box plots indicate mean ± SD and error bars are in the 5–95% range (n = 50). The FTIR spectra of aSyn fibrils formed with or without inhibitors (G) and their second derivatives (H).

Author Contributions: A.S. and V.S. designed the experiments, A.S., A.J., G.Z., M.Z. and K.M. performed the experiments, A.S., M.Z. and V.S. analyzed the data and prepared the manuscript. All authors have read and agreed to the published version of the manuscript.

Funding: European Social Fund under the Global Grant Measure, project number VP1-3.1-ŠMM-07-K-02-020 and Marie Curie Career Integration Grant 293476.

Institutional Review Board Statement: Not applicable.

Informed Consent Statement: Not applicable.

Data Availability Statement: The data presented in this study are available on request.

Conflicts of Interest: The authors declare no conflict of interest.

References

1. Chiti, F.; Dobson, C.M. Protein Misfolding, Amyloid Formation, and Human Disease: A Summary of Progress Over the Last Decade. *Annu. Rev. Biochem.* **2017**, *86*, 27–68. [[CrossRef](#)] [[PubMed](#)]
2. Anand, A.; Patience, A.A.; Sharma, N.; Khurana, N. The present and future of pharmacotherapy of Alzheimer's disease: A comprehensive review. *Eur. J. Pharmacol.* **2017**, *815*, 364–375. [[CrossRef](#)] [[PubMed](#)]
3. World Health Organization. Dementia Fact Sheet. Available online: <https://www.who.int/news-room/fact-sheets/detail/dementia> (accessed on 10 June 2022).
4. Vaz, M.; Silvestre, S. Alzheimer's disease: Recent treatment strategies. *Eur. J. Pharmacol.* **2020**, *887*, 173554. [[CrossRef](#)] [[PubMed](#)]
5. Lebouvier, T.; Chaumette, T.; Paillusson, S.; Duyckaerts, C.; Bruley Des Varannes, S.; Neunlist, M.; Derkinderen, P. The second brain and Parkinson's disease. *Eur. J. Neurosci.* **2009**, *30*, 735–741. [[CrossRef](#)]
6. Ball, N.; Teo, W.P.; Chandra, S.; Chapman, J. Parkinson's disease and the environment. *Front. Neurol.* **2019**, *10*, 218. [[CrossRef](#)]
7. Söderbom, G. Status and future directions of clinical trials in Parkinson's disease. *Int. Rev. Neurobiol.* **2020**, *154*, 153–188. [[CrossRef](#)]
8. Athar, T.; Al Balushi, K.; Khan, S.A. Recent advances on drug development and emerging therapeutic agents for Alzheimer's disease. *Mol. Biol. Rep.* **2021**, *48*, 5629–5645. [[CrossRef](#)]
9. Peña-Bautista, C.; Casas-Fernández, E.; Vento, M.; Baquero, M.; Cháfer-Pericás, C. Stress and neurodegeneration. *Clin. Chim. Acta* **2020**, *503*, 163–168. [[CrossRef](#)]
10. Molino, S.; Dossena, M.; Buonocore, D.; Ferrari, F.; Venturini, L.; Ricevuti, G.; Verri, M. Polyphenols in dementia: From molecular basis to clinical trials. *Life Sci.* **2016**, *161*, 69–77. [[CrossRef](#)]
11. Ji, C.; Sigurdsson, E.M. Current Status of Clinical Trials on Tau Immunotherapies. *Drugs* **2021**, *81*, 1135–1152. [[CrossRef](#)]
12. Velander, P.; Wu, L.; Henderson, F.; Zhang, S.; Bevan, D.R.; Xu, B. Natural product-based amyloid inhibitors. *Biochem. Pharmacol.* **2017**, *139*, 40–55. [[CrossRef](#)] [[PubMed](#)]
13. Mullard, A. Controversial Alzheimer's drug approval could affect other diseases. *Nature* **2021**, *595*, 162–163. [[CrossRef](#)] [[PubMed](#)]
14. Srivastava, S.; Ahmad, R.; Khare, S.K. Alzheimer's disease and its treatment by different approaches: A review. *Eur. J. Med. Chem.* **2021**, *216*, 113320. [[CrossRef](#)] [[PubMed](#)]
15. Verma, A.K.; Pratap, R. The biological potential of flavones. *Nat. Prod. Rep.* **2010**, *27*, 1571–1593. [[CrossRef](#)] [[PubMed](#)]
16. Wang, X.; Cao, Y.; Chen, S.; Lin, J.; Bian, J.; Huang, D. Anti-Inflammation Activity of Flavones and Their Structure-Activity Relationship. *J. Agric. Food Chem.* **2021**, *69*, 7285–7302. [[CrossRef](#)]
17. Es-Safi, N.E.; Ghidouche, S.; Ducrot, P.H. Flavonoids: Hemisynthesis, reactivity, characterization and free radical scavenging activity. *Molecules* **2007**, *12*, 2228–2258. [[CrossRef](#)]
18. Singh, M.; Silakari, O. *Flavone: An Important Scaffold for Medicinal Chemistry*; Elsevier: Amsterdam, The Netherlands, 2018; ISBN 9780081020838.
19. Singh, M.; Kaur, M.; Silakari, O. Flavones: An important scaffold for medicinal chemistry. *Eur. J. Med. Chem.* **2014**, *84*, 206–239. [[CrossRef](#)]

20. Sato, M.; Murakami, K.; Uno, M.; Nakagawa, Y.; Katayama, S.; Akagi, K.I.; Masuda, Y.; Takegoshi, K.; Irie, K. Site-specific inhibitory mechanism for amyloid β 42 aggregation by catechol-type flavonoids targeting the lys residues. *J. Biol. Chem.* **2013**, *288*, 23212–23224. [[CrossRef](#)]
21. Sakalauskas, A.; Ziaunys, M.; Snieckute, R.; Smirnovas, V. Autoxidation Enhances Anti-Amyloid Potential of Flavone Derivatives. *Antioxidants* **2021**, *10*, 1428. [[CrossRef](#)]
22. Matos, A.M.; Cristóvão, J.S.; Yashunsky, D.V.; Nifantiev, N.E.; Viana, A.S.; Gomes, C.M.; Rauter, A.P. Synthesis and effects of flavonoid structure variation on amyloid- β aggregation. *Pure Appl. Chem.* **2017**, *89*, 1305–1320. [[CrossRef](#)]
23. Khan, H.; Marya, A.; Amin, S.; Kamal, M.A.; Patel, S. Flavonoids as acetylcholinesterase inhibitors: Current therapeutic standing and future prospects. *Biomed. Pharmacother.* **2018**, *101*, 860–870. [[CrossRef](#)] [[PubMed](#)]
24. Yiannopoulou, K.G.; Papageorgiou, S.G. Current and Future Treatments in Alzheimer Disease: An Update. *J. Cent. Nerv. Syst. Dis.* **2020**, *12*, 1–12. [[CrossRef](#)]
25. Uriarte-Pueyo, I.; Calvo, I.M. Flavonoids as Acetylcholinesterase Inhibitors. *Curr. Med. Chem.* **2011**, *18*, 5289–5302. [[CrossRef](#)]
26. Sneideris, T.; Sakalauskas, A.; Sternke-Hoffmann, R.; Peduzzo, A.; Ziaunys, M.; Buell, A.K.; Smirnovas, V. The Environment Is a Key Factor in Determining the Anti-Amyloid Efficacy of EGCG. *Biomolecules* **2019**, *9*, 855. [[CrossRef](#)] [[PubMed](#)]
27. Ziaunys, M.; Mikalauskaitė, K.; Sakalauskas, A.; Smirnovas, V. Interplay between epigallocatechin-3-gallate and ionic strength during amyloid aggregation. *PeerJ* **2021**, *9*, e12381. [[CrossRef](#)] [[PubMed](#)]
28. Ramešová, Š.; Sokolová, R.; Tarábek, J.; Degano, I. The oxidation of luteolin, the natural flavonoid dye. *Electrochim. Acta* **2013**, *110*, 646–654. [[CrossRef](#)]
29. Sokolová, R.; Ramešová, Š.; Degano, I.; Hromadová, M.; Žabka, J. The oxidation of natural flavonoid quercetin. *Chem. Commun.* **2012**, *48*, 3433–3435. [[CrossRef](#)]
30. Bijlsma, J.; de Bruijn, W.J.C.; Velikov, K.P.; Vincken, J.P. Unravelling discolouration caused by iron-flavonoid interactions: Complexation, oxidation, and formation of networks. *Food Chem.* **2022**, *370*, 131292. [[CrossRef](#)]
31. Masuda, T.; Nojima, S.; Miura, Y.; Honda, S.; Masuda, A. An oxidative coupling product of luteolin with cysteine ester and its enhanced inhibitory activity for xanthine oxidase. *Bioorganic Med. Chem. Lett.* **2015**, *25*, 3117–3119. [[CrossRef](#)]
32. Di Gennaro, P.; Sabatini, V.; Fallarini, S.; Pagliarini, R.; Sello, G. Polyphenol Polymerization by an Alternative Oxidative Microbial Enzyme and Characterization of the Biological Activity of Oligomers. *Biomed. Res. Int.* **2018**, *2018*, 12–14. [[CrossRef](#)]
33. Tan, J.; De Bruijn, W.J.C.; Van Zadelhoff, A.; Lin, Z.; Vincken, J.P. Browning of Epicatechin (EC) and Epigallocatechin (EGC) by Auto-Oxidation. *J. Agric. Food Chem.* **2020**, *68*, 13879–13887. [[CrossRef](#)] [[PubMed](#)]
34. Chaaban, H.; Ioannou, I.; Paris, C.; Charbonnel, C.; Ghoul, M. The photostability of flavanones, flavonols and flavones and evolution of their antioxidant activity. *J. Photochem. Photobiol. A Chem.* **2017**, *336*, 131–139. [[CrossRef](#)]
35. Šneideris, T.; Baranauskienė, L.; Cannon, J.G.; Rutkienė, R.; Meškys, R.; Smirnovas, V. Looking for a generic inhibitor of amyloid-like fibril formation among flavone derivatives. *PeerJ* **2015**, *2015*, 1–17. [[CrossRef](#)]
36. Ziaunys, M.; Sakalauskas, A.; Mikalauskaitė, K.; Smirnovas, V. Polymorphism of Alpha-Synuclein Amyloid Fibrils Depends on Ionic Strength and Protein Concentration. *Int. J. Mol. Sci.* **2021**, *22*, 12382. [[CrossRef](#)] [[PubMed](#)]
37. Vonk, E.C.; Langeveld-Voss, B.M.W.; Van Dongen, J.L.J.; Janssen, R.A.J.; Claessens, H.A.; Cramers, C.A. Separation and characterization of oligomers by reversed-phase high-performance liquid chromatography; a study on well-defined oligothiophenes. *J. Chromatogr. A* **2001**, *911*, 13–26. [[CrossRef](#)] [[PubMed](#)]
38. Mastrangelo, I.A.; Ahmed, M.; Sato, T.; Liu, W.; Wang, C.; Hough, P.; Smith, S.O. High-resolution atomic force microscopy of soluble A β 42 oligomers. *J. Mol. Biol.* **2006**, *358*, 106–119. [[CrossRef](#)] [[PubMed](#)]
39. Banerjee, S.; Sun, Z.; Hayden, E.Y.; Teplow, D.B.; Lyubchenko, Y.L. Nanoscale Dynamics of Amyloid β -42 Oligomers as Revealed by High-Speed Atomic Force Microscopy. *ACS Nano* **2017**, *11*, 12202–12209. [[CrossRef](#)]



Article

The Major Components of Cerebrospinal Fluid Dictate the Characteristics of Inhibitors against Amyloid-Beta Aggregation

Andrius Sakalauskas *[†], Mantas Ziaunys, Ruta Snieckute [†], Agne Janoniene, Dominykas Veiveris, Mantas Zvirblis, Virginija Dudutiene and Vytautas Smirnovas *[†]

Institute of Biotechnology, Life Sciences Center, Vilnius University, LT-10257 Vilnius, Lithuania

* Correspondence: andrius.sakalauskas@gmc.vu.lt (A.S.); vytautas.smirnovas@bti.vu.lt (V.S.)

Abstract: The main pathological hallmark of Alzheimer’s disease (AD) is the aggregation of amyloid- β into amyloid fibrils, leading to a neurodegeneration cascade. The current medications are far from sufficient to prevent the onset of the disease, hence requiring more research to find new alternative drugs for curing AD. In vitro inhibition experiments are one of the primary tools in testing whether a molecule may be potent to impede the aggregation of amyloid-beta peptide ($A\beta_{42}$). However, kinetic experiments in vitro do not match the mechanism found when aggregating $A\beta_{42}$ in cerebrospinal fluid. The different aggregation mechanisms and the composition of the reaction mixtures may also impact the characteristics of the inhibitor molecules. For this reason, altering the reaction mixture to resemble components found in cerebrospinal fluid (CSF) is critical to partially compensate for the mismatch between the inhibition experiments in vivo and in vitro. In this study, we used an artificial cerebrospinal fluid that contained the major components found in CSF and performed $A\beta_{42}$ aggregation inhibition studies using oxidized epigallocatechin-3-gallate (EGCG) and fluorinated benzenesulfonamide VR16-09. This led to a discovery of a complete turnaround of their inhibitory characteristics, rendering EGCG ineffective while significantly improving the efficacy of VR16-09. HSA was the main contributor in the mixture that significantly increased the anti-amyloid characteristics of VR16-09.

Keywords: protein aggregation; amyloid-beta; inhibition; EGCG; VR16-09; aggregation kinetics; near-physiological conditions



Citation: Sakalauskas, A.; Ziaunys, M.; Snieckute, R.; Janoniene, A.; Veiveris, D.; Zvirblis, M.; Dudutiene, V.; Smirnovas, V. The Major Components of Cerebrospinal Fluid Dictate the Characteristics of Inhibitors against Amyloid-Beta Aggregation. *Int. J. Mol. Sci.* **2023**, *24*, 5991. <https://doi.org/10.3390/ijms24065991>

Academic Editor: Bruno Imbimbo

Received: 27 February 2023

Revised: 20 March 2023

Accepted: 21 March 2023

Published: 22 March 2023



Copyright: © 2023 by the authors. Licensee MDPI, Basel, Switzerland. This article is an open access article distributed under the terms and conditions of the Creative Commons Attribution (CC BY) license (<https://creativecommons.org/licenses/by/4.0/>).

1. Introduction

Alzheimer’s disease (AD) belongs to a group of disorders identified as neurodegenerative diseases [1]. The main pathophysiological hallmark of AD is the accumulation of extracellular senile plaques (SPs) and neurofibrillary tangles [2]. Amyloid β ($A\beta$) is considered the main component of these plaques and influences the onset of AD [3]. The constant production of 40-amino acid-long $A\beta$ ($A\beta_{40}$) by proteolysis of the integral membrane protein called amyloid precursor protein (APP) is a normal process that occurs throughout the entire lifespan of humans [4]. However, the dysregulation or an incorrect proteolytic cleavage of APP, producing 42-amino acid-long $A\beta$ ($A\beta_{42}$), may lead to a continuous imbalance between the production and elimination of the peptide, resulting in elevated levels of $A\beta_{40}$ and $A\beta_{42}$ [5]. This cascade step is followed by the oligomerization and fibrillation of $A\beta$ that drives the accumulation of SPs [6].

Various therapies aim to reduce or prevent the progression of AD [7]. While the efficiency of these established programs is minimal, the development of drugs against this neurodegenerative disorder is carried out through different strategies aimed at one or more targets, including $A\beta$ (production, anti-aggregation, and immunotherapy), Tau protein (immunotherapy, phosphorylation, and aggregation), neuroinflammation, and ease of the behavioral, psychological symptoms of dementia [8,9].

One of the strategies is to search for an active anti-amyloid compound that would interact with A β ₄₂ and prevent or slow the aggregation process. The primary step for this approach is screening the potential molecules *in silico* and *in vitro* [10]. *In vitro* screening experiments using different origins of A β ₄₂ peptides (synthetic or recombinant) found that specific reaction mixtures may lead to a distinct aggregation mechanism that could affect the inhibition studies [11,12]. First, there are studies where inhibition of A β ₄₂ was performed in a purification buffer after the final chromatographic step. In this case, the reaction mixture contained elevated pH (8.0–8.5) and reduced ionic strength compared to physiological conditions, resulting in aggregates with different morphologies and secondary structures [13]. Second, synthetic A β ₄₂ peptide aggregates slower than the recombinant version, affecting the aggregation pathway and cell toxicity [12]. In addition, a prolonged aggregation may lead to secondary events, such as degradation and modification of the inhibitor or the fluorescent dye used in the aggregation assay [14], that could shift the perception of the inhibition process. Finally, PBS is the most common buffered system where A β ₄₂ is aggregated. While the medium possesses similar pH and ionic strength, it lacks the main components typically found in cerebrospinal fluid (CSF) [15].

CSF surrounds the brain tissue, and A β ₄₂ aggregation may occur in the drainage of brain interstitial fluid [16]. CSF is a clear, colorless fluid and contains more sodium ions, chloride ions, and glucose but less calcium and potassium ions than in the blood [17]. A β ₄₂ assembly into fibrillar aggregates differs in CSF than in PBS or Hepes buffered systems [18,19]. It is known that both non-chaperone [20–22] and chaperone [23] proteins affect the aggregation of A β *in vivo* and *in vitro*. One of these proteins is albumin, found in CSF (<0.4 mg/mL), and is up to 90% of the total protein count in the fluid [24]. Stanyon and Viles showed that human serum albumin (HSA) regulates the aggregation of A β ₄₂ by binding to the peptide and trapping it in a nonfibrillar form [25]. In addition to HSA, transthyretin [26], transferrin [27], immunoglobulins, and other proteins are found in nanomolar concentrations [24]. Furthermore, CSF contains amino acids that may also contribute to altering the aggregation. According to research by Rainesalo, glutamine (450 μ M–900 μ M) was the main amino acid found in the CSF (control subjects). In contrast, the concentration of all other amino acids was up to 25 μ M [28].

Although it is impossible to recreate CSF perfectly to contain the equivalent levels of the vast number of components, it is necessary to improve the search for anti-amyloid compounds *in vitro* by mimicking the composition of CSF. Specific molecules present in CSF, such as albumin [20] or metal ions [29,30], may alter the aggregation pathway, which could completely change the properties of the inhibitor. The composition of artificial cerebrospinal fluid (aCSF) should minimize the barrier between the results *in vitro* and *in vivo*.

In this work, we have created an aCSF containing major components of CSF and tested how it affects the A β ₄₂ aggregation process. Two inhibitors were used to inhibit A β ₄₂ aggregation in PBS and the aCSF. One is fluorinated benzenesulfonamide VR16-09, previously shown to possess anti-amyloid characteristics against A β , α -synuclein, and insulin aggregation [31]. The other inhibitor used in this study was oxidized EGCG. EGCG was found to be unstable and prone to autoxidize at neutral or higher pH, which enhances its potency to inhibit various protein aggregation, including A β and α -synuclein [32,33]. We show that both inhibitors acted differently in the selected solutions, altering the conclusions drawn about their anti-amyloid properties.

2. Results

A β ₄₂ and its aggregates are found in the cerebrospinal fluid surrounding brain tissues [3]. This is why it is essential to alter the *in vitro* screening conditions to closely match the main components of the cerebrospinal fluid in order to gain confidence in the results. The created aCSF used in the experiments contained glucose, CaCl₂, MgCl₂, glutamine, urea, cholesterol, lactate, and human serum albumin.

In this work, we compared A β ₄₂ aggregation in PBS and aCSF (Figure 1). The two chemically different inhibitors, fluorinated benzenesulfonamide VR16-09 (Figure S1A) [31]

and oxidized polyphenol EGCG (Figure S1B) [32], were used to account for the aggregation inhibition changes among the selected solutions. In PBS (Figure 1A), oxidized EGCG increased $A\beta_{42}$ aggregation half-time two-fold and reduced the final ThT fluorescence intensity. This intensity reduction was previously shown to be related to ThT fluorescence quenching due to its interaction with the oxidated polyphenols or inner filter effects [34,35]. VR16-09, on the other hand, proved to be less impactful, with almost no reduction in the aggregation half-time compared with the control sample. However, there was a significantly higher baseline of VR16-09 than oxidized EGCG (intrinsic fluorescence in the selected emission wavelength range). Fluorescence intensity curves of inhibitor compounds in the absence of $A\beta_{42}$ are presented in Supplementary Materials (Figure S2). A completely opposite result was observed when $A\beta_{42}$ aggregated in the aCSF (Figure 1B). While oxidized EGCG reduced the final ThT fluorescence intensity level, the aggregation curves reached a plateau earlier than the control sample. In the sample where $A\beta_{42}$ aggregated with VR16-09, the aggregation half-time was increased with no shift of the ThT fluorescence intensity. It is important to note that in both reaction solutions, $A\beta_{42}$ aggregation half-time with oxidized EGCG was of a similar value (Figure 1C), while VR16-09 had a complete turnover, significantly slowing $A\beta_{42}$ aggregation in the aCSF reaction mixture. This shift, however, was not observed during the MTT assay in cells (Figure S3).

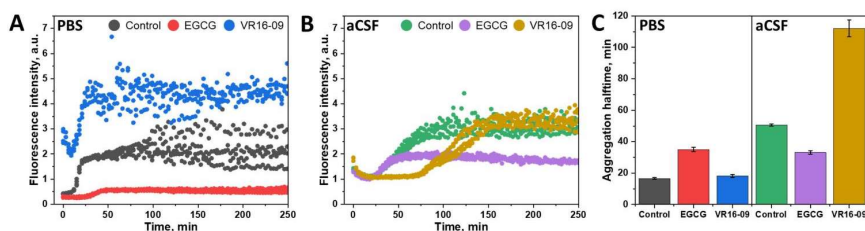


Figure 1. $A\beta$ (2 μ M) aggregation kinetics in PBS (A) and aCSF (B) in the absence or presence of 25 μ M of oxidized EGCG or VR16-09 and their respective relative half-time values (C). The three separate repeats of each kinetic experiment are shown in the graphs. Error bars are one standard deviation (n = 4).

Further, it was decided to compare the morphology of $A\beta_{42}$ aggregates formed in PBS and aCSF using AFM (Figure 2A,D). The $A\beta$ fibrils in PBS and aCSF were mostly clumped together into larger structures with a limited number of single fibrils. The fibril height distribution of control samples (Figure 2G) showed no significant difference and correlated to fibril heights found in the literature [36]. A similar view was seen in AFM images of samples where $A\beta_{42}$ was aggregated with oxidized EGCG (Figure 2B,E). However, in the case of aCSF, a vast number of smaller, round-shape structures was observed, while in PBS, the structures were less abundant and larger. Despite this fact, there was no significant difference in their height distribution (Figure 2H). In contrast, $A\beta_{42}$ aggregates formed with VR16-09 in PBS were shorter and significantly higher compared to the fibrils formed in the aCSF (Figure 2C,F,I). Additionally, $A\beta$ fibrils formed in the aCSF with VR16-09 were longer than in the sample with oxidized EGCG.

The aCSF is a more complex reaction mixture than PBS, containing glucose, Ca^{2+} , Mg^{2+} ions, urea, cholesterol, lactate, glutamine, and HSA. For this reason, experiments were conducted where each of the aforementioned components was used in $A\beta_{42}$ aggregation assays with and without VR16-09 (Figure 3). $CaCl_2$, $MgCl_2$, and urea sped up the $A\beta_{42}$ aggregation, while glutamine and HSA contributed to a longer fibrillation time (Figure 3H). Cholesterol, lactate, and glucose did not significantly affect the assembly of $A\beta_{42}$ fibrils. The $A\beta_{42}$ aggregation inhibition using VR16-09 was not achieved in the reaction without additional aCSF components, where only NaCl, KCl, KH_2PO_4 , Na_2HPO_4 , and NaH_2PO_4 components were present (Figure 3A) (Further referred to as w/o aCSF components). In

the presence of any component, the inhibition of VR16-09 was altered. All the components, except glutamine, enhanced the inhibitory effect of VR16-09. The most impactful element was HSA (Figure 3D), increasing both to $A\beta_{42}$ aggregation halftime and the inhibitory effect of VR16-09 more than two-fold. On the other hand, glutamine negatively contributed to the inhibitory potential of VR16-09. When all the components were present (Figure 3G), the inhibitory effect was increased, although the aggregation halftime of the control sample was reduced compared to the sample with HSA.

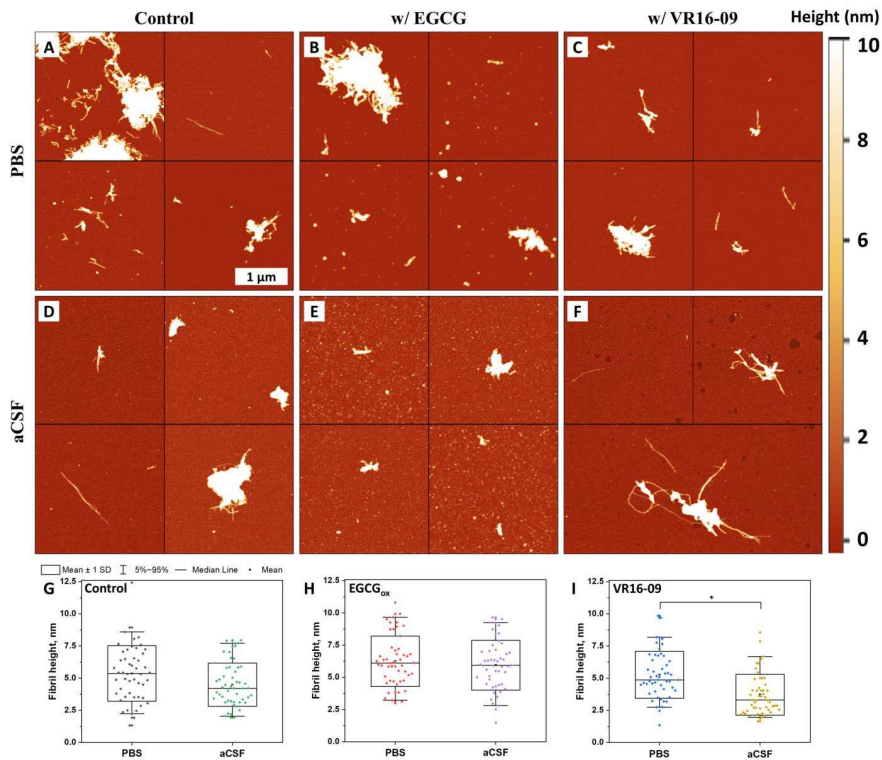


Figure 2. Atomic force microscopy (AFM) images of $A\beta_{42}$ aggregates formed without (A,D) and with 25 μM of oxidized EGCG (B,E) or with 25 μM of VR16-09 (C,F) in PBS and aCSF, respectively. The fibril height distribution among aggregates formed in PBS and aCSF without (G) and with oxidized EGCG (H) or VR16-09 (I), where box plots indicate mean \pm SD and error bars are in the 5–95% range ($n = 50$). ANOVA (Bonferroni) significance values were compared. * $p < 0.01$.

AFM images revealed that $A\beta_{42}$ aggregates formed without additional aCSF components (Figure 3B,I) were up to several micrometers in length and 2–6 nm in height while being irregularly clumped together or dispersed throughout the mica. When VR16-09 was present in the sample (Figure 3C), fibrils were of similar length but more clumped together, forming larger structures. Even larger clusters of aggregates were found when $A\beta_{42}$ was aggregated with HSA (Figure 3E). However, the samples had visually longer fibrils than in the previous cases. When HSA and VR16-09 were present in the reaction mixture (Figure 3F), fewer fibrils were found on the mica. They were up to 2–3 μm in length and 3–8 nm in height. No larger clumps of aggregates were found in this particular

case. An interesting instance to note, the addition of VR16-09 significantly increased the height of the fibrils, but it did not contribute to any significant height difference among the samples with the inhibitor, regardless of whether HSA was present or not.

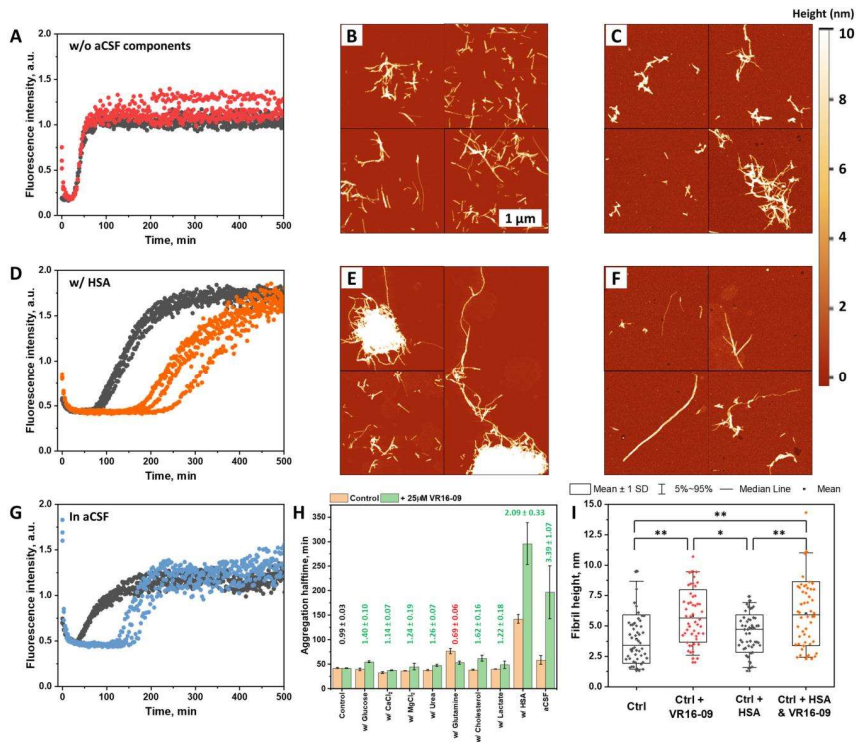


Figure 3. $A\beta_{42}$ (2 μM) aggregation kinetics in the reaction mixture without aCSF components (control) (A), with HSA (D), and with all aCSF components (G) in the absence (black) or presence (colored) of 25 μM of VR16-09. $A\beta_{42}$ aggregation half-time values (H) when aggregated with each aCSF component in the absence and presence of 25 μM of VR16-09. Relative aggregation half-time values calculated between the sample with and without the inhibitor are listed above each column in green. Error bars are one standard deviation ($n = 4$). Atomic force microscopy (AFM) images of $A\beta_{42}$ aggregates formed in the reaction mixture without aCSF components (B,C) or with HSA (E,F) in the absence or presence of 25 μM of VR16-09, respectively. Their height distribution box plot (I) indicates mean \pm SD, and error bars are in the 5–95% range ($n = 50$). ANOVA (Bonferroni) significance values were compared, * $p < 0.01$, ** $p < 0.001$.

To further determine the impact of VR16-09 on the aggregation of $A\beta_{42}$ in aCSF, $A\beta_{42}$ was aggregated under a range of protein concentrations from 0.75 to 2.0 μM , with or without 25 μM of VR16-09 (Figure 4A,B). To compare the inhibition, $A\beta_{42}$ was also aggregated in aCSF without serum albumin (Figure 4C,D), which seemed to make the greatest impact on the inhibitory effect of VR16-09 (Figure 3) as well as on the morphology of the fibrils formed and $A\beta_{42}$ toxic impact on cells during MTT assay (Figure S4). Instead of measuring the aggregation half-time, global fitting of the data was performed using a four-step model (nucleation, elongation, secondary nucleation, and fragmentation), as described previously [37]. The data were corrected for the initial signal intensity

drop to allow for a more accurate fitting procedure. The entire procedure is described in the Materials and Method section. Fit aided in calculating combined rate constants of primary nucleation–elongation (Figure 4E), elongation–secondary nucleation (Figure 4F), and elongation–fragmentation (Figure 4G). The kinetic and global-fitting data suggested that the addition of albumin and VR16-09 prolongs the aggregation of $A\beta_{42}$; however, in a different pattern. Removal of HSA from the aCSF formulation, whether VR16-09 was present or not, contributed to a sizeable decrease in the combined elongation–fragmentation rate constant (Figure 4G) while revealing an increase in primary nucleation–elongation and elongation–secondary nucleation (Figure 4E,F) rate constants in the environment with the VR16-09 compound. Accordingly, a lower fragmentation was visible in the previously shown AFM images (Figure 3).

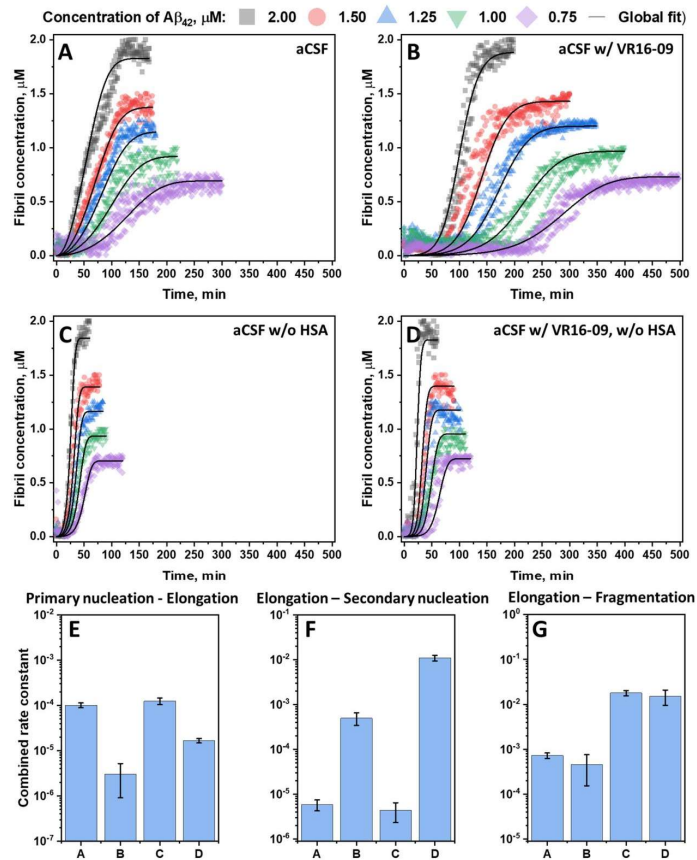


Figure 4. $A\beta_{42}$ aggregation kinetics in aCSF (A), aCSF with 25 μM VR16-09 (B), aCSF without HSA (C), and aCSF with 25 μM VR16-09 and without HSA (D). The fibril concentration in the Y axis is the concentration of monomers in their aggregated state (assuming the aggregation efficiency was 100%). For each condition, a four-step global-fitting aggregation model was used. Combined primary nucleation–elongation (E), elongation–secondary nucleation (F), and elongation–fragmentation (G) rate constants were obtained at each condition by global-fit of the $A\beta_{42}$ concentration range (0.75–2 μM). Error bars are one standard deviation ($n = 3$).

On the other hand, VR16-09 had a profound effect on the combined rate constants by significantly decreasing primary nucleation–elongation and considerably reducing elongation–secondary nucleation, while the elongation–fragmentation constant was unaffected. Specifically, this trend was visible to the naked eye in aCSF when VR16-09 was added. The $A\beta_{42}$ aggregation lag time increased, but the slope of the kinetic curves remained similar.

3. Discussion

Perhaps because the initial screening experiments when searching for the anti-amyloid compound were initiated in PBS or other reaction mixtures used to aggregate $A\beta_{42}$ (not in CSF), the components of cerebrospinal fluid were overlooked as crucial contributors to the inhibition studies. Out of eight compounds chosen in the formulation of the aCSF (Figure 3), HSA and glutamine had an inhibitory effect against $A\beta_{42}$ aggregation. While the inhibitory effect of HSA is known to be a “Monomer-competitor” [20], there is no record of glutamine affecting the fibrillation process of $A\beta_{42}$. This amino acid may interact with $A\beta_{42}$ through the formation of hydrogen bonds, hence stabilizing the protein. Compared to studies with inhibitors [31,34,38], a 0.7 mM concentration would be considered very high. Such inhibitor levels should be avoided due to potential toxic side effects on cells. However, the glutamine levels in CSF of regular patients can be even higher (0.9 mM) [28], enabling the possible regulation of $A\beta_{42}$ aggregation. In addition to the inhibitors present in the aCSF (Figure 3), the addition of Ca^{2+} and Mg^{2+} sped up the aggregation. This correlates with previous observations, as it has been shown that Ca^{2+} promotes the oligomerization of intracellular $A\beta_{42}$ [29].

The more complex picture was when all the components were present in the reaction mixture. The aggregation of $A\beta_{42}$ in the aCSF was enhanced by Ca^{2+} , Mg^{2+} and inhibited by HSA and glutamine. Unfortunately, the situation became less clear because the components in the mixture were likely prone to cross-interactions. For example, Bode et al. showed that cholesterol, fatty acids, and warfarin suppress the inhibitory effect of HSA on $A\beta_{42}$ [39]. Both of these components were present in aCSF. However, $A\beta_{42}$ aggregation half-time was more than 2-fold higher in the aCSF compared to PBS but lower than in the reaction mixture with HSA only (Figure 3A,D,G). A similar trend was observed by Padayachee et al., who compared $A\beta_{42}$ aggregation in a Hepes buffered system and in CSF samples from human patients [18]. This could mean a close relationship between the components in CSF and aCSF, affecting $A\beta_{42}$ aggregation. Nonetheless, the link between the components and the aggregation mechanism of $A\beta_{42}$ remains convoluted.

In PBS, in the presence of oxidized EGCG, the $A\beta_{42}$ fibrillation process slowed (Figure 1A). As it is typical to polyphenolic molecules containing neighboring hydroxy groups, the oxidation of EGCG may lead to the formation of polymeric molecules that are capable of binding to lysine and arginine amine groups that stabilize the protein monomer [32,40,41]. This would help to explain the accelerated fibrillation process in aCSF (Figure 1B). HSA with both lysine and arginine groups was present in the reaction mixture, which may bind to and reduce the number of oxidized EGCG molecules that may covalently interact with $A\beta_{42}$. This hypothesis is supported by AFM images (Figure 2). A number of smaller spherical objects were seen in the sample of aCSF, while in PBS, the structures were larger and less abundant. In the case of VR16-09, the opposite effect was observed. PBS had no inhibitory effect, possibly due to the solubility issues. However, matters changed when $A\beta_{42}$ was aggregated in aCSF, where the inhibitory effect of VR16-09 was greatly enhanced. This could be explained by the combined inhibition reaction with the components of aCSF. The claim is supported by the results presented in Figure 3, where all the components, except glutamine, enhanced the inhibitory effect. This also explains why $A\beta_{42}$ aggregation without any aCSF components was not inhibited by VR16-09 (Figure 3A). This result, however, contradicts the previously published data [31]. This inconsistency may have appeared due to several layers of mismatch—the nature of

the A β ₄₂ peptide (synthetic or recombinant), the concentration of the inhibitor, and the difference in preparation procedures.

The experiments in aCSF revealed its profound effect on the potency of amyloid inhibitors. VR16-09 was previously introduced as an insulin aggregation inhibitor with only low-to-moderate applicability against A β ₄₂ aggregation [31] (at higher inhibitor concentrations). This fluorinated benzenesulfonamide showed a pronounced effect and inhibited A β ₄₂ aggregation in aCSF by suppressing primary nucleation (Figure 4), associated with an extended aggregation lag time [42]. The interesting aspect of this inhibition is that VR16-09 and HSA had a combined effect by suppressing primary nucleation. This could be related to the interaction between VR16-09 and A β ₄₂ that may reduce the number of free monomers in the sample capable of forming a nucleus. Further, it is possible that during A β ₄₂ aggregation, VR16-09 binds to the fibrils, accelerating the surface catalysis reflected in an increased secondary nucleation rate. When HSA was present, this effect may be countered by decreasing affinity between A β ₄₂ monomers and its fibrils' surface or by reducing the number of free monomers in the sample [20]. While VR16-09 was not the most potent, the need for screening in an altered medium consisting of molecules found in CSF that affect A β ₄₂ aggregation is critical. Molecules, such as EGCG, that did not pass clinical trials were thought to lack the oxidation step, which is a key factor enabling its inhibition against protein aggregation [32]. However, after analyzing the results presented in this manuscript, the oxidized EGCG did not show any inhibitory effect against A β ₄₂ aggregation in aCSF, except for the reduced ThT fluorescence intensity, which can be altered by the presence of exogenous compounds [43].

4. Materials and Methods

4.1. Preparation of aCSF Reaction Mixture

The artificial cerebrospinal fluid was prepared based on the findings of human cerebrospinal fluid [24,44,45] and previously published compositions of aCSF [28,46,47] to contain the main components that may interact with protein aggregation and inhibition processes. A concentrated aCSF solution was prepared in three separate parts, listed in Table 1. The three parts were selected in order to avoid Ca²⁺ and Mg²⁺ ion reactivity with phosphate when dissolving them. HSA, cholesterol, sodium lactate, and glutamine (Part 3) were chosen to be dissolved separately to prevent the impact of high salt concentration. To prepare 1× aCSF, three parts were mixed together and diluted using MilliQ water at the ratio 9:9:10:72 (Part 1:Part 2:Part 3:MilliQ water). To account for the pH difference between the prepared solutions and the one measured in CSF (7.33), 1.6 μ L (*v/v*) of 25% HCl was added to 10 mL of 1× aCSF, which yielded a pH of 7.33. 100× D-glucose, CaCl₂, MgCl₂, Urea, sodium lactate, 10× HSA, cholesterol, and glutamine stocks were prepared for the experiments where separate components were used.

4.2. Preparation of Epigallocatechin-3-Gallate (EGCG)

EGCG is prone to autooxidation at neutral or higher pH resulting in the formation of different autooxidation products. These products are shown to possess an elevated inhibitory effect against protein aggregation. In order to avoid EGCG autooxidation during the protein aggregation experiments that may render the process unstable, EGCG was fully autooxidized. EGCG powder (Fluorochem, Glossop, UK, cat. No. M01719) was dissolved in 100 mM potassium phosphate buffer, pH 7.4, to a final concentration of 10 mM. Then, 1 mL of the solution was placed into 1.5 mL test tubes and incubated for 72 h at 60 °C. After this procedure, the test tubes were stored at −20 °C.

4.3. A β ₄₂ Aggregation Experiments

The A β ₄₂ peptide was expressed in *E. coli* BL-21StarTM (DE3) (Invitrogen, Carlsbad, CA, USA) and purified using the expression vector, as described previously [34,48]. The purified peptide fraction (8–20 μ M) (1.5 mL, 20 mM sodium phosphate, 0.2 mM EDTA pH 8) was mixed together with 10× PBS or concentrated aCSF parts and 10 mM thioflavin-T

(ThT) stock solutions (Sigma-Aldrich, St. Louis, MO, USA, cat. No. T3516), MilliQ water, and 10 mM oxidized EGCG or 10 mM VR16-09 stock solutions (VR16-09 stock solution was prepared as previously described [31]) to yield 2 μM $\text{A}\beta_{42}$ and 20 μM ThT in PBS or aCSF with or without 25 μM of the corresponding inhibitor. For experiments where a range of $\text{A}\beta_{42}$ concentrations was used, the prepared solution (2 μM $\text{A}\beta_{42}$, 20 μM ThT in aCSF) was diluted using a reaction solution (without $\text{A}\beta_{42}$) and 10 mM VR16-09 stock solution (dissolved in DMSO) to yield 2, 1.5, 1.25, 1.0, 0.75 μM of $\text{A}\beta_{42}$, and 20 μM ThT with or without 25 μM VR16-09. The equivalent volume of DMSO was used for the control samples. Kinetic aggregation measurements were performed in Corning non-binding 96-well plates (Fisher, Waltham, MA, USA, cat. No. 10438082) (sample volume was 80 μL) at 37 °C by measuring ThT fluorescence, using 440 nm excitation and 480 emission wavelengths, in a ClarioStar Plus plate reader (BMG Labtech, Ortenberg, Germany).

Table 1. Composition of 10 \times aCSF.

Composition of Concentrated aCSF (in 3 Separate Parts)			
	Amount in Pt 1, mM	Amount in Pt 2, mM	Amount in Pt 3, mM
NaCl	1270	-	127
KCl	18	-	1.8
KH_2PO_4	12	-	1.2
Na_2HPO_4	78.1	-	7.81
NaH_2PO_4	31.9	-	3.19
D-glucose	-	40	-
CaCl_2	-	14	-
MgCl_2	-	13	-
Urea	-	6.5	-
HSA	-	-	0.0615
Cholesterol	-	-	0.052
Sodium lactate	-	-	24
Glutamine	-	-	7

4.4. Atomic Force Microscopy (AFM)

The samples for AFM images were taken after $\text{A}\beta_{42}$ kinetic aggregation measurements were completed and scanned similarly, as previously described [34]. In brief, 40 μL of 0.5% (*v/v*) APTES (Sigma-Aldrich, cat. No. 440140) in MilliQ water was distributed onto freshly cleaved mica to modify the surface in order to bind the negatively charged structures. After incubating for 5 min, the mica was washed with 2 mL of MilliQ water and then dried under modest airflow. Forty microliters of each sample was deposited on the functionalized surface, incubated for another 5 min, washed with 2 mL MilliQ water, and dried under airflow. Imaging was done using a Dimension Icon (Bruker, Billerica, MA, USA) atomic force microscope. One thousand and twenty-four-by one thousand and twenty-four-pixel resolution images were recorded using a Nanoscope 10.0 (Bruker) and analyzed using Gwyddion 2.57 software. The heights of the fibrillar structures found on the mica were determined by tracing perpendicular to each fibril axis.

4.5. Cell Culturing

SH-SY5Y human neuroblastoma cells were obtained from the American Type Culture Collection (ATCC, Manassas, VA, USA). The cells were grown in Dulbecco's Modified Eagle Medium (DMEM) (Gibco, Grand Island, NY, USA), supplemented with 10% Fetal Bovine Serum (FBS) (Sigma-Aldrich, St. Louis, MO, USA), 1% Penicillin–Streptomycin (10,000 U/mL) (Gibco, Grand Island, NY, USA) at 37 °C in a humidified, 5% CO_2 atmosphere in a CO_2 incubator.

4.6. MTT Assay

MTT assay of SH-SY5Y cells was performed as previously described [40]. In short, SH-SY5Y cells were seeded in a 96-well plate (~15,000 cells/well) and cultured overnight. The 2 μM $\text{A}\beta_{42}$ monomers with or without 25 μM oxidized EGCG or 25 μM VR16-09 in PBS or aCSF were diluted in half with DMEM and used to replace the cell medium in each well. The preformed fibrils were used for the cell metabolic activity experiment using $\text{A}\beta_{42}$ with or without 10 μM of BSA. After the kinetic experiments, samples were taken, diluted in half with DMEM, and placed onto the cells in a 96-well plate. After 48 h of incubation, 10 μM of MTT was added to each well and left to incubate for 2 h. One hundred microliters of 10% SDS with 0.01 M HCl solution was added on top to dissolve formazan crystals. Absorbances at 540 nm, 570 nm, and 690 nm (reference wavelength) of each well were measured using a ClarioStar Plus plate reader (BMG Labtech, Ortenberg, Germany).

4.7. Statistical Analysis

The aggregation kinetic data analysis was done by fitting the kinetic curves using Boltzmann's sigmoidal equation [49]. Halftime values are added in Supplementary Materials (Table S1). The relative halftime values were calculated using the control samples from their respective 96-well plates. For the experimental data fitting, the baseline signal intensity drop was corrected by subtracting the exponential fit from 6 initial points of each individual curve. Each kinetic curve was then normalized between 0 and their respective initial peptide concentration in order to prepare for the global-fitting procedure (raw data are provided as Supplementary Material). Data fitting using a four-step aggregation model (primary nucleation, elongation, secondary nucleation, and fragmentation) was done using rModeler (Ubicalc Software, Vilnius, Lithuania), as described previously [33]. The fibril height values of different samples ($n = 50$) measured from AFM images were statistically compared using the one-way analysis of variance (ANOVA). * $p < 0.01$ and ** $p < 0.001$ were accepted as statistically significant. The data were processed and analyzed using Origin software (OriginLab, Northampton, MA, USA).

5. Conclusions

In conclusion, $\text{A}\beta_{42}$ aggregation was slower in aCSF than in PBS due to the combination of components found in the cerebrospinal fluid. The oxidized EGCG inhibitory effect retarded when aggregating $\text{A}\beta_{42}$ in aCSF instead of PBS, while VR16-09 showed opposite results with significantly enhanced inhibition. Human serum albumin was the main component influencing the increased inhibitory effect of VR16-09, whereas glutamine was the only one contributing negatively to the inhibition of $\text{A}\beta_{42}$. On the other hand, the inhibitory effect of VR16-09 on $\text{A}\beta_{42}$ aggregation in aCSF was mainly due to a decreased combined primary nucleation–elongation and an increased elongation–secondary nucleation rate constants of the process.

Supplementary Materials: The following supporting information can be downloaded at: <https://www.mdpi.com/article/10.3390/ijms24065991/s1>.

Author Contributions: A.S. and V.S. designed the experiments, A.S., R.S., A.J., D.V., and M.Z. (Mantas Ziaunys) performed the experiments, V.D. and M.Z. (Mantas Zvirblis) synthesized VR16-09, A.S., M.Z. (Mantas Ziaunys) and V.S. analyzed the data and prepared the manuscript. All authors have read and agreed to the published version of the manuscript.

Funding: This research was funded by the Research Council of Lithuania, grant number 01.2.2-LMT-K-718-03-0003.

Institutional Review Board Statement: Not applicable.

Informed Consent Statement: Not applicable.

Data Availability Statement: The data presented in this study are available in this manuscript.

Conflicts of Interest: The authors declare no conflict of interest.

References

1. Lamptey, R.N.L.; Chaulagain, B.; Trivedi, R.; Gothwal, A.; Layek, B.; Singh, J. A Review of the Common Neurodegenerative Disorders: Current Therapeutic Approaches and the Potential Role of Nanotherapeutics. *Int. J. Mol. Sci.* **2022**, *23*, 1851. [[CrossRef](#)] [[PubMed](#)]
2. Breijyeh, Z.; Karaman, R. Comprehensive Review on Alzheimer's Disease: Causes and Treatment. *Molecules* **2020**, *25*, 5789. [[CrossRef](#)]
3. De, S.; Whiten, D.R.; Ruggeri, F.S.; Hughes, C.; Rodrigues, M.; Sideris, D.I.; Taylor, C.G.; Aprile, F.A.; Muyldermans, S.; Knowles, T.P.J.; et al. Soluble aggregates present in cerebrospinal fluid change in size and mechanism of toxicity during Alzheimer's disease progression. *Acta Neuropathol. Commun.* **2019**, *7*, 120. [[CrossRef](#)]
4. Ehehalt, R.; Keller, P.; Haass, C.; Thiele, C.; Simons, K. Amyloidogenic processing of the Alzheimer β -amyloid precursor protein depends on lipid rafts. *J. Cell Biol.* **2003**, *160*, 113–123. [[CrossRef](#)]
5. Zhang, Y.W.; Thompson, R.; Zhang, H.; Xu, H. APP processing in Alzheimer's disease. *Mol. Brain* **2011**, *4*, 3. [[CrossRef](#)]
6. Thal, D.R.; Walter, J.; Saïdo, T.C.; Fändrich, M. Neuropathology and biochemistry of A β and its aggregates in Alzheimer's disease. *Acta Neuropathol.* **2015**, *129*, 167–182. [[CrossRef](#)]
7. Castellani, R.J.; Plascencia-Villa, G.; Perry, G. The amyloid cascade and Alzheimer's disease therapeutics: Theory versus observation. *Lab. Investig.* **2019**, *99*, 958–970. [[CrossRef](#)]
8. Huang, L.K.; Chao, S.P.; Hu, C.J. Clinical trials of new drugs for Alzheimer disease. *J. Biomed. Sci.* **2020**, *27*, 18. [[CrossRef](#)]
9. Athar, T.; Al Balushi, K.; Khan, S.A. Recent advances on drug development and emerging therapeutic agents for Alzheimer's disease. *Mol. Biol. Rep.* **2021**, *48*, 5629–5645. [[CrossRef](#)]
10. Srivastava, S.; Ahmad, R.; Khare, S.K. Alzheimer's disease and its treatment by different approaches: A review. *Eur. J. Med. Chem.* **2021**, *216*, 113320. [[CrossRef](#)]
11. Benoit, S.L.; Maier, R.J. The nickel-chelator dimethylglyoxime inhibits human amyloid beta peptide in vitro aggregation. *Sci. Rep.* **2021**, *11*, 6622. [[CrossRef](#)] [[PubMed](#)]
12. Finder, V.H.; Vodopivec, I.; Nitsch, R.M.; Glockshuber, R. The Recombinant Amyloid- β Peptide A β 1–42 Aggregates Faster and Is More Neurotoxic than Synthetic A β 1–42. *J. Mol. Biol.* **2010**, *396*, 9–18. [[CrossRef](#)]
13. Kodali, R.; Williams, A.D.; Chemuru, S.; Wetzel, R. A β (1–40) Forms Five Distinct Amyloid Structures whose β -Sheet Contents and Fibril Stabilities Are Correlated. *J. Mol. Biol.* **2010**, *401*, 503–517. [[CrossRef](#)]
14. Foderà, V.; Groenning, M.; Vetri, V.; Librizzi, F.; Spagnolo, S.; Cornett, C.; Olsen, L.; van de Weert, M.; Leone, M. Thioflavin T Hydroxylation at Basic pH and Its Effect on Amyloid Fibril Detection. *J. Phys. Chem. B* **2008**, *112*, 15174–15181. [[CrossRef](#)]
15. Di Terlizzi, R.; Platt, S. The function, composition and analysis of cerebrospinal fluid in companion animals: Part I—Function and composition. *Vet. J.* **2006**, *172*, 422–431. [[CrossRef](#)] [[PubMed](#)]
16. Ashok, K.S.; Gabriele, Z. The Interstitial System of the Brain in Health and Disease. *Aging Dis.* **2020**, *11*, 200. [[CrossRef](#)]
17. Vernau, W.; Vernau, K.A.; Bailey, C.S. Cerebrospinal Fluid. In *Clinical Biochemistry of Domestic Animals*; Elsevier: Amsterdam, The Netherlands, 2008; pp. 769–819.
18. Padayachee, E.R.; Zetterberg, H.; Portelius, E.; Borén, J.; Molinuevo, J.L.; Andreassen, N.; Cukalevski, R.; Linse, S.; Blennow, K.; Andreasson, U. Cerebrospinal fluid-induced retardation of amyloid β aggregation correlates with Alzheimer's disease and the APOE ϵ 4 allele. *Brain Res.* **2016**, *1651*, 11–16. [[CrossRef](#)]
19. Frankel, R.; Törnquist, M.; Meisl, G.; Hansson, O.; Andreasson, U.; Zetterberg, H.; Blennow, K.; Frohm, B.; Cedervall, T.; Knowles, T.P.J.; et al. Autocatalytic amplification of Alzheimer-associated A β 42 peptide aggregation in human cerebrospinal fluid. *Commun. Biol.* **2019**, *2*, 365. [[CrossRef](#)]
20. Milojevic, J.; Raditsis, A.; Melacini, G. Human Serum Albumin Inhibits A β Fibrillization through a "Monomer-Competitor" Mechanism. *Biophys. J.* **2009**, *97*, 2585–2594. [[CrossRef](#)] [[PubMed](#)]
21. Luo, J.; Wärmländer, S.K.T.S.; Gräslund, A.; Abrahams, J.P. Non-chaperone Proteins Can Inhibit Aggregation and Cytotoxicity of Alzheimer Amyloid β Peptide. *J. Biol. Chem.* **2014**, *289*, 27766–27775. [[CrossRef](#)]
22. Baram, M.; Miller, Y. Inhibitory Activity of Insulin on A β Aggregation Is Restricted Due to Binding Selectivity and Specificity to Polymorphic A β States. *ACS Chem. Neurosci.* **2020**, *11*, 445–452. [[CrossRef](#)] [[PubMed](#)]
23. Kanekiyo, T.; Ban, T.; Aritake, K.; Huang, Z.-L.; Qu, W.-M.; Okazaki, I.; Mohri, I.; Murayama, S.; Ozono, K.; Taniike, M.; et al. Lipocalin-type prostaglandin D synthase/ β -trace is a major amyloid β -chaperone in human cerebrospinal fluid. *Proc. Natl. Acad. Sci. USA* **2007**, *104*, 6412–6417. [[CrossRef](#)] [[PubMed](#)]
24. Schilde, L.M.; Kösters, S.; Steinbach, S.; Schork, K.; Eisenacher, M.; Galozzi, S.; Turewicz, M.; Barkovits, K.; Mollenhauer, B.; Marcus, K.; et al. Protein variability in cerebrospinal fluid and its possible implications for neurological protein biomarker research. *PLoS ONE* **2018**, *13*, e0206478. [[CrossRef](#)] [[PubMed](#)]
25. Stanyon, H.F.; Viles, J.H. Human Serum Albumin Can Regulate Amyloid- β Peptide Fiber Growth in the Brain Interstitium. *J. Biol. Chem.* **2012**, *287*, 28163–28168. [[CrossRef](#)] [[PubMed](#)]
26. Serot, J.M.; Christmann, D.; Dubost, T.; Couturier, M. Cerebrospinal fluid transthyretin: Aging and late onset Alzheimer's disease. *J. Neurol. Neurosurg. Psychiatry* **1997**, *63*, 506–508. [[CrossRef](#)] [[PubMed](#)]
27. Zaret, D.L.; Morrison, N.; Gulbranson, R.; Keren, D.F. Immunofixation to quantify beta 2-transferrin in cerebrospinal fluid to detect leakage of cerebrospinal fluid from skull injury. *Clin. Chem.* **1992**, *38*, 1908–1912. [[CrossRef](#)] [[PubMed](#)]

28. Rainesalo, S.; Keränen, T.; Palmio, J.; Peltola, J.; Oja, S.S.; Saransaari, P. Plasma and Cerebrospinal Fluid Amino Acids in Epileptic Patients. *Neurochem. Res.* **2004**, *29*, 319–324. [[CrossRef](#)]
29. Itkin, A.; Dupres, V.; Dufrière, Y.F.; Bechinger, B.; Ruyschaert, J.-M.; Raussens, V. Calcium Ions Promote Formation of Amyloid β -Peptide (1–40) Oligomers Causally Implicated in Neuronal Toxicity of Alzheimer’s Disease. *PLoS ONE* **2011**, *6*, e18250. [[CrossRef](#)]
30. Maier, J.A.M.; Locatelli, L.; Fedele, G.; Cazzaniga, A.; Mazur, A. Magnesium and the Brain: A Focus on Neuroinflammation and Neurodegeneration. *Int. J. Mol. Sci.* **2022**, *24*, 223. [[CrossRef](#)]
31. Hadi Ali Janvand, S.; Ladefoged, L.K.; Zubrienè, A.; Sakalauskas, A.; Christiansen, G.; Dudutienè, V.; Schiøtt, B.; Matulis, D.; Smirnovas, V.; Otzen, D.E. Inhibitory effects of fluorinated benzenesulfonamides on insulin fibrillation. *Int. J. Biol. Macromol.* **2023**, *227*, 590–600. [[CrossRef](#)]
32. Sneideris, T.; Sakalauskas, A.; Sternke-Hoffmann, R.; Peduzzo, A.; Ziaunys, M.; Buell, A.K.; Smirnovas, V. The Environment Is a Key Factor in Determining the Anti-Amyloid Efficacy of EGCG. *Biomolecules* **2019**, *9*, 855. [[CrossRef](#)]
33. Ziaunys, M.; Mikalauskaite, K.; Sakalauskas, A.; Smirnovas, V. Interplay between epigallocatechin-3-gallate and ionic strength during amyloid aggregation. *PeerJ* **2021**, *9*, e12381. [[CrossRef](#)] [[PubMed](#)]
34. Sakalauskas, A.; Ziaunys, M.; Snieckute, R.; Smirnovas, V. Autoxidation Enhances Anti-Amyloid Potential of Flavone Derivatives. *Antioxidants* **2021**, *10*, 1428. [[CrossRef](#)] [[PubMed](#)]
35. Hudson, S.A.; Ecroyd, H.; Kee, T.W.; Carver, J.A. The thioflavin T fluorescence assay for amyloid fibril detection can be biased by the presence of exogenous compounds. *FEBS J.* **2009**, *276*, 5960–5972. [[CrossRef](#)] [[PubMed](#)]
36. Watanabe-Nakayama, T.; Ono, K.; Itami, M.; Takahashi, R.; Teplow, D.B.; Yamada, M. High-speed atomic force microscopy reveals structural dynamics of amyloid β 1–42 aggregates. *Proc. Natl. Acad. Sci. USA* **2016**, *113*, 5835–5840. [[CrossRef](#)]
37. Sakalauskas, A.; Ziaunys, M.; Smirnovas, V. Gallic acid oxidation products alter the formation pathway of insulin amyloid fibrils. *Sci. Rep.* **2020**, *10*, 14466. [[CrossRef](#)]
38. Griner, S.L.; Seidler, P.; Bowler, J.; Murray, K.A.; Yang, T.P.; Sahay, S.; Sawaya, M.R.; Cascio, D.; Rodriguez, J.A.; Philipp, S.; et al. Structure-based inhibitors of amyloid beta core suggest a common interface with tau. *eLife* **2019**, *8*, e46924. [[CrossRef](#)]
39. Bode, D.C.; Stanyon, H.F.; Hirani, T.; Baker, M.D.; Nield, J.; Viles, J.H. Serum Albumin’s Protective Inhibition of Amyloid- β Fiber Formation Is Suppressed by Cholesterol, Fatty Acids and Warfarin. *J. Mol. Biol.* **2018**, *430*, 919–934. [[CrossRef](#)]
40. Sakalauskas, A.; Janonienė, A.; Zvinys, G.; Mikalauskaite, K.; Ziaunys, M.; Smirnovas, V. Exploring the Formation of Polymers with Anti-Amyloid Properties within the 2’3’-Dihydroxyflavone Autoxidation. *Process. Antioxid.* **2022**, *11*, 1711. [[CrossRef](#)]
41. Sato, M.; Murakami, K.; Uno, M.; Nakagawa, Y.; Katayama, S.; Akagi, K.I.; Masuda, Y.; Takegoshi, K.; Irie, K. Site-specific inhibitory mechanism for amyloid β 42 aggregation by catechol-type flavonoids targeting the lys residues. *J. Biol. Chem.* **2013**, *288*, 23212–23224. [[CrossRef](#)]
42. Shen, J.-L.; Tsai, M.-Y.; Schafer, N.P.; Wolyne, P.G. Modeling Protein Aggregation Kinetics: The Method of Second Stochasticization. *J. Phys. Chem. B* **2021**, *125*, 1118–1133. [[CrossRef](#)] [[PubMed](#)]
43. Ziaunys, M.; Mikalauskaite, K.; Smirnovas, V. Amyloidophilic Molecule Interactions on the Surface of Insulin Fibrils: Cooperative Binding and Fluorescence Quenching. *Sci. Rep.* **2019**, *9*, 20303. [[CrossRef](#)]
44. Plum, F. The physiology and pathophysiology of the cerebrospinal fluid by Hugh Davson, Keasley Welch, and Malcolm B. Segal New York. Livingstone, 1987 1013 pp. illustrated, \$198.00. *Ann. Neurol.* **1988**, *24*, 106. [[CrossRef](#)]
45. Johnson, K.S.; Sexton, D.J. *Cerebrospinal Fluid: Physiology and Utility of an Examination in Disease States*; UpToDate: Waltham, MA, USA, 2022; pp. 1–14.
46. Elbohouty, M.; Wilson, M.T.; Voss, L.J.; Steyn-Ross, D.A.; Hunt, L.A. In vitro electrical conductivity of seizing and non-seizing mouse brain slices at 10 kHz. *Phys. Med. Biol.* **2013**, *58*, 3599–3613. [[CrossRef](#)] [[PubMed](#)]
47. Kozak, L.R.; Bango, M.; Szabo, M.; Rudas, G.; Vidnyanszky, Z.; Nagy, Z. Using diffusion MRI for measuring the temperature of cerebrospinal fluid within the lateral ventricles. *Acta Paediatr. Int. J. Paediatr.* **2010**, *99*, 237–243. [[CrossRef](#)] [[PubMed](#)]
48. Sneideris, T.; Baranauskienė, L.; Cannon, J.G.; Rutkienė, R.; Meškys, R.; Smirnovas, V. Looking for a generic inhibitor of amyloid-like fibril formation among flavone derivatives. *PeerJ* **2015**, *3*, e1271. [[CrossRef](#)] [[PubMed](#)]
49. Ziaunys, M.; Sakalauskas, A.; Mikalauskaite, K.; Smirnovas, V. Polymorphism of Alpha-Synuclein Amyloid Fibrils Depends on Ionic Strength and Protein Concentration. *Int. J. Mol. Sci.* **2021**, *22*, 12382. [[CrossRef](#)]

Disclaimer/Publisher’s Note: The statements, opinions and data contained in all publications are solely those of the individual author(s) and contributor(s) and not of MDPI and/or the editor(s). MDPI and/or the editor(s) disclaim responsibility for any injury to people or property resulting from any ideas, methods, instructions or products referred to in the content.

Vilniaus universiteto leidykla
Saulėtekio al. 9, III rūmai, LT-10222 Vilnius
El. p. info@leidykla.vu.lt, www.leidykla.vu.lt
Tiražas 10 egz.